PALACKÝ UNIVERSITY

FACULTY OF MEDICINE AND DENTISTRY

Program DSP: Pediatrics

SCREENING OF CHEMICAL COMPOUNDS *IN VITRO* –

Analysis of the biological activity of small molecules

Petr Konečný, M.Sc.

Supervising department:

Institute of Molecular and Translational Medicine, Faculty of Medicine and Dentistry, Palacký University and University Hospital in Olomouc

Supervisor:

Petr Džubák, MD, PhD

Olomouc 2015

Statement:

I declare that I wrote this dissertation: "Screening of chemical compounds *in vitro*." myself. The research was carried out in the space of the Institute of Molecular and Translational Medicine, Laboratory of Experimental Medicine.

Acknowledgment:

First, I want to thank my supervisor, Petr Džubák, M.D., Ph.D. for his invaluable help throughout my PhD program, secondly, to Marián Hajdúch, M.D., Ph.D. for facilitating the laboratory work at the Institute of Molecular and Translational Medicine, with the great advantage of state of the art equipment and guidance throughout the research.

My appreciation goes to my colleagues from the Departments of Microbiology and Organic Chemistry, of Palacký University, researchers from the Institute of Organic Chemistry and Biochemistry, Academy of Science in Prague, Department of Analytical Chemistry, University of Chemical Technology Prague and Department of General and Inorganic Chemistry and Research Institute for Organic Synthesis, based in Pardubice.

I express gratitude to all my colleagues, who assisted and advised me but especially, Gabriela Rylová, M.Sc and Renata Buriánová.

My special thanks go to my friends and colleagues from the Experimental Pharmacology Unit in Napoli, Italy.

Research on these projects was supported by grants: IGA MZČR NT13569, GAČR 303/09/H048, IGA LF_2012_017, IGA UP LF_2013_015 a BIOMEDREG CZ.1.05/2.1.00/01.0030., NPU1 LO1304

Olomouc …….

July 2015 Petr Konečný, M.Sc.

CONTENT

ABBREVIATIONS

2D	two dimensional
3D	three dimensional
7-AAD	7-aminoactinomycin D
A549	lung Adenocarcinoma
ADME	Absorption, Distribution, Metabolism, Excretion
APC	allophycocyanine
ATP	adenosine triphosphate
ATCC	American Type Culture Collection
BCG	bacilli calmette guerine
BJ	Human normal cells derived from foreskin fibroblasts
CCRF-CEM/CEM-DNR	Human acute lymphoblastic leukaemia cell line/ acute lymphoblastic leukaemia cell line resistant to Doxorubicin
CML	Chronic myeloid leukaemia
DAPI	4',6-diamidin-2-fenylindol
DNA	Deoxyribonucleic acid
DsRed	Red fluorescent protein
ECM	extracellular matrix
EGF(R)	epidermal growth factor (receptor)

ERBB2/HER2/neu	receptor tyrosine-protein kinase/human epidermal growth factor receptor 2
FITC	fluorescein isothiocyanate
FSC	forward scatter
GFP	green fuorescent protein
hADK	human adenosine kinase
HAMA	human anti-mouse antibodies
HATs	histone acetyl-transferase
HBV	Hepatitis B virus
HCS	high content screening
HCT116wt/HCT116p53-/-	Human colorectal carcinoma cell line/ colorectal carcinoma cell line with deleted gene p53
HCV	Hepatitis C virus
HDACs	histone deacetylases
HDACi	histone deacetylase inhibitor
HIV	human immunodeficiency virus
hiPSC	human inducible pluripotent stem cells
HTS	high throughput screening
IC50	50% Inhibition concentration
IL	interleukin

K562/K562-TAX	Human myeloid leukaemia cell line/ myeloid leukaemia cell line resistant to Paclitaxel
KRAS	Kirsten rat sarcoma
LE	Ligand efficiencies
Lux	Bacterial luciferase
mADK	mycobacterial adenosine kinase
MAPK	mitogen-activated protein kinase
MDR	multi-drug resistance
MIC	minimum inhibitory concentration
MRC-5	Human normal cells derived from lung tissue
MRSA	Methicilin-resistant
MTB	*Mycobacterium tuberculosis*
MTS	(3-(4,5-dimethylthiazol-2-yl)-5-(3-carboxymethoxyphenyl)-2-(4-sulfophenyl)-2H-tetrazolium) , *in vitro* viability test
MTT	3-[4,5-dimethyl(thiazol-2-yl)-3,5-diphenyl] tetrazolium bromide, *in vitro* viability test
NADH	nicotinamid adenin dinucleotide
NIH	National Institute of Health
NSCLC	Non-small cell lung cancer
PDGF(R)	Plateled-derived growth factor (receptor)
PE	phycoerythrin
PerCP	Perydinin chlorophyll
PerCP Cy 5.5	Perydinin chlorophyll tandem conjugate
PES	phenazine ethyl sulfate

PMS	phenazine methyl sulfate
PMT	photomultiplier
RFP	Red fluorescent protein
RNA	ribonucleic acid
RT	room temperature
SRB	Sulphorodamine B, cell viability assay
SSC	side scatter
TI	Therapeutic index
TKI´s	tyrosine kinase inhibitors
VEGF(R)	vascular growth factor (receptor)
WHO	world health organisation
WST	Water-soluble Tetrazolium salts
XTT	(2,3-bis-(2-methoxy-4-nitro-5-sulfophenyl)-2H-tetrazolium-5-carboxanilide), *in vitro* viability test

1 Introduction

1.1 Drug development and biologically active small molecules

Even though there is a plethora of therapeutics for different kinds of diseases, many of them, including various forms of cancer, parasitic and severe bacterial infections are lacking proper specific treatment and are burdened with newly developed resistance or adverse side-effects. For this reason, there is major emphasis on finding new drugs that overcome these drawbacks. For clinically approved anticancer drugs, there are two main objectives. First, pathologically dividing and proliferating cells are targeted by **conventional chemotherapeutic drugs**, focusing on processes that lead to cancer cell division and proliferation. DNA replication is a key element in cellular division when an exact copy of the genetic material is made. Several classes of chemotherapy drugs target DNA synthesis and replication:

Alkylating agents bind to the DNA in the cell to prevent it from dividing. They work throughout the cell cycle and directly damage DNA. Alkylating agents include drugs from the following groups: Triazines (dacarbazine, temozolomide), Alkyl sulfonates (Busulfan), Nitrogen mustards (chlorambucil, cyclophosphamide and melphalan), Nitrosoureas (streptozocin, carmustine), Platinum derivatives (cisplatin, oxaliplatin, carboplatin) and others. Long-term usage of these drugs can, via their DNA damaging properties, cause bone marrow damage and lead to the development of secondary leukaemias. Bone marrow damage and secondary leukaemia are dose-dependant; which means that lower doses of alkylating drug cause less risk of disease development (Kumar et al. 2015).

The mode of action of the **Antimetabolites** is replacement of functional DNA and RNA building blocks by their non-functional substances. Unlike the previously mentioned group of therapeutics, Antimetabolites affect cells mostly during the S phase of the cell (DNA replication). This group involves Antifolate drugs (methotrexate,

pemetrexed) Antipurines (mercaptopurine, thioguanine, cladribin, cytarabine, gemcitabine etc.) and Antipyrimidines (kapecitabine, 5-fluorouracil).

Antitumor antibiotics prevent DNA uncoiling and interfere with the DNA strucuture. They are cell cycle specific drugs. The most common ATBs used as anticancer drugs are the Anthracyclines (Daunorubicin, Doxorubicin, Idarubicin). Other non-anthracycline ATBs include Actinomycin D, the radiomimetic drug Bleomycin (induces DNA strand breaks), Mitomycin C and Mitoxantrone. The main issue with these drugs is dose-dependent cardiotoxicity. Hence their application must be strictly controlled (Sikic 1999, Kumar et al. 2015).

Inhibitors of Topoisomerase prevent DNA strand separation and therefore DNA replication during the S phase. There are two groups of **Topoisomerase Inhibitors which** vary in the target affected: Topoisomerase I inhibitors (Topotecan, Irinotecan) and Topoisomerase II inhibitors (Etoposide, Teniposide). This enzyme is targeted by Mitoxantrone (Antitumor ATB), as well.

Antimitotic drugs (Fig. 1)**;** represented mostly by plant alkaloids, prevent cell division by interfering with the cellular cytoskeleton; specifically with microtubules creating mitotic spindles. They can be divided into two groups: inhibitors of polymerization (Vinca Alkaloids – vinblastine, vincristine and vinorelbine) and inhibitors of depolymerization (Taxanes – paclitaxel, docetaxel; Epothilones – ixabepilone) (Klener 2010; Kumar et al. 2015). Other proteins, involved in mitotic spindle assembly, such as aurora kinases, can be targeted by Aurora kinase inhibitors (Marzo & Naval 2013).

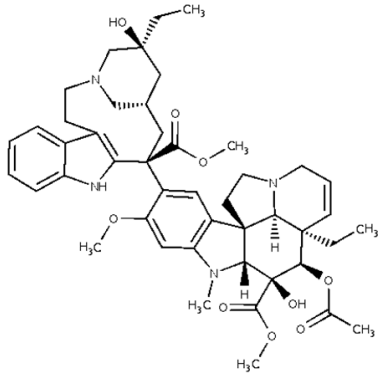

Vinblastine

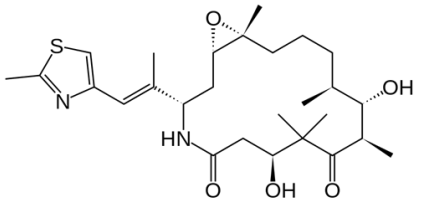

Ixabepilone

Fig. 1: Representatives of Antimitotic drugs: Vinblastine (Vinca Alkaloids), Ixabepilone (Epothilones).

Use of these drugs is however limited by their general cytotoxicity as they affect both cancer and normal cells even though cancer cells tend to be more sensitive to these drugs owing to their faster proliferation (conventional chemotherapeutics affect mostly fast dividing cells) and reduced threshold for further proapoptotic stimuli. This explains why this therapy does not affect non-dividing cancer stem cells and can cause relapses after treatment termination.

Cell division can be affected by other classes of chemotherapy in other ways as well. For example:

Antihormonal drugs suppress hormone dependent processes that stimulate cancer growth (Estrogenes, Androgenes, Glucocorticoids, Peptidic hormones) and commonly used in the treatment of breast, prostate cancer, leukaemia etc. Another approach to targeting pathologically proliferating cells is the **Induction of differentiation.** All-*trans* retinoic acid is successfully used in Promyelocytic leukaemia therapy (Mayer & Starý 2002). Another way is activation or reinforcement of the immune system components, called **Imunnotherapy**, targeting specifically cancer cells after stimulation by different cytokines (interferons, interleukins, hematopoetic growth factors, death ligands) or by synthetic immunomodulators (Thalidomide, Lenalidomide) or other immunomodulating drugs. Standard chemotherapy can be reinforced by addition of

chemoprotective drugs and antidotes (folic acid- decreases the toxicity of methotrexate) as well (Klener 2010).

Epigenetic modification provides another option for preventing cellular pathological behaviour. DNA methylation or histone modification is a way of gene expression control, which is often altered in cancer cells. DNA methyltransferase is an enzyme involved in DNA methylation and its inhibitors can cause reactivation of pathologically silenced gene expression (Howell et al. 2010). Regulation of transcription is provided by acetylation or deacetylation of histones as well. Enzymes involved in chromatin remodeling are histone deacetylases (HDACs) and histone acetyl-transferases (HATs). Histone acetylation opens chromatin structure and allows transcription of specific genes. In contrast, deacetylation causes closure of chromatin and disables gene transcription. In cancer cells, propapoptotic stimuli are often blocked by specific gene silencing via histone deacetylation. Histone deacetylase inhibitors (HDACi) can reactivate the transcription of silenced genes and induce apoptosis in cancer cells. It is also known that many other proteins involved in cell death and proliferation, are substrates for HDACs, such as cytoskeleton proteins, hormone receptors and chaperons (Xu et al. 2007).

The second approach is to target specific cellular pathways and the individual components involved in cancerogenesis. These are called **targeted therapies**. The advantage of this approach is high specifity, and therefore significantly lower cytotoxicity, with fewer side effects (compared to general cytostatics).

The two main categories of targeted therapy are currently **small molecules** and **monoclonal antibodies**. Monoclonal antibodies are artificial constructs prepared via hybridoma technology by fusion of spleen cells from mouse (immunized by specific antibody) and human myeloma cells. A broad spectrum of antibodies is in clinical use or being tested in clinical trials. Firstly, mouse antibodies were used but with little efficacy and causing systemic inflammatory response via production of human anti-mouse antibodies (HAMA). To avoid this, recombinant antibodies are now used. Today, we can find chimeric forms (rituximab, cetuximab), humanized antibodies (bevacizumab) and

completely human forms as well (panitumumab). These antibodies bind to a specific substance and are used in anticancer, anti-inflamatory, antiviral and other therapies, targeting different cellular proteins, such as growth factor receptors (VEGFR– bevacizumab, EGFR– cetuximab, ERBB2/HER2/neu receptor- trastuzumab), interleukins (IL-1β- canakinumab, IL-12, IL-23 ustekinumab) and many others (complement system proteins, integrines). Monoclonal antibodies are successfully used in the treatment of various cancers, such as breast and colorectal carcinoma, acute myeloid leukaemia, B-cell leukaemia and Non-Hodgkin´s lymphoma.

Although many new monoclonal antibodies as a form of specific targeting have recently been introduced into clinical treatment and even more are still in the clinical trials, the development of new active **small molecules** still stands as a solid and promising form of potential treatment discovery. The current focus is inhibition of particular targets and therefore we can talk about small molecular inhibitors. However, the process of the new drug development is time consuming, with low effectivity and highly expensive. **Chemical libraries** prepared by chemists subscribe to a few important rules, which improve the chances of finding molecular hits, with low initial cost and time, otherwise spent in preclinical testing. Based on their design, different kinds of libraries can be prepared; targeting specific molecular targets (proteases, kinases, G-protein coupled receptors), based on natural product molecule, protein-protein interaction, drug-like, lead-like (Lipinski 2000, Lipinski et al. 2004) or Fragment compounds Libraries. Fragment compound Libraries are the result of Fragment-based screening, focusing on drug leads discovery from small molecular fragments modification (Erlanson 2006). To obtain a lead drug candidate, many factors must be optimized, designed and modified to obtain the molecule with optimal physicochemical properties. So far the most common approach to finding these molecules is time consuming and financially demanding biological screening. Further, the number of successful drugs, leaving preclinical research is minimal, compared to the input amount of structures. There are different approaches to drug discovery. Drug development usually starts with the identification of lead molecule targeting specific molecular target (hit discovery), followed by optimization of its properties to obtain favourable binding efficiencies (hit-to-lead optimizition) (Keserü &

Makara 2009; Perola 2010). It has also been observed that clinical candidates are usually more complex than lead candidates because of modification during development (Keserü & Makara 2009).To avoid the necessity of testing a large number of promising compounds, *in silico* prediction models, which allow designing and optimizing different compounds with optimal properties before their direct synthesis, can be used. There are many ways for computing the potency of drug-like molecules. Prediction of ADME properties allows exclusion of compounds with poor accessibility and deliverance and selection of more potent structures with oral bioavailibility. ADME characteristics involve the evaluation of different biochemical parameters, such as blood-brain barrier permeability, whole molecule properties (solubility, hydrophobicity etc.), human bioavailability, intestinal absorption and metabolism. Various techniques can be used for ADME modelling involving patern recognition and classification models, molecular and quantum mechanics, statistical regression, using artificial neural networks and genetic algorithms, all contributing to distribution and toxicity profile establishment (Butina et al. 2002). For evaluation of interaction between small molecules with main classes of proteins, the QSAR modelling system (Bugrim et al. 2004) has been implemented. Toxicity, as a safety issue, is a very important limiting factor for drug modelling and causes a large number of failures in clinical trials. Many molecules have complex toxicity profiles (species- or organ-specific) and therefore its establishment is very difficult. Compounds with optimal toxicity profiles have high therapeutic index. Plasma levels together with toxicity manifestation are much higher than those for therapeutic efficiency. Thus, it is important to establish prediction and *in vitro* models for hepatotoxicity (main drug toxicity manifestation) or other system organ toxicity profiles (cardiotoxicity) (Li 2001).

Synthesis of chemical compounds is in theory not limited but can be focused and specified by application of different sets of predictors, such as the Lipinski rules, which define the desired properties for the best potential outcome for the drug, to become orally available and to have the best therapeutic absorption, distribution, metabolism and excretion (ADME) properties (Lipinski 2000, Lipiniski et al. 2001).

The Lipinski rules express the drug-likeness and basically focus on the molecular properties of the compound consisting of a:

- Maximum of 5 hydrogen bond donors (number of oxygen-hydrogen and nitrogen-hydrogen bonds
- Molecular mass lower than 500 Daltons
- A partition coefficient log P (a measure of lipophilicity) of less than 5
- No more than 10 hydrogen bond acceptors
- 40-130 molar refractivity

These ranges of chemical properties can predict the potential and capability of a small molecule to become an active compound and allow elimination of inconvenient candidates from development (Lipinski 2004). The number of hydrogen bond donors marks the ability of a compound to dissolve in an aqueous environment (blood, cytoplasm). Important characteristics which greatly affect the drug-likeness of compounds are lipophilicity and molecular weight. Lipophilicity is measured as the octanol-water partition coefficient logarithm (Log P) and imposes the rate of permeability through membranes, toxicity profile, determines metabolism and pharmacokinetics and are important features for the lead optimization process (Perola 2010; Tarcsay et al. 2012). Molecular size has a major role in terms of ligand efficiency. It has been observed that the molecular weight of tested compounds has a strong influence on average and maximal computed ligand efficiencies (LE). Usually molecules with a large number of heavy atoms display lower rates of LE (Reynolds et al. 2007; Hann 2011). The lower molecular mass improves the diffusion properties of the compound and facilitates its accessibility. The rate of lipophilicity provides information on permeability through the cell membrane and predicts the solubility of small molecule (Lipinski 2000).These settings seem to be widely accepted these days. They are validated mostly for oral application. Attempts have been made to apply the “Rule of five” to non-oral administrations (ophthalmic, transdermal and inhalation) and although most traditionally used non-oral drugs proved to have properties within the Lipinski rules, this should not be used to predict non-oral candidates which may be more limited than those for oral administration. This can be caused by unsuitable lack of enzymes in the skin, eye cornea

or lung epithelium, shorter retention time than in the intestines or by stronger epithelial barrier (Choy & Prausnitz 2011). Nevertheless, even some compounds out of the "Lipinski rules" range became routinely used in clinical practice as a standard chemotherapy (Fig. 2).

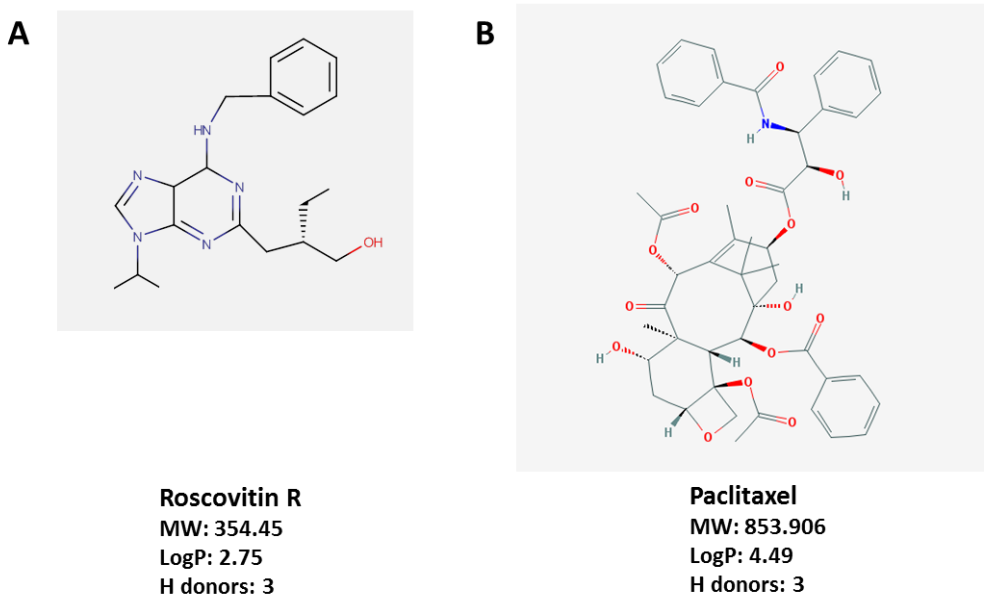

Fig. 2: Examples of molecules with (A) optimal properties according to Lipinski rules (Roscovitin R) and (B) non-Lipinski properties drugs (Paclitaxel).

There are also other definitions based on physicochemical properties, than Lipinsky rules, postulated by Veber, Oprea, Walters and Murcko, or by Rishton (Zhang et al. 2014).

Many different structures with various substituents are introduced into the initial screening and it is impossible to proceed to clinical trials with all of them. It is crucial to have a reliable model resembling the pathological and physiological properties of **tumors**, parasitic or bacterial infections and inflammation. This is one way of diminishing the number of potentially unsuccessful compounds in clinical trials and the financial costs their development.

In this work, we have focused on two major diseases, cancer and tuberculosis, diseases with several things in common. Apart from the for global and constantly increasing incidence and high mortality, newly developed resistance towards commonly applied drugs is a huge problem in both cases and needs to be dealt with. Although the origin, development, symptoms and prognosis of these illnesses are completely different and therefore comparison is not in place, they have features in common which can be used in drug development, such as similar or even identical therapeutic targets. For instance, even though there are structural and species related differences, drugs designed as tyrosine kinase inhibitors can affect both human and mycobacterial adenosine kinase and therefore represent potent molecules for future application to both these diseases.

This approach (application of standardized therapeutic to a different disease), called **Repurposing**, may be a way of discovering multi-potent drugs with interesting and unexpected activities and there is a tendency in research to do so. Repurposing or repositioning of clinically approved drugs for different applications has many advantages. It decreases the cost of new drug development as for the preclinical data (pharmacokinetics, pharmacodynamics, toxicity and side effects) are already known. It can improve success rate of treatment and exploit all possible applications of known molecules. Moreover, the active compound is usually easily available, there are vast libraries with drug-like compounds for this purpose and the possibility of clinical failure is greatly decreased (Geetharamani et al. 2015). The repositioning of drugs can be achieved via two options: as an "off target" approach, in which unknown new mechanisms of actions are explored or the "on target" approach, when an already known mechanism is used for different therapies (Kato et al. 2015). There are many drugs which have already been approved for different indications (Table 1). The libraries for drug repositioning are prepared by private institutions and public services as well. Except for patent agencies, where informations about various potent molecules are gathered and presented, other programs arise as a source of information for drug repurposing, such as National Institutes of Health (NIH) and the Chemical Genomics Centre which possess approved drug collection and contains bioinformatic and profiling data for many compounds. For example, the National Centre for Advancing Translational Sciences has a

programm for drug repurposing as well. Food and Drug Administration (USA) created a Rare Diseases Repurposing Database with all known molecular targets (Muthyala 2011).

Drug	Original indication	New indication	References
Amphotericin	Fungal infections	Leischmaniasis	Padhy 2011, Geetharamani 2015
Aspirin	Inflammation, pain	Antiplatelet	Padhy 2011, Geetharamani 2015
Bromocriptine	Parkinson´s disease	Diabetes mellitus	Padhy 2011, Geetharamani 2015
Celecoxib	Anti-inflammatory	STAT3 inhibitors – osteosarcoma therapy	Geetharamani 2015
Colchicine	gout	Recurrent pericarditis	Padhy 2011
Methotrexate	cancer	Psoriasis, reumathoid arthritis	Padhy 2011
Miltefosine	cancer	Visceral leishmaniasis	Padhy 2011
Raloxifene hydrochloride	Osteoporosis	Breast cancer	Geetharamani 2015
Retinoic acid	Acne	Acute promyelocitic leukaemia	Padhy 2011
Thalidomide	Morning sickness	Leprosy, multiple myeloma	Geetharamani 2015
Zidovudine	cancer	HIV/AIDS	Padhy 2011

Table 1: Selection of repurposed drugs.

1.2 Anticancer activities

1.2.1 Cancer cell lines and standard 2D experimental models

Identification of new potentional drugs and predicting drug response in cancer patients are major challenges in oncology. Scientists practicing clinical and translational research attempt to transform laboratory discoveries into new therapies for patients. **Tumor-derive**d cell lines have been used for many years as drug discovery tools. There are advantages to the use of **immortalized non-tumor cell lines** in drug discovery as well.

Traditionally, during the pre-clinical testing, immortalized cell lines bearing specific characteristics are used for observation of various effects caused by potential therapeutic drugs. Such cell lines represent libraries of different cancer and non-cancer cells derived from specific diseases´ manifestations. They usually tend to grow either in suspension or as a semi- or fully-adherent layers and are dependent on artificial environments and cultivation media supplements. The cultivation conditions and other variables greatly affect the reproducibility of results. The type of selected cultivation flask, plate or dish (different kinds of plastic, glass, porosity, adhesion surface structure etc.), as well as design of treatment (treatment after adhesion of the cells, or immediate treatment of cell suspension with compound, number of cultivation passage, lot of fetal calf serum which varies in endotoxins, Ig concentrations, growth factors, cell seeding concentration and eg.) can seriously contribute to variation in outcomes regarding growth, viability and response of cultured cells. Also, other microenvironment conditions (normoxic or hypoxic conditions) and usually the lack of its development in 2D cultures can decrease the reliability of experiments. Immortalized cell lines have many advantages for which they have become the most commonly used form of *in vitro* model tissues. Although, they have many disadvantages, which can cause misleading and false positivity of some compounds, and therefore selection of molecules which will eventually fail in clinical trials.

The establishment of the National Cancer Institute 60 **(NCI60)** cell line panel was a significant scientific commitment that required the development of a number of new technologies, such as the development of assays for measuring cytotoxicity, introduction of miniaturization in the form of microplates, automation of liquid handling and high volume data analysis on an unprecedented scale. Launched in 1990, the NCI60 platform consists of 60 human tumor cell lines, representing 9 cancer types; namely, leukemia (represented by 6 cell lines), melanoma (8 lines), cancers of the lung (9 non-small-cell lung cancer lines), colon (7 lines), brain (6 lines), ovary (7 lines), breast (6 lines), prostate (2 lines) and kidney (8 lines) (Stinson et al. 1992). Recently, advanced genetic techniques have revised the number of unique cell lines in the NCI60 panel to 57 (Lorenzi et al. 2009). However, the limitations imposed by the use of only 60 cell lines have become increasingly apparent in recent years. The recent introduction of "targeted anticancer drugs" show that clinical activity is often limited to small subsets of treated patients, rendering the composition of the NCI60 cell line panel somewhat inadequate for the task of capturing such low frequency responses.

In fact, the use of targeted therapeutics in the clinical setting has revealed that, as with the traditional cytotoxic chemotherapy agents, the clinical response to treatment with these agents varies substantially between patients — even among those with histologically indistinguishable disease. This is particularly well exemplified in the case of tyrosine kinase inhibitors (TKIs) that target epidermal growth factor receptor (EGFR) (Kris et al. 2003; Fukuoka et al. 2003; Thatcher et al. 2005; Shepherd et al. 2005; Moore et al. 2007; Saltz et al. 2004; Vermorken et al. 2007). The reasons for this are differences on the molecular level. Tyrosine kinases (TK´s) are enzymes which serve as modulators of growth factor signaling and through their activity- antiapoptotic effects, higher proliferation rate, angiogenic and metastatic activity can occur. Many inhibitors targeting specific tyrosine kinases were prepared and approved for clinical treatment. BCR-ABL fusion protein, typical for chronic myeloid leukaemia (CML) encoded by Philadelphia chromosme, is inhibited by Imatinib Mesylate (Gleevec). Other tyrosine kinases are overexpressed in different types of cancer as well. Epidermal growth factor (EGF) and the receptor for this protein (EGFR) overexpression occurring in non-small cell lung

cancer can be targeted by Gefitinib, Erlotinib, Lapatinib and other drugs. Semaxinib, Vatalanib and Sorafenib represent inhibtors for vascular endothelial growth factor (VEGF) or its receptor (VEGFR) and for example Leflunomide targets Plateled-derived growth factor (PDGF) (Arora & Scholar 2005). Nevertheless, molecular changes in TK´s can greatly affect the response to these drugs. Somatic mutations in these proteins can significantly alter the response to this treatment. It has been observed that treatment of NSCLC by Gefitinib was more successful in patients with somatic mutations (Paez et al. 2004). On the other hand, similar mutations occurring in KRAS protein in the same disease, predicted poor response to the same treatment. It is obvious that preceding genotyping is necessery for indication and selection of therapy (Massarelli 2007).

Other studies have suggested the need for larger and well characterised human cancer cell line panels, such as CMT1000 or the Cancer Cell Line Encyclopedia, to fully capture and mimic tumor heterogeneity (McDermott et al. 2008; Barretina et al. 2012).

However, it is only recently that investigators have begun to appreciate the enormous degree of genomic heterogenity across the human cancer patient population, and therefore across tumor-derived cell lines, and the crucial role that this diversity has in the variable clinical response to treatment.

In concordance with such approaches, other studies have used smaller cancer cell line panels consisting either of short-term tumor-derived cultures or established cell lines to recapitulate the genomic diversity of cancer. This model of tumor-derived cell lines is remarkably similar to that of the primary tumors from which they originated, implying that cultured tumor-derived cell lines are valid genetic surrogates of tumors *in vivo*. (Sos et al. 2009; Neve et al. 2006; Lin et al. 2008).

Many studies emphasize the necessity for new *in vitro* cancer models and the use of primary tumor models in which gene expression can be manipulated and small molecules tested in a setting that more closely mimics the *in vivo* cancer microenvironment so as to avoid radical changes in gene expression profiles produced by extended periods of cell culture. For example, Gillet J. and colleagues investigated the multidrug resistance (MDR) transcriptome of six cancer types in cancer established cell lines and clinical

samples and no correlation was found (Gillet et al. 2011). The cell lines bearing specific mutations with characterized cellular pathways are now used to identify targeted inhibitors of molecular processes which are crucial for diseases treatment. They are called Reporter cell lines and their preparation uses the application of biological reporters, such as Bacterial Luciferase (Lux), Green Fluorescent protein (GFP), (Nivens et al. 2004) or Aequorin, Obelin, Clytin and Mitrocomin, which are usually isolated from different kinds of bacteria (Lux) or some marine invertebrates (GFP, Aequorin, Obelin, Mitrocomin, Clytin), (Malikova et al. 2014).

1.2.2 2D vs. 3D models

More effort should be directed toward the development of new ex vivo models that more closely mimic the *in vivo* cancer microenvironment. The role of microenvironment is particularly important, for it was shown, that cells tend to behave differently under more complex conditions, similar to *in vivo* tissues and therefore display different sensitivity to various drugs or in their capability and speed diversity of growth (Pampaloni et al. 2007). Present trends imply that for adaptation of experiments towards the most similar environment to that *in vivo*, as possible,relationships between different cell types and their biological/chemical dependences need to be considered. It is known that in 2D models, cell-cell and cell-stroma interactions are not involved and therefore do not exactly mimic the natural environment in the human body (Birgersdotter et al. 2005). It was observed that for example primary hepatocytes cultured under standard two-dimensional conditions lose their specific function very quickly. On the contrary, 3D culture was able to sustain these functions. For future research, factors such as electrophysiological properties (Mulhall et al. 2013), hypoxia, sensitivity towards different drugs, interactions with other cells and ECM and many others must be included (Fig. 3).

One very important factor, not considered in 2D culture screening, is hypoxia. Because of limited ability of oxygen diffusion (described maximum for O2 diffusion is

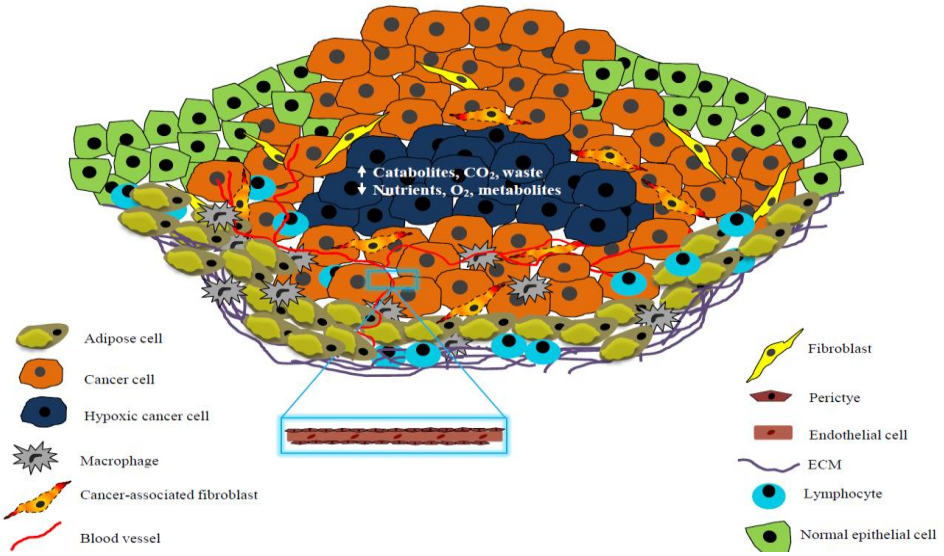

Fig. 3: Realistic model of cancerous tissue with its developed microenvironment. (Das, Konečný 2015)

100-200 μm), in 3D spherical forms of cultured tissues with greater size, this parameter can be taken for consideration. On the contrary, in 2D cultures, induction of hypoxia is almost impossible to achieve. According to Amish Astana, optimal size of aggregate preventing hypoxia is considered 250 μm (Asthana & Kissaalita 2012). The hypoxic conditions *in vitro* are nevertheless very important even in drug screening because hypoxia has been shown to be a significant factor affecting many biological processes and it is involved in tumor development and progression, for example, as an initiator of angiogenesis. Significant differences of VEGF and IL-8 expression (as the main angiogenesis inducing factors) were observed in 2D and 3D models, especially alterations in expression of IL-8, which is several-fold higher in 3D cultures than in 2D (Fischbach et al. 2007).

Apropos drug sensitivity/resistance, a number of studies have shown high reliance of spatial dimensions towards this factor. Pickl and Ries (2009) found that cells

growing under different spatial conditions, have different levels of HER family gene expression and even the form of dimerization, from heterodimers in 2D model, to homodimers localized in membrane rafts in 3D, which resulted in switch in signaling pathways from phosphoinosite 3-kinase (PI3K) to mitogen-activated protein kinase (MAPK), activation of integrin β4/rac1/PAK2 signaling cascade and therefore different response to trastuzumab treatment, favoring those in 3D cultures (Pickl & Ries 2009). In some cases, IC50 values significantly vary in 2D and 3D models, which can be caused by different levels of targeting molecules produced by 3D growing cells or by more difficult transport of drug throughout all spheroid, due the individual cells´heterogenity (Pickl & Ries 2009; Mehta et al. 2012; Sun et al. 2006; Fischbach et al. 2007).

There are several 3D platforms available today using different methods for establishing 3D cultures. Each of them has its advantages and disadvantages and not all can be used for HTS under current conditions (Breslin & O'Driscoll 2012; Pampaloni et al. 2007; Mehta et al. 2012; Kim 2005; Li et al. 2013). They can have different physical properties (rigid/pliable), creating matrix nets for cells adhesion or scaffold-free 3D cultures accomplished by hanging drops method or by Rotating Wall vessel, spinner vessels or microfluidic chambers (Astana and Kisaalita 2012; Pampaloni et al. 2007; Rimann & Graf-Hausner 2012; Fennema et al. 2013). The selection of spheroids preparation method is dependent on the design and purpose of the experiment.

To summarize, the main attributes of consideration. The direction of screening properties development leads toward the cheapest, fastest and most accurate, standardized, method. With 3D models, not all these characteristics can be achieved easily and it is necessary to make more effort in the evolution of new possibilities and approaches.

1.2.3 Drug discovery with High Throughput screening

High throughput screening is a powerful tool for drug screening, widely used for identification of active compounds in the thousands of chemical molecules (Fig. 4).

Basically, to test such a quantity of molecules is impossible without automatization and therefore a robotization and automatization of different processes is needed. Liquid handling, compound management system and data storage and evaluation, are processes which have to be automatized and electronically tracked. Current development in the field is enabling us to automatise quite complex tasks with multiple methodology steps which may vary, based on the interim results.

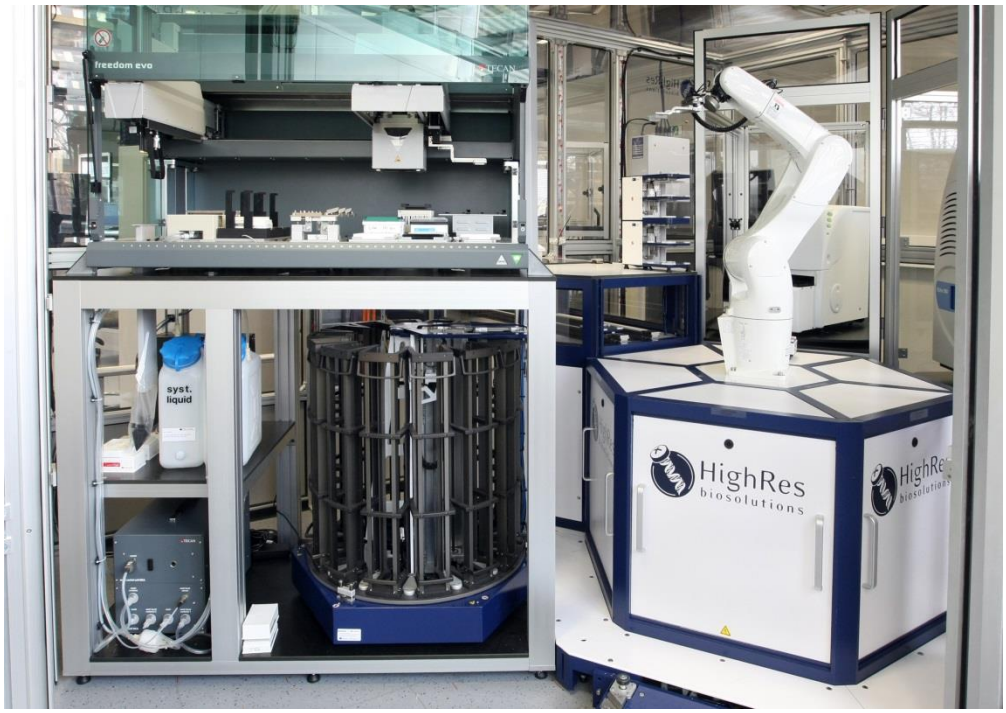

Fig. 4: Atomated robotic platform. (Institute of Molecular and Translational Medicine, Olomouc)

However, limitations occur even here. So far, mostly 2D models are used for HTS. Therefore, 3D cultures, for their closer relevance to living tissues, are thought to be implied in this screening and currently, many studies are engaged in this field. A few practical models have been introduced in these studies (Fernandes et al. 2009; Gidrol et al. 2009; Castel et al. 2006; Yliperttula et al. 2008). Although most of the issues were resolved, some of them complicate the situation, considering the cost of the assays or the quantitative analysis issue, for example. Also, in specific experiments, the size of 3D

structures must be evaluated. Due to hypoxia factors, a certain size of the culture must be achieved.

For drug discovery, different types of cell cultures are used. Together with traditionally used immortalized cell lines, primary cells, embryonic stem cells and human (or animal) pluripotent cells are being lately implemented in HTS as well. The 3D experimental models provide more specific and suitable conditions, resembling those *in vivo*. Nevertheless, not all of the issues have been solved so far and much has to be done for optimization of methodology, for cultures derived directly from patient samples evince different properties and complexity (Eglen et al. 2008). Several HTS platforms have been introduced lately using 3D models. Gidrol et al. (2009) summarized different approaches in 2 and 3D cell microarrays including modified glass slides, soft lithography based microfabrication of microwells in hydrogel or using microfluidic systems (Gidrol et al 2009).

3D cellular structures were successfully introduced for HTS by Horman et al. (2013). They were able to screen a library of 1528 compounds using soft agar assays, in which colorectal carcinoma cells HCT116 were grown and created multicellular spheroids. Compounds activity were then observed and characterized by different impact, into groups of non-active, cytotoxic, cytostatic or suppressive compounds. Moreover, the selectivity towards cancer cells was evaluated by co-culture with normal colon derived epithelial cells (Horman et al. 2013).

1.2.4 Primary cultures and third dimension

The other question rises, considering the cell types, used for drug screening. Comparison of genetic behavioral and other studies between commercially available cell lines and primary tissues obtained from cancer patients has provided interesting information about alterations between these two types. Even though cell lines are originally derived from tumors, immortalization and continuous cultivation under different conditions (than those in human bodies) caused several significant

transformations that can substantially affect therapeutic activity of tested drugs. The estimation of genes with different expression between primary cell cultures and cell lines is about 30%. Most of the alterations were observed in genes involved in cell cycle regulation which were upregulated in cell lines and caused therefore faster growth and proliferation in comparison with 3D structures (Bigersdotter et al. 2005). Lately, primary cells, derived from patient samples or embryonic tissues have been introduced into the HTS. With their phenotype and physiological properties, simulating those *in vivo*, these cells could become a more valuable model for preclinical studies, than immortalized cells. However, primary cells used in many experiments are mostly derived from animal models so far. Some of **human normal cells** have been used in drug screening too, for example human hepatocytes, neural cells, myocytes or pituitary cells. One possible implementation of primary cells was demonstrated by Sudo et al. 2009, discussed above. Although primary cells could be suitable, powerful tools for drug and HTS, the present direction of research abandons cells derived directly from patient samples and is more focused on embryonic stem cells and **inducible pluripotent stem cells** (hiPSC), which could actually overcome some of the issues connected with the cultivation and handling of primary cells, such as low proliferation activity, low transfectability and low survival susceptibility towards freezing and thawing. In fact, stem cells have been proved to display even better physiological properties, significantly higher potential of disease modeling and higher human relevance then primary cells. For example, Gao et al. (2014) stimulated differentiation of adipose derived stem cells into osteoblasts and endothelial cells and compared the growth characteristics of mono- and co-culture with relevance to the bone tissue engineering. This could solve the problem of insufficient vascularization during bone grafts fabrication (Gao et al. 2014). However, many HTS platforms use primary cells, and proved it to be a relatively suitable model for some important cellular properties, such as in toxicity assays or as patient derived xenografts, implanted in animal tissues and allowing growth under *in vivo* conditions (Eglen et al. 2008).

Not only cancer primary cells but **normal tissues** derived from patients have their place **in drug screening**. It is important to minimize compound toxicity and therefore potential side effects in early drug discovery phases. 3D screening and co-culture can

provide some of the information but it is necessary to perform parallel toxicity studies on normal tissue. In 2D models and with commercially available cell lines, this has been done traditionally. For application of primary cells, studies have been done, using several model tissue derived cells important in toxicity evaluation, including liver hepatocytes, neural cells and for example cardio myocytes. These are one of most affected tissues in humans, as targets for non-specific toxicity effects after drug treatment (Eglen et al. 2008). It is then very important to establish the so called **therapeutic index (TI),** expressing specific toxicity towards cancer cells and normal tissue (as mentioned above). It is one way of distinguishing compounds targeting directly cancer cells in early screening. For that reason, some researchers have focused their attention in this direction. Primary cardio myocytes were cultivated to obtain information about growth properties, gene expression and migratory characteristics in both, 2D and 3D models. Significantly different results were observed under these two different spatial conditions, confirming the theory, that cells in 3D environment evince similar development and response to external stimuli as *in vivo* (Akins et al. 2010). Application of primary cells *in vitro* has major relevance for therapeutic response of different drugs, chemotherapy and radiotherapy especially for specific types of tumors, such as head and neck cancer, which are situated in sensitive and risk locations and therefore application of radiotherapy has serious side effects. Jiglaire et al (2013), achieved successful establishment of glioblastoma primary cells, obtained from seven patients, in *ex-vivo* 3D hydrogel cultures and compared the results from toxicity and sensitivity/resistance assays from 3D and 2D cultivated cells. They discovered that sensitivity of tumor cells towards traditionally used drugs (cisplatin, temozolomide, carmusin) was significantly different in primary cells cultured under 2D and 3D spatial conditions. Glioblastoma cells were generally more resistant in three-dimensional environment. These cells proved to grow much more slowly in 3D than those in 2D (Jiglaire et al 2013).

1.2.5 The challenge of primary cells´ isolation

The challenge that requires specialized techniques is the isolation and culture of solid tumor cells and placing the cells in an *in vitro* environment similar to that *in vivo*. There are several methods for disrupting the extracellular matrix (ECM) and this is critical for successful isolation of primary cells. Additional problems include: non tumor cells contamination, few viable cells due to the resection from a necrotic area and stromal cells that compete with the listless cancer cells.

Tumor resection is an important step in isolating neoplastic masses with minimal damage to normal tissue, blood vessels and nervous system. The methodologies to isolate the tumor specimen vary and depend on tissue of origin. (Torzilli et al. 2011; Ayabe et al. 2011; Billis et al. 2012; Theodosopoulos et al. 2012; Yamamoto et al. 2012). After tumor resection, the next step is to isolate the cells from primary mass using different methods that dissociate the tumor to obtain a relative uniform population of cells. The neoplastic mass is dissociated by enzymatic, chemical or mechanical methods according to tissue of origin. Enzymatic dissociation is a common method to digest the specimens by enzymes including trypsin, collagenase, ialuronidase, pronase and deoxyribonuclease and certain enzymes are more effective than others for dissociation of specific tissues (Worthington Biochemical Online Tissue Dissociation Guide, Santangelo 2011). The chemical dissociation is based on the use of EDTA or EGTA that act by sequestration of numerous types of cations, such as Ca^{2+} and Mg^{2+}, from epithelial cells to release intercellular bonds. Another approach is the mechanical dissociation of tissue with scissors or sharp blades, homogenization, filtration and so on. This process is quick but is not appropriate for obtaining tumor cells because it results in a high percentage of dead cells with secretion of degrading enzymes. After dissociation the next step is to culture and maintain the cells.

There are several methods but very few are reproducible to generate primary tumor cell lines. For example, the **2D** monolayer culture was used first to elucidate the basic cell biology but in the case of primary culture, this fails because the cells are grown as a monolayer and lack architectural diversity. This method is not widely used to

establish primary tumor cell lines. In contrast, the **3D** methodology mimics the natural environmental conditions. The cells grow on a synthetic scaffold (hydrogel, matrigel and collagen) that reproduce extracellular matrix (ECM). This kind of approach facilitates numerous features of tumor cell lines such as proliferation, secretion of a large number of factors, immune evasion strategies, hypoxic condition, angiogenic properties, anchorage-independent growth, and metastatic potential. A recent paper, by Jiguet-Jiglaire and colleagues, described glioma cell growth and viability under various conditions in a 3D culture system. In particular, they characterized the three-dimensional culture system based on a hyaluronic acid-rich hydrogel, demonstrating that this culture model allows cell survival and proliferation, preserves cell morphology and is suitable for testing sensitivity to drugs and radiation (Jiguet-Jiglaire et al. 2014). The problems with this method are the appropriate seeding density, the tissue specific ECM and the composition of culture medium.

Other methods as well as explant-cell culture systems, precision-cut slice cultures, partial enzymatic degradation, sandwich cultures have been used and each is suitable for developing primary tumor cells but several issues remain: maintain good characteristics like polarity, morphology, gene expression and population purity.

It is still clear that primary tumors and cells derived from them are seldom used for primary research. The reason is poor and irregular availability. Hence these cells have become quite rare material and usually can be used only for advanced experiments.

1.2.6 Three dimensional experimental models and methods

The standardization of experiments is a big issue because for screening purposes it is necessary to achieve as identical as possible in culture conditions which is difficult in advanced and complexed systems, such as 3D models. This can be achieved especially with the **„Hanging drop" method**, using **matrices and scaffolds** or by **microfluidic cell culture platforms**. The disadvantage of these methods, is that they can be expensive or, in case of „Hanging drops", difficulties with exchange of culture media without

disturbing cells, may occur. Matrices, scaffolds and culture platforms may cause difficulties in further analyses because of problematic isolation of cells from formation.

The Forced-floating method is a relatively simple way of 3D spheroid forming. It is also quite inexpensive and suitable for HTS. On the other hand, there is rather large variability in cell size and shape and plate-coating can be time consuming.

Agitation-based methods are a more expensive model for the preparation of 3D structures due to the specialized equipment needed. Moreover, it is quite time consuming for HTS purposes and there is no control over spheroid size because of individual spontaneous adhesion of cells in suspension. In contrast, this option provides easy exchange of media (although in large amounts) but cultivating cells is very easy and so is the manipulation with spheroids, due to their accessibility. Another type of preparation is the **Rotary Cell Culture System**, developed by NASA which basically simulates microgravity, forcing the cells to flow in suspension. This allows continuous supply of nutrients from media and transfer of waste (Breslin & O'Driscoll 2012; Kim 2005; Mehta et al. 2012). Sudo and his team (2009) used primary rat hepatocytes to establish an assay for angiogenesis evaluation. They also co-cultured the primary cells with rat or human microvascular endothelial cells and compared the vascularization in 2D and 3D forms. They were able to establish viable and functional 3D hepatocyte cultures using a **microfluidic system**. This system involves a polydimethyl siloxande (PDMS) device with coverslip and two microfluidic channels together with intermediate 3D gel scaffold (Sudo et al. 2009).

A different way of creating 3D scaffolds was demonstrated by Gao et al. (2014). For establishing a suitable environment, poly (lactic-co-glycolic acid) (PLGA) and amorphous calcium phosphate nanoparticles in the form of **electrospun nanocomposite** was used for cell seeding. Electrospun poly -Ɛ-caprolactone scaffolds (PCL) have been used for successful growth and proliferation of murine astrocytes with phenotype of *in vivo* cells. Different nanofiber patterns (random, aligned) have demonstrated the different behavior of cells in various spatial environments with astrocytes in a random fiber field

growing deep within the scaffold in circular colonies and cells on aligned fibers creating colonies along the direction of the fibers (Lau et al. 2014).

3D scaffold are constantly being updated and individualized for specific cell types and their needs, to create environments that approximate *in vivo* conditions and the microenvironment. For example, Florczyk et al. (2013) adjusted a porous scaffold with hyaluronic acid used for cultivation of 3D human glioblastoma. To improve the adhesion properties of the system, polysaccharide chitosan was added. Their results suggest that cells exhibit more natural phenotype and growth properties and they confirm the possibilities for further specification for individual cell types (Florczyk et al. 2013).

In general, **hydrogels** represent a useful tool for 3D cultures. The material is easy to maintain and many different porous scaffolds made from different polymers can be prepared. Hydrogels of different compositions are commercially available, for example BD Bioscience (Li et al. 2013), Tebu-bio (Jiglaire 2014), Lifecore Biomedical, Rheometric Scientific (Beck et al. 2013) or many other. Hydrogels represent a form of 3D environment with various applications adaptable for different platforms (Asthana & Kisaalita 2013, Dixon et al. 2014). One possible 3D structure preparation, using hydrogel technology, suitable for HTS and drug screening, is **Microfluidic encapsulation**, which allows enclose of a specific number of of cells inside the capsules composed of different natural or synthetic polymeric hydrogels. Apart from cancer cells, other particles or chemicals can be captured within these capsules, for example ECM components, such as proteins. This allows preparation of populations with specific microenvironments. Large-particle flow cytometer subpopulations, consisting of cells expressing different fluorescence, can be sorted, re-cultivated and observed for specific markers or controlled micro environmental characteristics (Li et al 2013). Hydrogel scaffolds can be easily adapted for 96-well plates (Jiglaire 2014) and miniaturization for formats of 384 or even 1536 well- microtiter plates is being developed and optimized (Fig. 5).

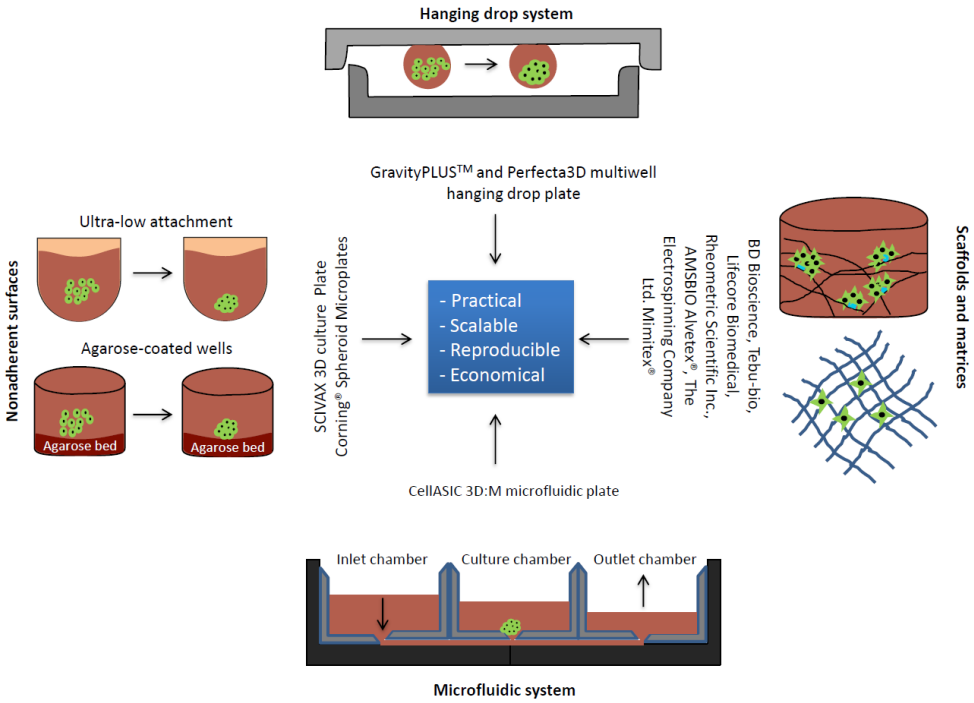

Fig. 5: 3D experimental culture models. (Das, Konečný et al. 2015)

The potential of different 3D models and their applicability in High Throughput (HTS) or High Content screening (HCS) is summarized by Kimlin et al. (2013) or by Reid et al. (2014) and will not be discussed in detail here.

One factor, which has to be considered in the **transfer of 3D cultures into HTS, is** easy, fast and precise visualization of produced spheroids and following their modifications after drug treatment. It is clear that 3D models will present challenges compared to monolayers which can be analyzed by optical and other methods. Many forms of microscopy can be used for appropriate visualization of 3D cultures, though not all of them provide the same outcome. Verveer at al. (2007) evaluated the differences between light-sheed based microscopy (SPIM) and **fluorescence confocal microscopy** with better outcome for SPIM, due to its higher resolution even without deconvolution, minimal photo damage and fast acquisition. The excitation light extends photo bleaching and phototoxic effect. Other microscopic methods have been described by Pampaloni et

al. (2007). These compare the methods outlined with electron micrograph and microscopy, immunohistochemical staining, multiphoton microscopy and optical coherence tomography (OCT), optical projection tomography (OPT), which were developed primarily for imaging of large 3D samples. Friedrich et al. (2009) established a drug screening protocol using phase contrast automated microscope which can easily be implemented in HTS platform and Horman et al (2013) implemented laser scanning fluorescence cytometer in the HTS screening of compounds activities of cells enclosed in different polymer hydrogel capsules.

1.3 Targeting of *Mycobacterium* by small molecules

1.3.1 General Antimycobaterial activity

Tuberculosis is a pulmonary disease in most cases caused by the pathogenic bacterium *Mycobacterium tuberculosis*. It is the cause of death in almost 1.5 million people of the more than 9 million infected, every year (WHO 2014). Its frequency decreases every year due to early and precise diagnosis but its prevalence is still enormous. Almost 25 percent (480 000) of infected patients were diagnosed as MDR-TB cases (WHO 2014). In some parts of the world, such as equatorial Africa, the treatment of TBC is burdened with a high incidence of HIV (or other) co-infection and combination of antiviral agents together with antituberculotics decreases the efficacy of the treatment. It is then necessary, to introduce more efficient compounds, with different mechanisms of action, targeting multidrug-resistant strains (MDR) and avoiding the contraindications between different drugs (Du et al. 2013, Bakuła et al. 2015). The ability to successfully target is rendered more difficult as different local strains have adapted during evolution to human population migrations. This correlates with the host immune system response (Gagneux et al. 2006; Gagneux & Small 2007). The *Mycobacterium* is a Gram-positive bacterium, although it cannot be visualized by Gram staining. This is due to lack of outer cell wall. Usually such bacteria are identified as acid-fast Gram-positive bacteria. They are oxygen dependent and transmission is usually airborne, or by soil, dust, water or by ingestion. When the mycobacteria are inhaled, they are phagocytised by pulmonary macrophages (Fig. 6). *Mycobacterium* uses several receptors for entry in the cell. Mostly Fc receptors, manose receptors and complement receptors (Glickman et al. 2001). The *Mycobacterium* enclosed in the phagosome prevents the fusion of the phagosome with lysosome and remains inside the cell, altering its surroundings to benefit itself. The bacterial cell wall is the main compartment in bacteria-cell interaction. It produces many different proteins, preventing the fusion, acidification of the phagosome, providing a way for nutrient supply from the outside and enabling its reproduction. This structure can

persist and thrive inside the cell. Eventually the cells are destroyed causing failure of lungs (Keane et al. 1997).

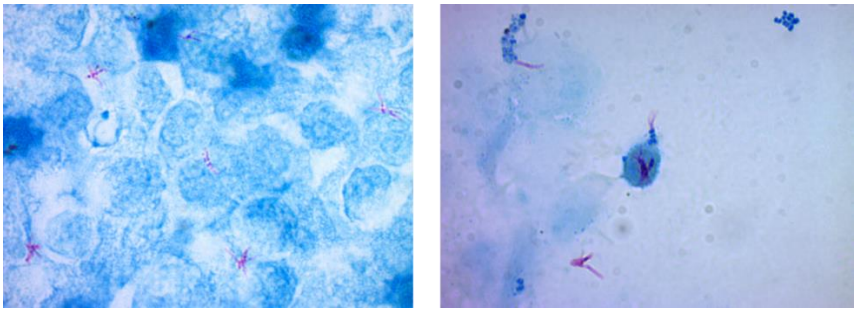

Fig. 6: *Mycobacterium smegmatis* phagocyted by B10A#4 macrophages– Ziehl-Neelsen acid staining. (40x)

Mycobacterium can be found in many other body tissues, such as kidneys, liver or spleen and it can persist in a dormant state for a very long time (Barrios-Payán et al. 2012). Properties, behaviour, and persistence of dormant *M. tuberculosis* change during its adaptation to non-active state.

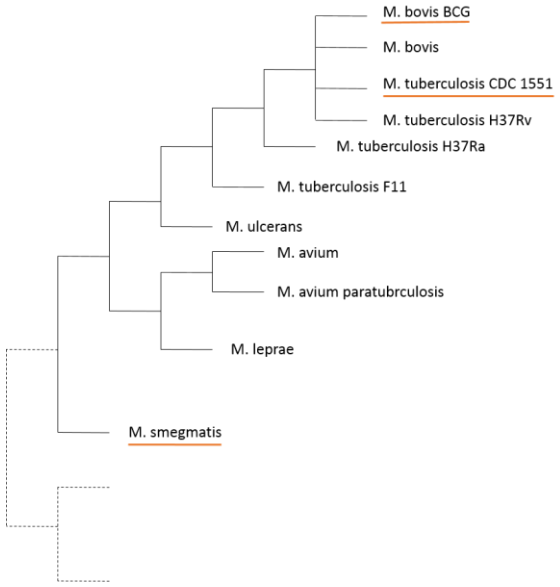

Fig. 7: *Mycobacterium*- Evolutionary tree.

This involves different protein expression, respiratory inhibition, slower growth and reproduction rate and invasion of non-respiratory phagocytes. This leads to a number of adverse outcomes, such as more difficult diagnosis, late manifestation and resistance to many commonly used drugs, such as rifampicin and isoniazid (Betts et al. 2002, Du 2013). For the purposes of screening, model strains used to obtain information about toxicity and specific activity, *M. bovis* and *M. smegmatis* can be obtained. ***M. bovis*** was derived from the standard vaccination strain BCG (Bacillus Calmette–Guérin). This bacterial strain has many advantages, such as non-pathogenicity, similar properties to standard *M. tuberculosis* and they are evolutionarily on the same level (Fig. 7). The main problem is the slow growth rate. On the other hand, M. smegmatis, is a distant relative of *M. tuberculosis*, has similar protein structures as well as growth properties, useful for screening. We have tested several groups of potentially active compounds for their toxicity towards these bacterial strains, targeting different proteins or interfering with specific metabolic agents. *Mycobacterium bovis* is a slow growing bacterial strain, closely related to *Mycobacterium tuberculosis*. It causes tuberculosis in cattle. In medicine it is used in the BCG vaccine (Bacillus Callmate Guérin), with reduced virulence (Fig. 8). Usually it is applied subcutaneously as a vaccine against *Mycobacterium tuberculosis.*

Fig. 8 : BCG (Bacillus Calmette- Guérin). Statents Serum Institute - Copenhagen

1.3.2 Potential mycobacterial targets

In the case of *Mycobacterium*, few cellular structures can be specifically targeted by different compounds (Table 2). There are a number of ways, to fight *Mycobacterium* and the approach should be focused on circumstances around the mechanism of infection. Treatment can be targeted to the bacteria itself, its metabolism or signalling properties, or it can concentrate on supporting a hostile environment of infected macrophage, mostly in

induction of autophagy and maturation of phagosome (Harris et al. 2007, 2009; Gutierrez et al. 2004; Houben et al. 2006; Mueller & Pieter 2006; Pieters 2008; Sundaramurthy & Pieters 2007). In the beginning, quinolone and its derivatives were standardly used. This causes arrest of bacterial replication. Although it was very efficient, many strains acquired multi-drug resistance towards these agents and diminished their application. As mentioned above, most of the bacteria's pathogenicity, adaptability to intracellular persistence and ability to transform its surroundings is provided by its cell wall components. The cell wall comprises peptidoglycans, galactofurans, arabinofuran and mycolic acids (Brennan 2003). Present-day approaches involve more specific targets, such as inhibition of these cell wall compartments, affecting mycolic acid, necessary for the cell wall build up (ethambutol, isoniazid), inhibition of mycobacterial RNA polymerase, therefore inhibiting RNA synthesis (Rifampicin) and interference with the energetic systems of bacteria (Bedaquiline). Another possibility is the inhibition of important bacterial protein kinases using different serine/ threonine protein kinases inhibitors (Rapamycine, meridianine derivatives) (Leiba et al. 2014; Yadav et al. 2015). Specific mechanism of action involves inhibition of peptidoglycan, arabinogalactan, fatty and amino acids and cofactor biosynthesis. This decreases the capability of mycobacterial cell walls to make a full contribution to bacterial survival. Another way of targeting *Mycobacterium* directly is to disrupt any of its typical pathways, such as mycothiol synthesis (oxidative stress protection) or non-mevalonate pathway of terpenoid synthesis; both non existent in humans (Table 2). There are other structures existing only in *Mycobaterium* and therefore potential targets for different drugs including regulatory proteins for glutamine synthase and iron-responsive regulators, menaquinone synthesis (vitamin K_2 homologues) or stringent response enzymes. Stringent response is a process providing adaptation for *in vivo* conditions (Mdluli & Spigelman 2006). Apart from these, two other basic mechanisms can be affected by different kinds of chemical compounds. Firstly, they can interfere with the iron metabolism of bacteria, which is crucial for its growth and reproduction. A second way is the inhibition of adenosine kinase (ADK), purine salvage enzyme involved in phosphorylation of adenosine to adenosine monophosphate (Long & Parker 2006), (Fig. 9). Very few bacterial species are known to express ADK. Of Gram-positive bacteria, *Mycobacterium* and Streptomyces lividans are

the only examples. As a representative of the group of Gram-negative category, Xanthomonas campestris was proven to express it as well. Nevertheless, *Mycobacterium* has ADK with a unique structure, unknown in any other species, which makes it a highly relevant target (Liu & Modlin 2008). For *Mycobacterium*, as well as for many other microorganisms, iron metabolism involves a series of processes crucial to survival and bacterial reproduction. It is essentially provided by proteins, called siderophores. *Mycobacterium* produces several siderophores called mycobactins and exochelins. Mycobactins are hydrophobic siderophores associated with the cell wall as porins, while exochelins are hydrophilic chelating receptors. Both of them are capable of attracting and reducting of Fe^{3+} ions and its further internalization into storage depots or for direct metabolism. Fe^{3+} ions are taken up from the host environment through these structures and reduced through exochelins and Fxu complex to Fe2+ actively while creating ATP from ADP or passively through porins. These ions are then stored as bacterioferritin iron storage proteins (Fig. 10). Compounds with higher Fe^{3+} affinity may prevent the storage of iron by the bacteria and therefore negatively affect its viability (Olakanmi et al. 2000).

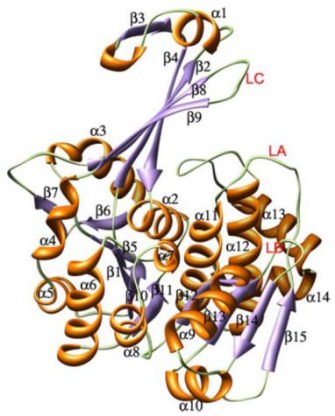

Fig. 9: Structure of mycobacterial Adenosine kinase. (Reddy et al. 2007)

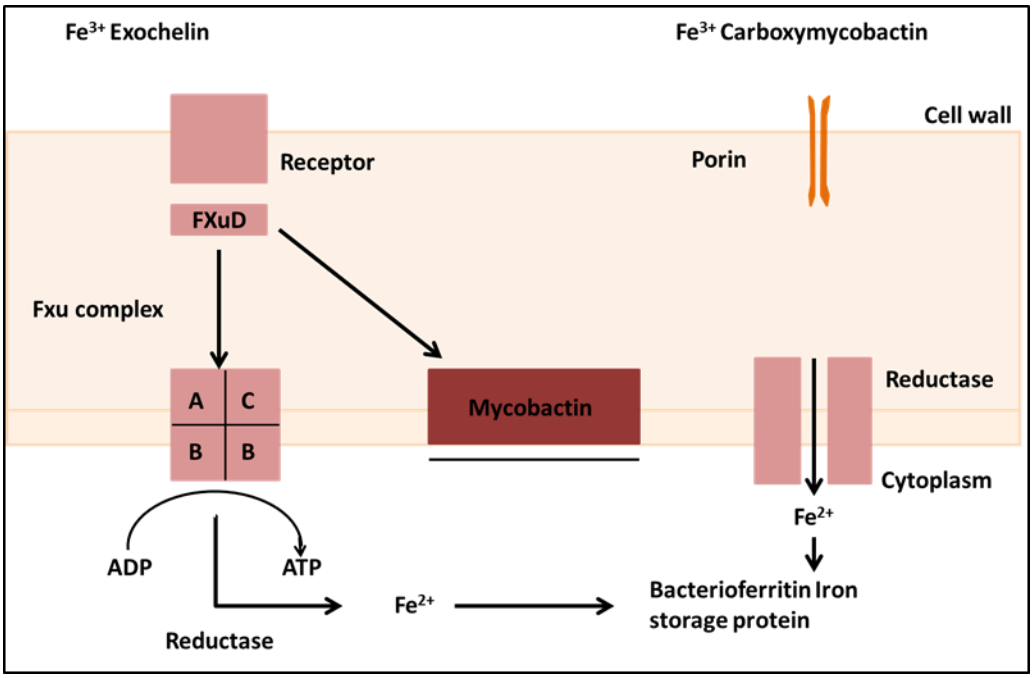

Fig. 10: Iron uptake in *Mycobacterium* – siderophore system of iron metabolism. (modified from Schaible & Kaufmann 2004)

Mechanism of action	Drugs	Molecular target	Line of treatment	References
Fatty acids biosynthesis inhibitors	Isoniazid	Alkyl hydroperoxidase; Enoyl ACP reductase; Catalase-peroxidase, NADH dehydrogenase	1st line	Zhang 2006, Janin 2007, Zumla 2013
	Pyranizamide	Nicotinamidase; Pyranizamidase	1st line	Zhang 2006, Janin 2007
	Ethionamide	Flavoprotein monooxygenase	2nd line	Zhang 2006, Janin 2007
	Prothionamide	Flavoprotein monooxygenase	2nd line	Janin 2007
Arabinogalactan and peptidoglycan biosynthesis inhibitors	Ethambutol	Arabinosyl transferase	2nd line	Berning 2001, Zhang 2006, Takiff 2011
	Amoxicillin	transpeptidase	-	Janin 2007
Inhibitors of protein synthesis	Streptomycine	S12 ribosomal protein; 16S rRNA of 30S ribosomal subunit	1st line	Zhang 2006, Janin 2007, Zumla 2013
	Kanamycin	30S ribosomal subunit	2nd line	Zhang 2006, Janin 2007, Zumla 2013
	Capreomycin	16S rRNA	2nd line	Zhang 2006, Janin 2007, Zumla 2013
	Clarithromycin	50S ribosomal subunit	3rd line	Janin 2007
	Linezolid	50S ribosomal subunit	3rd line	Janin 2007
DNA- based processess inhibitors	Rifampicin	DAN-dependent RNA polymerase	1st line	Zhang 2006, Janin 2007, Zumla 2013
	Rifapentin	DNA-dependent RNA polymerase	combination	Janin 2007, Zumla 2013
	Fluoroquinolones	DNA gyrase subunits A, B; DNA topoisomerase	-	Berning 2001, Takiff 2011
Energy depletion	Bedaquiline	ATP synthase *c* subunit	3rd line	Zumla 2013

Table 2: Clincally used anti-tuberculotic drugs with their mechanism of action and targeted molecular structures

1.3.3 Intracellular Antimycobacterial activity

Many compounds have been proven to be highly selective *in vitro* antimycobacterial activity, ranging from micromolar to sub-micromolar concentration, similar towith the positive control, Rifampicin. However, *Mycobacterium tuberculosis* is usually an intracellular bacterium, thriving in macrophages´ phagosomes. The compound therefore, must be able to penetrate the cell membrane and still affect the enclosed bacteria. For that, an intracellular activity assay was established, using macrophages as Mycobacterial carriers and performed for two groups of compounds, Nucleosides and Chelators. B10A#4 cells, a cell line derived from mouse macrophages were seeded, incubated with *Mycobacterium smegmatis* and allowed to phagocytose. Treatment followed and after incubation, phagocytosed bacteria were released and seeded on agar plates and observed for their viability. As expected, in some cases, IC50 values dramatically increased compared to previous results obtained from direct exposure. Some compounds had poor permeability and did not reach the targeted structure. The methodology is presented in detail in the Methodology section.

2 Experimental part

2.1 Methodology

2.1.1 Cytotoxity evaluation

In the first steps of research, it is important to determine the general cytotoxicity of tested compounds. For this purpose, many different assays have been developed. Sulphorhodamine B, MTT, MTS, XTT and WST assays are the most common (Riss et al. 2013). The MTT (3-(4,5-dimethylthiazol-2-yl)-2,5-diphenyltetrazolium bromide) tetrazolium reduction assay was the first homogeneous cell viability assay developed for a 96-well format that was suitable for high throughput screening (HTS) (Mosmann 1983). The MTT tetrazolium assay technology has been widely adopted and remains popular in academic labs as evidenced by thousands of published articles. MTT is positively charged and readily penetrates viable eukaryotic cells. Viable cells with active metabolism convert MTT into a purple colored formazan product with an absorbance maximum near 570 nm. When cells die, they lose the ability to convert MTT into formazan, thus color formation serves as a useful and convenient marker of only the viable cells. The exact cellular mechanism of MTT reduction into formazan is not well understood, but likely involves reaction with NADH or similar reducing molecules that transfer electrons to MTT (Marshall et al. 1995). Speculation in the early literature involving specific mitochondrial enzymes has led to the assumption mentioned in numerous publications that MTT measures mitochondrial activity (Berridge et al. 1996). One disadvantage of MTT is low solubility of the purple formazan product and subsequent solubilization step before spectrometry measurement.

Curently there are alternatives to MTT like XTT, MTS and WST class compounds. Their disadvantage is that the negative charge of the formazan products that contribute to solubility in cell culture mediums are thought to limit the cell permeability of the tetrazolium. This set of tetrazolium reagents is therefore used in combination with intermediate electron acceptor reagents such as phenazine methyl sulfate (PMS) or

phenazine ethyl sulfate (PES) which can penetrate viable cells, become reduced in the cytoplasm or at the cell surface and exit the cells where they can convert the tetrazolium into the soluble formazan product (Berridge et al. 2005). Another disadvantage is the price of the substrate. The cytotoxicity assays are usually performed using different cancer, bacterial, fungal or parasitic models as well as a healthy tissue representative. The obtained value is called IC50 (half maximal inhibitory concentration) (Pharm Stat. 2011). The optimal outcome is to have as low toxicity towards normal tissue as possible. This specific toxicity is expressed by a therapeutic index (TI), ratio between IC50 for normal tissue and IC50 for potential target (cell, bacteria, etc.). The higher the number, the more specific toxicity the drug evinces. In the case of antibacterial agents, comparison of toxicity towards bacteria and healthy tissue is very important. Compounds with an archaic general toxicity profile, must be excluded from the screening and attention must be focused on structures with narrow activitytoward specific therapeutic target. Cell lines selected for cytotoxicity assays were chosen across representatives of both haematological and solid tumours, the same as its sensitive and resistant forms and consist of a panel of CCRF-CEM (a cell line derived from acute lymphoblastic leukaemia), CEM-DNR (doxorubicin resistant variant) (Nosková et al. 2002), K562 (acute myeloid leukaemia), K562-TAX (paclitaxel resistant variant) (Nosková et al. 2002) as haematological representatives and A549 (lung adenocarcinoma), HCT116 (colorectal carcinoma), HCT166p53$^{-/-}$ (cell line with deletion of p53 gene) from solid tumours. The final IC50 value computed from absorbance measurement indicating the capacity of tested compound for further research. Compounds with IC50 lower than 10 μM for sensitive CEM cell line qualified for **cell cycle evaluation** (Bourderioux et al. 2011; Jansa et al. 2014; Kaplánek et al. 2015).

2.1.2 Flow cytometry

Flow cytometry is a biotechnological method that first appeared in the middle of 1950´s, and provides a useful and simple option for cellular properties evaluation.

Currently, this is routinely used in clinical and research facilities for cell counting, biomarker detection, cell sorting and for the diagnosis determination or confirmation. Other applications involve cell kinetics, cancer therapy monitoring, cell function analysis, tumor cell identification and chromosome karyotyping. Different properties (cell diameter, volume, membrane potential, internal structure etc.) and components (DNA, nuclear antigens, enzymes, proteins, RNA, surface antigene etc.) can be analysed by FC.

Flow cytometer usually consists of three main systems: Optical systems (with analogue to digital signal converting detectors), fluidic system providing sheath and cleaning solutions and computer systems for processing the data. The heart of the cytometer is a flow cell, which allows redistribution of cell suspension and laser beam exposure of cells. Based on hydrodynamic focusing, a sheatfluid mixes with the cell suspension and creates a stream consisting of specifically stabilized droplets containing embedded cells. This stream passes through a quartz-glass cuvette. The stream usually has a higher flow rate (~5ml/min) than the sample (~100 µl/min). This allows the cells to be constrained in the center of the flow chamber.

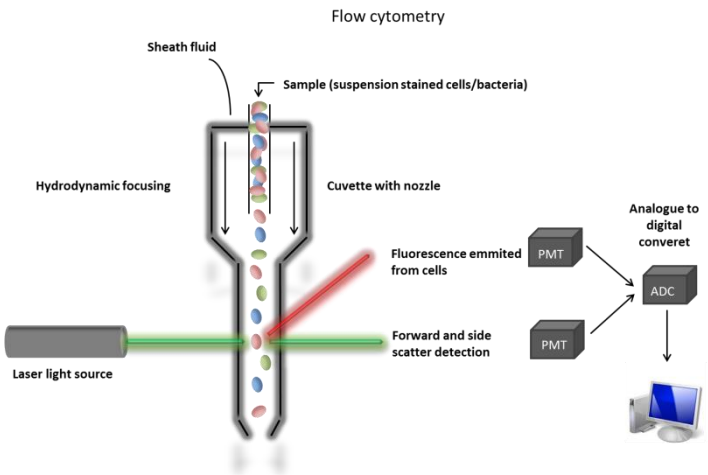

Fig. 11: Scheme of flow cytometry.

The cuvette is aligned with the laser beams and creates an optimal optical pathway, ensuring the highest sensitivity with a relatively low laser power. Optical systems can be covered by lapms, high-powered water- cooled lasers, low-powered air-cooled lasers or

laser diods. Usually low-powered air-cooled lasers are provided with different wavelength (488 nm, 633 nm or UV laser). Older cytometers consist of only two basic lasers. Modern instruments can possess multiple lasers with wide wavelength ranges. These laser beams pass through the cell flow and fall on the passing stream containing the analysed cells. Lasers have a Gaussian intensity distribution, which means, that the maximal intensity is in the centre of the beam. Therefore, the stream must be very stable at the same time, as well. Light scattered after the cell passes the stream allows us to analyse some of the basic physical properties, such as size (FSC) or granularity (SSC) of the cells. These two parameters are detected by a photodiode with a 488/10 nm bandpass filter (Forward scatter detection) and PMT detector with beam splitter (side scatter). Cell fluorescence is a form of luminescence and it stands for a light emmited by a cell or bacteria after light absorption (emission usually has a longer wavelength) (Fig. 11). After the laser falls on the cell surface, light excitation/emission is measured by PMT detectors and converted into an electrical signal enabled for processing and analysis (Kachel et al. 1990). Visualisation of various cellular components is enabled by application of molecules called fluorophores/fluorochromes. **Fluorophores** are fluorescent small molecules (200 – 1000 Daltons) emitting light and staining different cellular structures. Their excitation/emission parameters are the most important features for precise analysis. Among the most common fluorophores are nucleic acid dyes (Hoechst, DAPI, ethidium bromide, 7-AAD, propidium iodide etc.), fluorescent proteins (GFP, RFP, DsRed, APC, PerCP etc.) and cell function dyes (Fluo 3, Fluo 4, SNARF). Usually, some of these dyes are used as conjugates with macromolecules called **Antibodies**; structures specifically binding to different intra- or extra-cellular markers (Fig. 12). For the purpose of detailed analysis, many fluorophores have been developed

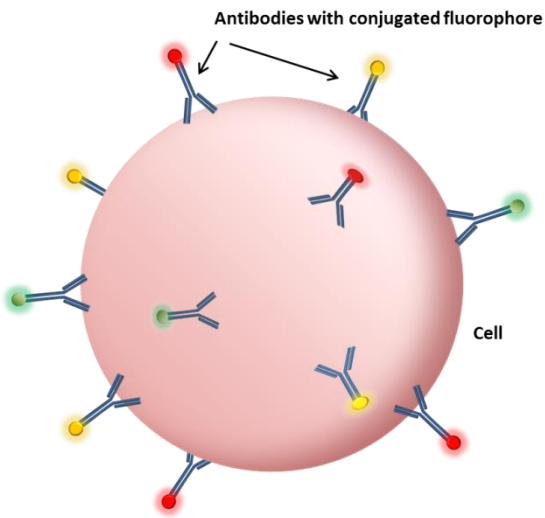

Fig. 12: Cell with attached antibodies conjugated with different fluorophores.

for the fluorescent labelling but they are usually represented by fluorescein isothiocyanate (FITC; 494/520 nm), phycoerythrin (PE; 496/578 nm), perydinine chlorophyll (PerCP; 482/678 nm) with its **tandem** conjugates PerCP Cy 5.5 (482/695 nm), allophycocyanine (APC; 650/660 nm), Alexa Fluore 488 (495/519 nm) and few others (Shapiro 2003).

Flow cytometer used for cell cycle analysis is the BD FACS (Fluorescence-activated cell sorting) Calibur from Becton Dickinson Company. Instrument contains two lasers- 488 nm 15mW air-cooled low-powerd laser and 633 nm 10mW laser. As a fluorescence detection system, four PMT detectors are used; three for the 488 nm laser (530/30 nm; 585/42 nm; > 670 nm) and one for the 633 nm laser (661/16 nm). According to screening requirements, several related parameters are analysed. These include apoptosis, distribution of cells in different cell cycle phases, synthesis of DNA, RNA and phosphorylation of phosphor histone ($pH3^{Ser10}$). Additionally, information about compound activity related protein biosynthesis alterations can by analysed. This method uses the ability of propidium iodide to intercalate into DNA, therefore visualize the cell cycle according to its DNA content. For DNA, RNA synthesis, $pH3^{Ser10}$ phosphorylation and protein synthesis, additional staining with primary and secondary antibodies is necessary. All these parameters were measured and analysed using BD software CellQuest with the exception of cell cycle analysis, which was performed in specialized Cell Cycle Analysis Software developed by Verity Software House, Inc. The final flow cytometry analysis provides closer information about the compounds´ basic mechanism of action and indications for further research, or consecutive modification of tested compounds. These modifications may serve for adjustment or enhancement of their therapeutic properties (Bourderioux et al. 2011; Jansa et al. 2014; Kaplánek et al. 2015).

2.1.2.1 Cell cycle and apoptosis analysis (Fig. 13, 14)

Cultivated CEM cells were maintained in a CO_2 incubator, seeded at standard density 1 x 10^6 cells/ well in 6-well plates. 24 hours later, compounds were added to the cell suspension (1x IC50, 5x IC50) and the sample was incubated until the next day. The

cell suspension was harvested after 24 hours, washed with 5 ml of PBS and fixed in 2 ml of 70% ice-cold ethanol. Cells in ice-cold ethanol were centrifuged at 800 g, for 7 min at room temperature and washed with 4 ml of citrate buffer. 500 µl of RNAase was added to the pellet and incubated for 15 min. Then, 600 µl of propidium iodide were added, incubated for 15 min in waterbath and samples were stored in a fridge for 1 hour and analysed using FACS Calibur (Bourderioux et al. 2011; Jansa et al. 2014; Kaplánek et al. 2015).

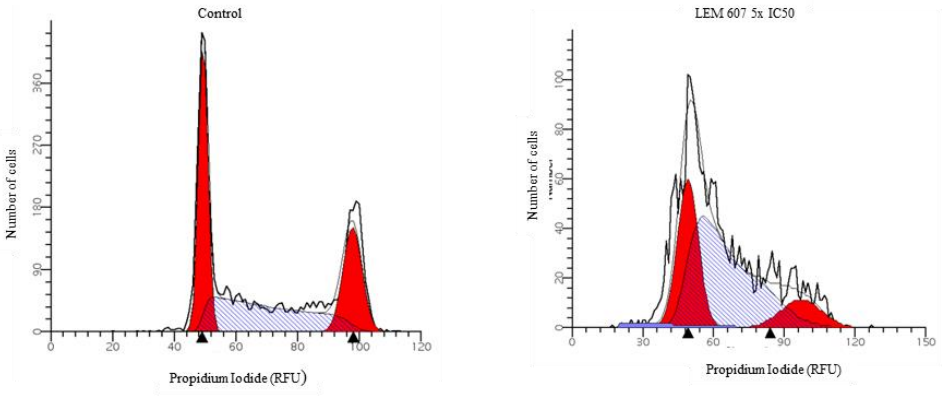

Fig. 13: Cell cycle analysis- Untreated control and cells treated with compound LEM 607 5x IC50.

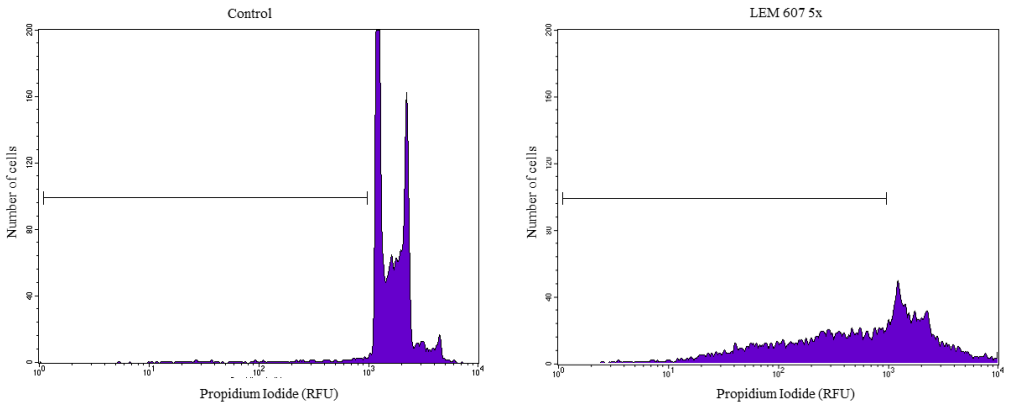

Fig. 14: Apoptosis analysis– Untreated control and cells treated with compound LEM 607 5x IC50 (compound 7).

2.1.2.2 pH3^{Ser10}staining – marker of M-phase initiation analysis (Fig. 15)

Cultivated CEM cells were maintained in a CO_2 incubator seeded at standard density 1 x 10^6 cells per well in 6-well plates. Following day, compound at desired concentration (1x IC50, 5x IC50) was added and cells were incubated for 24 hours. The cell suspension was harvested, washed with 5 ml of PBS and fixed in 2 ml of 70% ethanol. Cells fixed with ice-cold ethanol were used for phosphohistone phosphorylation analysis. Cells were washed with 1ml of PBS with 1% fetal bovine serum (FBS) and centrifuged at room temperature and 2000 rpm, for 5 min. Then they were incubated with 1 ml of 1x PBS containing 0.25% Triton X-100 for 15 minutes, washed with 5 ml of PBS + 1% FBS again and centrifuged (2000 rpm, 5min, RT). Primary antibody Anti-phospho-Histone pH3^{Ser10} antibody (Millipore) was prepared in PBS + 1% FBS and 100 µl was added to each sample. After 1 hour of incubation, samples were washed with 5 ml of washing solution (PBS + 1% FBS) and centrifuged again (2000 rpm, 5 min, RT). 30 minutes incubation with 100 µl of secondary antibody Alexa Fluor 488 goat anti-rabbit IgG (Invitrogen) followed. Samples were washed afterwards and incubated for 30 minutes with 700 µl of Propidium iodide with RNAase (PI – 50 µg/ml, RNAase – 0.5 mg/ml in PBS + 1% FBS). For analysis, FACS Calibur (Becton-Dickinson) was used (Bourderioux et al. 2011; Jansa et al. 2014; Kaplánek et al. 2015).

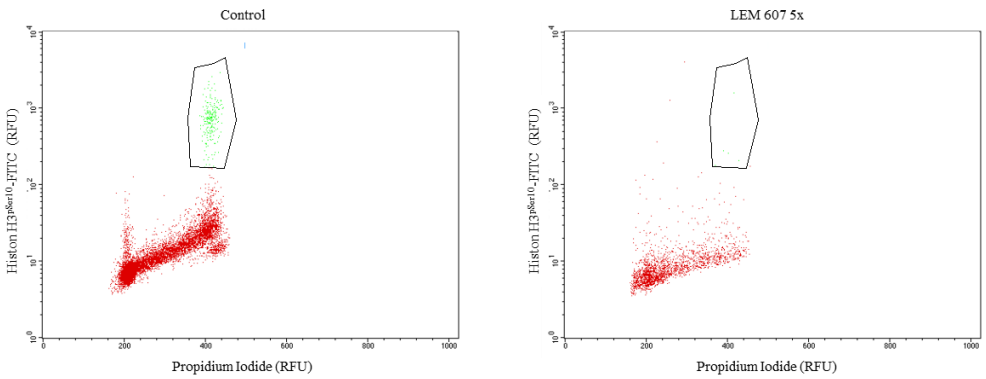

Fig. 15: Analysis of phosphorylation of histone H3 on Serin 10 (pH3^{Ser10}) – Untreated control and cells treated with compound LEM 607 5x IC50 (compound 7).

2.1.2.3 BrU incorporation analysis (Fig. 16)

Cultivated CEM cells were maintained in a CO_2 incubator seeded at standard density 1 x 10^6 cells per well in 6-well plates. The following day, compound at desired concentration (1x IC50, 5x IC50) was added and the cells were incubated for 24 hours. Then, 40 µl of 100 mM of 5-bromouridine (BrU) was added and suspension was incubated for a further 30 min. Cell suspension was harvested after 30 min, washed with PBS and fixed in 2 ml of 1% paraformaldehyde (added drop-wise). Cells fixed in 1% paraformaldehyde were used for this analysis. Suspensions were centrifuged and washed with 3 ml of cold PBS containing 1% glycine and then again with PBS at 500 g, for 5 min, RT. 100 µl of primary antibody Antimouse BrdU (cross-reactive to BrU), clone MOBu-1 (Exbio, Cat. No. 11-286-C100) prepared in PBS + 0.1% BSA + 0.1% NP40 was added afterwards and cells were incubated for 45 minutes. Then, the cells were washed with 3ml of PBS + 0.1% BSA + 0.1% NP40 and centrifuged (500 g, 5 min, RT), labelled with 100 µl of secondary antibody Anti-Mouse IgG (whole molecule) with FITC (Sigma, Cat. No. F28883) and incubated for half an hour. Samples were washed again in the same way as before (PBS + 0.1% BSA + 0.1% NP40 and centrifuged at 500 g, 5 min, RT) and fixed in 1 ml of PBS containing 1% formaldehyde and 0.05% NP-40, mixed by rotating for 15 minutes and then incubated for 1 hour at 4°C. Samples were then washed again with 3 ml of cold PBS containing 1% glycine, 100 µl of RNAase (10 mg/ml of PBS + 0.1 % BSA + 0.1 % NP40) and 600 µl of propidium iodide (50 µg/ml of PBS + 0.1 % BSA + 0.1 % NP40) were added and cells were analysed with FACS Calibur (Bourderioux et al. 2011 ; Jansa et al. 2014; Kaplánek et al. 2015).

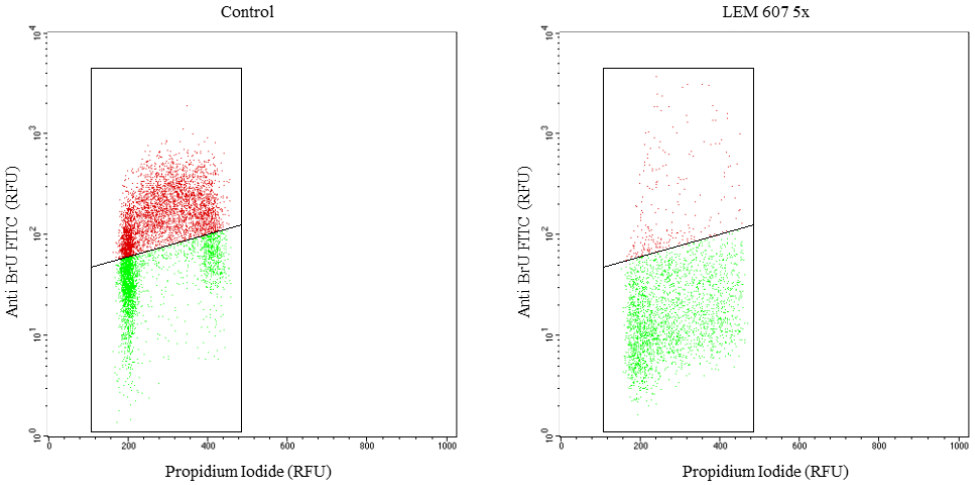

Fig. 16: RNA synthesis analysis (BrU) – Untreated control and cells treated with compound LEM 607 5x IC50 (compound 7).

2.1.2.4 BrdU incorporation analysis (Fig. 17)

Cultivated CEM cells were maintained in a CO_2 incubator seeded at standard density 1 x 10^6 cells per well in 6-well plates. The following day, compound at desired concentration (1x IC50, 5x IC50) was added and cells were incubated for 24 hours. Then, 40 µl of 1 mM of 5-bromodeoxyuridine (BrdU) was added and the suspension was incubated for a further 30 min. The cell suspension was harvested, washed with PBS and fixed in 2 ml of 70% ethanol. Cells fixed in ice-cold ethanol were centrifuged at 500 g, for 5 min, RT and 2 ml of 2N HCl/ Triton X-100 was added. Samples were mixed by vortexing and incubated for 30 min. Afterwards, cells were centrifuged again, (500 g, for 5 min, RT). 2 ml of borax (0.1 M $Na_2B_4O_7.10.H_2O$) were added. The suspension was centrifuged, and after washing with 2 ml of PBS + 0.5% Tween + 0.1% BSA, 200 µl of primary antibody Antimouse BrdU, clone MOBu-1 (Exbio, Cat. No. 11-286-C100) prepared in PBS was used for labeling. Suspensions were then incubated for 30 min and washed again with 2 ml of PBS + 0.5% Tween + 0.1% BSA. Addition of 200 µl of secondary antibody Anti-Mouse IgG (whole molecule) with FITC (Sigma, Cat. No.

F28883) (prepared in the same way as the primary) followed. After 30 min of incubation, cell suspensions were washed again as mentioned above (500g, 5 min, RT). 100 µl of RNAase (10 mg/ml of PBS) was added to the cells and incubated for 15 minutes at RT. 600 µl of propidium iodide (50 µg/ml of PBS) were added, incubated for 15 minutes at RT and samples were stored in a fridge for 30 min. Measurement was performed on FACS Calibur (Bourderioux et al. 2011; Jansa et al. 2014; Kaplánek et al. 2015).

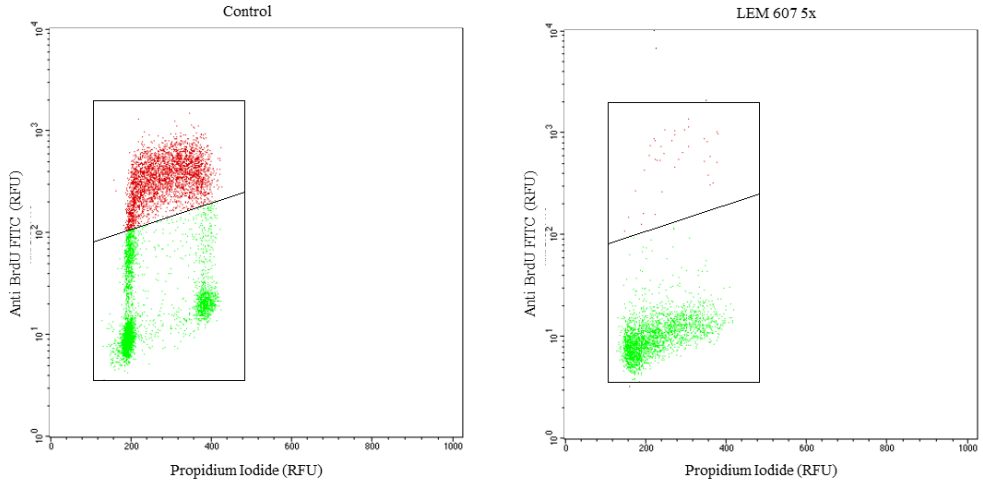

Fig. 17: DNA synthesis analysis (BrdU) – Untreated control and cells treated with compound LEM 607 5x IC50 (compound 7).

2.1.3 Antibacterial and antifungal activity

Many compounds derived from basic natural or synthetic active molecules evince different potential therapeutic effects. Diverse groups of compounds with anticancer, antibacterial, antifungal, immunosuppressive or anti-inflammatory agents can be distinguished. As a part of standard screening, activity against several common bacterial and fungal strains together with their drug-resistant equivalents are simultaneously explored. The main panel consists of bacteria Enterococcus faecalis CCM 4224, Staphylococcus aureus CCM 3953, Escherichia coli CCM 3954, Pseudomonas aeruginosa CCM 3955, Staphylococcus aureus (MRSA) 4591, Staphylococcus

haemoliticus 16568, Escherichia coli 16702, Pseudomonas aeruginosa 16575 and fungi Candida albicans, Candida crusei, Candida tropicalis and Candida parapsilosis. This panel is assembled from basic bacterial and fungial representatives. Bacterial and yeast liquid cultures were seeded on blood agar soils and incubated for 24 hours at 37°C. Grown colonies were dissolved in broth and allowed to incubate for 1hour. The MIC assessment was performed using standard dilution micromethod, described below (Kaplánek et al. 2015). Nevertheless, some tested compounds were synthesized with already known potential targets, such as mycobacterial ADK. For this purpose, *Mycobacterium bovis* and *Mycobacterium smegmatis* were added for extension of the tested platform (chapter 2.1.4).

2.1.4 Antimycobacterial activity

For evaluation of specific antimycobacterial activity, model strains- ***M. bovis*** and later, ***M. smegmatis*** were used. Standard BCG vaccine lyophilized bacteria was resuspended in attached solvent and seeded on 7H11 agar plates (7H11 agar + OADC enrichment). For suspension culture, grown colony was inoculated in 7H9 Broth media, containing 0.05% of Tween 80. This prevents bacteria from creating clusters. M. smegmatis was prepared in the same way, although this strain was already obtained as an agar seeded culture. Both M. bovis (isolated from BCG vaccine) and M. smegmatis (ATCC) are known to process tetrazolium salt in the same way as human tissue cells do, through mitochondrial activity. Therefore the standard MTT test was performed for these bacterial strains to distinguish compounds with selective antimycobacterial activity. Suspension bacteria M. boivs and smegmatis) were cultivated in 7H9 Broth (Difco, BD). Then, 80 µl of suspension was seeded on 96-well plates and treated with the desired compounds in dilution series, the highest concentration at 100 µM and the following 4x dilutions with the minimum in the range of sub µM to nanomols. The culture was then incubated for 120 hours at 37°C and 5% CO_2. After incubation, 20 µl of MTT were added and allowed to react for 1-4 hours, depending on the individual strain. Afterwards, 100 µl

of SDS, as a detergent, were added to the wells and IC50 values were assessed from absorbance measurement. The whole methodology is described in detail in Kaplánek et al. (2015).

2.1.4.1 Assesment of intracellular activity

The intracellular activity assay was newly established and optimized for analysis of intracellular antimycobacterial potential but results are not yet published. As a carrier for M. smegmatis, mouse derived macrophage cell line B10A#4 was used (Radzioch et al. 1991). These cells were seeded on 6- or 12-well plates containing 2 - 4 ml of RPMI medium and allowed to adhere. Afterwards, M. smegmatis strain was added at different densities (10 – 20 bacteria per one cell) and incubated for a few hours (4 - 5) to allow the process of phagocytosis. Then, not-phagocyted extracellular bacteria were thoroughly washed out. Tested compounds at desired concentrations were added to the well and incubated for 120 hours. Macrophages were then lysed using 0.2% digitonin for a certain amount of time (to release enclosed bacteria) and the final suspension was harvested in 7H9 broth medium and inoculated on 7H11 (Difco, BD) agar plates. The culture was allowed to grow for 10 days and the final CFU was counted and compared to the untreated control sample (Fig. 18). This assay was performed for two different groups of compounds – Nucleoside derivatives, as a potential MTB ADK inhibitors and Benzothiazole hydrazones, due to their chelating properties (Fig. 19, 20).

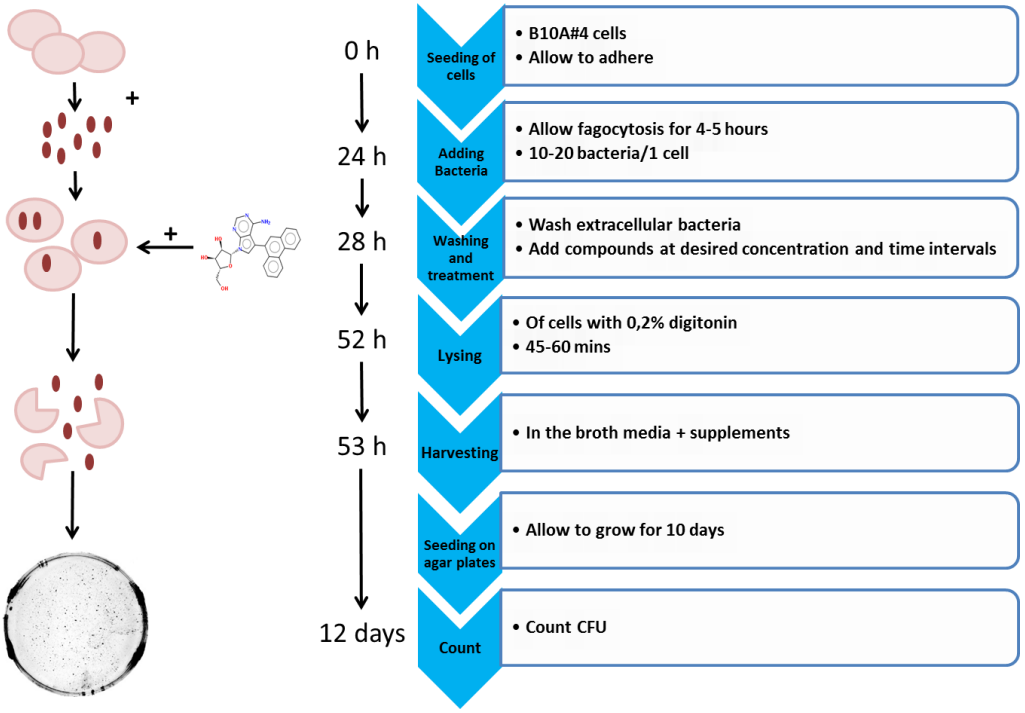

Fig. 18: Workflow of intracellular activity assay. (Unpublished data)

2.2 Aim of study:

Identification of biological activities of tested molecules

1. **Nucleoside derivatives**:

    a) 7-hetaryl-7-deazaadenosines

    b) 6-alkyl, 6-aryl, 6-hetaryl deazapurines)

    c) 6-substituted 7-het (aryl) deazapurines

2. **Cytosine derivatives**

3. **Hydrazones with Tröger base skelet**

2.3 Tested compounds

Many substances naturally occurring in plants have proven to have potent biological activity including anticancer, antibacterial, antifungal, and anti-inflammatory among others; however, the basic active molecules frequently fail due to inaccessibility and lack of natural occurrence. The chemists´ effort then relies on the preparation of derivatives, based on these molecules, with enhanced biological properties. This is usually achieved by structural modification and by addition of different substituents that improve the accessibility and deliverance. To date, three classes of chemical compounds have passed through basic screening profiling and allowed the selection of the most potent compounds with dual biological activities (anticancer and antibacterial).

2.3.1 Nucleoside derivatives

Nucleosides (Fig. 21), as anticancer drugs have been known since the 1950´s. These are now used in the treatment of different kinds of malignancies. However, a number of reviews have described the problematics of the anticancer and antiviral activity of nucleoside derivatives (Pastor-Anglada et al. 1998; Younger et al. 2004; Bobeck et al. 2010; Jordheim et al. 2013). Briefly, nucleosides represent nucleic acid analogues based on purine (thymine/cytosine, uracil) or pyrimidine (adenosine, guanine) bases and belong to the class of antimetabolites (Jordheim 2013; Pałasz & Cieź 2015; Jahnz-Wechmann et al. 2015).

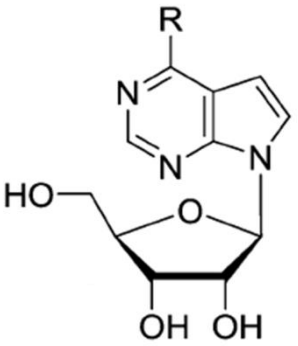

Fig. 21 : Basic skeleton of nucleoside. (Nauš et al 2014)

They have been successfully applied in the treatment of haematological malignancies and solid tumours. Nucleosides are multifunctional structures that target cell proliferation and growth (Fig. 22). They successfully incorporate into the DNA or RNA and therefore significantly alter their synthesis; they are able to affect metabolism, cell signalling and other vital cellular processes. Specifically, they are able to inhibit human and viral polymerases, different kinases, thymidylate synthase, DNA methyltransferase and many others (Pastor-Anglada et al. 1998; Jordheim et al. 2013). These structures are known as prodrugs – compounds that need to be activated into a cytotoxic state by metabolic processes in the cell, specifically by phosphorylation (Matsuda & Sasaki 2004).

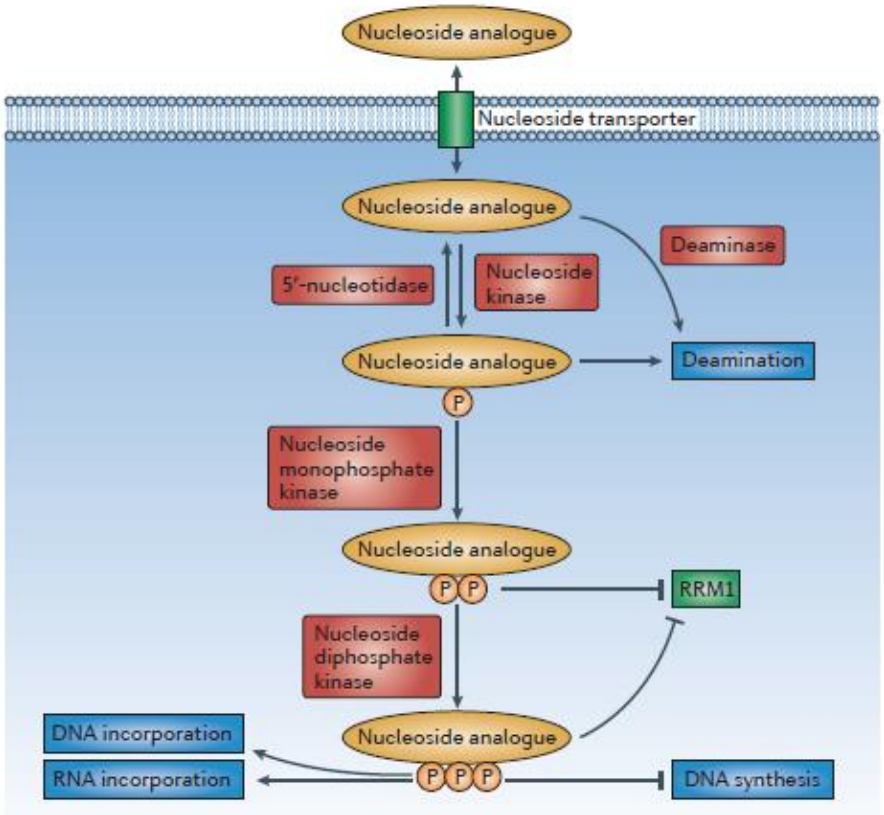

Fig. 22: Mechanism of action – Nucleoside analogues

Nucleoside analogues are actively transported through the cell membrane as a inactive pro-drug and undergo three phosphorylation steps (addition of one phosphate group) until they become therapeutically active, compete with their natural counterparts and incorporate into DNA/RNA. (Jordheim et al. 2013)

Except for cancer, these molecules are also known for their high antiviral activity, especially as anti-HIV agents (Xu et al. 2014), anti-HBV (Younger et al. 2004; Menéndez-Arias et al. 2014) and anti-HCV (Bobeck et al. 2010). Derivatives of nucleosides therefore represent active structures with extensive antiviral and antitumor activities. In common practice, derivatives of both, purine and pyrimidine analogues are used for the treatment of a wide range of malignancies. Compounds such as mercaptopurine, tioguanine and cladribine have been used as a treatment for acute lymphocytic and acute myeloblastic leukaemia. Gemcitabine, capecitabine and 5-

fluorouracil (Fig. 23), are mainly applied against colorectal, breast, lung, bladder, esophageal cancer (Klener 2010; Pałasz & Cieź 2015).

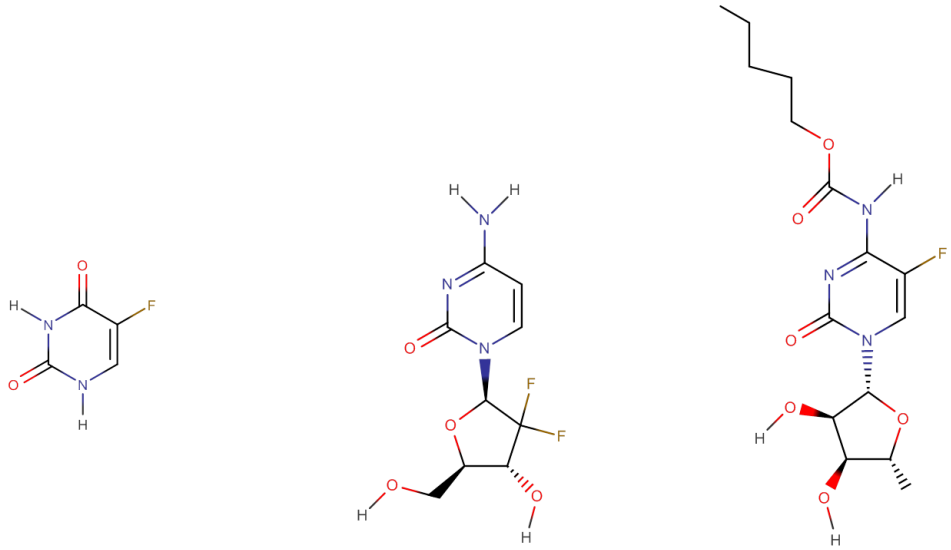

Fig. 23: Chemical structures of nucleosidic drugs (5-FU, Gemcitabine and Capecitabine).

However, increasing of drug-resistant forms of cancer urgently require new analogues with improved activities. For this reason, derivatives of deazapurine ribonucleosides have been prepared that evince nanomolar cytostatic activity towards different cancer cell lines (Bourderioux et al. 2011). Moreover, these compounds are potent antibacterial, antiviral and antiparasitic agents, acting mostly through adenosine kinase inhibitory activity. The addition of 6-alkyl-, 6-aryl- or 6-hetaryl- groups allowed synthesis of very potent structures specifically targeting adenosine kinase, both human and mycobacterial. Inhibition of Mtb ADK was observed at submicromolar and nanomolar concentration. That is in contrast with the observation in *in vitro* experiments, where IC50 values were usually higher than 30 μM. Intracellular activity assay was performed and this confirmed our findings. Significant differences between activity towards Mtb ADK and *in vitro* experiments might be caused by poor permeability of compounds through mycobacterial cell wall (Perlíková et al. 2013; Snášel et al. 2014).

2.3.1.1 Nucleosides with significant cytostatic activity

BOURDERIOUX, A. – NAUŠ, P. – PERLÍKOVÁ, P. – POHL, R. – PICHOVÁ, I. – VOTRUBA, I. – DŽUBÁK, P. – KONEČNÝ, P. – HAJDÚCH, M. – STRAY, K.M. – WANG, T. – RAY, A. S. – FENG, J.Y. – BIRKUS, G. – CIHLÁŘ, T. – HOCEK, M. (2011). Synthesis and Significant Cytostatic Activity of 7-Hetaryl-7-deazaadenosines. *Journal of Medicinal Chemistry* , vol. 2011, no. 54, s. 5498-2623

Journal of Medicinal Chemistry

ARTICLE

pubs.acs.org/jmc

Synthesis and Significant Cytostatic Activity of 7-Hetaryl-7-deazaadenosines

Aurelie Bourderioux,[†] Petr Nauš,[†] Pavla Perlíková,[†] Radek Pohl,[†] Iva Pichová,[†] Ivan Votruba,[†] Petr Džubák,[¶] Petr Konečný,[¶] Marián Hajdúch,[¶] Kirsten M. Stray,[‡] Ting Wang,[‡] Adrian S. Ray,[‡] Joy Y. Feng,[‡] Gabriel Birkus,[‡] Tomas Cihlar,[‡] and Michal Hocek*[,†]

[†]Institute of Organic Chemistry and Biochemistry, Academy of Sciences of the Czech Republic, Gilead Sciences & IOCB Research Center, Flemingovo nam. 2, CZ-16610 Prague 6, Czech Republic

[¶]Laboratory of Experimental Medicine, Institute of Molecular and Translational Medicine, Faculty of Medicine and Dentistry, Palacky University, Puškinova 6, Olomouc 77520, Czech Republic

[‡]Gilead Sciences, Inc., 333 Lakeside Drive, Foster City, California 94404, United States

Supporting Information

ABSTRACT: A series of 7-aryl- and 7-hetaryl-7-deazaadenosines were prepared by the cross-coupling reactions of unprotected or protected 7-iodo-7-deazaadenosines with (het)arylboronic acids, stannanes, or zinc halides. Nucleosides bearing 5-membered heterocycles at the position 7 exerted potent in vitro antiproliferative effects against a broad panel of hematological and solid tumor cell lines. Cell cycle analysis indicated profound inhibition of RNA synthesis and induction of apoptosis in treated cells. Intracellular conversion to triphosphates has been detected with active compounds. The triphosphate metabolites showed only a weak inhibitory effect on human RNA polymerase II, suggesting potentially other mechanisms for the inhibition of RNA synthesis and quick onset of apoptosis. Initial in vivo evaluation demonstrated an effect of 7-(2-thienyl)-7-deazaadenine ribonucleoside on the survival rate in syngeneic P388D1 mouse leukemia model.

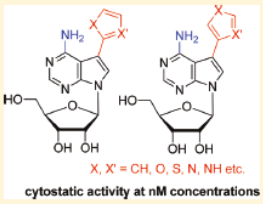

INTRODUCTION

Purine nucleosides and their analogues display a wide range of biological activities. Their antiviral and antitumor properties are particularly important. Many purine (fludarabine, cladribine, nelarabine, and clofarabine),[1] pyrimidine (gemcitabine, cytarabine, 5-fluoro deoxyuridine, capecitabine, and decitabine),[2] and other (e.g., 2-deoxycoformycin) nucleosides are clinically used for treatment of both solid and hematological malignancies. Despite extensive research over the last five decades, there still remains a space for the design of new purine nucleoside analogues and development of novel nucleoside-based anticancer therapeutics[3] for the treatment of drug-resistant tumors. In our previous works, we have reported on significant cytostatic effects of 6-(het)arylpurine nucleosides **1** (Chart 1).[4] Recently, we have discovered[5] 6-hetaryl-7-deazapurine ribonucleosides **2**−**4** with nanomolar cytostatic activities toward a wide panel of leukemia and cancer cell lines. The most active were derivatives bearing furyl or thienyl groups at the position 6 and either hydrogen or fluorine at position 7 of the 7-deazapurine. Surprisingly, their cyclo-Sal-phosphate and phosphoramidate prodrugs[6] were less active due to increased efflux from the cells.

7-Deazaadenosine (Tubercidin) is a natural cytostatic antibiotic.[7] Numerous studies[8] were devoted to the synthesis of diverse derivatives of Tubercidin and related natural nucleosides Toyocamycin and Sangivamycin. A variety of 7-substituted derivatives of **5** bearing halogens, carboxamides, or alkynes were prepared[9] and many of them exerted significant cytotoxic, antiparasitic, and antiviral activities mostly through inhibition of adenosine kinase. An important group of Tubercidin derivatives are 7-substituted 2′-C-methylribonucleosides that are selective inhibitors of HCV replication.[10] Although some 7-phenyltubercidin derivatives and analogues have been reported,[11] no systematic study of 7-aryl- and 7-hetaryl-7-deazaadenosines has been reported in the literature. Therefore, we report here on the synthesis and significant cytostatic activities of the title 7-hetaryl-7-deazaadenosines.

CHEMISTRY

The synthesis of the majority of the target 7-aryl- and 7-hetaryltubercidins **6** (Chart 1) was envisaged by the cross-coupling reactions of either unprotected 7-iodotubercidin[12] or its sugar-protected derivatives with the corresponding aryl- or hetaryl boronic acids. Whenever possible, we have employed the previously developed aqueous Suzuki−Miyaura cross-couplings[13] for the reactions of 7-iodotubercidin **7** with boronic acids in the presence of $Pd(OAc)_2$, TPPTS ligand, and Na_2CO_3 in acetonitrile/water. In this way, the desired 7-(het)aryl substituted 7-deazaadenosines **6a**−**n** were prepared in a single step mostly in good yields (Scheme 1).

Received: April 28, 2011
Published: June 29, 2011

Chart 1. Structures of Cytostatic 6-(Het)arylpurines 1 and -7-Deazapurine Ribonucleosides 2−4 and Tubercidin Derivatives 5

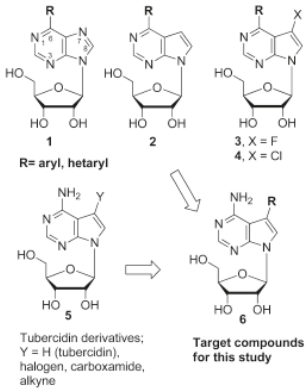

It should be noted that *N*-protecting group in both starting pyrrolyl boronic acids were removed under the conditions of coupling (products **6k** and **6l**). Because of low yield of 4-pyrazolyl derivative **6m** by Suzuki reaction, the compound was alternatively prepared by Stille reaction of 7-iodotubercidin **7** with 1-dimethylsulfamoyl-4-tributylstannylpyrazole[14] and subsequent removal of dimethylsulfamoyl group under acidic conditions (1 M aq HCl) in 68% overall yield after crystallization.

Ethynyl derivative **6o** was prepared by Sonogashira reaction of **7** (Scheme 2) with trimethylsilylacetylene and protodesilylation of TMS-ethynyl derivative **8** under basic conditions. Copper-catalyzed [3 + 2] cycloaddition[15] of ethynyl derivative **6o** with trimethylsilyl azide afforded triazolyl derivative **6p** in 24% yield.

Thiazolyl and imidazolyl derivatives **6q**−**s** were prepared by the Stille or Negishi cross-coupling reactions of per-*O*-silyl protected 7-iodotubercidin **9** (Scheme 3) with thiazolyl-stannane or *N*-protected imidazolyl zinc reagents[16] and subsequent acidic deprotections. It should be noted that attempted Stille cross-coupling of 2-(tributylstannyl)thiazole with *O*-unprotected 7-iodotubercidin **7** failed, presumably due to hydrolytic protodestannylation of organotin by ribose hydroxyl groups under the reaction conditions.

In addition, as standards for metabolism studies, we have prepared several nucleoside 5′-*O*-monophosphate (NMP) and nucleoside 5′-*O*-triphosphate (NTP) derivatives. The target 7-substituted-7-deazaadenosine 5′-*O*-triphosphates **10a,f**−**i** and 5′-*O*-monophosphates **11a,f**−**i** were synthesized by the aqueous Suzuki−Miyaura reactions[17] (Scheme 4) of 7-iodo-7-deazaadenosine 5′-*O*-triphosphate **12** and 5′-*O*-monophosphate **13** with the corresponding boronic acids. Starting 7-iodotubercidine triphosphate **12** and monophosphate **13** were prepared by convenient phosphorylation methods from 7-iodotubercidin **7**.

BIOLOGICAL PROFILING

Cytostatic Activity. Cytostatic activity of prepared compounds was initially evaluated against eight different cell lines derived from various human solid tumors including lung (A-549

Scheme 1

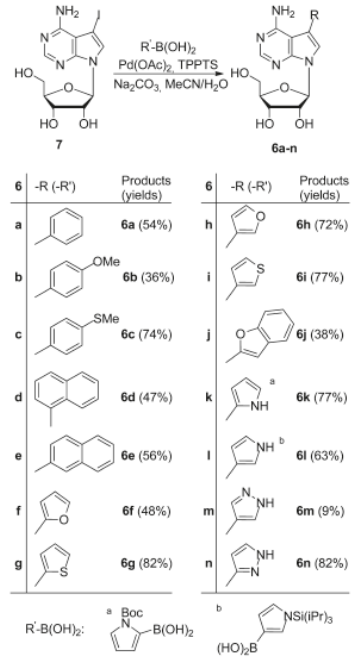

Scheme 2[a]

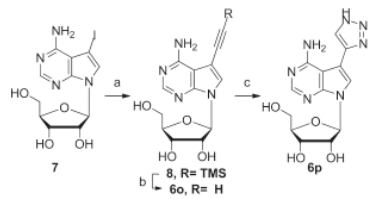

[a] Conditions: (a) trimethylsilylacetylene, $PdCl_2(PPh_3)_2$, CuI, NEt_3, DMF (100%); (b) K_2CO_3, MeOH (96%); (c) $TMSN_3$, CuI, DMF/MeOH (24%).

cells and NCI-H23), prostate (Du145 and PC3), colon (HCT116 and HCT15), and breast (Hs578 and BT549) carcinomas. Concentrations inhibiting the cell growth by 50% (GIC_{50}) were determined using a quantitative cellular staining with sulforhodamine B (SRB)[18] following a 5-day treatment. The SRB method allowed for a quantitative measurement of a net effect on cell growth by subtracting background signal generated by the cell culture inoculum at the beginning of treatment. In

Scheme 3

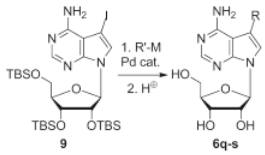

6	-R	R'-M	Products (yields)
q			**6q** (76%)
r			**6r** (77%)
s			**6s** (13%)

Scheme 4

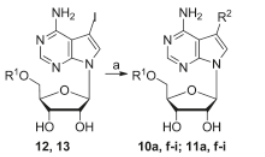

12, 10a, f-i R^1= 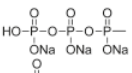

13, 11a, f-i R^1= 

10, 11	R^2	Products (yields)
a		**10a** (46%) **11a** (94%)
f		**10f** (27%) **11f** (34%)
g		**10g** (53%) **11g** (51%)
h		**10h** (37%) **11h** (45%)
i		**10i** (67%) **11i** (47%)

general, 7-substituted 7-deazaadenine nucleosides modified with a phenyl or naphthyl ring either with or without substitution (compounds **6a,c**−**e**) or bulky benzofuryl (**6j**) showed minimal to no cytostatic activity against the tested cell lines (Table 1). The only exception was 7-(4-methoxyphenyl)tubercidin **6b** that exerted submicromolar activities. In contrast, the nucleosides containing 5-member heterocyclic moiety at 7-position (**6f**−**6i**, **6k**−**6n**, and **6p**−**6s**) exhibited potent cytostatic effects (nanomolar GIC_{50}) over a wide range of the tested cell lines comparable to Tubercidin or Doxorubicin and better than Clofarabin. Interestingly, also 7-ethynyltubercidin **6o** exerted nanomolar cytostatic affect.

In addition, the antiproliferative effect of prepared compounds was tested against a human T-lymphoblastic leukemia line CCRF-CEM, promyelocytic leukemia HL-60, and cervical carcinoma HeLa S3 growing in liquid suspension. Cell viability was determined following a 3-day incubation using metabolic 2,3-bis-(2-methoxy-4-nitro-5-sulfophenyl)-2*H*-tetrazolium-5-carboxanilide (XTT) based method.[19] The average IC_{50} values for all compounds in the XTT-based assays were higher compared to the SRB-based assays, but the potency ranking followed similar trends as those observed in the SRB assays. Shorter duration of incubation during the XTT-based assay and/or different genetic background of the cells are likely the main reason for the lower activities.

All the nucleosides **6a**−**6s** were also tested for their inhibition of human adenosine kinase (ADK). Most of the compounds were only weak inhibitors with $IC_{50} > 5\,\mu M$. The exceptions were the 7-pyrazolyl- **6m** and 7-ethynyl- **6o** derivatives that showed IC_{50} in submicromolar range. Therefore, we can conclude that the strong cytostatic effect of this class of compounds is not due to the ADK inhibition.

In addition, selected five compounds, **6m**, **6i**, **6g**, **6h**, and **6l**, were subjected for expanded cytotoxic activity profiling against a panel of 26 human or rodent cancer cell lines (Table 2). The most potent (nanomolar) activity was confirmed against leukemia (K562, BV-173), including the drug resistant subline (CEM-DNR-Bulk), breast (BT-549 and MDA-MB 231), colon (HT-29 and HCT116), prostate (LNCaP), cervix (HeLa), leiomyosarcoma (MES-SA), and pancreatic (HPAC) cancers; the cytotoxic activities were comparable or slightly lower than gemcitabine and better than clofarabine. However, low potency was observed in neural (SK−N-As, C6 U-87 MG), androgen refractory, and p53 mutant prostate (PC-3), melanoma (SK-Mel-2), lung (NCi-H146), and ovarian (SK-OV-3) tumors. Importantly, the compounds **6m**, **6i**, **6g**, **6h**, and **6l** were generally noncytotoxic against normal human fibroblasts (BJ), demonstrating promising therapeutic index under in vitro conditions.

Metabolism and Cell-Cycle Studies. As one of the expected mode of action of the cytostatic nucleosides is the phosphorylation to NTPs, which downregulates the RNA synthesis through the inbibition of RNA polymerases, we have studied intracellular phosphorylation of nucleosides **6g** (active) and **6a** (inactive) in drug sensitive Du145 cells (Table 3). Both nucleosides are phosphorylated to the corresponding NMPs (**11g,a**) and NTPs (**10g,a**). Notably, the more active nucleoside **6g** is phosphorylated significantly better than the inactive one (**6a**) after 24 h. The first phosphorylation step to NMP appears to be significantly more efficient than the formation of triphosphate.

Further, four NTPs (**10f**−**10i**) derived from the corresponding strongly cytostatic nucleosides (**6f**−**6i**) were tested for the inhibition of human RNA polymerase II in a nuclear extract-based assay. The results indicated relatively low inhibition, with the IC_{50} values in the range of 54 to >400 μM (Table 4). Interestingly, Tubercidin triphosphate inhibited the RNA polymerase II with the efficiency similar to that of the other tested analogues. These data suggest that the direct inhibition of mRNA transcript synthesis by RNA polymerase II is unlikely to be the primary mode of action for tubercidine and its 7-substituted derivatives, although a possibility of stable internal incorporation into RNA with subsequent inhibition of translation should be addressed in future studies.

Table 1. Cytostatic, Cytotoxic, and ADK Inhibition Activities of Nucleosides 6a−6s

	GIC_{50} (μM)[a]									IC_{50} (μM)[b]			IC_{50} (μM)
compd	A549	NCIH23	Du145	PC3	HCT116	HCT15	HS578	BT549	MT-4	HL60	HeLa S3	CCRF-CEM	human ADK
6a	>20	>20	>20	>20	>20	>20	>20	>20	>20	>10	>10	>10	>5
6b	0.701	0.856	0.152	1.106	0.633	0.544	0.811	nd	4.3	>10	>10	>10	>2
6c	nd	0.39	1.87	nd	1.29	nd	1.97	nd	4.4	>10	>10	>10	>10
6d	nd	>10	>10	nd	>10	nd	>10	nd	nd	>10	>10	>10	>10
6e	nd	5.35	1.05	nd	5.67	nd	2.16	nd	nd	>10	>10	>10	>5
6f	0.035	0.294	0.019	0.004	0.048	0.003	0.017	nd	0.086	11.64	0.05	0.10	>2
6g	0.0070	0.0037	0.133	1.62	0.0026	0.011	0.012	nd	0.035	0.95	0.02	0.05	>5
6h	0.034	0.198	0.330	0.418	0.015	nd	0.021	0.028	0.170	9.06	0.02	0.07	>5
6i	0.016	0.073	0.097	1.323	0.007	nd	0.050	0.028	0.124	6.62	0.06	0.11	>5
6j	7.02	5.40	nd	6.29	3.74	nd	6.73	>10	4.8	>10	>10	3.95	>10
6k	0.1604	0.333	nd	0.0878	0.0652	nd	0.1129	0.1292	nd	2.04	1.04	0.16	
6l	0.0053	0.033	nd	0.0290	0.0059	nd	0.0044	0.0080	0.024	0.84	0.07	0.11	>5
6m	0.192	0.144	nd	0.014	0.970	nd	0.012	0.050	0.110	>25	0.22	0.56	0.05
6n	nd	0.035	nd	0.015	0.018	nd	0.008	nd	0.018	>20	0.69	0.13	>10
6o	nd	0.001	nd	0.011	0.002	nd	0.001	nd	0.001	0.09	0.02	0.01	0.2
6p	nd	0.004	nd	0.005	0.004	nd	0.003	nd	0.018	0.31	0.09	0.06	
6q	nd	0.005	nd	0.042	0.093	nd	0.015	nd	0.042	1.61	0.04	0.02	
6r	nd	0.002	nd	0.002	0.003	nd	0.002	nd	0.028	0.13	0.07	0.07	>10
6s	nd	0.006	nd	0.001	0.002	nd	0.001	nd	0.049	0.10	0.44	0.07	>5
Doxorubicin	0.016	0.005	nd	0.021	0.011	nd	0.006	0.010	nd				
Tubercidin	0.001	0.011	0.018	0.048	0.001	0.011	0.098	nd	0.021				
Clofarabin	0.086	0.040	0.125	0.063	0.106	0.180	1.241	0.065	0.051				

[a] Cytostatic activity (GIC_{50}) was determined by SRB assay following a 5-day incubation with tested compounds. Values represent means from two independent experiments. [b] Cytotoxic activity was determined by XTT assay following a 3-day incubation. Values represent means from four independent experiments.

Cell-cycle study of compound **6g** has been performed on CCRF-CEM lymphoblasts at 1× GIC_{50} and at 5× GIC_{50} concentrations within 12 h (Figure 1). At the higher concentration (5×GIC_{50}), the compound induces apoptosis within 4−8 h and at later times also accumulation of cells in G2/M phase was observed. The compound produces potent and fast onset of the inhibition of RNA synthesis at both concentrations, whereas the synthesis of DNA is inhibited only after longer incubations at high concentration. This indicates that the inhibition of DNA synthesis is likely a secondary effect, and the RNA synthesis is primary target of compound **6g**, although the direct inhibition of RNA polymerase II is unlikely to be involved (Table 4).

This study shows that the 7-hetaryltubercidins **6** are strongly cytostatic compounds that inhibit RNA synthesis and induce apoptosis. Although they are phosphorylated to NTPs, the activity is not due to inhibition of RNA polymerase II. Our future studies are scheduled to elucidate the detailed mechanisms of action of 7-hetaryl-7-deazaadenine nucleotides and their potential biological use.

Initial in Vivo Evaluation of Antitumor Activity in Mouse Model. To evaluate anticancer activity of **6g** under in vivo conditions, the P388D1 leukemia survival model was employed. The compound was dosed at maximum tolerated dose (MTD) and appoximately 0.5× MTD, corresponding to 75 and 35 mg/kg, respectively, in two cycles. Administration of **6g** prolonged mean survival time (MST), increased lifespan percentage (ILS), and significantly increased overall survival (Figure 2). These data warrant further more detailed exploration of compound **6g** in additional in vivo pharmacokinetics/pharmacodynamics and anticancer models.

CONCLUSIONS

7-Hetaryl-7-deazaadenine ribonucleosides (bearing 5-membered heterocycles at position 7) have been found to possess cytostatic effects at low nanomolar concentrations with the potency comparable to clofarabine. On the other hand, the corresponding 7-aryl-7-deazaadenine ribonucleosides were much less active. The compounds effectively inhibit RNA synthesis in treated cells and induce apoptosis at their cytotoxic concentrations. The molecular mechanism of this effect requires additional investigation. Thus far, our experiments detected the formation of intracellular triphosphate metabolites in treated cells and ruled out the inhibition of ADK and RNA polymerase II by parent nucleosides and corresponding triphosphates, respectively, as the major targets of the observed antiproliferative effects. Encouraging in vivo activity has been observed in the syngeneic mouse P388D1 leukemia model, warranting additional studies of the mechanism together with further characterization of the in vivo cytostatic activity and pharmacokinetics.

EXPERIMENTAL SECTION

General Methods. Melting points were determined on a Kofler block and are uncorrected. Optical rotations were measured at 25 °C, $[\alpha]_D^{20}$ values are given in 10^{-1} deg cm^2 g^{-1}. NMR spectra were measured at 400 MHz for ^{1}H and 100.6 MHz for ^{13}C nuclei, or at 500 MHz for ^{1}H and 125.8 MHz for ^{13}C, or at 600 MHz for ^{1}H and 151 MHz for ^{13}C in $CDCl_3$ (TMS was used as internal standard), MeOH-d_4 (referenced to the residual solvent signal), or DMSO-d_6 (referenced to the residual solvent signal). Chemical shifts are given in ppm (δ scale),

Table 2. Cytotoxic Activity Profiling of the Most Potent Compounds 6m, 6i, 6g, 6h, and 6l on Expanded Panel of Cancer Cell Lines and Normal Human Fibroblasts

	IC_{50}[a] (μM)								
	leukemia						breast		
compd	K562	K526-tax	BV-173	CEM-DNR-Bulk	L1210 (mouse)	EL4 (mouse)	MCF-7	BT-549	MDA-MB 231
6g	0.025	0.047	0.105	0.091	0.115	9.30	0.528	0.119	0.026
6h	0.200	0.147	0.068	0.364	0.445	>10	9.74	0.452	0.126
6i	0.067	0.093	0.029	0.110	0.199	>10	7.25	0.120	0.082
6l	0.033	0.009	0.004	0.008	0.084	9.42	6.31	0.006	0.027
6m	9.83	0.092	9.78	0.104	0.258	>10	>10	0.108	>10
Gemcitabine	0.718	0.006	0.001	0.022	0.007	0.007	0.149	0.008	0.245
Cladribine	7.69	0.170	0.0008	0.352	0.393	0.848	2.35	0.123	>10

	neural			colon			prostate		
	SK-N-As	U-87 MG	C6 (rat)	HT-29	HCT116	CT-26 (mouse)	PC-3	LNCaP	Mat-LyLu (rat)
6g	>10	>10	4.54	0.096	0.060	0.124	8.73	0.018	0.180
6h	>10	>10	>10	0.394	0.425	1.67	>10	0.112	1.86
6i	>10	>10	8.29	0.184	0.194	0.225	>10	0.068	0.525
6l	>10	>10	3.68	4.05	nd	0.017	>10	0.021	nd
6m	>10	>10	0.538	0.136	>10	0.396	>10	9.55	>10
Gemcitabine	1.10	1.49	0.504	1.53	nd	0.006	nd	0.512	nd
Cladribine	>10	>10	9.07	9.44	9.43	0.131	8.28	>10	nd

	others							
	NCi-H146 (lung)	MES-SA (leiomyo-sarcoma)	HeLa (cervix)	SK-OV-3 (ovary)	SK-Mel2 (mela-noma)	HPAC (pan-creas)	P388D1 (mouse)	BJ (fibro-blasts)
6g	>10	0.232	0.033	>10	1.98	0.070	0.028	9.85
6h	>10	1.33	0.350	>10	>10	0.133	0.139	>10
6i	>10	0.076	0.124	>10	>10	0.110	0.076	>10
6l	>10	0.081	0.040	>10	8.71	0.068	0.010	6.09
6m	>10	7.74	0.185	>10	>10	0.141	0.093	>10
Gemcitabine	2.78	0.005	4.12	>10	7.11	0.073	0.019	9.88
Cladribine	>10	0.165	>10	>10	>10	9.32	0.285	>10

[a] Cytotoxic activity was determined by MTT assay following a 3-day incubation. Values represent means from four independent experiments.

Table 3. Intracellular Phosphorylation of Nucleosides 6g and 6a

	dosing					
	6 h (pmol/million)			24 h (pmol/million)		
compd	nucleoside	NMP (11)	NTP (10)	nucleoside	NMP (11)	NTP (10)
6g	4.66	5.04	0.53	30.4	64.0	1.96
6a	32.91	6.23	0.13	68.8	6.68	0.27

Table 4. Inhibition of RNA Pol II by NTPs 10f–10i

entry	compd	IC_{50} (μM)
1	**10f**	148
2	**10g**	54
3	**10h**	>400
4	**10i**	91
5	Tubercidin triphosphate	93
6	α-amanitin	2.2 ng/mL

coupling constants (J) in Hz. Complete assignment of all NMR signals was performed using a combination of H,H-COSY, H,H-ROESY, H,C-HSQC, and H,C-HMBC experiments. High resolution mass spectra were measured using electrospray ionization. Reverse phase high performance flash chromatography (HPFC) purifications were performed with Biotage SP1 apparatus on with KP-C18-HS columns. All final free nucleosides for testing were >95% pure as determined by combustion analysis. Synthetic procedures and characterization data of compounds **6b–e**, **6g–s**, **12**, **10f–i**, and **11f–i** are given in the Supporting Information.

*4-Amino-5-phenyl-7-(β-D-ribofuranosyl)-7H-pyrrolo[2,3-d]pyrimidine (**6a**).* An argon purged mixture of 7-iodotubercidin [7][12] (200 mg, 0.51 mmol), phenylboronic acid (93 mg, 0.76 mmol), Na_2CO_3 (502 mg, 4.74 mmol), $Pd(OAc)_2$ (6.6 mg, 0.029 mmol), and TPPTS (42 mg, 0.07 mmol) in water/MeCN (2:1, 3.6 mL) was stirred at 100 °C for 1 h. After cooling, the mixture was neutralized by the addition of

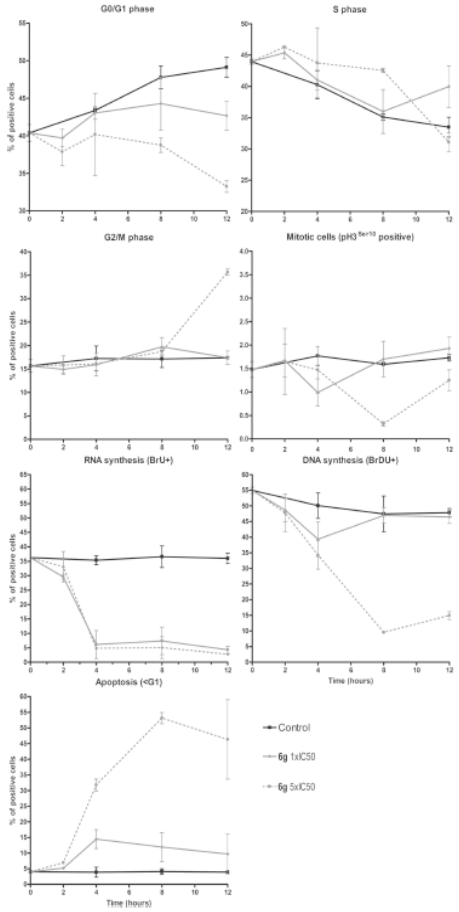

Figure 1. Effects of compound **6g** on cell cycle, apoptosis, and DNA/RNA synthesis in CCRF-CEM lymphoblasts.

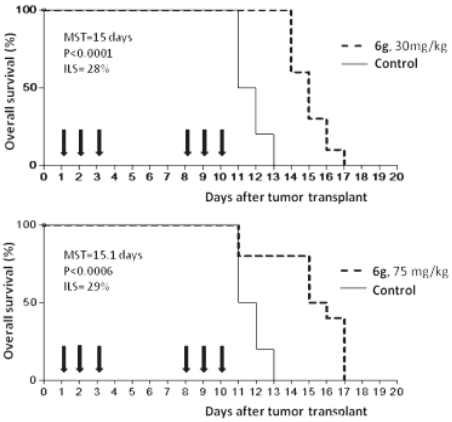

Figure 2. In vivo antitumor activity of the compound **6g** in P388D1 syngeneic tumor model is demonstrated by prolonged MST, ILS and significant increase of overall survival when administered at MTD or 1/2MTD. Arrows indicate administration of active molecule or vehicle in control animals.

aqueous HCl (1M), volatiles were removed in vacuo and the residue was purified by reverse phase chromatography (0→100% MeOH in water), affording title compound **6a** as white solid (94 mg, 54%); mp 119 °C; $[\alpha]^{20}_D$ −49.8 (*c* 0.301, MeOH). UV (MeOH): λ_{max} (ε) 282 (12900). ^{1}H NMR (600 MHz, DMSO-d_6): 3.53 (ddd, 1H, J_{gem} = 11.9, $J_{5'b,OH}$ = 6.1, $J_{5'b,4'}$ = 3.9, H-5′b), 3.63 (ddd, 1H, J_{gem} = 11.9, $J_{5'a,OH}$ = 5.2, $J_{5'a,4'}$ = 3.4, H-5′a), 3.90 (ddd, 1H, $J_{4',5'}$ = 3.9, 3.4, $J_{4',3'}$ = 3.5, H-4′), 4.10 (bm, 1H, H-3′), 4.46 (bm, 1H, H-2′), 5.16 (d, 1H, $J_{OH,3'}$ = 3.5, OH-3′), 5.22 (dd, 1H, $J_{OH,5'}$ = 6.1, 5.2, OH-5′), 5.36 (d, 1H, $J_{OH,2'}$ = 4.8, OH-2′), 6.12 (d, 1H, $J_{1',2'}$ = 6.3, H-1′), 7.37 (m, 1H, H-*p*-Ph), 7.47 (m, 2H, H-*o*-Ph), 7.49 (m, 2H, H-*m*-Ph), 7.54 (s, 1H, H-6), 8.15 (s, 1H, H-2). ^{13}C NMR (151 MHz, DMSO-d_6): 61.93 (CH_2-5′), 70.89 (CH-3′), 74.05 (CH-2′), 85.38 (CH-4′), 87.27 (CH-1′), 100.73 (C-4a), 116.57 (C-5), 121.41 (CH-6), 127.20 (CH-*p*-Ph), 128.70 (CH-*o*-Ph), 129.28 (CH-*m*-Ph), 134.71 (C-*i*-Ph), 151.10 (C-7a), 151.95 (CH-2), 157.57 (C-4). MS (FAB) *m*/*z* 343 (M + H), 365 (M + Na). HRMS (FAB) for $C_{17}H_{19}N_4O_4$ [M + H] calcd, 343.1406; found, 343.1409. Anal. ($C_{17}H_{18}N_4O_4 \cdot 0.8H_2O$): C, H, N.

4-Amino-5-(furan-2-yl)-7-(β-D-ribofuranosyl)-7H-pyrrolo[2,3-d]-pyrimidine (**6f**). Compound **6f** was prepared as described for **6a** from compound **7** and furan-2-boronic acid; yield 48%; tan solid after recrystallization from MeOH; mp 118 °C; $[\alpha]^{20}_D$ −52.5 (*c* 0.287, MeOH). UV (MeOH): λ_{max} (ε) 288 (13200), 258 (12500). ^{1}H NMR (500 MHz, DMSO-d_6): 3.55 and 3.65 (2 × dd, 2H, J_{gem} = 11.9, $J_{5',4'}$ = 3.9, H-5′), 3.91 (td, 1H, $J_{4',5'}$ = 3.9, $J_{4',3'}$ = 3.4, H-4′), 4.11 (dd, 1H, $J_{3',2'}$ = 5.2, $J_{3',4'}$ = 3.4, H-3′), 4.41 (dd, 1H, $J_{2',1'}$ = 6.1, $J_{2',3'}$ = 5.2, H-2′), 5.00−5.50 (bs, 2H, OH-2′,3′,5′), 6.09 (d, 1H, $J_{1',2'}$ = 6.1, H-1′), 6.61 (dd, 1H, $J_{4,3}$ = 3.3, $J_{4,5}$ = 1.9, H-4-furyl), 6.67 (dd, 1H, $J_{3,4}$ = 3.3, $J_{3,5}$ = 0.8, H-3-furyl), 6.88 (bs, 2H, NH_2), 7.78 (dd, 1H, $J_{5,4}$ = 1.9, $J_{5,3}$ = 0.8, H-5-furyl), 7.83 (s, 1H, H-6), 8.13 (s, 1H, H-2). ^{13}C NMR (125.7 MHz, DMSO-d_6): 61.81 (CH_2-5′), 70.67 (CH-3′), 74.00 (CH-2′), 85.33 (CH-4′), 87.27 (CH-1′), 99.55 (C-4a), 105.50 (CH-3-furyl), 106.34 (C-5), 112.09 (CH-4-furyl), 120.70 (CH-6), 142.16 (CH-5-furyl), 148.77 (C-2-furyl), 151.04 (C-7a), 152.26 (CH-2), 157.45 (C-4). MS (FAB): *m*/*z* 333 (M + H), 355 (M + Na). HRMS (FAB) for $C_{15}H_{17}N_4O_5$ [M + H] calcd, 333.1199; found, 333.1202. Anal. ($C_{15}H_{16}N_4O_5 \cdot H_2O$): C, H, N.

4-Amino-5-phenyl-7-(β-D-ribofuranosyl)-7H-pyrrolo[2,3-d]pyrimidine 5′-O-triphosphate Sodium Salt (**10a**). An argon purged mixture of $Pd(OAc)_2$ (1.5 mg, 6.7 μmol) and TPPTS (17.3 mg, 30 μmol) in water/MeCN (2:1, 1.2 mL) was sonicated to full dissolution, and one-quarter of this preprepared solution (0.3 mL, 1/4 of total amount) was added to an argon purged mixture of compound **12** (20.1 mg, 29 μmol), phenylboronic acid (5.3 mg, 43 μmol), and Cs_2CO_3 (28 mg, 87 μmol) in water/MeCN (2:1, 0.6 mL), and the mixture was stirred at 100 °C for 30 min. After cooling, the mixture was filtered through microfilter and purified by HPLC on C-18 phase (0→100% MeOH in 0.1 M aq TEAB) affording after ion exchange on Dowex 50 (Na^+ form) and lyophilization title compound **10a** as white cotton (8.6 mg, 46%). ^{1}H NMR (500 MHz, D_2O + phosphate buffer, pH = 7.1, $ref_{dioxane}$ = 3.75 ppm): 4.14 (ddd, 1H, J_{gem} = 11.6, $J_{H,P}$ = 4.7, $J_{5'b4'}$ = 3.5, H-5′b), 4.25 (ddd, 1H, J_{gem} = 11.6, $J_{H,P}$ = 6.5, $J_{5'a,4'}$ = 3.3, H-5′a), 4.35 (m, 1H, $J_{4',5'}$ = 3.5, 3.3, $J_{4',3'}$ = 2.9,

$J_{H,P}$ = 1.7, H-4′), 4.57 (dd, 1H, $J_{3',2'}$ = 5.4, $J_{3',4'}$ = 2.9, H-3′), 4.73 (dd, 1H, $J_{2',1'}$ = 6.9, $J_{2',3'}$ = 5.4, H-2′), 6.30 (d, 1H, $J_{1'2'}$ = 6.9, H-1′), 7.45 (m, 1H, H-*p*-Ph), 7.49−7.56 (m, 4H, H-*o*,*m*-Ph), 7.57 (s, 1H, H-6), 8.16 (s, 1H, H-2). ^{13}C NMR (125.7 MHz, D_2O + phosphate buffer, pH = 7.1, $ref_{dioxane}$ = 69.3 ppm): 68.22 (d, $J_{C,P}$ = 5, CH_2-5′), 73.26 (CH-3′), 76.24 (CH-2′), 86.31 (d, $J_{C,P}$ = 9, CH-4′), 88.34 (CH-1′), 103.75 (C-4a), 121.56 (C-5), 122.86 (CH-6), 130.41 (CH-*p*-Ph), 131.59 and 131.94 (CH-*o*,*m*-Ph), 136.10 (C-*i*-Ph), 153.15 (C-7a), 153.67 (CH-2), 159.61 (C-4). ^{31}P (^{1}H dec) NMR (202.4 MHz, D_2O + phosphate buffer, pH = 7.1, ref_{H3PO4} = 0 ppm): −21.32 (dd, J = 19.3, 19.0, P_β), −10.45 (d, J = 19.3, P_α), −6.98 (d, J = 19.0, P_γ). MS (ESI, negative mode) m/z 581 (M-3Na + 2H), 603 (M-2Na + H), 625 (M-Na). HRMS (ESI, negative mode)$^-$ for $C_{17}H_{20}N_4O_{13}P_3$ [M-3Na + 2H] calcd, 581.0240; found, 581.0253.

*4-Amino-5-phenyl-7-(β-D-ribofuranosyl)-7H-pyrrolo[2,3-d]pyrimidine 5′-O-monophosphate Sodium Salt (**11a**).* An argon purged mixture of $Pd(OAc)_2$ (1.7 mg, 7.6 μmol) and TPPTS (21.7 mg, 38 μmol) in water/MeCN (2:1, 1.6 mL) was sonicated until dissolution, and one-quarter of resulting solution (0.4 mL, 1/4 of total amount, 1.9 μmol Pd) was added to an argon purged mixture of compound **13** (21 mg, 38 μmol), phenylboronic acid (6.9 mg, 57 μmol), and Na_2CO_3 (12 mg, 114 μmol) in water/MeCN (2:1, 0.8 mL), and the mixture was stirred at 100 °C for 1.5 h. After cooling, the mixture was filtered through microfilter and purified by HPLC on C-18 phase (0→100% MeOH in 0.1 M aq TEAB), affording after ion exchange on Dowex 50 (Na^+ form) and lyophilization title compound **11a** as white solid (15.8 mg, 94%). ^{1}H NMR (500 MHz, D_2O, $ref_{dioxane}$ = 3.75 ppm): 3.91 (dt, 1H, J_{gem} = 11.4, $J_{H,P}$ = $J_{5'b,4'}$ = 4.4, H-5′b), 3.95 (ddd, 1H, J_{gem} = 11.4, $J_{H,P}$ = 5.6, $J_{5'a,4'}$ = 4.2, H-5′a), 4.30 (ddd, 1H, $J_{4',5'}$ = 4.4, 4.2, $J_{4',3'}$ = 2.7, H-4′), 4.46 (dd, 1H, $J_{3',2'}$ = 5.4, $J_{3',4'}$ = 2.7, H-3′), 4.75 (dd, 1H, $J_{2',1'}$ = 7.1, $J_{2',3'}$ = 5.4, H-2′), 6.31 (d, 1H, $J_{1'2'}$ = 7.1, H-1′), 7.46 (m, 1H, H-*p*-Ph), 7.54 (m, 2H, H-*m*-Ph), 7.56 (m, 2H, H-*o*-Ph), 7.58 (s, 1H, H-6), 8.18 (s, 1H, H-2). ^{13}C NMR (125.7 MHz, D_2O, $ref_{dioxane}$ = 69.3 ppm): 66.53 (d, $J_{C,P}$ = 5, CH_2-5′), 73.61 (CH-3′), 76.15 (CH-2′), 86.94 (d, $J_{C,P}$ = 9, CH-4′), 88.22 (CH-1′), 103.97 (C-4a), 121.38 (C-5), 122.79 (CH-6), 130.44 (CH-*p*-Ph), 131.72 (CH-*o*-Ph), 131.91 (CH-*m*-Ph), 136.31 (C-*i*-Ph), 153.35 (C-7a), 154.40 (CH-2), 160.15 (C-4). ^{31}P (^{1}H dec) NMR (202.4 MHz, D_2O, ref_{H3PO4} = 0 ppm): 4.64. MS (ESI) m/z 445 (M + H), 467 (M + Na). HRMS (ESI) for $C_{17}H_{19}N_4NaO_7P$: [M + H] calcd, 445.0884; found, 445.0880.

Biology. *Cytostatic Activity Assays.* All cell lines were obtained from ATCC (Manassas, VA). Colon (HCT116, HCT 15), breast (BT549, HS 578), lung (A549, NCI-H23), and T-lymphoblastic (CCRF-CEM) cell lines were maintained in the RPMI cultivation medium (Invitrogen, Carlsbad, CA) supplemented with 10% fetal bovine serum (FBS). Prostate cell lines (Du145, PC3) were cultivated in MEM/F12K medium containing 10% FBS, respectively. Doxorubicin, clofarabine, trichloroacetic acid (TCA), and sulforhodamine B (SRB) were from Sigma-Aldrich (St. Louis, MO). Gemcitabine was obtained from Moravek Biochemicals (Brea, CA)

A modified protocol of sulforhodamine B colorimetric assay was used for the cytostatic activity screening.[18] Cells were distributed into the 96-well plates in 150 μL of media (HCT116 and Du145 5300 cell/mL, HCT15 and A549 10600cells/mL, Hs578 and BT549 26600 cells/mL, PC3 16600 cells/mL, NCI-H23 40000 cells/mL) and incubated overnight in humidified CO_2 incubator at 37 °C. Next day, one plate of each cell line was fixed with TCA by removing media and adding 100 μL of cold 10% (v/v) TCA to each well. After 1 h incubation at 4 °C, TCA was discarded and plates were washed four times with tap water. These plates represented cell counts at day zero. The tested compounds were 5-fold serially diluted and distributed to cells in 50 μL of media. After five days of incubation, the plates were fixed with TCA as mentioned above and 100 μL of 0.057% SRB solution in 1% (v/v) acetic acid was added to each well. After 30 min incubation at room temperature, SRB was removed and the plates were rinsed four times 1% (v/v) acetic acid. Next, 200 μL of 10 mM Tris base solution (pH 10.5) was added to each well of completely dried plates and absorbance of cell associated SRB was read at 500 nm. The percentage of cell-growth inhibition was calculated using the following formula: % of control cell growth = 100 × (OD_{sample} − mean OD_{day0})/($OD_{neg\ control}$ − mean OD_{day0}). For GIC_{50} determination, dose−response curves between the compound concentration and percent of growth inhibition were plotted. GIC_{50} values can be derived by fitting dose−response curves using a sigmoidal dose−response equation.

Cytotoxic 3-(4,5-Dimethylthiazol-2-yl)-2,5-diphenyltetrazolium Bromide (MTT) Assay[20]. The most cytostatic compounds were further tested in cytotoxic MTT assay on extended cancer cell line panel. All cells were purchased from the ATCC (Manassas, VA), unless otherwise indicated. The daunorubicin resistant subline of CEM cells (CEM-DNR bulk) and paclitaxel resistant subline K562-tax were selected in our laboratory by the cultivation of maternal cell lines in increasing concentrations of daunorubicine or paclitaxel, respectively.[21] The cells were cultured in DMEM/RPMI 1640 with 5 g/L glucose, 2 mM glutamine, 100 U/mL penicillin, 100 μg/mL streptomycin, 10% fetal calf serum, and $NaHCO_3$.

Cell suspensions were prepared and diluted according to the particular cell type and the expected target cell density (2500−30000 cells/well based on cell growth characteristics). Cells were added by pipet (80 μL) into 96-well microtiter plates. Inoculates were allowed a preincubation period of 24 h at 37 °C and 5% CO_2 for stabilization. Four-fold dilutions, in 20 μL aliquots, of the intended test concentration were added to the microtiter plate wells at time zero. All test compound concentrations were examined in duplicate. Incubation of the cells with the test compounds lasted for 72 h at 37 °C, in a 5% CO_2 atmosphere at 100% humidity. At the end of the incubation period, the cells were assayed using MTT. Aliquots (10 μL) of the MTT stock solution were pipetted into each well and incubated for a further 1−4 h. After this incubation period, the formazan produced was dissolved by the addition of 100 μL/well of 10% aq SDS (pH = 5.5), followed by a further incubation at 37 °C overnight. The optical density (OD) was measured at 540 nm with a microplate reader. Tumour cell survival (IC_{50}) was calculated using the following equation: IC = ($OD_{drug\text{-}exposed\ well}$/mean $OD_{control\ wells}$) × 100%. The IC_{50} value, the drug concentration lethal to 50% of the tumor cells, was calculated from appropriate dose−response curves.

Human ADK Inhibition[6]. The standard reaction mixture (50 μL) contained 50 mM HEPES pH 6.2, 10 mM KCl, 1 mM $MgCl_2$, 1 mM ATP, 80 μg BSA, 1 μCi of [^{3}H]-adenosine (20 Ci/mmol), 1 μM unlabeled adenosine, various concentration of tested compounds, and 0.94 ng of adenosine kinase. The mixtures were incubated at 37 °C and separated on PEI cellulose plate (prespotted with 0.01 AMP). The plates were developed in the solvent system 2-propanol−NH_4OH−water (7:1:2). The spots were visualized under UV light (254 nm) and cut out for radioactivity determination in the toluene-based scintillation cocktail.

Intracellular Metabolism. Du145 cells were seeded into T25 flasks at 60% confluence in the MEM medium supplemented with 10% FBS. Next day, the medium was replaced with fresh media containing the tested compounds at 10 μM concentration. After 6 and 24 h of incubation, cells were washed with phosphate buffer and detached with trypsin. Trypsin was neutralized by adding cultivation medium, and the cells were spun for 5 min at 500g. The supernatants were removed, and cell pellets were resuspended in 0.5 mL of media. Cell suspension was layered onto 0.25 mL of Nyosil M25 oil and centrifuged for 3 min. The media was aspirated off, and the top of the oil layer was washed with water. Both water and oil were aspirated off without disturbing the cell pellet. The cells were extracted with 500 μL of 70% MeOH, and cell lysates were centrifuged, supernatants collected, dried by vacuum, and samples were resuspended in 1 mM Ammonium phosphate pH 8.5.

Transient ion-pairing high-performance liquid chromatography using dimethylhexylamine coupled to positive ion electrospray tandem mass spectrometery (LC/MS/MS) was used to quantitate intracellular nucleotides.[22] Standard curves and quality control samples were generated for all analytes using extracts from untreated cells. Methods were adapted from those described for the acyclic phosphonate nucleotide analogue adefovir, its phosphorylated metabolites, and natural nucleotides.[23]

RNA Polymerase II Inhibition Assay. The assay was performed using a HeLaScribe nuclear extract (Promega). The reaction mixture (25 μL) contained 7.5 μL 1× HeLaScribe transcription buffer, 3 mM $MgCl_2$, 100 ng CMV(+) control DNA, 400 μM CTP, GTP, UTP, and 25 μM [^{33}P]ATP. The mixture was preincubated with various concentrations of the inhibitor for 5 min at 30 °C, followed by the addition of 3.5 μL of HeLaScribe nuclear extract. After 1 h incubation at 30 °C, the polymerase reaction was stopped by adding Proteinase K, SDS, and EDTA. After additional incubation at 37 °C for 3 h and denaturation at 75 °C, the reaction mixture was separated on 6% polyacrylamide gel with 8 M urea. The full-length product of transcription was quantified using Typhoon Trio imager and Image Quant TL software (GE Healthcare), and the IC_{50} value was defined as the concentration of inhibitor at which a 50% decrease in the product formation was observed.

Cell Cycle and Apoptosis Analysis. Subconfluent CCRF-CEM cells (ATCC), seeded at the density of 5×10^5 cells/ml in 6-well panels, were cultivated with the 1× or 5× GIC_{50} of tested compounds in a humidified CO_2 incubator at 37 °C in RPMI 1640 cell culture medium containing 10% fetal calf serum, 10 mM glutamine, 100 U/mL penicillin, and 100 μg/mL streptomycin. Controls containing vehicle were harvested at the same time points (2−24 h). Cells were washed with cold PBS and fixed in 70% ethanol overnight at −20 °C. The next day, the cells were washed in hypotonic citrate buffer, treated with RNase (50 μg/mL), stained with propidium iodide, and analyzed by flow cytometry using a 488 nm single beam laser (Becton Dickinson). Cell cycle was analyzed in the program ModFitLT (Verity), and apoptosis was measured in logarithmic mode as a percentage of the particles with propidium content lower than cells in G0/G1 phase (sub-G1) of the cell cycle. Half of the sample was used for phospho-histon $H3^{Ser10}$ antibody (Sigma) labeling and subsequent flow cytometry analysis of mitotic cells.[24]

BrdU Incorporation Analysis. Cells were cultured as for cell cycle analysis. Before harvesting, they were pulse-labeled with 10 μM 5-bromo-2′-deoxyuridine (BrdU) for 30 min. The cells were trypsinized, fixed with ice-cold 70% ethanol, incubated on ice for 30 min, washed with PBS, and resuspended in 2 M HCl for 30 min at room temperature to denature their DNA. Following neutralization with 0.1 M $Na_2B_4O_7$, the cells were washed with PBS containing 0.5% Tween-20 and 1% BSA. They were then stained with primary anti-BrdU antibody (Exbio) for 30 min at room temperature in the dark. Cells were than washed with PBS and stained with secondary antimouse-FITC antipody (Sigma). The cells were then washed with PBS and incubated with propidium iodide (0.1 mg/mL) and RNase A (0.5 mg/mL) for 1 h at room temperature in the dark and finally analyzed by flow cytometry using a 488 nm single beam laser (FACSCalibur, Becton Dickinson).[25]

BrU Incorporation Analysis. Cells were cultured as for cell cycle analysis. Before harvesting, they were pulse-labeled with 1 mM 5-bromouridine (BrU) for 30 min. The cells were fixed in 1% buffered paraformaldehyde with 0.05% of NP-40, incubated in room temperature for 15 min, and then in the refridgerator overnight. They were then washed in 1% glycin in PBS, washed in PBS, and stained with primary anti-BrdU antibody crossreacting to BrU (Exbio) for 30 min at room temperature in the dark. Cells were than washed with PBS and stained with secondary antimouse-FITC antibody (Sigma). Following the staining, the cells were washed with PBS and fixed with 1% PBS buffered paraformaldehyde with 0.05% of NP-40. The cells were then washed with PBS, incubated with propidium iodide (0.1 mg/mL) and RNase A (0.5 mg/mL) for 1 h at room temperature in the dark, and finally analyzed by flow cytometry using a 488 nm single beam laser (FACSCalibur, Becton Dickinson).[25]

In Vivo Activity in P388D1 Leukemia Model. The P388D1 mouse leukemia cells were obtained from ATCC (Manassas, VA) and grown in the RPMI cultivation medium (Sigma Aldrich, Prague, Czech Republic) supplemented with 10% fetal bovine serum. DBA/2 mice were obtained from Charles River Laboratories (Sulzfeld, Germany) and maintained in specific pathogen free facility. Then 10^5 of P388D1 leukemia cells per mice were transplanted intraperitoneally on day 0 to 18−22 g female mice, and animals were randomized into control and treatment groups (10 mice per group). The testing regiment included administering **6g** once a day intraperitoneally dissolved in 50% solution of PEG400/deionized water (pH 7.0) in two cycles on day 1−3 and 8−10. Animals were treated at MTD and 1/2 MTD (70 and 35 mg/kg of **6g**, respectively), and control mice received volume equivalent of the vehicle. Animal weights and deaths were recorded daily. Survival parameters (MST and percentage of ILS) were calculated. Kaplan−Meier survival curves were constructed and the significant difference in overall survival (control versus treatment groups) was evaluated by log-rank test (Figure 2).

■ ASSOCIATED CONTENT

Supporting Information. Synthetic procedures and characterization data of compounds **6b**−**e**, **6i**−**n**, **10h,i**, and **11h,i** and analytical characterization data for the final nucleosides. This material is available free of charge via the Internet at http://pubs.acs.org.

■ AUTHOR INFORMATION

Corresponding Author

*To whom the correspondence should be addressed: Phone: +420 220183324. Fax: +420 220183559. E-mail: hocek@uochb.cas.cz.

■ ACKNOWLEDGMENT

This work is a part of the research project Z4 055 0506 from the Academy of Sciences of the Czech Republic. It was supported by the Ministry of Education, Youth and Sports (grant 1M0508 and LC07017), by the Czech Science Foundation (P207/11/0344), and by Gilead Sciences, Inc. Infrastructural part of this project (Institute of Molecular and Translational Medicine) was supported from the Operational Programme Research and Development for Innovations (project CZ.1.05/2.1.00/01.0030).

■ ABBREVIATIONS USED

ADK, adenosine kinase; BrdU, 5-bromo-2′-deoxyuridine; BrU, 5-bromouridine; HPFC, high performance flash chromatography; ILS, increased lifespan percentage; MTD, maximum tolerated dose; MST, mean survival time; MTT, 3-(4,5-dimethylthiazol-2-yl)-2,5-diphenyltetrazolium bromide; NMP, nucleoside 5′-*O*-monophosphate; NTP, nucleoside 5′-*O*-triphosphate; SRB, sulforhodamine B; TCA, trichloroacetic acid; TDA-1, tris(2-(2-methoxyethoxy)ethyl)amine; TMS, trimethylsilyl; TPPTS, tris(3-sulfonatophenyl)phosphine; XTT, 2,3-bis-(2-methoxy-4-nitro-5-sulfophenyl)-2H-tetrazolium-5-carboxanilide

■ REFERENCES

(1) Johnson, S. A.; Thomas, W. Therapeutic potential of purine analogue combinations in the treatment of lymphoid malignancies. *Hematol. Oncol.* **2000**, *18*, 141–153. (b) Johnson, S. A. Nucleoside

analogues in the treatment of haematological malignancies. *Expert Opin. Pharmacother.* **2001**, *2*, 929–943. (c) Parker, W. B.; Secrist, J. A., III; Waud, W. R. Purine nucleoside antimetabolites in development for the treatment of cancer. *Curr. Opin. Invest. Drugs* **2004**, *5*, 592–596.

(2) (a) Galmarini, C. M.; Mackey, J. R.; Dumontet, C. Nucleoside analogues and nucleobases in cancer treatment. *Lancet Oncol.* **2002**, *3*, 415–242. (b) Galmarini, C. M.; Popowycz, F.; Joseph, B. Cytotoxic nucleoside analogues: different strategies to improve their clinical afficacy. *Curr. Med. Chem.* **2008**, *15*, 1072–1082.

(3) (a) Robins, R. K.; Revankar, G. R. Purine analogs and related nucleosides and nucleotides as antitumor agents. *Med. Res. Rev.* **1985**, *5*, 273–296. (b) Plunkett, W.; Saunders, P. P. Metabolism and action of purine nucleoside analogs. *Pharmacol. Ther.* **1991**, *49*, 239–268. (c) Robak, T.; Korycka, A.; Kasznicki, M.; Wrzesien-Kus, A.; Smolewski, P. Purine nucleoside analogues for the treatment of hematological malignancies: pharmacology and clinical applications. *Curr. Cancer Drug Targets* **2005**, *5*, 421–444. (d) Jordheim, L.; Galmarini, C. M.; Dumontet, C. Drug resistance to cytotoxic nucleoside analogues. *Curr. Drug Targets* **2003**, *4*, 443–460. (e) Jordheim, L. P.; Galmarini, C. M.; Dumontet, C. Recent developments to improve the efficacy of cytotoxic nucleoside analogues. *Recent Patents Anti-Cancer Drug Discovery* **2006**, *1*, 163–170. (f) Parker, W. B. Enzymology of Purine and Pyrimidine Antimetabolites Used in the Treatment of Cancer. *Chem. Rev.* **2009**, *109*, 2880–2893.

(4) (a) Hocek, M.; Holý, A.; Votruba, I.; Dvořáková, H. Synthesis and Cytostatic Activity of Substituted 6-Phenylpurine Bases and Nucleosides: Application of the Suzuki−Miyaura Cross-Coupling Reactions of 6-Chloropurine Derivatives with Phenylboronic Acids. *J. Med. Chem.* **2000**, *43*, 1817–1825. (b) Hocek, M.; Holý, A.; Votruba, I.; Dvořáková, H. Cytostatic 6-arylpurine nucleosides III. Synthesis and structure−activity relationship study in cytostatic activity of 6-aryl-, 6-hetaryl- and 6-benzylpurine ribonucleosides. *Collect. Czech. Chem. Commun.* **2001**, *66*, 483–499. (c) Hocek, M.; Nauš, P.; Pohl, R.; Votruba, I.; Furman, P. A.; Tharnish, P. M.; Otto, M. J. Cytostatic 6-arylpurine Nucleosides 6. SAR in Anti-HCV and Cytostatic Activity of Extended Series of 6-Hetarylpurine Ribonucleosides. *J. Med. Chem.* **2005**, *48*, 5869–5873.

(5) Nauš, P.; Pohl, R.; Votruba, I.; Džubák, P.; Hajdúch, M.; Ameral, R.; Birkus, G.; Wang, T.; Ray, A. S.; Mackman, R.; Cihlar, T.; Hocek, M. 6-(Het)aryl-7-Deazapurine Ribonucleosides as Novel Potent Cytostatic Agents. *J. Med. Chem.* **2010**, *53*, 460–470.

(6) (a) Spáčilová, P.; Nauš, P.; Pohl, R.; Votruba, I.; Snášel, J.; Zábranská, H.; Pichová, I.; Ameral, R.; Birkuš, G.; Cihlář, T.; Hocek, M. CycloSal-phosphate Pronucleotides of Cytostatic 6-(Het)aryl-7-deazapurine Ribonucleosides: Synthesis, Cytostatic Activity, and Inhibition of Adenosine Kinases. *ChemMedChem* **2010**, *5*, 1386–1396. (b) Perlíková, P.; Pohl, R.; Votruba, I.; Shih, R.; Birkuš, G.; Cihlář, T.; Hocek, M. Phosphoramidate pronucleotides of cytostatic 6-aryl-7-deazapurine ribonucleosides. *Bioorg. Med. Chem.* **2011**, *19*, 229–242.

(7) (a) Anzai, K.; Nakamura, G.; Suzuki, S. A New Antibiotic, Tubercidin. *J. Antibiot.* **1957**, *10*, 201–204. (b) Suzuki, S.; Marumo, S. Chemical Structure of Tubercidin. *J. Antibiot., Series A* **1961**, *13*, 360–360. (c) Acs, G.; Mori, M.; Reich, E. Biological + Biochemical Properties of Analogue Antibiotic Tubercidin. *Proc. Natl. Acad. Sci. U.S.A.* **1964**, *52*, 493–501.

(8) (a) Ramasamy, K.; Imamura, N.; Robins, R. K.; Revankar, G. R. A Facile Synthesis of Tubercidin And Related 7-Deazapurine Nucleosides via The Stereospecific Sodium Salt Glycosylation Procedure. *Tetrahedron Lett.* **1987**, *28*, 5107–5110. (b) Tolman, R. L.; Robins, R. K.; Townsend, L. B. Pyrrolopyrimidine Nucleosides. III. The Total Synthesis of Toyocamycin, Sangivamycin, Tubercidin and Related Derivatives. *J. Am. Chem. Soc.* **1969**, *91*, 2102–2108. (c) Bergstrom, D. E.; Brattesani, A. J.; Ogawa, M. K.; Reddy, A. T.; Schweickert, M. J.; Balzarini, J.; De Clercq, E. Antiviral Activity of C-5 Substituted Tubercidin Analogues. *J. Med. Chem.* **1984**, *27*, 285–292. (d) Wu, R.; Smidansky, E. D.; Oh, H. S.; Takhampunya, R.; Padmanabhan, R.; Cameron, C. E.; Peterson, B. R. Synthesis of a 6-Methyl-7-deaza Analogue of Adenosine That Potently Inhibits Replication of Polio and Dengue Viruses. *J. Med. Chem.* **2010**, *53*, 7958–7966.

(9) (a) Cook, A. F.; Holman, M. J. Synthesis of the Natural Product 5′-Deoxy-5-iodotubercidin and Related Halogenated Analogues. *Nucleosides Nucleotides* **1984**, *3*, 401–411. (b) Ugarkar, B. G.; DaRe, J. M.; Kopcho, J. J.; Browne, C. E., III; Schanzer, J. M.; Wiesner, J. B.; Erion, M. D. Adenosine Kinase Inhibitors. 1. Synthesis, Enzyme Inhibition and Antiseizure Activity of 5-Iodotubercidin Analogues. *J. Med. Chem.* **2000**, *43*, 2883–2893. (c) Ugarkar, B. G.; Castellino, A. J.; DaRe, J. S.; Ramirez-Weinhouse, M.; Kopcho, J. J.; Rosengren, S.; Erion, M. D. Adenosine Kinase Inhibitors. 3. Synthesis, SAR and Antiinflammatory Activity of a Series of L-Lyxofuranosyl Nucleosides. *J. Med. Chem.* **2003**, *46*, 4750–4760. (d) Kim, Y. A.; Sharon, A.; Chu, C. K.; Rais, R. H.; Al Safarjalani, O. N.; Naguib, F. N. M.; el Kouni, M. H. Structure−Activity Relationships of 7-Deaza-6-benzylthioinosine Analogues as Ligands of *Toxoplasma gondii* Adenosine Kinase. *J. Med. Chem.* **2008**, *51*, 3934–3945.

(10) (a) Eldrup, A. B.; Prhavc, M.; Brooks, J.; Bhat, B.; Prakash, T. P.; Song, Q. L.; Bera, S.; Bhat, N.; Dande, P.; Cook, P. D.; Bennett, C. F.; Carroll, S. S.; Ball, R. G.; Bosserman, M.; Burlein, C.; Colwell, L. F.; Fay, J. F.; Flores, O. A.; Getty, K.; LaFemina, R. L.; Leone, J.; MacCoss, M.; McMasters, D. R.; Tomassini, J. E.; Von Langen, D.; Wolanski, B.; Olsen, D. B. Structure−activity relationship of heterobase-modified 2′-C-methyl ribonucleosides as inhibitors of hepatitis C virus RNA replication. *J. Med. Chem.* **2004**, *47*, 5284–5297. (b) Eldrup, A. B.; Allerson, C. R.; Bennett, C. F.; Bera, S.; Bhat, B.; Bhat, N.; Bosserman, M. R.; Brooks, J.; Burlein, C.; Carroll, S. S.; Cook, P. D.; Getty, K. L.; MacCoss, M.; McMasters, D. R.; Olsen, D. B.; Prakash, T. P.; Prhavc, M.; Song, Q. L.; Tomassini, J. E.; Xia, J. Structure−activity relationship of purine ribonucleosides for inhibition of hepatitis C virus RNA-dependent RNA polymerase. *J. Med. Chem.* **2004**, *47*, 2283–2295. (c) Olsen, D. B.; Eldrup, A. B.; Bartholomew, L.; Bhat, B.; Bosserman, M. R.; Ceccacci, A.; Colwell, L. F.; Fay, J. F.; Flores, O. A.; Getty, K. L.; Grobler, J. A.; LaFemina, R. L.; Markel, E. J.; Migliaccio, G.; Prhavc, M.; Stahlhut, M. W.; Tomassini, J. E.; MacCoss, M.; Hazuda, D. J.; Carroll, S. S. A 7-deaza-adenosine analog is a potent and selective inhibitor of hepatitis C virus replication with excellent pharmacokinetic properties. *Antimicrob. Agents Chemother.* **2004**, *48*, 3944–3953.

(11) (a) Ugarkar, B. G.; Castellino, A. J.; DaRe, J. M.; Kopcho, J. J.; Wiesner, J. B.; Schanzer, J. M.; Erion, M. D. Adenosine Kinase Inhibitors. 2. Synthesis, Enzyme Inhibition and Antiseizure Activity of Diarylturbercidin Analogues. *J. Med. Chem.* **2000**, *43*, 2894–2905. (b) Boyer, S. H.; Ugarkar, B. G.; Solbach, J.; Kopcho, J.; Matelich, M. C.; Ollis, K.; Gomez-Galeno, J. E.; Mendonca, R.; Tsuchiya, M.; Nagahisa, A.; Nakane, M.; Wiesner, J. B.; Erion, M. D. Adenosine Kinase Inhibitors. 5. Synthesis, Enzyme Inhibition and Analgesic Activity of Erythro Diarylturbercidin Analogs. *J. Med. Chem.* **2005**, *48*, 6430–6441. (c) Bookser, B. C.; Matelich, M. C.; Ollis, K.; Ugarkar, B. G. Adenosine Kinase Inhibitors. 4. 6,8-Disubstituted Purine Nucleoside Derivatives. Synthesis, Conformation, and Enzyme Inhibition. *J. Med. Chem.* **2005**, *48*, 3389–3399.

(12) Seela, F.; Ming, X. 7-Functionalized 7-deazapurine β-D and β-L-ribonucleosides related to tubercidin and 7-deazainosine: glycosylation of pyrrolo[2,3-*d*]pyrimidines with 1-*O*-acetyl-2,3,5-tri-*O*-benzoyl-β-D or β-L-ribofuranose. *Tetrahedron* **2007**, *63*, 9850–9861.

(13) (a) Western, E. C.; Daft, J. R.; Johnson, E. M.; Gannett, P. M.; Shaughnessy, K. H. Efficient One-Step Suzuki Arylation of Unprotected Halonucleosides, Using Water-Soluble Palladium Catalysts. *J. Org. Chem.* **2003**, *68*, 6767–6774. (b) Čapek, P.; Pohl, R.; Hocek, M. Cross-Coupling Reactions of Unprotected Halopurine Bases, Nucleosides, Nucleotides and Nucleoside Triphosphates with 4-Boronophenylalanine in Water. Synthesis of (Purin-8-yl)- and (Purin-6-yl)phenylalanines. *Org. Biomol. Chem.* **2006**, *4*, 2278–2284.

(14) Park, S. B.; Dekeyser, M. A.; McDonald, P. T. Pesticidal fluoroethyl pyrazoles. U.S. Patent US 2004/157892 A1, August 12, 2004.

(15) Jin, T.; Kamijo, S.; Yamamoto, Y. Copper-Catalyzed Synthesis of *N*-Unsubstituted 1,2,3-Triazoles from Nonactivated Terminal Alkynes. *Eur. J. Org. Chem.* **2004**, 3789–3791.

(16) (a) Jetter, M. C.; Reitz, A. B. Synthesis of 4-Substituted Imidazoles via Palladium-Catalyzed Cross-Coupling Reactions. *Synthesis* **1998**, 829–831. (b) Bell, A. S.; Roberts, D. A.; Ruddock, K. S. A synthesis

of 2- and 4(5)-(2-pyridinyl)imidazoles by palladium-catalysed cross-coupling reactions. *Tetrahedron Lett.* **1988**, *29*, 5013–5016.

(17) For aqueous-phase Suzuki—Miyaura cross-coupling reactions of nucleoside triphosphates, see:(a) Čapek, P.; Cahová, H.; Pohl, R.; Hocek, M.; Gloeckner, C.; Marx, A. An Efficient Method for the Construction of Functionalized DNA Bearing Amino Acid Groups through Cross-Coupling Reactions of Nucleoside Triphosphates Followed by Primer Extension or PCR. *Chem.—Eur. J.* **2007**, *13*, 6196–6203. (b) Cahová, H.; Havran, L.; Brázdilová, P.; Pivoňková, H.; Pohl, R.; Fojta, M.; Hocek, M. Aminophenyl- and Nitrophenyl-Labeled Nucleoside Triphosphates: Synthesis, Enzymatic Incorporation, and Electrochemical Detection. *Angew. Chem., Int. Ed.* **2008**, *47*, 2059–2062. (c) Raindlová, V; Pohl, R.; Šanda, M.; Hocek, M. Direct Polymerase Synthesis of Reactive Aldehyde-Functionalized DNA and Its Conjugation and Staining with Hydrazines. *Angew. Chem., Int. Ed.* **2010**, *49*, 1064–1066.

(18) Vichai, V.; Kirtikara, K. Sulforhodamine B colorimetric assay for cytotoxicity screening. *Nature Protoc.* **2006**, *1*, 1112–1116.

(19) Scudiero, D. A.; Shoemaker, R. H.; Paull, K. D.; Monks, A.; Tierney, S.; Nofziger, T. H.; Currens, M. J.; Seniff, D.; Boyd, M. R. Evaluation of a Soluble Tetrazolium/Formazan Assay for Cell Growth and Drug Sensitivity in Culture Using Human and Other Tumor Cell Lines. *Cancer Res.* **1988**, *48*, 4827–4833.

(20) Hajduch, M.; Kolar, Z.; Novotny, R.; Hanus, J.; Mihal, V.; Hlobilkova, A.; Noskova, V.; Strnad, M. Induction of apoptosis and regression of spontaneous dog melanoma following in vivo application of synthetic cyclin-dependent kinase inhibitor olomoucine. *Anticancer Drugs* **1997**, *8*, 1007–1013.

(21) Noskova, V.; Dzubak, P.; Kuzmina, G.; Ludkova, A.; Stehlik, D.; Trojanec, R.; Janostakova, A.; Korinkova, G.; Mihal, V.; Hajduch, M. In vitro chemoresistance profile and expression/function of MDR associated proteins in resistant cell lines derived from CCRF-CEM, K562, A549 and MDA MB 231 parental cells. *Neoplasma* **2002**, *49*, 418–425.

(22) Durand-Gasselin, L.; Van Rompay, K. K. A.; Vela, J. E.; Henne, I. N.; Lee, W. A.; Rhodes, G. R.; Ray, A. S. Nucleotide Analogue Prodrug Tenofovir Disoproxil Enhances Lymphoid Cell Loading following Oral Administration in Monkeys. *Mol. Pharmaceutics* **2009**, *6*, 1145–1151.

(23) Vela, J. E.; Olson, L. Y.; Huang, A.; Fridland, A.; Ray, A. S. Simultaneous quantitation of the nucleotide analog adefovir, its phosphorylated anabolites and 2′-deoxyadenosine triphosphate by ion-pairing LC/MS/MS. *J. Chromatogr., B: Anal. Technol. Biomed. Life Sci.* **2007**, *848*, 335–343.

(24) Spacilova, L.; Dzubak, P.; Hajduch, M.; Krupkova, S.; Hradil, P.; Hlavac, J. Synthesis and cytotoxic activity of various 5-[alkoxy-(4-nitro-phenyl]-methyl]-uracils in their racemic form. *Bioorg. Med. Chem. Lett.* **2007**, *17*, 6647–6650.

(25) Krystof, V.; Cankar, P.; Frysova, I.; Slouka, J.; Kontopidis, G.; Dzubak, P.; Hajduch, M.; Srovnal, J.; De Azavedo, W. F.; Orsag, M.; Paprskarova, M.; Rolcik, J.; Latr, A.; Fischer, P.; Strnad, M. 4-Arylazo-3,5-diamino-1*H*-pyrazole CDK Inhibitors: SAR Study, Crystal Structure in Complex with CDK2, Selectivity, and Cellular Effects. *J. Med. Chem.* **2006**, *49*, 6500–6509.

2.3.1.2 Nucleosides as a potential mycobacterial ADK inhibitors

PERLÍKOVÁ, P., P. KONEČNÝ, P. NAUŠ, J. SNÁŠEL, I. VOTRUBA, P. DŽUBÁK, I. PICHOVÁ, M. HAJDÚCH a M. HOCEK. (2013). 6-Alkyl-, 6-aryl- or 6-hetaryl-7-deazapurine ribonucleosides as inhibitors of human or MTB adenosine kinase and potential antimycobacterial agents. *MedChemComm*, 4(11),1497-1500

MedChemComm

RSC Publishing

CONCISE ARTICLE

View Article Online
View Journal | View Issue

Cite this: *Med. Chem. Commun.*, 2013, **4**, 1497

6-Alkyl-, 6-aryl- or 6-hetaryl-7-deazapurine ribonucleosides as inhibitors of human or MTB adenosine kinase and potential antimycobacterial agents†

Pavla Perlíková,‡[a] Petr Konečný,‡[b] Petr Nauš,[a] Jan Snášel,[a] Ivan Votruba,[a] Petr Džubák,[b] Iva Pichová,[a] Marián Hajdúch[b] and Michal Hocek*[ac]

Received 21st August 2013
Accepted 16th September 2013

DOI: 10.1039/c3md00232b

www.rsc.org/medchemcomm

Title 6-alkyl-, 6-aryl- and 6-hetaryl-7-deazapurine ribonucleosides previously known as nanomolar cytostatics were found to be potent inhibitors of either human or mycobacterial (MTB) adenosine kinase (ADK). Several new derivatives bearing bulky substituents at position 6 were non-cytotoxic but selectively inhibited MTB ADK. However, most of the nucleosides (ADK inhibitors) as well as their octadecylphosphate prodrugs were inactive in the whole cell assay of inhibition of *Mycobacterium bovis* growth. 6-Methyl-7-deazapurine ribonucleoside was found to be a potent antimycobacterial agent.

Introduction

Modified purine nucleoside derivatives and analogs display a wide range of biological activities. Their antiviral[1] and antitumor[2] properties are particularly important and used in clinical therapeutics. However, purine derivatives[3] and nucleosides[4] also are potent antimycobacterial agents, *i.e.* for treatment of *Mycobacterium tuberculosis* (MTB). Out of the variety of possible target enzymes from the purine salvage pathway in MTB,[5] adenosine kinase (ADK)[6] is considered as a promising target for drug development since it is structurally very different from the human ADK.[7]

Recently, we have discovered 6-hetaryl-7-deazapurine ribonucleosides **1–3** with nanomolar cytostatic activities towards a wide panel of leukemia and cancer cell-lines.[8] Their *cyclo*Sal-phosphate[9] and phosphoramidate prodrugs[10] were less active due to increased efflux from the cells. However, *cyclo*Sal-phosphates were also found[9] to be potent inhibitors of human and moderate inhibitors of MTB ADKs. Since also other 7-deazapurine nucleosides are known as inhibitors of ADKs,[11] we have revisited the whole class of 7-deazapurine nucleosides with diverse aryl and hetaryl groups at position 6 and systematically studied their activity toward human and MTB ADKs.

Results and discussion

The synthesis of a series of nineteen 6-alkyl, 6-aryl- and 6-hetaryl-7-deazapurine ribonucleosides **1b–t**, nine 7-fluoro derivatives **2e**, **j–m**, **o–r** and six 7-chloro derivatives **3e**, **g**, **j–m** has been reported earlier,[8] as well as the 6-methyl derivative **1a** (ref. 12) (Chart 1). Most of these derivatives exhibited strong cytostatic or cytotoxic activities.[8,12]

In order to get less cytotoxic derivatives, we have extended the series by synthesis of other six derivatives bearing bulky (het)aryl groups at position 6 (Scheme 1). The dibenzofuryl and benzofuryl derivatives **1u** and **v** were prepared by the Suzuki coupling of isopropylidene-protected nucleoside **4** followed by deprotection. The other derivatives **1w–z** were synthesized by direct aqueous Suzuki coupling of 6-chloro-7-deazapurine ribonucleoside with the corresponding hetarylboronic acid in the presence of $Pd(OAc)_2$, triphenylphosphine-3,3′,3″-trisulfonate (TPPTS) and Na_2CO_3. In the case of indole derivative **1x**, the coupling was performed with the Boc-protected indole-2-boronic acid and the TFA treatment was used for deprotection. In all cases, the products were obtained in good 71–85% yields.

A synthetic path to 6-(het)aryl-7-deazapurine ribonucleoside-5′-octadecylphosphates, as potential lipophilic phosphate prodrugs, was developed starting from isopropylidene-protected ribonucleoside **4**. An octadecylphosphate group was attached by reaction with octadecylphosphate in the presence of 2,4,6-trimethylbenzene-1-sulphonyl chloride (MtsCl) in pyridine. Nucleoside-5′-octadecylphosphate **7** was obtained in 58% yield. Deprotection by treatment with 90% aqueous TFA provided free

[a]*Institute of Organic Chemistry and Biochemistry, Academy of Sciences of the Czech Republic, Gilead Sciences & IOCB Research Center, Flemingovo nam. 2, CZ-16610 Prague 6, Czech Republic. E-mail: hocek@uochb.cas.cz; Tel: +420 220183324*

[b]*Institute of Molecular and Translational Medicine, Laboratory of Experimental Medicine, Palacky University and University Hospital in Olomouc, Faculty of Medicine and Dentistry, Hněvotínská 5, CZ-775 15 Olomouc, Czech Republic*

[c]*Department of Organic Chemistry, Faculty of Science, Charles University in Prague, Hlavova 8, CZ-12843 Prague 2, Czech Republic*

† Electronic supplementary information (ESI) available: Experimental part and characterization data for all new compounds. See DOI: 10.1039/c3md00232b

‡ These authors contributed equally.

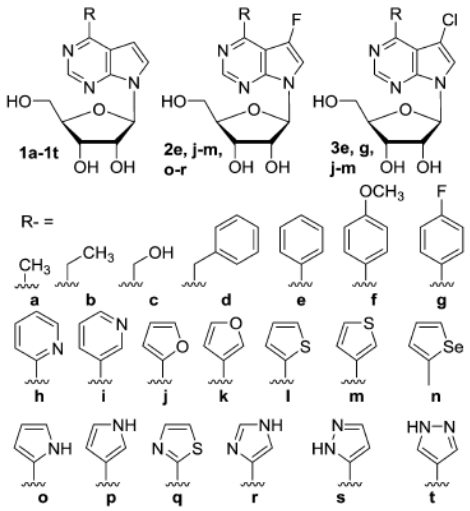

Chart 1 Structures of previously known nucleosides **1a–t**.

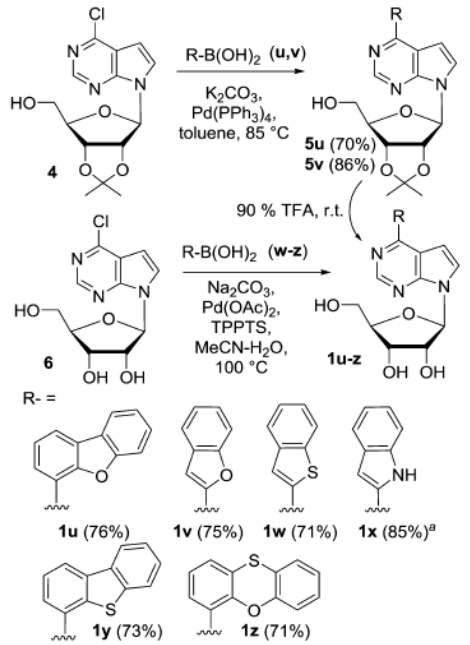

Scheme 1 Synthesis of nucleosides **1u–z**. [a] *N*-Boc-protected indole-2-boronic acid was used and the Boc was cleaved off by 90% TFA at rt; the yield is given over two steps.

nucleoside-5′-octadecylphosphate **8** (94%), which was used as a starting material for a series of Stille and Suzuki cross-coupling reactions. Stille cross-coupling reactions with hetaryltributylstannanes were performed in the presence of $PdCl_2(PPh_3)_2$ in DMF at 105 °C. As 5′-octadecylphosphate **8** is insoluble in toluene, standard conditions for the Suzuki cross-coupling reaction had to be slightly modified. The reactions with (het) arylboronic acids were performed in the presence of potassium carbonate and $Pd(PPh_3)_4$ in DMF/water (8 : 1) at 105 °C. 6-(Het) aryl-7-deazapurine ribonucleoside-5′-octadecylphosphates **9e, j–m** and **v** were obtained in 62–85% yields (Scheme 2).

All the title nucleosides **1a–z, 2e, j–m, o–r, 3e, g, j–m** and nucleotides **9e, j–m, v** were tested for the inhibition of human and MTB ADKs (for cloning expression and purification of these enzymes, see ref. 9) and most of them also for substrate activity to the kinases, *i.e.* for phosphorylation. The results were correlated with their *in vitro* cytotoxicity (MTT) against non-malignant BJ and MRC-5 human fibroblast cell lines. The cytotoxicity strongly depended on the bulkiness of the substituent at position 6. Most active were derivatives bearing five-membered heterocycles, whereas derivatives bearing bulky aryl groups were generally not cytotoxic, which was consistent with previously published[8] cytostatic and cytotoxic activities on leukemia and solid tumor cell lines. Most of the nucleosides did not show significant inhibition to human ADK with the exception of bulky derivatives **1u–z**, which showed inhibition with micromolar IC_{50} values. On the other hand, most of the nucleosides were moderate to good substrates for the human ADK and were readily phosphorylated to nucleoside 5′-*O*-monophosphates, which is a necessary step in their activation for eventual inhibition of RNA synthesis in their cytostatic or cytotoxic effect.[8] On the other hand, none of the compounds was found to be a substrate for MTB ADK and most compounds efficiently inhibited this enzyme. While the alkyl-substituted derivatives **1a–d** were weak inhibitors of MTB ADK, all the aryl-

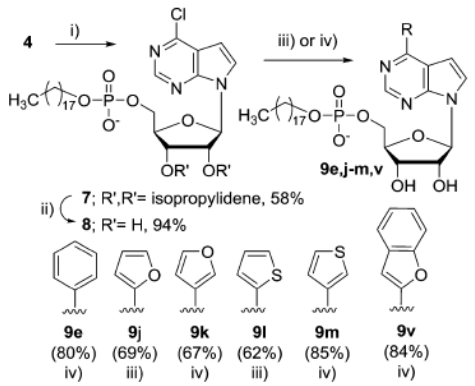

Scheme 2 *Reagents and conditions*: (i) $C_{18}H_{37}OP(O)(OH)_2$ (1.5 equiv), MtsCl (6 equiv), pyridine, rt; (ii) 90% TFA, rt; (iii) R-$SnBu_3$ (1.5 equiv), $PdCl_2(PPh_3)_2$ (0.05 equiv)/DMF, 105 °C; (iv) R-$B(OH)_2$ (1.5 equiv), K_2CO_3 (2 equiv), $Pd(PPh_3)_4$ (0.05 equiv), DMF/H_2O (8 : 1), 105 °C.

Table 1 Cytotoxicity, human and MTB ADK inhibition and antimycobacterial activity

			ADK substrate[b] (%)	ADK inhibition IC_{50} (μM)		
Compd	BJ[a] CC_{50} (μM)	MRC-5 CC_{50} (μM)	Human	Human	MTB	*Mycobacterium bovis*[c] IC_{50} (μM)
1a	0.098	0.081	54	>10	8.8 ± 0.03	0.30
1b	2.70	50	n.d.	>20	8.1 ± 0.9	88.84
1c	0.34	0.28	26	>10	>5.00	32.61
1d	36.92	>50		>20	>20	>100
1e	44.15	>50	n.d.	>10	0.12 ± 0.03	75.16
1f	>50	>50	n.d.	>10	0.058 ± 0.003	56.88
1g	>50	>50	17	>10	0.08 ± 0.008	93.82
1h	1.74	>50	39	>10	0.12 ± 0.02	38.22
1i	50	>50	n.d.	>10	1.00 ± 0.11	>100
1j	0.23	11.83	56	1.30 ± 0.25	0.32 ± 0.05	>100
1k	1.20	45.38	32	>10	0.32 ± 0.04	83.67
1l	0.31	>50	n.d.	>5	0.046 ± 0.003	>100
1m	21.33	>50	56	>10	0.195 ± 0.05	81.00
1n	1.52	>50	43	>10	0.030 ± 0.005	>100
1o	>50	>50	40	>10	0.073 ± 0.007	56.44
1p	1.87	40.15	70	>10	0.30 ± 0.04	98.23
1q	0.26	37.00	41	>20	0.023 ± 0.003	80.53
1r	0.21	>50	28	>10	0.78 ± 0.10	15.55
1s	43.93	1.16	31	>20	0.059 ± 0.005	91.10
1t	42.13	>50	7	>20	0.67 ± 0.10	>100
1u	>50	>50	n.d.	5.26 ± 0.66	2.35 ± 0.35	>100
1v	>50	>50	n.d.	2.10 ± 0.03	0.0145 ± 0.001	>100
1w	>50	>50	n.d.	0.30 ± 0.02	0.0075 ± 0.0007	>100
1x	>50	>50	n.d.	8.35 ± 0.75	0.04 ± 0.005	>100
1y	>50	43.76	n.d.	15.4 ± 1.2	0.15 ± 0.007	>100
1z	>50	>50	n.d.	3.07 ± 0.40	1.46 ± 0.07	>100
2e	>50	>50	17	>10	0.20 ± 0.05	74.81
2j	0.31	29.04	50	1.30 ± 0.25	0.19 ± 0.10	73.20
2k	0.35	15.38	n.d.	>10	0.15 ± 0.05	91.19
2l	0.17	47.21	52	1.10 ± 0.20	0.035 ± 0.005	>100
2m	0.62	50	51	>10	0.063 ± 0.003	>100
2o	2.99	44.45	76	>10	0.070 ± 0.010	45.78
2p	2.02	48.94	97	>10	0.40 ± 0.06	>100
2q	0.63	>50	75	>20	0.028 ± 0.007	68.99
2r	>50	>50	11	>20	1.00 ± 0.12	11.73
3e	44.49	>50	29	>10	0.22 ± 0.05	>100
3g	49.52	>50	n.d	>20	0.40 ± 0.02	89.63
3j	37.25	>50	77	0.29 ± 0.03	0.11 ± 0.01	89.23
3k	21.62	>50	100	3.4	0.30 ± 0.03	97.10
3l	4.97	>50	100	1.20 ± 0.20	0.07 ± 0.007	96.38
3m	1.72	>50	97	>10	0.25 ± 0.03	99.57
9e	>50	>50	—	4.40 ± 0.10	>20	>100
9j	>50	45.26	—	2.4 ± 0.11	>20	>100
9k	44.20	>50	—	5.15 ± 0.35	>20	56.56
9l	n.d.	n.d.	—	1.97 ± 0.16	>20	n.d.
9m	>50	>50	—	6.35 ± 0.34	>20	82.78
9v	>50	>50	—	2.9 ± 0.30	>20	93.39

[a] Cytotoxicity (MTT test) in BJ and MRC-5 fibroblasts. [b] ADK substrate activity, conversion to 5′-phosphate (%). [c] 50% growth inhibitory concentration of *in vitro* cultivated *Mycobacterium bovis* BCG.

and hetaryl-substituted 7-deazapurine ribonucleosides (**1e–z**), including 7-fluoro- (**2**) and 7-chloro-derivatives (**3**) were strong inhibitors of this enzyme with submicromolar to low nanomolar IC_{50} values. Most of the derivatives bearing phenyl and five-membered hetaryl groups at position 6 (**1e–i, k–t, 2e, k, m–r** and **3e, g, m**) were selective inhibitors of the MTB ADK and did not significantly inhibit the human enzyme (but were strongly cytotoxic). 6-Furyl derivatives **1j** and **2j** and the thienyl derivative **2l** were less selective, inhibited both enzymes and were cytotoxic. The derivatives bearing bulky aryl groups **1u–z** inhibited the MTB ADK in low nanomolar concentrations while the inhibition of human enzyme was observed at micromolar concentrations, and so the selectivity index was 2–3 orders of magnitude. These bulky derivatives were not cytotoxic. The octadecylphosphate prodrugs **9** were moderate inhibitors of the human ADK and inactive against MTB enzyme.

All the derivatives were also tested for *in vivo* inhibition of *Mycobacterium bovis* growth (Table 1). From all tested nucleosides only compound **1a** displayed very significant antimycobacterial activity (IC_{50} = 0.3 μM) but showed the highest cytotoxicity. This derivative, however, only weakly inhibited *in vitro* MTB ADK (IC_{50} = 8.8 μM) which may indicate that the mode of antimycobacterial activity of this compound is independent of MTB ADK and rather suggests a more general cytotoxic mechanism. Two 6-(imidazolyl)deazapurine nucleosides **1r** and **2r** exerted moderate antimycobacterial activity (IC_{50} = 15.6 and 11.7 μM, respectively) accompanied by preferential inhibition of MTB ADK and low cytotoxicity, whereas all other nucleosides were virtually inactive. The octadecylphosphate prodrugs **9e**, **j–m** and **v**, which were designed as lipophilic derivatives with increased penetration through the mycobacterial cell wall, did not show any antimycobacterial activity either.

Conclusions

It can be concluded that the 6-(het)aryl-7-deazapurine ribonucleosides are strong and mostly selective inhibitors of MTB ADK but not the human ADK. Nonetheless, they showed only limited potential to inhibit growth of mycobacteria. One reason could be their poor penetration through the mycobacterial cell wall. Alternatively, the mycobacterial ADK may not be a suitable target for therapy since AMP also can be biosynthesized by the salvage pathway from adenine utilizing adenine phosphoribosyl transferase or by a reaction sequence from IMP.[5]

Acknowledgements

This work was supported by the institutional support from the Academy of Sciences of the Czech Republic (RVO: 61388963), a grant of the Czech Science Foundation (P207/11/0344), EU-PF7 SysteMtb Collaborative Project no. 241587, and by Gilead Sciences, Inc. Infrastructural part of this project (Institute of Molecular and Translational Medicine) was supported by the Operational Programme Research and Development for Innovations (project CZ.1.05/2.1.00/01.0030). We thank Mrs Dagmar Grundová for excellent technical assistance.

Notes and references

1 Reviews: (*a*) E. De Clercq, *J. Med. Chem.*, 2010, 53, 1438–1450; (*b*) E. De Clercq, *Nucleosides, Nucleotides Nucleic Acids*, 2012, **31**, 339–352.

2 Reviews: (*a*) W. B. Parker, J. A. Secrist, III and W. R. Waud, *Curr. Opin. Invest. Drugs*, 2004, **5**, 592–596; (*b*) C. M. Galmarini, F. Popowycz and B. Joseph, *Curr. Med. Chem.*, 2008, **15**, 1072–1082; (*c*) W. B. Parker, *Chem. Rev.*, 2009, **109**, 2880–2893.

3 Examples: (*a*) A. Scozzafava, A. Mastrolorenzo and C. T. Supuran, *Bioorg. Med. Chem. Lett.*, 2001, **11**, 1675–1678; (*b*) A. K. Pathak, V. Pathak, L. E. Seitz, W. J. Suling and R. C. Reynolds, *J. Med. Chem.*, 2004, **47**, 273–276; (*c*) L.-L. Gundersen, J. Nissen-Meyer and B. Spilsberg, *J. Med. Chem.*, 2002, **45**, 1383–1386; (*d*) A. K. Bakkestuen, L.-L. Gundersen and B. T. Utenova, *J. Med. Chem.*, 2005, **48**, 2710–2723; (*e*) M. Braendvang and L.-L. Gundersen, *Bioorg. Med. Chem.*, 2005, **13**, 6360–6373.

4 Reviews: (*a*) M. C. Long and W. B. Parker, *Biochem. Pharmacol.*, 2006, **71**, 1671–1682; (*b*) M. C. Long, S. C. Shaddix, O. Moukha-Chafiq, J. A. Maddry, L. Nagy and W. B. Parker, *Biochem. Pharmacol.*, 2008, **75**, 1588–1600.

5 Reviews: (*a*) W. B. Parker and M. C. Long, *Curr. Pharm. Des.*, 2007, **13**, 599–608; (*b*) R. G. Ducati, A. Breda, A. Basso, L. A. Basso and D. S. Santos, *Curr. Med. Chem.*, 2011, **18**, 1258–1275.

6 M. C. M. Reddy, S. K. Palaninathan, N. D. Shetty, J. L. Owen, M. D. Watson and J. C. Sacchettini, *J. Biol. Chem.*, 2007, **282**, 27334–27342.

7 S. W. Muchmore, R. A. Smith, A. O. Stewart, M. D. Cowart, A. Gomtsyan, M. A. Matulenko, H. Yu, J. M. Severin, S. S. Bhagwat, C.-H. Lee, E. A. Kowaluk, M. F. Jarvis and C. L. Jakob, *J. Med. Chem.*, 2006, **49**, 6726–6731.

8 P. Nauš, R. Pohl, I. Votruba, P. Džubák, M. Hajdúch, R. Ameral, G. Birkus, T. Wang, A. S. Ray, R. Mackman, T. Cihlar and M. Hocek, *J. Med. Chem.*, 2010, **53**, 460–470.

9 P. Spáčilová, P. Nauš, R. Pohl, I. Votruba, J. Snášel, H. Zábranská, I. Pichová, R. Ameral, G. Birkuš, T. Cihlář and M. Hocek, *ChemMedChem*, 2010, **5**, 1386–1396.

10 P. Perlíková, R. Pohl, I. Votruba, R. Shih, G. Birkuš, T. Cihlář and M. Hocek, *Bioorg. Med. Chem.*, 2011, **19**, 229–242.

11 Examples: (*a*) B. G. Ugarkar, J. M. DaRe, J. J. Kopcho, C. E. Browne, III, J. M. Schanzer, J. B. Wiesner and M. D. Erion, *J. Med. Chem.*, 2000, **43**, 2883–2893; (*b*) B. G. Ugarkar, A. Castellino, J. M. DaRe, J. J. Kopcho, J. B. Wiesner, J. M. Schanzer and M. D. Erion, *J. Med. Chem.*, 2000, **43**, 2894–2905; (*c*) B. G. Ugarkar, A. J. Castellino, J. S. DaRe, M. Ramirez-Weinhouse, J. J. Kopcho, S. Rosengren and M. D. Erion, *J. Med. Chem.*, 2003, **46**, 4750–4760; (*d*) B. C. Bookser, M. C. Matelich, K. Ollis and B. G. Ugarkar, *J. Med. Chem.*, 2005, **48**, 3389–3399; (*e*) S. H. Boyer, B. G. Ugarkar, J. Solbach, J. J. Kopcho, M. C. Matelich, K. Ollis, J. E. Gomez-Galeno, R. Mendonca, M. Tsuchiya, A. Nagahisa, M. Nakane, J. B. Wiesner and M. D. Erion, *J. Med. Chem.*, 2005, **48**, 6430–6441; (*f*) Y. A. Kim, A. Sharon, C. K. Chu, R. H. Rais, O. N. Al Safarjalani, F. N. M. Naguib and M. H. el Kouni, *J. Med. Chem.*, 2008, **51**, 3934–3945.

12 R. Wu, E. D. Smidansky, H. S. Oh, R. Takhampunya, R. Padmanabhan, C. E. Cameron and B. R. Peterson, *J. Med. Chem.*, 2010, **53**, 7958–7966.

2.3.1.3 Identification of the most potent nucleosides with various biological activities

NAUŠ, P., O. CALETKOVÁ, P. KONEČNÝ, P. DŽUBÁK, K. BOGDANOVÁ, M. KOLÁŘ, J. VRBKOVÁ, L. SLAVĚTÍNSKÁ, E. TLOUŠŤOVÁ, P. PERLÍKOVÁ, M. HAJDÚCH a M. HOCEK. (2014). Synthesis, cytostatic, antimicrobial, and anti-HCV activity of 6-substituted 7-(het)aryl-7-deazapurine ribonucleosides. *Journal of Medicinal Chemistry*, **57**(3), 1097-1110.

Journal of Medicinal Chemistry

Article

pubs.acs.org/jmc

Synthesis, Cytostatic, Antimicrobial, and Anti-HCV Activity of 6-Substituted 7-(Het)aryl-7-deazapurine Ribonucleosides

Petr Nauš,[†] Olga Caletková,[†] Petr Konečný,[‡] Petr Džubák,[‡] Kateřina Bogdanová,[‡] Milan Kolář,[‡] Jana Vrbková,[‡] Lenka Slavětínská,[†] Eva Tloušťová,[†] Pavla Perlíková,[†] Marián Hajdúch,[‡] and Michal Hocek*[,†,§]

[†]Institute of Organic Chemistry and Biochemistry, Academy of Sciences of the Czech Republic, Gilead Sciences & IOCB Research Center, Flemingovo nam. 2, CZ-16610 Prague 6, Czech Republic

[‡]Institute of Molecular and Translational Medicine, Faculty of Medicine and Dentistry, Palacky University and University Hospital in Olomouc, Hněvotínská 5, CZ-775 15 Olomouc, Czech Republic

[§]Department of Organic Chemistry, Faculty of Science, Charles University in Prague, Hlavova 8, CZ-12843 Prague 2, Czech Republic

Supporting Information

ABSTRACT: A series of 80 7-(het)aryl- and 7-ethynyl-7-deazapurine ribonucleosides bearing a methoxy, methylsulfanyl, methylamino, dimethylamino, methyl, or oxo group at position 6, or 2,6-disubstituted derivatives bearing a methyl or amino group at position 2, were prepared, and the biological activity of the compounds was studied and compared with that of the parent 7-(het)aryl-7-deazaadenosine series. Several of the compounds, in particular 6-substituted 7-deazapurine derivatives bearing a furyl or ethynyl group at position 7, were significantly cytotoxic at low nanomolar concentrations whereas most were much less potent or inactive. Promising activity was observed with some compounds against *Mycobacterium bovis* and also against hepatitis C virus in a replicon assay.

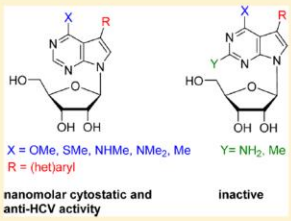

INTRODUCTION

Purine nucleosides and their analogues display a wide range of antiviral and antitumor activities,[1] but there is still a room for development of new nucleoside-based anticancer drugs[2] targeting malignant versus nonmalignant cells as well as drugs for the treatment of resistant tumors. We have previously observed significant cytotoxic activity among certain 6-(het)arylpurine[3] and 6-(het)aryl-7-deazapurine[4] nucleosides. More recently we discovered 7-hetaryl-7-deazaadenine ribonucleosides **1**[5] (Chart 1) with nanomolar cytostatic activities against leukemia and cancer cell lines and found[6] that some sugar-modified compounds derived from **1** are still cytotoxic but less so than the parent compounds. The mechanism of action of **1** has not yet been fully explored. We previously reported[5] that these nucleosides interfere with RNA synthesis, although their triphosphates are only weak inhibitors of RNA polymerases. To analyze the SAR of these compounds and their mode of action, we have now prepared and tested a series of base-modified derivatives of **1** (Chart 1). The first group (compounds **2**−**7**) was characterized by replacement of the amino group (H-bond donor) at position 6 by diverse H-bond acceptors (methoxy, methylsulfanyl, dimethylamino, oxo), methylamino (which can serve as either a donor or acceptor), and the isosteric but nonpolar methyl group. The second group of derivatives (compounds **8**−**11**) were 2,6-disubstituted 7-deazaguanine, 7-deazadiaminopurine, and 2-methyl-7-deazaadenine nucleosides. In each class, a series of 7-substituted derivatives bearing (het)aryl, ethynyl, and halogen groups, as well as 7-unsubstituted derivatives, were studied.

As a group, these derivatives may be viewed as analogues of the antibiotic tubercidin.[7] Many other tubercidin analogues have been studied,[8] including 7-halogen, 7-carboxamido, and 7-alkynyl derivatives,[9] some of which showed cytotoxic, antiparasitic, and antiviral activities. Several related 6-substituted analogues of tubercidin[10] were likewise cytostatic, whereas 6-substituted analogues of toyocamycin possessed anti-HCV[11] activity. 6-Methyl-7-deazapurine ribonucleoside **6h**[12] was also recently reported to have an antiviral effect.

RESULTS AND DISCUSSION

Chemistry. The synthetic strategy for preparation of 6-monosubstituted 7-(hetaryl)-7-deazapurine nucleosides **2**−**7** was based on aqueous-phase Suzuki cross-coupling reactions of the corresponding 6-substituted 7-iodo-7-deazapurine ribonucleosides **13**−**16**. These key intermediates were obtained in good yields from 4-chloro-5-iodo-7-(2,3,5-tri-*O*-benzoyl-*β*-D-ribofuranosyl)-7*H*-pyrrolo[2,3-*d*]pyrimidine **12**[13] through nucleophilic substitution at position 6 with NaOMe, NaSMe, CH_3NH_2, or $(CH_3)_2NH$ (Scheme 1). Concomitant nucleophilic debenzoylation of the sugar proceeded in all cases under the reaction conditions, affording directly free nucleosides.

Received: December 10, 2013
Published: January 7, 2014

dx.doi.org/10.1021/jm4018948 | J. Med. Chem. 2014, 57, 1097−1110

Chart 1. Previously Reported Cytostatic Nucleosides 1 and the Design of Derivatives in This Study

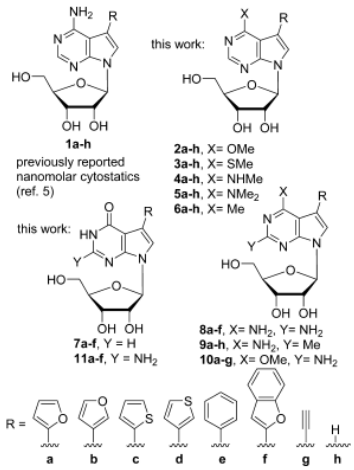

Scheme 1. Nucleophilic Substitution at Position 6[a]

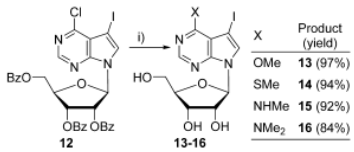

X	Product (yield)
OMe	**13** (97%)
SMe	**14** (94%)
NHMe	**15** (92%)
NMe_2	**16** (84%)

[a]Conditions: (i) for **13**: MeONa/MeOH; for **14**: MeSNa/EtOH; for **15**: $MeNH_2$/EtOH; for **16**: aq Me_2NH/dioxane.

The synthesis of 7-halogenated 6-methyl-7-deazapurine ribonucleosides was more complicated due to the need for cross-coupling methylation at position 6, which on 6-chloro-7-iodo-7-deazapurine nucleoside **12** would not proceed chemoselectively. Attempted "classical" S_NAr methylation of **12** using either Wittig reagent[14] or enolates of 1,3-dicarbonyl compounds (acetylacetone,[15] ethyl acetoacetate[16]) failed to give desired product. Attempted methylation via iron-catalyzed[17] reaction of **12** with methylmagnesium chloride also failed resulting in deiodination, presumably by iodine−magnesium exchange. Thus we decided to first selectively hydrodeiodinate **12** followed by C-6 methylation and reintroduction of the halogen at position 7 (Scheme 2). Deiodination of **12** was achieved by iodine−magnesium exchange reaction using Knochel's Turbo-Grignard reagent[18] (*i*PrMgCl·LiCl) and subsequent hydrolysis of magnesium intermediate to give 6-chloro-7-deazapurine riboside **17**[19] in almost quantitative yield without need for purification. This process is a useful alternative route to 6-chloro-7-deazapurine ribonucleosides, because the glycosylation of the 7-unsubstituted 6-chloro-7-deazapurine base is troublesome,[19,20] whereas that of 7-halogenated 6-chloro-7-deazapurines is convenient under Vorbrüggen conditions using commercialy available 1-*O*-acetyl-2,3,5-tri-*O*-benzoyl-β-D-ribofuranose.[13] The 6-chloro-7-deazapurine **17**

Scheme 2. Synthesis of 7-Halogenated 6-Methyl-7-deazapurine Ribonucleosides[a]

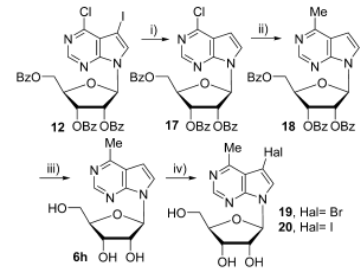

[a]Conditions: (i) 1. iPrMgCl·LiCl, THF, −10 °C. 2. aq workup (quant); (ii) $AlMe_3$, $Pd(PPh_3)_4$, THF, 100 °C (92%); (iii) MeONa, MeOH, rt (97%); (iv) for **19**: NBS, DMF, rt (66%); for **20**: NIS, DMF, rt (58%).

was converted to 6-methyl derivative **18** by palladium-catalyzed reaction with trimethylaluminum in 92% yield, and the follow-up Zemplén deprotection furnished free 6-methyl-7-deazapurine ribonucleoside **6h**[12] in 97% yield. Compound **6h** was then brominated by *N*-bromosuccinimide (NBS) in DMF to give 7-bromo derivative **19** in 66% yield. Analogous 7-iodo derivative **20** was prepared by treatment with *N*-iodosuccinimide (NIS), but the reaction was more sluggish, giving **20** in 58% yield with 18% recovery of unreacted **6h**.

The halogenated nucleoside intermediates **13**−**16** and **19** served as starting points for the synthesis of the target 7-(het)aryl 7-deazapurine ribonucleosides via the Suzuki−Miyaura reactions with (het)aryl boronic acids (Scheme 3).

Scheme 3. Suzuki Cross-Coupling Reactions of 13−16 and 19

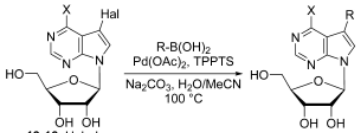

	Product (yield)				
R-	X= OMe	X= SMe	X= NHMe	$X= NMe_2$	X= Me
furan-2-yl	**2a** (75%)	**3a** (46%)	**4a** (86%)	**5a** (49%)	**6a** (83%)
furan-3-yl	**2b** (73%)	**3b** (90%)	**4b** (96%)	**5b** (44%)	**6b** (78%)
thiophen-2-yl	**2c** (86%)	**3c** (67%)	**4c** (94%)	**5c** (49%)	**6c** (78%)
thiophen-3-yl	**2d** (79%)	**3d** (81%)	**4d** (98%)	**5d** (55%)	**6d** (82%)
phenyl	**2e** (82%)	**3e** (49%)	**4e** (95%)	**5e** (42%)	**6e** (71%)
benzofuran-2-yl	**2f** (85%)	**3f** (23%)	**4f** (64%)	**5f** (69%)	**6f** (79%)

The Pd-catalyzed reactions were conducted under aqueous conditions[21] in the presence of TPPTS and sodium carbonate. The reactions in a water/acetonitrile 2:1 mixture at 100 °C proceeded smoothly within 3 h to give the desired library of 30 (5 × 6) 7-(het)aryl derivatives **2a**−**f**, **3a**−**f**, **4a**−**f**, **5a**−**f**, and **6a**−**f** in moderate to good yields. In most cases, except for methylamino derivatives **4a**−**f**, the reaction mixtures also

dx.doi.org/10.1021/jm4018948 | J. Med. Chem. 2014, 57, 1097−1110

contained minor byproducts of concomitant reductive deiodination, **2h**, **3h**, **5h**, or **6h**, which were easily removed by chromatography. For methylsulfanyl derivatives **3a**, **3c**, and **3f**, the cross-coupling reactions did not reach full conversions of starting iodide **14**, and separation from the products required crystallization. This could be due to sulfur poisoning of the palladium catalytic species, resulting in a decreased reaction rate and hence premature decomposition of labile hetarylboronic acids[22] (furan[23] and thiophene[24] boronic acids are prone to fast protodeboronation).

Ethynyl derivatives **2g**–**6g** were prepared from the corresponding iododeazapurines **13**–**16** and **20** by Sonogashira reaction with (trimethylsilyl)acetylene followed by cleavage of the trimethylsilyl group by treatment with K_2CO_3 in methanol (Scheme 4). It is noteworthy that methyl derivative **6g** had to be synthesized from a more reactive iododeazapurine **20** because the bromo derivative **19** failed to react under these conditions.

Scheme 4. Preparation of Ethynyl Derivatives 2g–6g[a]

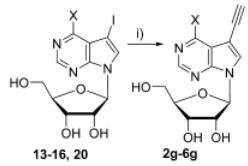

X	Product (yield)
OMe	**2g** (88%)
SMe	**3g** (66%)
NHMe	**4g** (78%)
NMe_2	**5g** (81%)
Me	**6g** (81%)

[a]Conditions: (i) 1. trimethylsilylacetylene, $PdCl_2(PPh_3)_2$, CuI, NEt_3, DMF, 100 °C. 2. K_2CO_3, MeOH, rt. The yields are given as overall isolated yields over the two steps.

For comparison of biological activity, 7-unsubstituted 7-deazapurine ribonucleosides **2h**–**4h**[10] were prepared from 6-chlorodeazapurine nucleoside **17** by substitution/deprotection (Scheme 5). Dimethylamino compound **5h**[10] was isolated as a byproduct from Suzuki reactions in the synthesis of compounds **5a**–**e** (Scheme 3).

Scheme 5. Preparation of 7-Unsubstituted 7-Deazapurine Ribonucleosides 2h–4h[a]

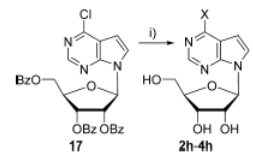

X	Product (yield)
OMe	**2h** (89%)
SMe	**3h** (46%)
NHMe	**4h** (91%)

[a]Conditions: (i) for **2h**: MeONa/MeOH; for **3h**: MeSNa/EtOH; for **4h**: $MeNH_2$/EtOH.

7-(Het)aryl-7-deazainosines (**7a**–**f**) synthesized directly from 7-iodo-7-deazainosine[13] using Pd-catalyzed Suzuki or Stille cross-couplings were obtained in very low yields. Therefore, **7a**–**f** were prepared by O-demethylation of 6-methoxy derivatives **2a**–**f** (Scheme 6). Application of the Seela's basic hydrolysis[13] (aq KOH, dioxane, reflux) to 7-(het)aryl-6-methoxy-7-deazapurine ribosides **2a**–**f** surprisingly failed to give even trace of desired products **7a**–**f**, although this protocol perfectly works for demethylation of 7-halogenated congeners

Scheme 6. Preparation of 7-(Het)aryl-7-deazainosines 7a–f[a]

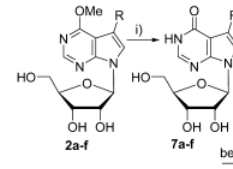

R	Product (yield)
furan-2-yl	**7a** (61%)
furan-3-yl	**7b** (68%)
thiophen-2-yl	**7c** (87%)
thiophen-3-yl	**7d** (92%)
phenyl	**7e** (77%)
benzofuran-2-yl	**7f** (93%)

[a]Conditions: (a) NaI, TMSCl, MeCN, rt.

such as **13** to yield 7-iodo-7-deazainosine. Instead, cleavage of methyl ethers **2a**–**f** with in situ generated iodotrimethylsilane[25] (from TMSCl and NaI) in acetonitrile was found to give 7-(het)aryl-7-deazainosines **7a**–**f** in good yields. Only with 2-furyl derivative **7a**, shorter reaction time and modified workup had to be used due to decomposition during standard conditions.

Synthetic pathway toward 2-methyl-7-deazaadenosines began with the preparation of 2-methyl-7-deazahypoxanthine **21** as reported[26] (Scheme 7). Deoxychlorination of **21** via a slight

Scheme 7. Preparation of 2-Methyl-7-deazaadenosine 9h[a]

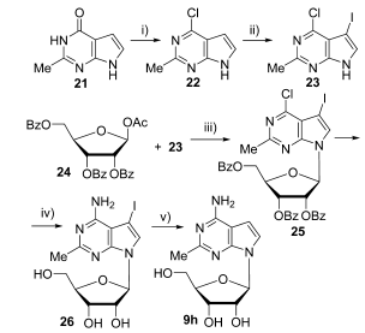

[a]Conditions: (i) $POCl_3$, *N*,*N*-dimethylaniline, BTEACl, MeCN, 100 °C (82%); (ii) NIS, CH_2Cl_2, rt (87%); (iii) 1. BSA, MeCN. 2. TMSOTf, 50 °C (35%); (iv) aq NH_3 (27% w/w), dioxane, 120 °C (92%); (v) H_2, Pd/C, NEt_3, DMF, rt (97%).

modification of literature conditions[27] produced 6-chloro-2-methyl-7-deazapurine **22**[28] (82%) whose further iodination using NIS provided **23** in 87% yield. Nucleobase **23** was converted to nucleoside **25** via a silyl-Hilbert–Johnson reaction with 1-*O*-acetyl-2,3,5-tri-*O*-benzoyl-β-D-ribofuranose **24** under Vorbrüggen conditions. Thus, silylation of **23** with BSA and treatment with **24** in the presence of TMSOTf catalyst afforded crystalline nucleoside **25** in 35% yield. The formation of **25** was slow due to extensive decomposition of **24** at the usual reaction temperature of 80 °C. Therefore, the reaction was run at only 50 °C with 2 equiv of **24** being added to the reaction in three portions. Essentially this is a protocol developed by Seela for analogous ribosylation of 7-halogenated 2-pivaloylamino-6-chloro-7-deazapurine[29] (we also used these conditions to obtain iodides **27** and **28**, vide infra). Amination of **25** with benzoyl deprotection by treatment with ammonia gave 7-iodo-2-methyl-7-deazaadenosine **26** in 92% yield. Reduction of iodo

dx.doi.org/10.1021/jm4018948 | J. Med. Chem. 2014, 57, 1097–1110

derivative **26** by catalytic hydrogenation on Pd/C furnished 2-methyl-7-deazaadenosine **9h**.[30]

7-(Het)aryl-substituted 2-amino-7-deazaadenosines **8a–f**, 2-methyl-7-deazaadenosines **9a–f**, and 2-amino-6-methoxy-7-deazapurine ribonucleosides **10a–f** were synthesized once again by aqueous Suzuki cross-couplings from iodo derivatives **26–28**[29] with the coresponding boronic acids (Scheme 8). The

Scheme 8. Suzuki Cross-Coupling Reactions of 26–28

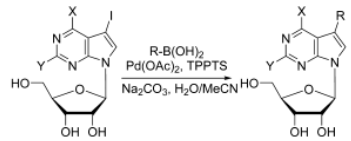

26, X= NH_2, Y= Me
27, X= NH_2, Y= NH_2
28, X= OMe, Y= NH_2

8a-f, **9a-f**, **10a-f**

R	Product (yield) X= NH_2 Y= NH_2	X= NH_2 Y= Me	X= OMe Y= NH_2
furan-2-yl	**8a** (80%)	**9a** (78%)	**10a** (59%)
furan-3-yl	**8b** (67%)	**9b** (76%)	**10b** (62%)
thiophen-2-yl	**8c** (83%)	**9c** (70%)	**10c** (58%)
thiophen-3-yl	**8d** (88%)	**9d** (93%)	**10d** (58%)
phenyl	**8e** (87%)	**9e** (90%)	**10e** (44%)
benzofuran-2-yl	**8f** (80%)	**9f** (77%)	**10f** (44%)

reactions leading to 2,6-diamino compounds **8a–f** and 2-methyl derivatives **9a–f** proceeded cleanly without significant side reactions, but those leading to 2-amino-6-methoxy 7-deazapurines **10a–f** were accompanied by reductive dehalogenation of iodide **28** (<14% as determined by NMR), and this byproduct was removed during reverse phase chromatography.

7-Ethynyl nucleosides **9g** and **10g** were synthesized by the Sonogashira reaction of 7-iodo-7-deazapurine nucleosides **26** or **28** followed by desilylation (Scheme 9).

Scheme 9. Sonogashira Reaction of 26 and 28[a]

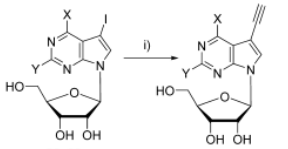

26, **28**

9g, X= NH_2, Y= Me, 79%
10g, X= OMe, Y= NH_2, 56%

[a]Conditions: (i) 1. trimethylsilylacetylene, $PdCl_2(PPh_3)_2$, CuI, NEt_3, DMF, 100 °C. 2. K_2CO_3, MeOH, rt. The yields are given as overall isolated yields over the two steps.

Similarly to the synthesis of inosines **7a–f**, 7-(het)aryl 7-deazaguanosines **11a–f** were obtained from the corresponding 6-methoxy compounds **10a–f** by demethylation using TMSCl/NaI reagent (Scheme 10). The products **11a–f** were isolated in only moderate unoptimized yields, as they were somewhat unstable during prolonged treatment under reaction and workup conditions. Again similarly to inosines **7a–f**, attempted direct synthesis of 7-deazaguanosines **11a–f** by cross-coupling

Scheme 10. Synthesis of 7-Deazaguanosines 11a–f[a]

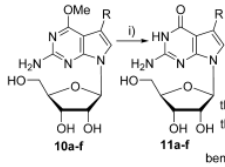

10a-f **11a-f**

R	Product (yield)
furan-2-yl	**11a** (21%)
furan-3-yl	**11b** (55%)
thiophen-2-yl	**11c** (71%)
thiophen-3-yl	**11d** (36%)
phenyl	**11e** (56%)
benzofuran-2-yl	**11f** (39%)

[a]Conditions: (i) NaI, TMSCl, MeCN, rt.

reactions from 7-iodo-7-deazaguanosine was found to be of little use because of low conversions.

Biological Activity Profiling. *Cytotoxic/Cytostatic Activity.* In vitro cytotoxic/cytostatic activity of final nucleosides **2–26** was initially evaluated against six cell lines derived from human solid tumors including lung (A549 cells) and colon (HCT116 and HCT116p53−/−) carcinomas, as well as leukemia cell lines (CCRF-CEM, CEM-DNR, K562, and K562-TAX) and, for comparison, nonmalignant BJ and MRC-5 fibroblasts. Concentrations inhibiting the cell growth by 50% (IC_{50}) were determined using a quantitative metabolic staining with 3-(4,5-dimethylthiazol-2-yl)-2,5-diphenyltetrazolium bromide (MTT)[31] following a 3-day treatment.

In addition, the antiproliferative effect was tested against a human T-lymphoblastic leukemia line CCRF-CEM, promyelocytic leukemia HL-60, and cervical carcinoma HeLa S3 growing in liquid suspension. Cell viability was determined following a 3-day incubation using 2,3-bis(2-methoxy-4-nitro-5-sulfophenyl)-2*H*-tetrazolium-5-carboxanilide (XTT) assay.[32]

Table 1 summarizes the cytotoxic activities of **2–26** in comparison with the previously published[5] 7-hetaryl-7-deazaadenosines **1a** and **1c**. In the 6-substituted series, the 7-(2-furyl) derivatives **2a**, **3a**, **4a**, and **6a** were the most potent, showing low nanomolar cytostatic effects similar to those of **1a** and **1c**, whereas the IC_{50} values of the bulkier 6-dimethylamino derivative **5a** were in micromolar range. These derivatives, however, were also the most cytotoxic to fibroblasts, suggesting a nonspecific cytotoxic effect. On the other hand, analogous 7-(3-furyl)-, 7-(2-thienyl)-, and 7-(3-thienyl) derivatives **2–6b**, **2–6c**, and **2–6d** were less active or inactive. The 6-methoxy derivatives **2b–d** still showed significant activities but with low toxicity to fibroblasts showing promissing in vitro therapeutic index. The more bulky 7-phenyl **2–6e** and 7-benzofuryl **2–6f** derivatives were generally inactive. On the other hand, 6-substituted 7-deazapurine nucleosides bearing a small ethynyl group at position 7 (**2–6g**) displayed considerable activity against several cell lines; in particular, the 6-methylsulfanyl derivative had a low nanomolar IC_{50} value against most tumor cells but had little effect on fibroblasts. The 7-unsubstituted derivatives **2–5h** (analogous to tubercidin) did not show a significant cytotoxic effect with the exception of 6-methyl derivative **6h**[12], which was the most cytotoxic compound of the entire set to both cancer cells and fibroblasts. The 7-deazahypoxanthine derivatives **7**, as well as all the 2-substituted derivatives **8–11**, were devoid of any significant cytotoxic effect. The unusual specific effect of 2-furyl and ethynyl substitution on cytostatic activity was the major difference from the rest of the 7-deazaadenosine **1a–g**, where all compounds bearing five-membered heterocyclic substituents exerted similar low nanomolar effects. On the other hand, the SAR analysis of

Table 1. Cytotoxic Activity and Antimycobacterial Activity of Compounds 2–26

	MTT, IC_{50} (μM)								XTT, IC_{50} (μM)			IC_{50} (μM)
compd	CCRF-CEM	CEM -DNR-bulk	K562	K562 -TAX	A549	HCT116	HCT116p53−/−	BJ	MRC-5	HepG2	HL60	HeLa S3	*Mycobacterium bovis*
1a[a]	0.04	0.21	0.04	0.05	0.03	0.03	0.17	18.3	36.5	–	11.6	0.05	17.4
1c[a]	0.02	0.17	0.03	0.02	0.04	0.01	0.06	65.6	39.4	–	0.95	0.02	4.73
2a	0.02	0.16	0.06	0.38	0.03	0.04	0.04	0.43	1.70	0.30	0.10	1.02	>100
2b	0.11	>20	0.19	2.82	1.16	0.11	0.13	28.8	29.4	0.29	0.15	1.79	>100
2c	0.09	12.1	0.07	6.20	4.85	0.08	0.44	62.8	43.2	13.9	0.08	1.76	>100
2d	2.57	7.64	0.09	3.45	5.17	0.12	0.14	64.3	75.3	0.43	0.13	3.35	>100
2e	>20	>20	>20	>20	>20	>20	>20	>100	>100	>20	>20	>20	>100
2f	5.37	10.8	20.9	13.1	17.7	13.8	14.5	22.4	65.6	>20	4.47	9.24	73.5
2g	>20	3.49	0.30	0.38	8.16	4.06	5.14	98.4	>100	12.7	0.19	1.73	>100
2h	>20	>20	>20	>20	>20	>20	>20	>100	>100	>20	>20	>20	>100
13	1.15	>20	>20	14.8	>20	>20	>20	91.0	63.0	>20	2.30	14.3	>100
3a	0.05	0.23	0.04	0.21	0.05	0.02	0.01	0.26	73.9	0.22	0.12	0.54	>100
3b	14.2	>20	0.06	3.25	0.28	0.04	0.10	98.8	>100	>15	0.36	5.39	>100
3c	>20	>20	11.6	>20	>20	>20	>20	96.9	>100	>20	1.13	1.96	>100
3d	>20	>20	0.45	>20	>20	>20	>20	95.8	>100	>15	4.59	>20	98.6
3e	>20	>20	>20	>20	>20	>20	>20	>100	>100	>20	>20	>20	>100
3f	>20	>20	17.2	>20	>20	>20	>20	67.2	70.8	>20	1.21	1.93	>100
3g	>20	0.11	0.03	0.07	0.14	0.03	0.09	68.6	>100	>15	0.05	0.11	>100
3h	>20	3.61	>20	0.10	>20	>20	>20	>100	>100	>20	7.19	11.9	96.8
14	>20	>20	10.5	7.73	>20	>20	>20	86.1	>100	>20	0.05	0.25	87.1
4a	0.18	>20	0.22	15.1	2.57	0.23	0.44	5.04	90.8	0.85	0.62	5.00	>100
4b	>20	>20	>20	>20	>20	>20	>20	96.3	>100	>20	>15	>20	>100
4c	>20	>20	>20	>20	>20	>20	>20	>100	>100	>20	>20	>20	>100
4d	>20	>20	>20	>20	>20	>20	>20	>100	>100	>20	>20	>20	>100
4e	>20	>20	>20	>20	>20	>20	>100	>100	>100	>20	>20	>20	>100
4f	>20	>20	>20	>20	>20	>20	>20	75.6	75.3	>20	8.95	>20	>100
4g	>20	18.5	>20	1.38	>20	>20	>20	86.0	>100	>15	9.06	>20	>100
4h	>20	4.89	>20	0.92	>20	>20	>20	91.4	97.8	>20	12.8	>20	87.1
15	>100	>20	>100	>20	>100	>100	>100	>100	>100	>20	>20	>20	99.9
5a	2.91	3.14	0.15	1.28	4.60	0.25	0.32	>100	>100	>15	0.22	1.19	>100
5b	13.3	>20	1.54	14.9	>20	>20	>20	99.2	>100	12.5	1.16	9.06	>100
5c	>20	>20	>20	>20	>20	>20	>20	>100	>100	>20	11.8	>20	>100
5d	3.48	>20	0.53	>20	>20	>20	>20	>100	>100	>20	1.92	>15	>100
5e	>20	>20	>20	>20	>100	>20	>20	>100	>100	>20	>20	>20	>100
5f	>20	>20	>20	>20	>20	>20	>20	>100	>100	>20	>20	>20	>100
5g	0.09	0.24	0.11	0.26	0.39	0.18	0.29	0.41	36.1	1.32	0.29	0.81	>100
5h	0.63	2.60	5.28	0.89	>20	18.4	5.09	5.30	58.2	1.81	0.87	10.6	>100
16	1.59	0.10	0.07	0.05	0.34	0.09	0.12	45.7	91.7	13.9	0.05	0.19	>100
6a	0.04	0.07	0.04	0.11	0.11	0.04	0.04	0.07	0.61	0.30	0.21	1.33	38.9
6b	>20	>20	>20	>20	>20	>20	>20	89.2	98.3	5.32	>15	>20	9.30
6c	>20	>20	>20	>20	>20	>20	>20	>100	>100	>15	5.73	>15	14.0
6d	11.2	8.56	0.32	5.55	>20	0.46	1.43	96.9	>100	4.72	0.35	14.3	18.5

dx.doi.org/10.1021/jm4018948 | J. Med. Chem. 2014, 57, 1097−1110

Table 1. continued

	MTT, IC_{50} (μM)									XTT, IC_{50} (μM)			
compd	CCRF-CEM	CEM -DNR-bulk	K562	K562 -TAX	A549	HCT116	HCT116p53−/−	BJ	MRC-5	HepG2	HL60	HeLa S3	IC_{50} (μM)*Mycobacterium bovis*
6e	>20	>20	>20	>20	>20	>100	95.3	>100	>100	>20	>20	>20	26.5
6f	17.3	>20	19.5	>20	>20	>20	>20	93.9	84.4	>20	>20	>20	2.10
6g	5.60	0.16	6.92	0.11	19.2	>20	>20	0.05	1.44	0.29	1.11	14.7	42.9
6h	0.01	0.05	0.01	0.05	0.03	0.03	0.06	0.07	0.09	0.06	0.02	0.02	0.30
20	5.48	12.6	17.8	>20	12.2	4.72	7.57	>100	13.3	3.46	2.65	4.08	51.4
19	15.0	>20	>20	15.8	>20	15.7	19.6	>100	24.4	5.55	7.24	13.8	20.8
7a	>20	>20	15.5	17.8	>20	18.3	>20	>100	>100	>15	2.20	5.78	>100
7b	9.03	>20	12.5	14.5	>20	10.3	14.8	>100	>100	12.1	6.37	>20	>100
7c	>20	>20	>20	>20	>20	>20	>20	>100	>100	>20	>20	>20	>100
7d	14.5	>20	>20	>20	>20	>20	>20	>100	>100	>15	12.0	>20	>100
7e	>100	>20	>20	>20	>100	>100	>20	>100	>100	>20	>20	>20	>100
7f	>20	>20	>20	>20	>20	>20	>20	62.7	>100	>20	>20	>20	>100
8a	>20	>20	>20	>20	>20	>20	>20	>100	>100	>20	>20	>20	84.0
8b	>20	>20	>20	>20	>20	>20	>20	>100	>100	>20	>20	>20	71.5
8c	>20	>20	>20	>20	>20	>20	>20	>100	>100	>20	>20	>20	2.44
8d	>20	>20	>20	>20	>100	>20	>20	>100	>100	>20	>20	>20	>100
8e	>20	>20	>20	>20	>20	>20	>20	>100	>100	>20	>15	>20	8.53
8f	>20	>20	18.6	>20	>20	>20	14.0	>100	78.5	>20	>15	>20	24.6
9a	>100	>20	>20	>20	>20	>20	>20	>100	>100	>20	>20	>20	>100
9b	>100	>20	>20	>20	>20	>20	>20	>100	>100	>20	>20	>20	>100
9c	>20	>20	>20	>20	>20	>20	>20	>100	>100	>20	>20	>20	82.7
9d	>20	>20	>20	>20	>20	>20	>20	>100	>100	>20	>20	>20	>100
9e	>20	>20	>20	>20	>20	>100	>20	>100	>100	>20	>20	>20	>100
9f	>20	6.31	15.7	4.99	>20	>20	13.1	>100	91.8	>20	>20	>20	>100
9g	>20	12.6	>20	3.29	>20	>20	>20	>100	>100	>20	>20	>20	>100
9h	>20	>20	>20	>20	>100	>20	>20	>100	>100	>20	>20	>20	>100
26	9.03	3.48	5.12	1.11	12.1	>20	>20	24.6	85.8	6.31	2.05	4.18	>100
10a	>20	>20	>20	>20	>20	>20	>20	>100	89.7	>20	>20	>20	>100
10b	>20	>20	>20	>20	>20	>20	>20	>100	>100	>20	>20	>20	>100
10c	>20	>20	>20	>20	>20	>20	>20	99.9	>100	>20	>20	>20	>100
10d	>20	>20	>20	>20	>100	>20	>20	>100	>100	>20	>20	>20	>100
10e	>20	>20	>20	>20	>20	>20	>20	>100	>100	>20	>20	>20	>100
10f	12.7	16.7	14.6	15.5	>20	>20	>20	25.6	22.7	>20	>20	>20	>100
10g	>100	>20	>20	>20	>100	>20	>20	>100	>100	>20	>20	>20	>100
11a	>20	>20	>20	>20	>20	>20	>20	>100	>100	>20	>20	>20	>100
11b	17.9	15.0	19.6	12.5	>20	14.2	17.6	21.5	86.1	>20	>15	10.7	>100
11c	>20	>20	>20	16.8	>20	>20	19.8	>100	>100	>20	>20	>20	>100
11d	>20	>20	>20	18.3	>20	>20	>20	>100	>100	>20	>20	>20	>100
11e	>100	>20	>20	>20	>100	>20	>20	>100	>100	>20	>20	>20	>100
11f	>20	>20	>20	>20	>100	>100	>100	>100	>100	>20	>20	>20	>100

[a]Compounds **1a,c** were reported in ref 5; the data presented here are from fresh retesting.

dx.doi.org/10.1021/jm401894f | J. Med. Chem. 2014, 57, 1097−1110

Table 2. Anti-HCV Activities of Selected Compounds[a]

	replicon 1B		replicon 2A	
	EC_{50} (μM)	CC_{50} (μM)	EC_{50} (μM)	CC_{50} (μM)
2a	0.02	>44	0.03	>44
2b	0.33	>44	8.28	>44
2c	1.08	>44	>44	>44
2d	0.55	>44	>44	>44
2e	20.98	>44	>44	>44
2f	2.64	>44	10.23	>44
2g	0.18	>44	>44	>44
3a	0.07	38.58	0.05	>44
3b	4.72	>44	>44	>44
3c	5.42	>44	>44	>44
3d	10.93	>44	>44	>44
3e	23.27	>44	>44	>44
3f	8.03	>44	29.64	>44
3g	0.21	>44	>44	>44
3h	29.89	>44	>44	>44
14	19.21	>44	>44	>44
4a	0.06	>44	0.14	>44
4b	35.93	>44	>44	>44
4f	2.05	>44	13.57	>44
4g	0.35	>44	>44	>44
4h	0.82	>44	>44	>44
5a	1.49	>44	1.35	>44
5b	7.88	>44	>44	>44
5c	16.76	>44	>44	>44
5d	38.41	>44	>44	>44
5e	26.88	>44	>44	>44
5f	19.20	>44	>44	>44
5g	0.07	>44	0.10	>44
5h	0.27	>44	0.97	>44
16	0.69	>44	>44	>44
6a	0.07	6.62	0.15	43.60
6b	4.43	>44	>44	>44
6c	6.67	>44	>44	>44
6d	4.47	>44	>44	>44
6e	34.83	>44	>44	>44
6f	6.76	>44	40.20	>44
6g	0.23	>44	21.60	>44
6h	0.02	0.23	0.02	0.12
20	2.16	20.85	8.75	13.81
19	12.01	35.61	20.74	28.17
7b	4.54	>44	22.34	>44
7d	14.35	>44	>44	>44
7f	7.21	>44	17.45	>44
8a	12.45	>44	n.t.[b]	n.t.
8b	21.29	>44	n.t.	n.t.
8c	10.03	>44	n.t.	n.t.
8f	5.58	>44	11.49	>44
9d	28.73	>44	>44	>44
9f	6.14	39.25	18.25	39.10
9g	8.00	>44	n.t.	n.t.
26	2.45	>44	>44	>44
10a	2.44	>44	n.t.	n.t.
10b	19.74	>44	n.t.	n.t.
10c	6.07	>44	n.t.	n.t.
10d	14.45	>44	n.t.	n.t.
10f	8.98	>44	20.66	>44
11b	25.66	>44	40.71	>44
11c	18.80	>44	n.t.	n.t.

[a]Compounds not listed in this table were inactive (EC_{50} and CC_{50} >44 μM). [b]n.t. = not tested.

the entire panel of compounds shows that the H-bond-donating NH_2 group at position 6 can be replaced by H-bond acceptor groups or even by an isosteric but nonpolar methyl group, with some analogues retaining high cytotoxic activity.

Multidrug resistance is a major therapeutic problem in cancer chemotherapy. It is associated with overexpression of drug transporters, typically multidrug resistance protein 1 (*mrp-1*), and multidrug resistance gene 1 (*mdr-1*), which transport drugs extracellularly in an ATP-dependent manner.[33] To assess efficacy of our compounds in multidrug resistant cancers, we have tested their cytotoxic potency in drug-resistant sublines derived from chemosensitive CCRF-CEM T-lymphoblastic and K562 myeloid leukemia cells. CEM daunorubicine-resistant (CEM-DNR-bulk) and K562 paclitaxel-resistant (K562-TAX) lines were originally prepared by increasing the concentration of cytotoxic compounds and then characterization. While CEM-DNR-bulk cells stabily overexpress *mrp-1*, K562-TAX cells express only *mdr-1* gene.[34] Unfortunately, the vast majority of cytotoxic compounds with submicromolar activity showed decreased potency in drug-resistant sublines over-expressing multidrug transporters. Similarly to the multidrug resistance phenomenon, functional inactivation of p53 tumor suppressor is associated with poor prognosis and therapeutic response in many cancers.[35] Therefore, we have evaluated in vitro therapeutic potency of nucleoside derivatives using isogenic colorectal cancer cells bearing wild type (HCT116) or deleted p53 gene (HCT116p53−/−). Interestingly, the compounds were equally toxic for tumor cells bearing wild-type or null alleles of p53 gene, indicating potential therapeutic activity in p53 mutant tumors.

Antimicrobial Activity. Antibacterial activity was tested against *Enterococcus faecalis* CCM 4224, *Staphylococcus aureus* CCM 3953, *Escherichia coli* CCM 3954, *Pseudomonas aeruginosa* CCM 3955, methicillin-resistant staphylococci (*Staphylococcus aureus* MRSA 4591 and *Staphylococcus haemolyticus* A/16568), multiresistant strains of *Escherichia coli* C/16702, and *Pseudomonas aeruginosa* A/16575. None of the tested compounds exerted any activity in these assays. None of the compounds showed antifungal activity against *Candida albicans*, *Candida parapsilosis*, *Candida crusei*, and *Candida tropicalis*. On the othe hand, significant antimycobacterial effects of several compounds against *Mycobacterium bovis* were found (Table 1, last column). The most active (but also most cytotoxic) was 6-methyl-7-deazapurine ribonucleoside **6h**. Bulky and nonpolar 7-benzofuryl-6-methyldeazapurine nucleoside **6f** and 2,6-diamino-7-thienyldeazapurine **8c** showed low micromolar antimycobacterial activity with no cytotoxicity, which makes them promising candidates for further development as antituberculotics.

Antiviral Activity. Compounds were also tested in Huh-7 cells harboring subgenomic reporter replicons derived from HCV subtypes 1B and 2A. Partial inhibition of the replicon reporter was observed with most of the compounds (Table 2). Activity correlated with cytotoxicity in most cases, suggesting

that the activity detected by the replicon assay was a reflection of interference with host target(s). Several 2,6-disubstituted 7-deazapurine nucleosides (e.g., **8f**, **26**, **10a**, **10c**, and **10f**) showed low micromolar anti-HCV effects without significant cytotoxicity.

Cell Cycle Analysis. Cell cycle analysis of selected compounds with low-micromolar cytotoxicity in cancer cells (**2a**, **2b**, **2c**, **2d**, **3a**, **4a**, **5a**, **5d**, **5g**, **13**, and **16**) was performed on CCRF-CEM lymphoblasts at the concentration corresponding to the IC_{50} after 24 h of incubation and compared to that of the previously published compound **1c** (Table 3). Some of the compounds induced major apoptosis (**2d**) as early as after 24 h. However, the major mechanism of action was inhibition of RNA synthesis (BrU incorporation), and all tested compounds (**1c**–**16**) were more active than parent compound **1c**. DNA synthesis was barely inhibited by compounds **3a**, **5d**, and **13**, and this most probably occurred via action at the level of cellular signaling and metabolic pathways. Cell cycle alterations (G1, S, G2/M) were not observed in treated cells under specified experimental conditions.

Table 3. Summary of Cell Cycle, Apoptosis (sub-G1), Mitosis ($pH3^+$), RNA (BrU+), and DNA (BrdU+) Synthesis Analysis[a]

	% of total cell populations						
	sub-G1	G1	S	G2/M	$pH3^{Ser10+}$	BrdU+	BrU+
control	9.6	41	44.8	14.2	1.4	50.1	43.3
1c	18.6	50.6	39.2	10.1	1.4	52.4	15.2
2a	6.8	42.8	44.3	12.9	1.4	45.3	13.8
2b	8.5	43.5	44.2	12.3	1.6	44.2	0.7
2c	7.5	41.5	48.7	9.8	1.1	38.6	0.1
2d	75	40.8	46.5	12.7	2.9	44.4	0.5
3a	7.9	43.5	45.3	11.3	0.7	29.5	5.0
4a	10.6	42.2	45.8	12.1	1.4	47.2	1.0
5a	10.2	31	53.6	15.4	1.5	50.6	0.4
5d	6.8	41.4	47.4	11.2	0.7	36.1	0.7
5g	8.9	38.5	46.8	14.7	1.3	43.4	8.6
13	6.0	37.9	49.2	12.9	0.9	38.9	0.2
16	9.4	39.8	46.7	13.5	1.3	48.7	4.8

[a]In CCRF-CEM cells treated with selected nucleosides at IC_{50} for 24 h.

■ CONCLUSIONS

Synthesis of a large series (80 derivatives) of diverse 6-substituted 7-(het)aryl- or 7-ethynyl-7-deazapurine ribonucleosides was developed, and a systematic biological activity screening was performed in comparison with the parent 7-(het)aryl-7-deazaadenosine series published previously.[5] Several title nucleosides, in particular 6-methoxy-, 6-methylsulfanyl-, 6-methylamino-, and 6-methyl-7-(2-furyl)-deazapurine nucleosides **2a**, **3a**, **4a**, and **6a**, as well as some 7-ethynyl derivatives **3g**, **5g**, and **6g**, have been found to possess cytostatic effects at low nanomolar concentrations with the potency comparable to **1a** and **1c**. On the other hand, most other derivatives were much less active compared to analogously substituted 7-deazaadenosines **1**. A striking difference was found in activities of certain 7-(2-furyl)- and 7-(2-thienyl)-7-deazapurine derivatives (compare highly active derivatives **3a**–**6a** with inactive derivatives **3c**–**6c**, whereas the parent compounds **1a** and **1c** showed comparably high cytostatic/cytotoxic effects). This can be attributed to the higher polarity of the furyl substituent (compared to thienyl), resulting in lower expected log *P* values. However, this difference suggests that the mechanism of action of compounds **1a**–**d** may not necessarily be the same as that of **2**–**6**. All the 7-deazahypoxanthine derivatives, as well as all the 2-substituted derivatives, were inactive. The compounds inhibited RNA synthesis in treated cells and induced apoptosis at their cytotoxic concentrations. Nonetheless, molecular target(s) identification requires additional investigation.

None of the title compounds showed antibacterial or antifungal effects, but some compounds (i.e., **6f** and **8c**) showed promising activity against *Mycobacterium bovis*. Most of the compounds also exerted a significant (and mostly nonspecific) anti-HCV effect in a replicon assay accompanied by cytotoxicity, but some derivatives showed a low micromolar anti-HCV effect without in vitro toxicity.

■ EXPERIMENTAL SECTION

General. NMR spectra were recorded on a 400 MHz (^{1}H at 400 MHz, ^{13}C at 100.6 MHz), a 500 MHz (^{1}H at 500 MHz, ^{13}C at 125.7 MHz), or a 600 MHz (^{1}H at 600 MHz, ^{13}C at 150.9 MHz) spectrometer. Melting points were determined on a Kofler block and are uncorrected. Optical rotations were measured at 25 °C, and $[\alpha]_D^{20}$ values are given in 10^{-1} deg cm^2 g^{-1}. High resolution mass spectra were measured using electrospray ionization. Reverse-phase high performance flash chromatography (HPFC) was performed on KP-C18-HS columns with Biotage SP1 system, and the sample was loaded as a solution in pure water or in water/DMSO (5:1) mixture. FT IR spectra were measured on a Bruker Alpha spectrometer using the ATR technique. The purity of all tested compounds was confirmed by HPLC analysis and was >95%.

*5-Iodo-4-methylsulfanyl-7-(β-D-ribofuranosyl)-7H-pyrrolo[2,3-d]pyrimidine (**14**).* A mixture of 4-chloro-5-iodo-7-(2,3,5-tri-*O*-benzoyl-β-D-ribofuranosyl)-7*H*-pyrrolo[2,3-*d*]pyrimidine **12**[13] (5.37 g, 7.42 mmol) and sodium thiomethoxide (1.1 g, 15.7 mmol) in EtOH (150 mL) was stirred at rt for 4 h. The volatiles were removed in vacuo, and the residue was coevaporated several times with water and crystallized from water to furnish **14** (2.94 g, 94%) as a white solid. Mp 217–219 °C. $[\alpha]^{20}_D$ −69.8 (*c* 0.242, DMSO). ^{1}H NMR (500 MHz, DMSO-d_6): 2.63 (s, 3H, CH_3S); 3.55 (ddd, 1H, J_{gem} = 12.0 Hz, $J_{5'a,OH}$ = 5.5 Hz, $J_{5'a,4'}$ = 4.0 Hz, H-5′a); 3.63 (ddd, 1H, J_{gem} = 12.0 Hz, $J_{5'b,OH}$ = 5.2 Hz, $J_{5'b,4'}$ = 4.0 Hz, H-5′b); 3.91 (bq, 1H, $J_{4',5'a}$ = $J_{4',5'b}$ = $J_{4',3'}$ = 3.6 Hz, H-4′); 4.09 (m, 1H, H-3′); 4.36 (m, 1H, H-2′); 5.09 (bt, 1H, $J_{OH,5'a}$ = $J_{OH,5'b'}$ = 5.4 Hz, OH-5′); 5.18 (bd, 1H, $J_{OH,3'}$ = 3.9 Hz, OH-3′); 5.40 (bs, 1H, OH-2′); 6.15 (d, 1H, $J_{1',2'}$ = 6.2 Hz, H-1′); 7.99 (s, 1H, H-6); 8.62 (s, 1H, H-2). ^{13}C NMR (125.7 MHz, DMSO-d_6): 12.13 (CH_3S); 53.17 (C-5); 61.56 (CH_2-5′); 70.62 (CH-3′); 74.38 (CH-2′); 85.54 (CH-4′); 86.77 (CH-1′); 117.20 (C-4a); 130.87 (CH-6); 148.74 (C-7a); 150.86 (CH-2); 161.82 (C-4). IR (ATR): ν 3386, 3132, 1556, 1449, 1220, 1113, 1066, 954, 492 cm^{-1}. MS (ESI) *m*/*z* 424 (M + H), 446 (M + Na). HRMS (ESI) for $C_{12}H_{13}IN_3O_4S$ [M + H] calcd: 423.98279; found: 423.98216. Anal. ($C_{12}H_{14}IN_3O_4S^{\cdot 3}/_4H_2O$): C, H, N.

*5-Iodo-4-methylamino-7-(β-D-ribofuranosyl)-7H-pyrrolo[2,3-d]pyrimidine (**15**).* A mixture of 4-chloro-5-iodo-7-(2,3,5-tri-*O*-benzoyl-β-D-ribofuranosyl)-7*H*-pyrrolo[2,3-*d*]pyrimidine **12**[13] (2.4 g, 3.31 mmol) in methylamine (33 wt % in absolute EtOH, 25 mL) was stirred in a pressure tube at 100 °C for 5 h. After cooling, the mixture was evaporated to dryness and purified by column chromatography (SiO_2, 3% MeOH in chloroform) to afford **15** (1.24 g, 92%) as a white solid. Crystallization from MeOH afforded colorless needles. Mp 218–223 °C. $[\alpha]^{20}_D$ −61.3 (*c* 0.419, DMSO). ^{1}H NMR (500 MHz, DMSO-d_6): 3.02 (d, 3H, $J_{CH3,NH}$ = 4.7 Hz, CH_3); 3.52 (ddd, 1H, J_{gem} = 12.0 Hz, $J_{5'a,OH}$ = 6.1 Hz, $J_{5'a,4'}$ = 3.8 Hz, H-5′a); 3.61 (ddd, 1H, J_{gem} = 12.0 Hz, $J_{5'b,OH}$ = 5.1 Hz, $J_{5'b,4'}$ = 3.8 Hz, H-5′b); 3.88 (bq, 1H, $J_{4',5'a}$ = $J_{4',5'b}$ = $J_{4',3'}$ = 3.5 Hz, H-4′); 4.06 (td, 1H, $J_{3',2'}$ = $J_{3',OH}$ = 4.9 Hz, $J_{3',4'}$ = 3.1 Hz, H-3′); 4.35 (td, 1H, $J_{2',1'}$ = $J_{2',OH}$ = 6.4 Hz, $J_{2',3'}$ = 5.1 Hz, H-2′); 5.12 (d, 1H, $J_{OH,3'}$ = 4.7 Hz, OH-3′); 5.16 (dd, 1H, $J_{OH,5'a}$ = 6.1 Hz, $J_{OH,5'b'}$ = 5.1 Hz, OH-5′); 5.31 (d, 1H, $J_{OH,2'}$ = 6.5 Hz, OH-2′); 6.03

(d, 1H, $J_{1',2'}$ = 6.3 Hz, H-1′); 6.44 (q, 1H, J_{NH,CH_3} = 4.7 Hz, NH); 7.66 (s, 1H, H-6); 8.19 (s, 1H, H-2). ^{13}C NMR (125.7 MHz, DMSO-d_6): 27.90 (CH_3NH); 51.25 (C-5); 61.74 (CH_2-5′); 70.70 (CH-3′); 74.10 (CH-2′); 85.37 (CH-4′); 86.99 (CH-1′); 103.73 (C-4a); 127.17 (CH-6); 149.70 (C-7a); 152.07 (CH-2); 156.62 (C-4). IR (ATR): ν 3387, 3323, 1603, 1550, 1305, 1090, 866, 596 cm^{-1}. MS (ESI) m/z 407 (M + H), 429 (M + Na). HRMS (ESI) for $C_{12}H_{16}IN_4O_4$ [M + H] calcd: 407.02162; found: 407.02111. Anal. ($C_{12}H_{15}IN_4O_4$): C, H, N.

*4-Dimethylamino-5-iodo-7-(β-D-ribofuranosyl)-7H-pyrrolo[2,3-d]pyrimidine (**16**).* A mixture of 4-chloro-5-iodo-7-(2,3,5-tri-*O*-benzoyl-β-D-ribofuranosyl)-7*H*-pyrrolo[2,3-*d*]pyrimidine **12**[13] (5.79 g, 8 mmol), aq dimethylamine (40% w/w, 10 mL) in dioxane (10 mL) was stirred in a steel bomb at 120 °C for 8 h. After cooling, the mixture was evaporated to dryness and the residue was coevaporated several times with water. Crystallization from water afforded **16** (2.84 g, 84%) as white needles. Mp 195−197 °C. $[\alpha]_D$ −39.0 (*c* 0.290, DMSO). ^{1}H NMR (500 MHz, DMSO-d_6): 3.16 (s, 6H, $(CH_3)_2$N); 3.54 (ddd, 1H, J_{gem} = 11.9 Hz, $J_{5'a,OH}$ = 5.8 Hz, $J_{5'a,4'}$ = 3.8 Hz, H-5′a); 3.62 (ddd, 1H, J_{gem} = 11.9 Hz, $J_{5'b,OH}$ = 5.2 Hz, $J_{5'b,4'}$ = 3.9 Hz, H-5′b); 3.89 (bq, 1H, $J_{4',5'a}$ = $J_{4',5'b}$ = $J_{4',3'}$ = 3.5 Hz, H-4′); 4.07 (td, 1H, $J_{3',2'}$ = $J_{3',OH}$ = 5.0 Hz, $J_{3',4'}$ = 3.2 Hz, H-3′); 4.36 (td, 1H, $J_{2',1'}$ = $J_{2',OH}$ = 6.3 Hz, $J_{2',3'}$ = 5.1 Hz, H-2′); 5.13 (t, 1H, $J_{OH,5'a}$ = $J_{OH,5'b}$ = 5.5 Hz, OH-5′); 5.13 (d, 1H, $J_{OH,3'}$ = 4.7 Hz, OH-3′); 5.33 (d, 1H, $J_{OH,2'}$ = 6.4 Hz, OH-2′); 6.11 (d, 1H, $J_{1',2'}$ = 6.3 Hz, H-1′); 7.86 (s, 1H, H-6); 8.24(s, 1H, H-2). ^{13}C NMR (125.7 MHz, DMSO-d_6): 43.28 ($(CH_3)_2$N); 53.85 (C-5); 61.66 (CH_2-5′); 70.65 (CH-3′); 74.12 (CH-2′); 85.36 (CH-4′); 86.77 (CH-1′); 106.62 (C-4a); 129.62 (CH-6); 150.46 (CH-2); 152.13 (C-7a); 160.31 (C-4). IR (ATR): ν 1580, 1536, 1422, 1222, 1127, 1060, 1013, 947, 760, 600 cm^{-1}. MS (ESI) m/z 421 (M + H), 443 (M + Na). HRMS (ESI) for $C_{13}H_{18}N_4O_4I$ [M + H] calcd: 421.03672; found: 421.03663. Anal. ($C_{13}H_{17}N_4O_4I$): C, H, N.

*5-Bromo-4-methyl-7-(β-D-ribofuranosyl)-7H-pyrrolo[2,3-d]-pyrimidine (**19**).* To a stirred solution of **6h**[12] (1061 mg, 4 mmol) in DMF (10 mL) was added dropwise *N*-bromosuccinimide (748 mg, 4.2 mmol) in DMF (4 mL) within 3 min. The mixture was stirred at rt for 40 min followed by addition of solid Na_2SO_3 (50 mg) and dilution with water (66 mL). This solution was separated (in portions according to column capacity) using reverse-phase HPFC (C-18, 0→100% MeOH in water) to obtain a crude product, which after crystallization from iPrOH afforded **19** (913 mg, 66%) as white solid. Mp 188−189 °C. $[\alpha]_D$ −61.1 (*c* 0.229, DMSO). ^{1}H NMR (500 MHz, DMSO-d_6): 2.85 (s, 3H, CH_3); 3.55 (ddd, 1H, J_{gem} = 11.9 Hz, $J_{5'a,OH}$ = 5.5 Hz, $J_{5'a,4'}$ = 4.0 Hz, H-5′a); 3.64 (ddd, 1H, J_{gem} = 11.9 Hz, $J_{5'b,OH}$ = 5.2 Hz, $J_{5'b,4'}$ = 4.1 Hz, H-5′b); 3.91 (bq, 1H, $J_{4',5'a}$ = $J_{4',5'b}$ = $J_{4',3'}$ = 3.6 Hz, H-4′); 4.10 (td, 1H, $J_{3',2'}$ = $J_{3',OH}$ = 4.9 Hz, $J_{3',4'}$ = 3.3 Hz, H-3′); 4.38 (td, 1H, $J_{2',1'}$ = $J_{2',OH}$ = 6.2 Hz, $J_{2',3'}$ = 5.1 Hz, H-2′); 5.10 (t, 1H, $J_{OH,5'a}$ = $J_{OH,5'b}$ = 5.4 Hz, OH-5′); 5.19 (d, 1H, $J_{OH,3'}$ = 4.8 Hz, OH-3′); 5.40 (d, 1H, $J_{OH,2'}$ = 6.3 Hz, OH-2′); 6.21 (d, 1H, $J_{1',2'}$ = 6.2 Hz, H-1′); 8.06 (s, 1H, H-6); 8.70 (s, 1H, H-2). ^{13}C NMR (125.7 MHz, DMSO-d_6): 21.14 (CH_3); 61.58 (CH_2-5′); 70.64 (CH-3′); 74.33 (CH-2′); 85.54 (CH-4′); 86.66 (CH-1′); 88.18 (C-5); 115.68 (C-4a); 126.38 (CH-6); 149.75 (C-7a); 151.65 (CH-2); 159.54 (C-4). IR (ATR): ν 1593, 1563, 1345, 1211, 1119, 1092, 1058, 1032, 968, 921, 787 cm^{-1}. MS (ESI) m/z 344 (M + H), 366 (M + Na). HRMS (ESI) for $C_{12}H_{15}N_3O_4Br$ [M + H] calcd: 344.02405; found: 344.02407. Anal. ($C_{12}H_{14}N_3O_4Br$): C, H, N.

*5-Iodo-4-methyl-7-(β-D-ribofuranosyl)-7H-pyrrolo[2,3-d]-pyrimidine (**20**).* To a stirred solution of **6h** (796 mg, 3 mmol) in DMF (7 mL) was added dropwise *N*-iodosuccinimide (709 mg, 3.15 mmol) in DMF (3 mL) within 3 min. The mixture was stirred at rt for 16 h followed by addition of solid Na_2SO_3 (50 mg) and dilution with water (50 mL). This solution was directly separated (in portions according to column capacity) using reverse phase HPFC (C-18, 0→100% MeOH in water) to afford **20** (685 mg, 58%) as a white solid after crystallization from water. HPFC also recovered starting **6h** (145 mg, 18%). Mp 187−188 °C. $[\alpha]_D$ −58.3 (*c* 0.365, DMSO). ^{1}H NMR (500 MHz, DMSO-d_6): 2.88 (s, 3H, CH_3); 3.55 (ddd, 1H, J_{gem} = 11.9 Hz, $J_{5'a,OH}$ = 5.6 Hz, $J_{5'a,4'}$ = 3.9 Hz, H-5′a); 3.64 (ddd, 1H, J_{gem} = 11.9 Hz, $J_{5'b,OH}$ = 5.3 Hz, $J_{5'b,4'}$ = 4.0 Hz, H-5′b); 3.91 (btd, 1H, $J_{4',5'a}$ = $J_{4',5'b}$ = 3.9 Hz, $J_{4',3'}$ = 3.2 Hz, H-4′); 4.09 (td, 1H, $J_{3',2'}$ = $J_{3',OH}$ = 5.0 Hz, $J_{3',4'}$ = 3.2 Hz, H-3′); 4.38 (td, 1H, $J_{2',1'}$ = $J_{2',OH}$ = 6.3 Hz, $J_{2',3'}$ = 5.1 Hz, H-2′); 5.10 (t, 1H, $J_{OH,5'a}$ = $J_{OH,5'b}$ = 5.5 Hz, OH-5′); 5.18 (d, 1H, $J_{OH,3'}$ = 4.8 Hz, OH-3′); 5.38 (d, 1H, $J_{OH,2'}$ = 6.4 Hz, OH-2′); 6.18 (d, 1H, $J_{1',2'}$ = 6.2 Hz, H-1′); 8.06 (s, 1H, H-6); 8.66 (s, 1H, H-2). ^{13}C NMR (125.7 MHz, DMSO-d_6): 20.74 (CH_3); 54.05 (C-5); 61.61 (CH_2-5′); 70.67 (CH-3′); 74.30 (CH-2′); 85.52 (CH-4′); 86.66 (CH-1′); 118.04 (C-4a); 131.65 (CH-6); 150.27 (C-7a); 151.17 (CH-2); 159.76 (C-4). IR (ATR): ν 1584, 1562, 1347, 1335, 1207, 1122, 1078, 1059, 1031, 1000, 893 cm^{-1}. MS (ESI) m/z 392 (M + H), 414 (M + Na). HRMS (ESI) for $C_{12}H_{15}N_3O_4I$ [M + H] calcd: 392.01018; found: 392.01014. Anal. ($C_{12}H_{14}N_3O_4I$): C, H, N.

*5-(Furan-2-yl)-4-methoxy-7-(β-D-ribofuranosyl)-7H-pyrrolo[2,3-d]pyrimidine (**2a**).* An argon-purged mixture of **13**[13] (794 mg, 1.95 mmol), furan-2-boronic acid (328 mg, 2.93 mmol), Na_2CO_3 (620 mg, 5.85 mmol), $Pd(OAc)_2$ (22 mg, 98 μmol), and TPPTS (136 mg, 0.24 mmol) in water/MeCN (2:1, 10 mL) was stirred at 100 °C for 3 h. After cooling, the mixture was neutralized using aq HCl (1 M) and concentrated to dryness in vacuo and the residue purified by reverse phase HPFC (C-18, 0→100% MeOH in water). Repurification by column chromatography (SiO_2, 2.5% MeOH in chloroform) furnished **2a** (507 mg, 75%) as a beige solid, which was crystallized from water/MeOH. Mp 155−157 °C. $[\alpha]_D$ −78.2 (*c* 0.317, DMSO). ^{1}H NMR (500 MHz, DMSO-d_6): 3.58 (dd, 1H, J_{gem} = 11.9 Hz, $J_{5'a,4'}$ = 3.6 Hz, H-5′a); 3.65 (dd, 1H, J_{gem} = 11.9 Hz, $J_{5'b,4'}$ = 3.7 Hz, H-5′b); 3.94 (bq, 1H, $J_{4',5'a}$ = $J_{4',5'b}$ = $J_{4',3'}$ = 3.5 Hz, H-4′); 4.11 (s, 3H, CH_3O); 4.13 (dd, 1H, $J_{3',2'}$ = 5.0 Hz, $J_{3',4'}$ = 3.2 Hz, H-3′); 4.44 (bt, 1H, $J_{2',1'}$ = $J_{2',3'}$ = 5.6 Hz, H-2′); 5.14 (bs, 1H, OH-5′); 5.18 (bs, 1H, OH-3′); 5.38 (bs, 1H, OH-2′); 6.22 (d, 1H, $J_{1',2'}$ = 6.2 Hz, H-1′); 6.57 (dd, 1H, $J_{4,3}$ = 3.3 Hz, $J_{4,5}$ = 1.9 Hz, H-4-furyl); 6.93 (dd, 1H, $J_{3,4}$ = 3.3 Hz, $J_{3,5}$ = 0.9 Hz, H-3-furyl); 7.67 (dd, 1H, $J_{5,4}$ = 1.9 Hz, $J_{5,3}$ = 0.9 Hz, H-5-furyl); 7.98 (s, 1H, H-6); 8.47 (s, 1H, H-2). ^{13}C NMR (125.7 MHz, DMSO-d_6): 54.05 (CH_3O); 61.65 (CH_2-5′); 70.79 (CH-3′); 74.41 (CH-2′); 85.51 (CH-4′); 87.08 (CH-1′); 101.50 (C-4a); 107.17 (C-5); 107.42 (CH-3-furyl); 111.92 (CH-4-furyl); 121.09 (CH-6); 141.81 (CH-5-furyl); 148.27 (CH-2-furyl); 151.52 (CH-2); 152.54 (C-7a); 162.76 (C-4). IR (ATR): ν 1590, 1563, 1120, 1080, 1063, 1012, 795, 744 cm^{-1}. MS (ESI) m/z 348 (M + H), 370 (M + Na). HRMS (ESI) for $C_{16}H_{18}N_3O_6$ [M + H] calcd: 348.11901; found: 348.11899. Anal. ($C_{16}H_{17}N_3O_6$·1/4H_2O): C, H, N.

*5-(Furan-2-yl)-4-methylsulfanyl-7-(β-D-ribofuranosyl)-7H-pyrrolo[2,3-d]pyrimidine (**3a**).* An argon-purged mixture of **14** (313 mg, 0.74 mmol), furan-2-boronic acid (124 mg, 1.11 mmol), Na_2CO_3 (235 mg, 2.22 mmol), $Pd(OAc)_2$ (8 mg, 36 μmol) and TPPTS (53 mg, 0.093 mmol) in water/MeCN (2:1, 4 mL) was stirred at 100 °C for 1 h. After cooling the mixture was neutralized using aq HCl (1 M) and concentrated by evaporation. The residue was coevaporated with silica and purified by column chromatography (SiO_2, 1→3% MeOH in $CHCl_3$). Repurification by reverse-phase HPFC (C-18, 0→100% MeOH in water) and crystallization from water/MeOH afforded **3a** (123 mg, 46%) as a yellowish solid. Mp 150−152 °C. $[\alpha]^{20}_D$ −70.5 (*c* 0.237, DMSO). ^{1}H NMR (500 MHz, DMSO-d_6): 2.59 (s, 3H, CH_3S); 3.56 (ddd, 1H, J_{gem} = 12.0 Hz, $J_{5'a,OH}$ = 5.6 Hz, $J_{5'a,4'}$ = 3.8 Hz, H-5′a); 3.65 (ddd, 1H, J_{gem} = 12.0 Hz, $J_{5'b,OH}$ = 5.3 Hz, $J_{5'b,4'}$ = 3.9 Hz, H-5′b); 3.93 (bq, 1H, $J_{4',5'a}$ = $J_{4',5'b}$ = $J_{4',3'}$ = 3.6 Hz, H-4′); 4.12 (td, 1H, $J_{3',2'}$ = $J_{3',OH}$ = 5.0 Hz, $J_{3',4'}$ = 3.3 Hz, H-3′); 4.42 (td, 1H, $J_{2',1'}$ = $J_{2',OH}$ = 6.2 Hz, $J_{2',3'}$ = 5.1 Hz, H-2′); 5.10 (t, 1H, $J_{OH,5'a}$ = $J_{OH,5'b}$ = 5.4 Hz, OH-5′); 5.19 (d, 1H, $J_{OH,3'}$ = 4.8 Hz, OH-3′); 5.42 (d, 1H, $J_{OH,2'}$ = 6.3 Hz, OH-2′); 6.23 (d, 1H, $J_{1',2'}$ = 6.1 Hz, H-1′); 6.60 (dd, 1H, $J_{4,3}$ = 3.3 Hz, $J_{4,5}$ = 1.9 Hz, H-4-furyl); 6.71 (dd, 1H, $J_{3,4}$ = 3.3 Hz, $J_{3,5}$ = 0.9 Hz, H-3-furyl); 7.78 (dd, 1H, $J_{5,4}$ = 1.9 Hz, $J_{5,3}$ = 0.9 Hz, H-5-furyl); 8.01 (s, 1H, H-6); 8.68 (s, 1H, H-2). ^{13}C NMR (125.7 MHz, DMSO-d_6): 12.21 (CH_3S); 61.58 (CH_2-5′); 70.68 (CH-3′); 74.42 (CH-2′); 85.54 (CH-4′); 86.92 (CH-1′); 106.61 (C-5); 109.18 (CH-3-furyl); 111.68 (CH-4-furyl); 113.63 (C-4a); 125.13 (CH-6); 142.90 (CH-5-furyl); 146.82 (C-2-furyl); 148.92 (C-7a); 150.91 (CH-2); 161.69 (C-4). IR (ATR): ν 3166, 2937, 2903, 1547, 1446, 1062, 1029, 976, 594 cm^{-1}. MS (ESI) m/z 364 (M + H), 386 (M + Na). HRMS (ESI) for $C_{16}H_{18}N_3O_5S$ [M + H] calcd: 364.09672; found: 364.09609.

*5-(Furan-2-yl)-4-methylamino-7-(β-D-ribofuranosyl)-7H-pyrrolo-[2,3-d]pyrimidine (**4a**).* An argon-purged mixture of **15** (300 mg, 0.74

mmol), furan-2-boronic acid (124 mg, 1.11 mmol), Na_2CO_3 (235 mg, 2.22 mmol), $Pd(OAc)_2$ (8 mg, 36 μmol), and TPPTS (53 mg, 0.093 mmol) in water/MeCN (2:1, 4 mL) was stirred at 100 °C for 1 h. After cooling, the mixture was neutralized using aq HCl (1 M) and concentrated to dryness. The residue was coevaporated with silica and purified by column chromatography (SiO_2, 1→3% MeOH in $CHCl_3$) to afford product **4a** (220 mg, 86%) as a white solid, which was crystallized from water/MeOH. Mp 114−117 °C. $[\alpha]^{20}_D$ −70.6 (*c* 0.299, DMSO). ^{1}H NMR (500 MHz, DMSO-d_6): 3.04 (d, 3H, J_{CH_3NH} = 4.8 Hz, CH_3); 3.54 (dm, 1H, J_{gem} = 12.0 Hz, H-5′a); 3.64 (dm, 1H, J_{gem} = 11.9 Hz, H-5′b); 3.91 (q, 1H, $J_{4',5'a} = J_{4',5'b} = J_{4',3'}$ = 3.6 Hz, H-4′); 4.10 (td, 1H, $J_{3',2'} = J_{3',OH}$ = 4.9 Hz, $J_{3',4'}$ = 3.3 Hz, H-3′); 4.41 (td, 1H, $J_{2',1'} = J_{2',OH}$ = 6.3 Hz, $J_{2',3'}$ = 5.2 Hz, H-2′); 5.18 (d, 1H, $J_{OH,3'}$ = 4.8 Hz, OH-3′); 5.25 (m, 1H, OH-5′); 5.37 (d, 1H, $J_{OH,2'}$ = 6.4 Hz, OH-2′); 6.09 (d, 1H, $J_{1',2'}$ = 6.2 Hz, H-1′); 6.61 (dd, 1H, $J_{4,3}$ = 3.3 Hz, $J_{4,5}$ = 1.9 Hz, H-4-furyl); 6.66 (dd, 1H, $J_{3,4}$ = 3.3 Hz, $J_{3,5}$ = 0.8 Hz, H-3-furyl); 6.85 (q, 1H, $J_{NH,CH3}$ = 4.8 Hz, NH); 7.76 (dd, 1H, $J_{5,4}$ = 1.9 Hz, $J_{5,3}$ = 0.8 Hz, H-5-furyl); 7.82 (s, 1H, H-6); 8.22 (s, 1H, H-2). ^{13}C NMR (125.7 MHz, DMSO-d_6): 28.24 (CH_3NH); 61.92 (CH_2-5′); 70.81 (CH-3′); 74.12 (CH-2′); 85.45 (CH-4′); 87.31 (CH-1′); 100.03 (C-4a); 105.59 (CH-3-furyl); 106.35 (C-5); 112.20 (CH-4-furyl); 120.52 (CH-6); 142.39 (CH-5-furyl); 148.79 (C-2-furyl); 150.34 (C-7a); 152.27 (CH-2); 156.84 (C-4). IR (ATR): ν 3649, 2934, 1624, 1319, 1021, 585, 564 cm^{-1}. MS (ESI) *m*/*z* 347 (M + H), 369 (M + Na). HRMS (ESI) for $C_{16}H_{19}N_4O_5$ [M + H] calcd: 347.13554; found: 347.13496.

*4-Dimethylamino-5-(furan-2-yl)-7-(β-D-ribofuranosyl)-7H-pyrrolo[2,3-d]pyrimidine (**5a**).* An argon-purged mixture of iodide **16** (420 mg, 1 mmol), furan-2-boronic acid (168 mg, 1.5 mmol), Na_2CO_3 (318 mg, 3 mmol), $Pd(OAc)_2$ (11 mg, 49 μmol), and TPPTS (71 mg, 0.125 mmol) in water/MeCN (2:1, 5 mL) was stirred at 100 °C for 3 h. After cooling, the mixture was neutralized using aq HCl (1 M), concentrated to dryness in vacuo and the residue was purified by reverse phase HPFC (C-18, 0→100% MeOH in water). Repurification by column chromatography (SiO_2, 2.5% MeOH in chloroform) furnished **5a** (176 mg, 49%) as a beige foam. Reverse phase HPFC also provided product of reduction **5h** (73 mg, 25%). Mp 97−103 °C. $[\alpha]_D$ −42.8 (*c* 0.358, DMSO). ^{1}H NMR (500 MHz, DMSO-d_6): 2.84 (s, 6H, $(CH_3)_2N$); 3.54 (ddd, 1H, J_{gem} = 11.9 Hz, $J_{5'a,OH}$ = 6.0 Hz, $J_{5'a,4'}$ = 3.8 Hz, H-5′a); 3.62 (ddd, 1H, J_{gem} = 11.9 Hz, $J_{5'b,OH}$ = 5.1 Hz, $J_{5'b,4'}$ = 3.8 Hz, H-5′b); 3.90 (btd, 1H, $J_{4',5'a} = J_{4',5'b}$ = 3.8 Hz, $J_{4',3'}$ = 3.2 Hz, H-4′); 4.10 (m, 1H, H-3′); 4.42 (td, 1H, $J_{2',1'} = J_{2',OH}$ = 6.4 Hz, $J_{2',3'}$ = 5.1 Hz, H-2′); 5.14 (d, 1H, $J_{OH,3'}$ = 4.8 Hz, OH-3′); 5.15 (dd, 1H, $J_{OH,5'a}$ = 5.9 Hz, $J_{OH,5'b}$ = 5.1 Hz, OH-5′); 5.35 (d, 1H, $J_{OH2'}$ = 6.5 Hz, OH-2′); 6.17 (d, 1H, $J_{1',2'}$ = 6.4 Hz, H-1′); 6.51 (dd, 1H, $J_{3,4}$ = 3.2 Hz, $J_{3,5}$ = 0.9 Hz, H-3-furyl); 6.58 (dd, 1H, $J_{4,3}$ = 3.2 Hz, $J_{4,5}$ = 1.9 Hz, H-4-furyl); 7.75 (dd, 1H, $J_{5,4}$ = 1.9 Hz, $J_{5,3}$ = 0.9 Hz, H-5-furyl); 7.75 (s, 1H, H-6); 8.25 (s, 1H, H-2). ^{13}C NMR (125.7 MHz, DMSO-d_6): 39.44 ($(CH_3)_2N$); 61.73 (CH_2-5′); 70.74 (CH-3′); 74.10 (CH-2′); 85.35 (CH-4′); 86.98 (CH-1′); 102.05 (C-4a); 106.87 (C-5); 107.61 (CH-3-furyl); 111.74 (CH-4-furyl); 122.92 (CH-6); 142.56 (CH-5-furyl); 149.33 (C-2-furyl); 150.71 (CH-2); 152.01 (C-7a); 159.64 (C-4). IR (ATR): ν 1574, 1515, 1450, 1420, 1410, 1203, 1120, 1077, 1058 cm^{-1}. MS (ESI) *m*/*z* 361 (M + H), 383 (M + Na). HRMS (ESI) for $C_{17}H_{21}N_4O_5$ [M + H] calcd: 361.15065; found: 361.15057.

*5-(Furan-2-yl)-4-methyl-7-(β-D-ribofuranosyl)-7H-pyrrolo[2,3-d]pyrimidine (**6a**).* An argon-purged mixture of **19** (258 mg, 0.75 mmol), furan-2-boronic acid (126 mg, 1.125 mmol), Na_2CO_3 (239 mg, 2.25 mmol), $Pd(OAc)_2$ (8 mg, 35.6 μmol), and TPPTS (53 mg, 93 μmol) in water/MeCN (2:1, 5 mL) was stirred at 100 °C for 1 h. After cooling, the mixture was neutralized using aq HCl (1 M), concentrated to dryness in vacuo and the residue was purified by reverse phase HPFC (C-18, 0→100% MeOH in water) to furnish **6a** (207 mg, 83%) as an orange foam. $[\alpha]_D$ −75.3 (*c* 0.219, DMSO). ^{1}H NMR (500 MHz, DMSO-d_6): 2.65 (s, 3H, CH_3); 3.57 (bdt, 1H, J_{gem} = 11.9 Hz, $J_{5'a,OH} = J_{5'a,4'}$ = 4.5 Hz, H-5′a); 3.66 (bdt, 1H, J_{gem} = 11.9 Hz, $J_{5'b,OH} = J_{5'b,4'}$ = 4.4 Hz, H-5′b); 3.94 (bq, 1H, $J_{4',5'a} = J_{4',5'b} = J_{4',3'}$ = 3.6 Hz, H-4′); 4.13 (m, 1H, H-3′); 4.45 (btd, 1H, $J_{2',1'} = J_{2',OH}$ = 6.2 Hz, $J_{2',3'}$ = 5.3 Hz, H-2′); 5.10 (bt, 1H, $J_{OH,5'a} = J_{OH,5'b}$ = 5.4 Hz, OH-5′); 5.20 (d, 1H, $J_{OH,3'}$ = 4.8 Hz, OH-3′); 5.41 (d, 1H, $J_{OH,2'}$ = 6.4 Hz, OH-2′); 6.26 (d, 1H, $J_{1',2'}$ = 6.1 Hz, H-1′); 6.62 (dd, 1H, $J_{4,3}$ = 3.3 Hz, $J_{4,5}$ = 1.9 Hz, H-4-furyl); 6.66 (dd, 1H, $J_{3,4}$ = 3.3 Hz, $J_{3,5}$ = 0.9 Hz, H-3-furyl); 7.80 (dd, 1H, $J_{5,4}$ = 1.9 Hz, $J_{5,3}$ = 0.9 Hz, H-5-furyl); 8.07 (s, 1H, H-6); 8.71 (s, 1H, H-2). ^{13}C NMR (125.7 MHz, DMSO-d_6): 23.03 (CH_3); 61.63 (CH_2-5′); 70.71 (CH-3′); 74.31 (CH-2′); 85.50 (CH-4′); 86.79 (CH-1′); 106.79 (C-5); 108.50 (CH-3-furyl); 111.75 (CH-4-furyl); 115.36 (C-4a); 125.82 (CH-6); 142.93 (CH-5-furyl); 147.62 (C-2-furyl); 150.82 (C-7a); 151.38 (CH-2); 159.71 (C-4). IR (ATR): ν 1571, 1438, 1348, 1201, 1120, 1080, 1031, 968, 892, 792, 736, 637 cm^{-1}. MS (ESI) *m*/*z* 332 (M + H), 354 (M + Na). HRMS (ESI) for $C_{16}H_{18}N_3O_5$ [M + H] calcd: 332.12410; found: 332.12406. Anal. ($C_{16}H_{17}N_3O_5 \cdot {}^3/_4H_2O$): C, H, N.

*5-Ethynyl-4-methoxy-7-(β-D-ribofuranosyl)-7H-pyrrolo[2,3-d]-pyrimidine (**2g**).* An argon-purged mixture of **13** (407 mg, 1 mmol), $PdCl_2(PPh_3)_2$ (35 mg, 0.05 mmol), CuI (19 mg, 0.1 mmol), trimethylsilylacetylene (1.4 mL, 10 mmol), and triethylamine (0.5 mL) was stirred in DMF (2 mL) at rt for 16 h. The volatiles were removed in vacuo, and the residue was coevaporated several times with EtOH/toluene and loaded on silica by coevaporation. Column chromatography (SiO_2, 0→1.5% MeOH in $CHCl_3$) afforded trimethylsilylethynyl derivative contaminated by triethylammonium iodide. This material was directly deprotected by treatment with K_2CO_3 (207 mg, 1.5 mmol) in MeOH (5 mL) at rt for 5 h, followed by coevaporation with silica and final column chromatography (SiO_2, 2.5% MeOH in $CHCl_3$) afforded **2g** (268 mg, 88% in two steps), which was crystallized from MeOH. Mp 205−207 °C. $[\alpha]_D$ −78.4 (*c* 0.333, DMSO). ^{1}H NMR (500 MHz, DMSO-d_6): 3.56 (ddd, 1H, J_{gem} = 11.9 Hz, $J_{5'a,OH}$ = 5.7 Hz, $J_{5'a,4'}$ = 3.7 Hz, H-5′a); 3.65 (ddd, 1H, J_{gem} = 11.9 Hz, $J_{5'b,OH}$ = 5.3 Hz, $J_{5'b,4'}$ = 3.9 Hz, H-5′b); 3.92 (td, 1H, $J_{4',5'a} = J_{4',5'b}$ = 3.8 Hz, $J_{4',3'}$ = 3.5 Hz, H-4′); 4.06 (s, 3H, CH_3O); 4.10 (td, 1H, $J_{3',2'} = J_{3',OH}$ = 5.0 Hz, $J_{3',4'}$ = 3.4 Hz, H-3′); 4.11 (d, 1H, $J_{CH,6}$ = 0.4 Hz, C≡CH); 4.38 (td, 1H, $J_{2',1'} = J_{2',OH}$ = 6.2 Hz, $J_{2',3'}$ = 5.0 Hz, H-2′); 5.12 (t, 1H, $J_{OH,5'a} = J_{OH,5'b}$ = 5.5 Hz, OH-5′); 5.18 (d, 1H, $J_{OH,3'}$ = 4.9 Hz, OH-3′); 5.41 (d, 1H, $J_{OH2'}$ = 6.3 Hz, OH-2′); 6.14 (d, 1H, $J_{1',2'}$ = 6.0 Hz, H-1′); 8.05 (s, 1H, H-6); 8.47 (s, 1H, H-2). ^{13}C NMR (125.7 MHz, DMSO-d_6): 54.04 (CH_3O); 61.55 (CH_2-5′); 70.63 (CH-3′); 74.45 (CH-2′); 77.17 (C≡CH); 81.80 (C≡CH); 85.56 (CH-4′); 87.31 (CH-1′); 94.82 (C-5); 105.16 (C-4a); 130.01 (CH-6); 151.43 (C-7a); 151.93 (CH-2); 162.95 (C-4). IR (ATR): ν 1596, 1574, 1061, 1005, 653, 604, 535 cm^{-1}. MS (ESI) *m*/*z* 306 (M + H), 328 (M + Na). HRMS (ESI) for $C_{14}H_{15}N_3O_5$Na [M + Na] calcd: 328.0904; found: 328.0892. Anal. ($C_{14}H_{15}N_3O_5 \cdot 1/4H_2O$): C, H, N.

*5-(Furan-2-yl)-7-(β-D-ribofuranosyl)-7H-pyrrolo[2,3-d]pyrimidin-4(3H)-one (**7a**).* To a stirred slurry of **2a** (139 mg, 0.40 mmol) and NaI (300 mg, 2 mmol) in dry MeCN (5 mL) was slowly added TMSCl (253 μL, 2 mmol), and the mixture was stirred at rt for 4 h. The precipitate was filtered off, washed carefully with MeCN, and dissolved in water, and pH of the solution was quickly adjusted to 7 using solid K_2CO_3. The mixture was evaporated to dryness, and crystallization from water gave **7a** (50 mg, 38%) as a beige solid. Reverse phase HPFC (C-18, 0→100% MeOH in water) of the mother liquors provided additional **7a** (31 mg, 23%). Total yield of **7a** was 61%. Mp 184−186 °C. $[\alpha]_D$ −83.8 (*c* 0.216, DMSO). ^{1}H NMR (500 MHz, DMSO-d_6): 3.56 (ddd, 1H, J_{gem} = 11.8 Hz, $J_{5'a,OH}$ = 5.4 Hz, $J_{5'a,4'}$ = 3.7 Hz, H-5′a); 3.63 (ddd, 1H, J_{gem} = 11.9 Hz, $J_{5'b,OH}$ = 5.3 Hz, $J_{5'b,4'}$ = 3.7 Hz, H-5′b); 3.90 (q, 1H, $J_{4',5'a} = J_{4',5'b} = J_{4',3'}$ = 3.5 Hz, H-4′); 4.09 (td, 1H, $J_{3',2'} = J_{3',OH}$ = 4.9 Hz, $J_{3',4'}$ = 3.3 Hz, H-3′); 4.35 (td, 1H, $J_{2',1'} = J_{2',OH}$ = 6.3 Hz, $J_{2',3'}$ = 5.1 Hz, H-2′); 5.08 (t, 1H, $J_{OH,5'a} = J_{OH,5'b}$ = 5.3 Hz, OH-5′); 5.15 (d, 1H, $J_{OH,3'}$ = 4.8 Hz, OH-3′); 5.36 (d, 1H, $J_{OH,2'}$ = 6.4 Hz, OH-2′); 6.08 (d, 1H, $J_{1',2'}$ = 6.2 Hz, H-1′); 6.51 (dd, 1H, $J_{4,3}$ = 3.3 Hz, $J_{4,5}$ = 1.8 Hz, H-4-furyl); 7.37 (dd, 1H, $J_{3,4}$ = 3.3 Hz, $J_{3,5}$ = 0.9 Hz, H-3-furyl); 7.60 (dd, 1H, $J_{5,4}$ = 1.9 Hz, $J_{5,3}$ = 0.9 Hz, H-5-furyl); 7.68 (s, 1H, H-6); 7.96 (d, 1H, $J_{2,NH}$ = 3.8 Hz, H-2); 12.10 (d, 1H, $J_{NH,2}$ = 3.7 Hz, NH). ^{13}C NMR (125.7 MHz, DMSO-d_6): 61.61 (CH_2-5′); 70.75 (CH-3′); 74.60 (CH-2′); 85.41 (CH-4′); 86.93 (CH-1′); 104.08 (C-4a); 108.41 (CH-3-furyl); 111.14 (C-5); 111.75 (CH-4-furyl); 116.71 (CH-6); 141.42 (CH-5-furyl); 144.94 (CH-2); 148.68 (C-2-furyl); 148.82 (C-7a); 158.39 (C-4). IR (ATR): ν 1696, 1599, 1045, 788, 723 cm^{-1}. MS (ESI) *m*/*z* 334 (M + H), 356 (M + Na).

dx.doi.org/10.1021/jm4018948 | J. Med. Chem. 2014, 57, 1097−1110

HRMS (ESI) for $C_{15}H_{15}N_3O_6Na$ [M + Na] calcd: 356.0853; found: 356.0843. Anal. ($C_{15}H_{15}N_3O_6{\cdot}H_2O$): C, H, N.

*4-Chloro-5-iodo-2-methyl-7H-pyrrolo[2,3-d]pyrimidine (**23**).* A mixture of compound **22**[26] (4.51 g, 26.9 mmol) and *N*-iodosuccinimide (6.7 g, 29.8 mmol) in dichloromethane (80 mL) was stirred at rt for 4 h. The volatiles were removed under reduced pressure, and the residue was crystallized from MeCN, affording **23** (6.89 g, 87%) as pinkish-orange needles. Mp 229−231 °C. ^{1}H NMR (500 MHz, DMSO-d_6): 2.60 (s, 3H, CH_3); 7.80 (d, 1H, $J_{6,NH}$ = 2.5 Hz, H-6); 12.67 (bs, 1H, NH). ^{13}C NMR (125.7 MHz, DMSO-d_6): 25.07 (CH_3); 51.58 (C-5); 113.55 (C-4a); 133.02 (CH-6); 150.62 (C-4); 152.49 (C-7a); 160.04 (C-2). IR (ATR): ν 1607, 1550, 1463, 1402, 1245, 1196, 964, 897, 808, 779, 632, 609, 573 cm^{-1}. MS (ESI) m/z 294 (M + H), 316 (M + Na). HRMS (ESI) for $C_7H_6N_3ClI$ [M + H] calcd: 293.92894; found: 293.92895.

*4-Chloro-5-iodo-2-methyl-7-(2,3,5-tri-O-benzoyl-β-D-ribofuranosyl)-7H-pyrrolo[2,3-d]pyrimidine (**25**).* To a slurry of iodide **23** (3.39 g, 11.55 mmol) in dry MeCN (60 mL) was added *N*,*O*-bis(trimethylsilyl)acetamide [BSA] (3.44 mL, 13.87 mmol), and the mixture was stirred at rt for 20 min (clear solution was formed). Then TMSOTf (4.2 mL, 23.24 mmol) was added, 1-*O*-acetyl-2,3,5-tri-*O*-benzoyl-β-D-ribofuranose **24** (11.67 g, 23.13 mmol) was introduced in three portions (3 × 3.89 g, once per 8 h), and the mixture was stirred at 50 °C for 24 h. After cooling, the mixture was treated with saturated aq $NaHCO_3$ (150 mL) and extracted with $CHCl_3$ (300 mL, then 2 × 50 mL). Combined organic phases were dried over $MgSO_4$, concentrated in vacuo, and coevaporated with silica. Column chromatography (SiO_2, dichloromethane→2.5% EtOAc in dichloromethane) afforded fractions containing product contaminated to various extents with non-nucleoside sugar byproducts. Crystallization of these fractions from hexane/EtOAc afforded **25** (3.03 g, 35%) as a white crystalline solid. Mp 180−182 °C. ^{1}H NMR (500 MHz, DMSO-d_6): 2.58 (s, 3H, CH_3); 4.68 (dd, 1H, J_{gem} = 12.2 Hz, $J_{5'a,4'}$ = 5.0 Hz, H-5′a); 4.78 (dd, 1H, J_{gem} = 12.2 Hz, $J_{5'b,4'}$ = 3.9 Hz, H-5′b); 4.87 (ddd, 1H, $J_{4',3'}$ = 5.7 Hz, $J_{4',5'a}$ = 5.0 Hz, $J_{4',5'b}$ = 3.9 Hz, H-4′); 6.23 (t, 1H, $J_{3',4'} = J_{3',2'}$ = 5.9 Hz, H-3′); 6.30 (dd, 1H, $J_{2',3'}$ = 6.1 Hz, $J_{2',1'}$ = 4.5 Hz, H-2′); 6.63 (d, 1H, $J_{1',2'}$ = 4.5 Hz, H-1′); 7.40−7.52 (m, 6H, H-*m*-Bz); 7.60−7.70 (m, 3H, H-*p*-Bz); 7.84−7.97 (m, 6H, H-*o*-Bz); 8.17 (s, 1H, H-6). ^{13}C NMR (125.7 MHz, DMSO-d_6): 25.07 (CH_3); 54.44 (C-5); 63.52 (CH_2-5′); 70.93 (CH-3′); 73.82 (CH-2′); 79.34 (CH-4′); 86.89 (CH-1′); 114.83 (C-4a); 128.50 and 128.78 (C-*i*-Bz); 128.94, 128.96, and 128.98 (CH-*m*-Bz); 129.31 (C-*i*-Bz); 129.35 and 129.57 (CH-*o*-Bz); 133.68 (CH-6); 133.75, 134.08, and 134.19 (CH-*p*-Bz); 151.39 (C-7a); 151.48 (C-4); 160.86 (C-2); 164.66, 164.87, and 165.58 (CO). IR (ATR): ν 1729, 1720, 1593, 1415, 1267, 1248, 1212, 1103, 1071, 708 cm^{-1}. MS (ESI) m/z 738 (M + H), 760 (M + Na). HRMS (ESI) for $C_{33}H_{25}ClIN_3O_7Na$ [M + Na] calcd: 760.0318; found: 760.0314.

*4-Amino-5-iodo-2-methyl-7-(β-D-ribofuranosyl)-7H-pyrrolo[2,3-d]pyrimidine (**26**).* A suspension of nucleoside **25** (2.99 g, 4.05 mmol) in dioxane (20 mL) and aq ammonia (27% w/w, 15 mL) was stirred in a steel bomb at 120 °C for 24 h. After cooling, the volatiles were evaporated in vacuo, the residue was purified by reverse phase HPFC (C-18, 0→100% MeOH in water), and final recrystallization from MeOH/water (1:1) afforded **26** (1.51 g, 92%) as long colorless needles. Mp 236−239 °C. $[\alpha]_D$ −57.0 (*c* 0.316, DMSO). ^{1}H NMR (500 MHz, DMSO-d_6): 2.37 (s, 3H, CH_3); 3.52 (ddd, 1H, J_{gem} = 12.0 Hz, $J_{5'a,OH}$ = 6.6 Hz, $J_{5'a,4'}$ = 3.7 Hz, H-5′a); 3.60 (ddd, 1H, J_{gem} = 12.0 Hz, $J_{5'b,OH}$ = 4.7 Hz, $J_{5'b,4'}$ = 3.8 Hz, H-5′b); 3.88 (td, 1H, $J_{4',5'a} = J_{4',5'b}$ = 3.7 Hz, $J_{4',3'}$ = 2.7 Hz, H-4′); 4.05 (td, 1H, $J_{3',2'} = J_{3',OH}$ = 4.8 Hz, $J_{3',4'}$ = 2.7 Hz, H-3′); 4.40 (td, 1H, $J_{2',1'} = J_{2',OH}$ = 6.6 Hz, $J_{2',3'}$ = 5.1 Hz, H-2′); 5.12 (d, 1H, $J_{OH,3'}$ = 4.5 Hz, OH-3′); 5.28 (d, 1H, $J_{OH2'}$ = 6.5 Hz, OH-2′); 5.29 (dd, 1H, $J_{OH,5'a}$ = 6.6 Hz, $J_{OH,5'b}$ = 4.7 Hz, OH-5′); 5.97 (d, 1H, $J_{1',2'}$ = 6.8 Hz, H-1′); 6.60 (bs, 2H, NH_2); 7.56 (s, 1H, H-6). ^{13}C NMR (125.7 MHz, DMSO-d_6): 25.35 (CH_3); 51.79 (C-5); 61.93 (CH_2-5′); 70.90 (CH-3′); 73.71 (CH-2′); 85.53 (CH-4′); 87.10 (CH-1′); 101.42 (C-4a); 126.94 (CH-6); 151.19 (C-7a); 157.22 (C-4); 160.74 (C-2). IR (ATR): ν 1627, 1588, 1560, 1460, 1416, 1289, 1119, 1086, 1030, 786, 657 cm^{-1}. MS (ESI) m/z 407 (M + H), 429 (M + Na). HRMS (ESI) for $C_{12}H_{15}IN_4O_4Na$ [M + Na] calcd: 429.0030; found: 429.0029. Anal. ($C_{12}H_{15}N_4O_4I{\cdot}H_2O$): C, H, N.

*2,4-Diamino-5-(furan-2-yl)-7-(β-D-ribofuranosyl)-7H-pyrrolo[2,3-d]pyrimidine (**8a**).* An argon-purged mixture of 2,4-diamino-5-iodo-7-(β-D-ribofuranosyl)-7*H*-pyrrolo[2,3-*d*]pyrimidine **27**[29] (305 mg, 0.75 mmol), furan-2-boronic acid (126 mg, 1.125 mmol), Na_2CO_3 (239 mg, 2.25 mmol), $Pd(OAc)_2$ (8 mg, 0.036 mmol), and TPPTS (53 mg, 0.093 mmol) in water/MeCN (2:1, 5 mL) was stirred at 100 °C for 3 h. After cooling, the mixture was neutralized using aq HCl (1 M) and concentrated to dryness in vacuo, and the residue was purified by reverse phase HPFC (C-18, 0→100% MeOH in water) to afford **8a** (209 mg, 80%), which was crystallized from water as white needles. Mp 234−236 °C. $[\alpha]_D$ −71.9 (*c* 0.313, DMSO). ^{1}H NMR (500 MHz, DMSO-d_6): 3.52 (ddd, 1H, J_{gem} = 11.9 Hz, $J_{5'a,OH}$ = 6.0 Hz, $J_{5'a,4'}$ = 4.1 Hz, H-5′a); 3.61 (ddd, 1H, J_{gem} = 11.9 Hz, $J_{5'b,OH}$ = 5.2 Hz, $J_{5'b,4'}$ = 4.1 Hz, H-5′b); 3.84 (td, 1H, $J_{4',5'a} = J_{4',5'b}$ = 4.1 Hz, $J_{4',3'}$ = 3.3 Hz, H-4′); 4.06 (td, 1H, $J_{3',2'} = J_{3',OH}$ = 4.9 Hz, $J_{3',4'}$ = 3.3 Hz, H-3′); 4.34 (td, 1H, $J_{2',1'} = J_{2',OH}$ = 6.4, $J_{2',3'}$ = 5.2 Hz, H-2′); 5.08 (d, 1H, $J_{OH,3'}$ = 4.6 Hz, OH-3′); 5.18 (dd, 1H, $J_{OH,5'a}$ = 6.0 Hz, $J_{OH,5'b}$ = 5.2 Hz, OH-5′); 5.28 (d, 1H, $J_{OH2'}$ = 6.3 Hz, OH-2′); 5.77 (bs, 2H, NH_2-2); 5.96 (d, 1H, $J_{1',2'}$ = 6.4 Hz, H-1′); 6.47 (bs, 2H, NH_2-4); 6.55−6.59 (m, 2H, H-3,4-furyl); 7.40 (s, 1H, H-6); 7.73 (dd, 1H, $J_{5,4}$ = 1.7 Hz, $J_{5,3}$ = 1.0 Hz, H-5-furyl). ^{13}C NMR (125.7 MHz, DMSO-d_6): 61.95 (CH_2-5′); 70.77 (CH-3′); 73.50 (CH-2′); 84.91 (CH-4′); 86.35 (CH-1′); 93.16 (C-4a); 104.60 (CH-3-furyl); 106.73 (C-5); 112.00 (CH-4-furyl); 116.99 (CH-6); 141.56 (CH-5-furyl); 149.70 (C-2-furyl); 154.12 (C-7a); 157.84 (C-4); 160.13 (C-2). IR (ATR): ν 1609, 1579, 1478, 1444, 1126, 1010, 875, 792, 738 cm^{-1}. MS (ESI) m/z 348 (M + H), 370 (M + Na). HRMS (ESI) for $C_{15}H_{18}N_5O_5$ [M + H] calcd: 348.13025; found: 348.13034. Anal. ($C_{15}H_{17}N_5O_5$): C, H, N.

*4-Amino-5-(furan-2-yl)-2-methyl-7-(β-D-ribofuranosyl)-7H-pyrrolo[2,3-d]pyrimidine (**9a**).* An argon-purged mixture of **26** (305 mg, 0.75 mmol), furan-2-boronic acid (126 mg, 1.125 mmol), Na_2CO_3 (239 mg, 2.25 mmol), $Pd(OAc)_2$ (8 mg, 0.036 mmol), and TPPTS (53 mg, 0.093 mmol) in water/MeCN (2:1, 5 mL) was stirred at 100 °C for 3 h. After cooling, the mixture was neutralized using aq HCl (1 M) and concentrated to dryness in vacuo, and the residue was purified by reverse phase HPFC (C-18, 0→100% MeOH in water) to afford product **9a** (203 mg, 78%) as a beige solid, which was crystallized from water/MeOH to give beige needles. Mp 205−207 °C. $[\alpha]_D$ −74.7 (*c* 0.269, DMSO). ^{1}H NMR (500 MHz, DMSO-d_6): 2.39 (s, 3H, CH_3); 3.54 (ddd, 1H, J_{gem} = 12.0 Hz, $J_{5'a,OH}$ = 6.8 Hz, $J_{5'a,4'}$ = 3.7 Hz, H-5′a); 3.64 (ddd, 1H, J_{gem} = 12.0 Hz, $J_{5'b,OH}$ = 4.8 Hz, $J_{5'b,4'}$ = 3.9 Hz, H-5′b); 3.91 (td, 1H, $J_{4',5'a} = J_{4',5'b}$ = 3.8 Hz, $J_{4',3'}$ = 2.9 Hz, H-4′); 4.09 (btd, 1H, $J_{3',2'} = J_{3',OH}$ = 4.9 Hz, $J_{3',4'}$ = 2.9 Hz, H-3′); 4.47 (td, 1H, $J_{2',1'} = J_{2',OH}$ = 6.4 Hz, $J_{2',3'}$ = 5.1 Hz, H-2′); 5.15 (bd, 1H, $J_{OH,3'}$ = 4.6 Hz, OH-3′); 5.31 (bd, 1H, $J_{OH2'}$ = 6.5 Hz, OH-2′); 5.34 (dd, 1H, $J_{OH,5'a}$ = 6.8 Hz, $J_{OH,5'b}$ = 4.8 Hz, OH-5′); 6.03 (d, 1H, $J_{1',2'}$ = 6.7 Hz, H-1′); 6.60 (dd, 1H, $J_{4,3}$ = 3.3 Hz, $J_{4,5}$ = 1.9 Hz, H-4-furyl); 6.65 (dd, 1H, $J_{3,4}$ = 3.3 Hz, $J_{3,5}$ = 0.9 Hz, H-3-furyl); 6.86 (s, 2H, NH_2); 7.74 (s, 1H, H-6); 7.77 (dd, 1H, $J_{5,4}$ = 1.9 Hz, $J_{5,3}$ = 0.9 Hz, H-5-furyl). ^{13}C NMR (125.7 MHz, DMSO-d_6): 25.32 (CH_3); 62.04 (CH_2-5′); 70.96 (CH-3′); 73.61 (CH-2′); 85.55 (CH-4′); 87.32 (CH-1′); 97.50 (C-4a); 105.19 (CH-3-furyl); 106.21 (C-5); 112.09 (CH-4-furyl); 120.39 (C-6); 142.04 (CH-5-furyl); 148.99 (C-2-furyl); 151.93 (C-7a); 157.33 (C-4); 160.82 (C-2). IR (ATR): ν 1641, 1565, 1499, 1417, 1316, 1123, 1099, 1046, 1014, 983, 873, 792, 740 cm^{-1}. MS (ESI) m/z 347 (M + H), 369 (M + Na). HRMS (ESI) for $C_{16}H_{19}N_4O_5$ [M + H] calcd: 347.1350; found: 347.1340. Anal. ($C_{16}H_{18}N_4O_5{\cdot}^1/_2H_2O$): C, H, N.

*2-Amino-5-(furan-2-yl)-4-methoxy-7-(β-D-ribofuranosyl)-7H-pyrrolo[2,3-d]pyrimidine (**10a**).* An argon-purged mixture of 2-amino-5-iodo-4-methoxy-7-(β-D-ribofuranosyl)-7*H*-pyrrolo[2,3-*d*]pyrimidine **28**[29] (822 mg, 2 mmol), furan-2-boronic acid (336 mg, 3 mmol), Na_2CO_3 (636 mg, 6 mmol), $Pd(OAc)_2$ (22 mg, 98 μmol), and TPPTS (142 mg, 0.25 mmol) in water/MeCN (2:1, 10 mL) was stirred at 100 °C for 3 h. After cooling, the mixture was neutralized using aq HCl (1 M) and evaporated to dryness in vacuo, and the residue was purified by reverse phase HPFC (C-18, 0→100% MeOH in water). Repurification by column chromatography (SiO_2, 2.5% MeOH in

dx.doi.org/10.1021/jm4018948 | J. Med. Chem. 2014, 57, 1097−1110

chloroform) furnished **10a** (426 mg, 59%) as a beige solid, which was crystallized from MeOH. Mp 204−206 °C. $[\alpha]_D$ −63.7 (*c* 0.331, DMSO). ^{1}H NMR (500 MHz, DMSO-d_6): 3.53 (ddd, 1H, J_{gem} = 11.9 Hz, $J_{5'a,OH}$ = 5.5 Hz, $J_{5'a,4'}$ = 3.9 Hz, H-5′a); 3.59 (ddd, 1H, J_{gem} = 11.9 Hz, $J_{5'b,OH}$ = 5.3 Hz, $J_{5'b,4'}$ = 3.9 Hz, H-5′b); 3.85 (btd, 1H, $J_{4',5'a}$ = $J_{4',5'b}$ = 3.9 Hz, $J_{4',3'}$ = 3.1 Hz, H-4′); 3.99 (s, 3H, CH_3O); 4.06 (btd, 1H, $J_{3',2'}$ = $J_{3',OH}$ = 4.8 Hz, $J_{3',4'}$ = 3.0 Hz, H-3′); 4.34 (td, 1H, $J_{2',1'}$ = $J_{2',OH}$ = 6.4 Hz, $J_{2',3'}$ = 5.1 Hz, H-2′); 5.04 (t, 1H, $J_{OH,5'a}$ = $J_{OH,5'b}$ = 5.4 Hz, OH-5′); 5.07 (d, 1H, $J_{OH,3'}$ = 4.4 Hz, OH-3′); 5.27 (d, 1H, $J_{OH,2'}$ = 6.3 Hz, OH-2′); 6.03 (d, 1H, $J_{1',2'}$ = 6.5 Hz, H-1′); 6.36 (s, 2H, NH_2); 6.51 (dd, 1H, $J_{4,3}$ = 3.3 Hz, $J_{4,5}$ = 1.8 Hz, H-4-furyl); 6.82 (dd, 1H, $J_{3,4}$ = 3.3 Hz, $J_{3,5}$ = 0.9 Hz, H-3-furyl); 7.43 (s, 1H, H-6); 7.59 (dd, 1H, $J_{5,4}$ = 1.8 Hz, $J_{5,3}$ = 0.9 Hz, H-5-furyl). ^{13}C NMR (125.7 MHz, DMSO-d_6): 53.28 (CH_3O); 61.79 (CH_2-5′); 70.83 (CH-3′); 73.73 (CH-2′); 84.95 (CH-4′); 85.89 (CH-1′); 93.78 (C-4a); 106.50 (CH-3-furyl); 107.54 (C-5); 111.71 (CH-4-furyl); 116.53 (C-6); 141.13 (CH-5-furyl); 149.21 (C-2-furyl); 155.61 (C-7a); 159.86 (C-2); 163.29 (C-4). IR (ATR): ν 1626, 1597, 1575, 1486, 1442, 1411, 1308, 1213, 1043, 1004, 790, 739 cm^{-1}. MS (ESI) *m*/*z* 363 (M + H), 385 (M + Na). HRMS (ESI) for $C_{16}H_{18}N_4O_6Na$ [M + Na] calcd: 385.11186; found: 385.11168. Anal. ($C_{16}H_{18}N_4O_6 \cdot {}^1/_4H_2O$): C, H, N.

*2-Amino-5-(furan-2-yl)-7-(β-D-ribofuranosyl)-7H-pyrrolo[2,3-d]-pyrimidin-4(3H)-one (**11a**).* To a stirred slurry of **10a** (174 mg, 0.48 mmol) and NaI (360 mg, 2.4 mmol) in dry MeCN (5 mL) was slowly added TMSCl (304 μL, 2.4 mmol), and the mixture was stirred at rt for 4 h. The precipitate was filtered off, washed carefully with MeCN, and dried. The solid was then dissolved in water/MeOH, the pH of the solution was quickly adjusted to 7 using solid K_2CO_3, and the mixture was evaporated to dryness. The residue was desalted by reverse phase HPFC (C-18, 0→100% MeOH in water) and repurified by column chromatography (SiO_2, 6% MeOH in $CHCl_3$) to obtain **11a** (35 mg, 21%) as a yellowish foam. $[\alpha]_D$ −66.5 (*c* 0.200, DMSO). ^{1}H NMR (500 MHz, DMSO-d_6): 3.52 (ddd, 1H, J_{gem} = 11.9 Hz, $J_{5'a,OH}$ = 5.4 Hz, $J_{5'a,4'}$ = 4.0 Hz, H-5′a); 3.58 (ddd, 1H, J_{gem} = 11.9 Hz, $J_{5'b,OH}$ = 5.3 Hz, $J_{5'b,4'}$ = 3.9 Hz, H-5′b); 3.82 (td, 1H, $J_{4',5'a}$ = $J_{4',5'b}$ = 3.9 Hz, $J_{4',3'}$ = 3.2 Hz, H-4′); 4.05 (m, 1H, H-3′); 4.28 (td, 1H, $J_{2',1'}$ = $J_{2',OH}$ = 6.4 Hz, $J_{2',3'}$ = 5.1 Hz, H-2′); 5.00 (t, 1H, $J_{OH,5'a}$ = $J_{OH,5'b}$ = 5.4 Hz, OH-5′); 5.05 (d, 1H, $J_{OH,3'}$ = 4.4 Hz, OH-3′); 5.26 (d, 1H, $J_{OH,2'}$ = 6.5 Hz, OH-2′); 5.92 (d, 1H, $J_{1',2'}$ = 6.5 Hz, H-1′); 6.35 (s, 2H, NH_2); 6.46 (dd, 1H, $J_{4,3}$ = 3.3 Hz, $J_{4,5}$ = 1.8 Hz, H-4-furyl); 7.25 (s, 1H, H-6); 7.31 (dd, 1H, $J_{3,4}$ = 3.3 Hz, $J_{3,5}$ = 1.0 Hz, H-3-furyl); 7.54 (dd, 1H, $J_{5,4}$ = 1.9 Hz, $J_{5,3}$ = 0.9 Hz, H-5-furyl); 10.47 (s, 1H, NH). ^{13}C NMR (125.7 MHz, DMSO-d_6): 61.75 (CH_2-5′); 70.80 (CH-3′); 73.88 (CH-2′); 84.89 (CH-4′); 85.88 (CH-1′); 96.21 (C-4a); 107.66 (C-3-furyl); 110.89 (C-5); 111.56 (CH-4-furyl); 113.28 (C-6); 140.85 (CH-5-furyl); 149.42 (C-2-furyl); 152.33 (C-7a); 153.12 (C-2); 158.77 (C-4). IR (ATR): ν 1632, 1602, 1552, 1543, 1439, 1357, 1123, 1038, 1022, 999, 786 cm^{-1}. MS (ESI) *m*/*z* 349 (M + H), 371 (M + Na). HRMS (ESI) for $C_{15}H_{16}N_4O_6Na$ [M + Na] calcd: 371.09621; found: 371.09615.

■ ASSOCIATED CONTENT

Supporting Information

Synthetic procedures and characterization data of compounds **2b−h**, **3b−h**, **4b−h**, **5b−h**, **6b−h**, **7b−f**, **8b−f**, **9b−g**, **10b−g**, **11b−f**, **17**, **18**, and **22**; experimental procedures for biological activity profiling, and analytical characterization data for the final nucleosides. This material is available free of charge via the Internet at http://pubs.acs.org.

■ AUTHOR INFORMATION

Corresponding Author

*Phone: +420 220183324. E-mail: hocek@uochb.cas.cz.

Notes

The authors declare no competing financial interest.

■ ACKNOWLEDGMENTS

This work was supported by the Czech Science Foundation (P207/11/0344), Technology Agency of the Czech Republic (TE01020028), and by Gilead Sciences, Inc. The infrastructural part of this project (Institute of Molecular and Translational Medicine) was supported from the Operational Programme Research and Development for Innovations (project CZ.1.05/2.1.00/01.0030) and RVO:61388963. The authors thank Drs. Joy Feng and Gina Bahador (Gilead Sciences, Inc.) for anti-HCV testing.

■ ABBREVIATIONS USED

BrdU, 5-bromo-2′-deoxyuridine; BrU, 5-bromouridine; HPFC, high performance flash chromatography; MTT, 3-(4,5-dimethylthiazol-2-yl)-2,5-diphenyltetrazolium bromide; TCA, trichloroacetic acid; TDA-1, tris(2-(2-methoxyethoxy)ethyl)-amine; TMS, trimethylsilyl; TTPTS, triphenylphosphine-3,3′,3″-tris(sulfonate); XTT, 2,3-bis(2-methoxy-4-nitro-5-sulfophenyl)-2*H*-tetrazolium-5-carboxanilide

■ REFERENCES

(1) Johnson, S. A.; Thomas, W. Therapeutic potential of purine analogue combinations in the treatment of lymphoid malignancies. *Hematol. Oncol.* **2000**, *18*, 141−153. (b) Johnson, S. A. Nucleoside analogues in the treatment of haematological malignancies. *Expert Opin. Pharmacother.* **2001**, *2*, 929−943. (c) Parker, W. B.; Secrist, J. A., III; Waud, W. R. Purine nucleoside antimetabolites in development for the treatment of cancer. *Curr. Opin. Investig. Drugs* **2004**, *5*, 592−596.

(2) (a) Robins, R. K.; Revankar, G. R. Purine analogs and related nucleosides and nucleotides as antitumor agents. *Med. Res. Rev.* **1985**, *5*, 273−296. (b) Plunkett, W.; Saunders, P. P. Metabolism and action of purine nucleoside analogs. *Pharmacol. Ther.* **1991**, *49*, 239−268. (c) Robak, T.; Korycka, A.; Kasznicki, M.; Wrzesien-Kus, A.; Smolewski, P. Purine nucleoside analogues for the treatment of hematological malignancies: Pharmacology and clinical applications. *Curr. Cancer Drug Targets* **2005**, *5*, 421−444. (d) Jordheim, L.; Galmarini, C. M.; Dumontet, C. Drug resistance to cytotoxic nucleoside analogues. *Curr. Drug Targets* **2003**, *4*, 443−460. (e) Jordheim, L. P.; Galmarini, C. M.; Dumontet, C. Recent developments to improve the efficacy of cytotoxic nucleoside analogues. *Recent Pat. Anti-Cancer Drug Discovery* **2006**, *1*, 163−170. (f) Parker, W. B. Enzymology of Purine and Pyrimidine Antimetabolites Used in the Treatment of Cancer. *Chem. Rev.* **2009**, *109*, 2880−2893.

(3) (a) Hocek, M.; Holý, A.; Votruba, I.; Dvořáková, H. Synthesis and Cytostatic Activity of Substituted 6-Phenylpurine Bases and Nucleosides: Application of the Suzuki−Miyaura Cross-Coupling Reactions of 6-Chloropurine Derivatives with Phenylboronic Acids. *J. Med. Chem.* **2000**, *43*, 1817−1825. (b) Hocek, M.; Holý, A.; Votruba, I.; Dvořáková, H. Cytostatic 6-arylpurine nucleosides III. Synthesis and structure-activity relationship study in cytostatic activity of 6-aryl-, 6-hetaryl- and 6-benzylpurine ribonucleosides. *Collect. Czech. Chem. Commun.* **2001**, *66*, 483−499. (c) Hocek, M.; Nauš, P.; Pohl, R.; Votruba, I.; Furman, P. A.; Tharnish, P. M.; Otto, M. J. Cytostatic 6-arylpurine Nucleosides 6. SAR in Anti-HCV and Cytostatic Activity of Extended Series of 6-Hetarylpurine Ribonucleosides. *J. Med. Chem.* **2005**, *48*, 5869−5873.

(4) (a) Nauš, P.; Pohl, R.; Votruba, I.; Džubák, P.; Hajdúch, M.; Ameral, R.; Birkus, G.; Wang, T.; Ray, A. S.; Mackman, R.; Cihlar, T.; Hocek, M. 6-(Het)aryl-7-Deazapurine Ribonucleosides as Novel Potent Cytostatic Agents. *J. Med. Chem.* **2010**, *53*, 460−470. (b) Spáčilová, P.; Nauš, P.; Pohl, R.; Votruba, I.; Snášel, J.; Zábranská, H.; Pichová, I.; Ameral, R.; Birkuš, G.; Cihlář, T.; Hocek, M. CycloSal-phosphate Pronucleotides of Cytostatic 6-(Het)aryl-7-deazapurine Ribonucleosides: Synthesis, Cytostatic Activity, and Inhibition of Adenosine Kinases. *ChemMedChem* **2010**, *5*, 1386−

1396. (c) Perlíková, P.; Pohl, R.; Votruba, I.; Shih, R.; Birkuš, G.; Cihlář, T.; Hocek, M. Phosphoramidate pronucleotides of cytostatic 6-aryl-7-deazapurine ribonucleosides. *Bioorg. Med. Chem.* **2011**, *19*, 229−242.

(5) Bourderioux, A.; Nauš, P.; Perlíková, P.; Pohl, R.; Pichová, I.; Votruba, I.; Džubák, P.; Konečný, P.; Hajdúch, M.; Stray, K. M.; Wang, T.; Ray, A. S.; Feng, J. Y.; Birkus, G.; Cihlar, T.; Hocek, M. Synthesis and significant cytostatic activity of 7-hetaryl-7-deazaadenosines. *J. Med. Chem.* **2011**, *54*, 5498−5507.

(6) (a) Nauš, P.; Perlíková, P.; Bourderioux, A.; Pohl, R.; Slavětínská, L.; Votruba, I.; Bahador, G.; Birkuš, G.; Cihlář, T.; Hocek, M. Sugar-modified derivatives of cytostatic 7-(het)aryl-7-deazaadenosines: 2′-C-methylribonucleosides, 2′-deoxy-2′-fluoroarabinonucleosides, arabino-nucleosides and 2′-deoxyribonucleosides. *Bioorg. Med. Chem.* **2012**, *20*, 5202−5214. (b) Perlíková, P.; Eberlin, L.; Ménová, P.; Raindlová, V.; Slavětínská, L.; Tloušťová, E.; Bahador, G.; Lee, Y.-J.; Hocek, M. Synthesis, Cytostatic and Antiviral activity of 2′-Deoxy-2′,2′-difluororibo- and 2′-Deoxy-2′-fluororibonucleosides Derived from 7-(Het)aryl-7-deazaadenines. *ChemMedChem* **2013**, *8*, 832−846.

(7) (a) Anzai, K.; Nakamura, G.; Suzuki, S. A New Antibiotic, Tubercidin. *J. Antibiot.* **1957**, *10*, 201−204. (b) Suzuki, S.; Marumo, S. Chemical Structure of Tubercidin. *J. Antibiot., Ser. A* **1961**, *13*, 360−360. (c) Acs, G.; Mori, M.; Reich, E. Biological + Biochemical Properties of Analogue Antibiotic Tubercidin. *Proc. Natl. Acad. Sci. U.S.A.* **1964**, *52*, 493−501.

(8) (a) Ramasamy, K.; Imamura, N.; Robins, R. K.; Revankar, G. R. A Facile Synthesis of Tubercidin and Related 7-Deazapurine Nucleosides via the Stereospecific Sodium Salt Glycosylation Procedure. *Tetrahedron Lett.* **1987**, *28*, 5107−5110. (b) Tolman, R. L.; Robins, R. K.; Townsend, L. B. Pyrrolopyrimidine Nucleosides. III. The Total Synthesis of Toyocamycin, Sangivamycin, Tubercidin and Related Derivatives. *J. Am. Chem. Soc.* **1969**, *91*, 2102−2108. (c) Bergstrom, D. E.; Brattesani, A. J.; Ogawa, M. K.; Reddy, A. T.; Schweickert, M. J.; Balzarini, J.; De Clercq, E. Antiviral Activity of C-5 Substituted Tubercidin Analogues. *J. Med. Chem.* **1984**, *27*, 285−292.

(9) (a) Cook, A. F.; Holman, M. J. Synthesis of the Natural Product 5′-Deoxy-5-iodotubercidin and Related Halogenated Analogues. *Nucleosides Nucleotides* **1984**, *3*, 401−411. (b) Ugarkar, B. G.; DaRe, J. M.; Kopcho, J. J.; Browne, C. E., III; Schanzer, J. M.; Wiesner, J. B.; Erion, M. D. Adenosine Kinase Inhibitors. 1. Synthesis, Enzyme Inhibition and Antiseizure Activity of 5-Iodotubercidin Analogues. *J. Med. Chem.* **2000**, *43*, 2883−2893. (c) Ugarkar, B. G.; Castellino, A. J.; DaRe, J. S.; Ramirez-Weinhouse, M.; Kopcho, J. J.; Rosengren, S.; Erion, M. D. Adenosine Kinase Inhibitors. 3. Synthesis, SAR and Antiinflammatory Activity of a Series of L-Lyxofuranosyl Nucleosides. *J. Med. Chem.* **2003**, *46*, 4750−4760. (d) Kim, Y. A.; Sharon, A.; Chu, C. K.; Rais, R. H.; Al Safarjalani, O. N.; Naguib, F. N. M.; el Kouni, M. H. Structure−Activity Relationships of 7-Deaza-6-benzylthioinosine Analogues as Ligands of *Toxoplasma gondii* Adenosine Kinase. *J. Med. Chem.* **2008**, *51*, 3934−3945. (e) Ugarkar, B. G.; Castellino, A. J.; DaRe, J. M.; Kopcho, J. J.; Wiesner, J. B.; Schanzer, J. M.; Erion, M. D. Adenosine Kinase Inhibitors. 2. Synthesis, Enzyme Inhibition, and Antiseizure Activity of Diaryltubercidin Analogues. *J. Med. Chem.* **2000**, *43*, 2894−2905. (f) Boyer, S. H.; Ugarkar, B. G.; Solbach, J.; Kopcho, J.; Matelich, M. C.; Ollis, K.; Gomez-Galeno, J. E.; Mendonca, R.; Tsuchiya, M.; Nagahisa, A.; Nakane, M.; Wiesner, J. B.; Erion, M. D. Adenosine Kinase Inhibitors. 5. Synthesis, Enzyme Inhibition, and Analgesic Activity of Erythro Diarylturbercidin Analogues. *J. Med. Chem.* **2005**, *48*, 6430−6441. (g) Bookser, B. C.; Matelich, M. C.; Ollis, K.; Ugarkar, B. G. Adenosine Kinase Inhibitors. 4. 6,8-Disubstituted Purine Nucleoside Derivatives. Synthesis, Conformation, and Enzyme Inhibition. *J. Med. Chem.* **2005**, *48*, 3389−3399.

(10) Gerster, J. F.; Carpenter, B.; Robins, R. K.; Townsend, L. B. Pyrrolopyrimidine Nucleosides. I. The Synthesis of 4-Substituted 7-(-β-D-Ribofuranosyl)pyrrolo[2,3-*d*]pyrimidines from Tubercidin. *J. Med. Chem.* **1967**, *10*, 326−331.

(11) Varaprasad, C. V. N. S.; Ramasamy, K. S.; Girardet, J. -L.; Gunic, E.; Lai, V.; Zhong, W.; An, H.; Hong, Z. Synthesis of pyrrolo[2,3-*d*]pyrimidine nucleoside derivatives as potential anti-HCV agents. *Bioorg. Chem.* **2007**, *35*, 25−34.

(12) Wu, R.; Smidansky, E. D.; Oh, H. S.; Takhampunya, R.; Padmanabhan, R.; Cameron, C. E.; Peterson, B. R. Synthesis of a 6-Methyl-7-deaza Analogue of Adenosine That Potently Inhibits Replication of Polio and Dengue Viruses. *J. Med. Chem.* **2010**, *53*, 7958−7966.

(13) Seela, F.; Ming, X. 7-Functionalized 7-deazapurine β-D and β-L-ribonucleosides related to tubercidin and 7-deazainosine: Glycosylation of pyrrolo[2,3-*d*]pyrimidines with 1-*O*-acetyl-2,3,5-tri-*O*-benzoyl-β-D or β-L-ribofuranose. *Tetrahedron* **2007**, *63*, 9850−9861.

(14) Taylor, E. C.; Martin, S. F. General Method for Alkylation and Alkenylation of Heterocycles. *J. Am. Chem. Soc.* **1974**, *96*, 8095−8102.

(15) Guo, H. M.; Zhang, Y.; Niu, H. Y.; Wang, D. C.; Chu, Z. L.; Qu, G. R. Microwave promoted C6-alkylation of purines through SNAr-based reaction of 6-chloropurines with 3-alkyl-acetylacetone. *Org. Biomol. Chem.* **2011**, *9*, 2065−2068.

(16) Qu, G. R.; Mao, Z. J.; Niu, H. Y.; Wang, D. C.; Xia, C.; Guo, H. M. Straightforward and Highly Efficient Catalyst-Free One-Step Synthesis of 2-(Purin-6-yl)acetoacetic Acid Ethyl Esters, (Purin-6-yl)acetates, and 6-Methylpurines through SNAr-Based Reactions of 6-Halopurines with Ethyl Acetoacetate. *Org. Lett.* **2009**, *11*, 1745−1748.

(17) (a) Fürstner, A.; Leitner, A.; Méndez, M.; Krause, H. Iron-Catalyzed Cross-Coupling Reactions. *J. Am. Chem. Soc.* **2002**, *124*, 13856−13863. (b) Hocek, M.; Dvořáková, H. An Efficient Synthesis of 2-Substituted 6-Methylpurine Bases and Nucleosides by Fe- or Pd-Catalyzed Cross-Coupling Reactions of 2,6-Dichloropurines. *J. Org. Chem.* **2003**, *68*, 5773−5776.

(18) (a) Krasovskiy, A.; Knochel, P. A LiCl-Mediated Br/Mg Exchange Reaction for the Preparation of Functionalized Aryl- and Heteroarylmagnesium Compounds from Organic Bromides. *Angew. Chem., Int. Ed.* **2004**, *43*, 3333−3336. (b) Brückl, T.; Thoma, I.; Wagner, A. J.; Knochel, P.; Carell, T. Efficient Synthesis of Deazaguanosine-Derived tRNA Nucleosides $preQ_0$, $preQ_1$, and Archaeosine Using the Turbo-Grignard Method. *Eur. J. Org. Chem.* **2010**, 6517−6519.

(19) Tolman, R. L.; Tolman, G. L.; Robins, R. K.; Townsend, L. B. Pyrrolopyrimidine Nucleosides. VI. Synthesis of 1,3 and 7-β-D-Ribofuranosylpyrrolo[2,3-*d*]pyrimidines *via* Silylated Intermediates. *J. Heterocycl. Chem.* **1970**, *7*, 799−806.

(20) Rosemeyer, H.; Seela, F. Stereoselective Synthesis of Pyrrolo-[2,3-d]Pyrimidine α- and β-D-Ribonucleosides from Anomerically Pure D-Ribofuranosyl Chlorides: Solid-Liquid Phase-Transfer Glycosylation and ^{15}N-NMR Spectra. *Helv. Chim. Acta* **1988**, *71*, 1573−1585.

(21) (a) Western, E. C.; Daft, J. R.; Johnson, E. M.; Gannett, P. M.; Shaughnessy, K. H. Efficient One-Step Suzuki Arylation of Unprotected Halonucleosides, Using Water-Soluble Palladium Catalysts. *J. Org. Chem.* **2003**, *68*, 6767−6774. (b) Čapek, P.; Pohl, R.; Hocek, M. Cross-coupling Reactions of Unprotected Halopurine Bases, Nucleosides, Nucleotides and Nucleoside Triphosphates with 4-Boronophenylalanine in Water. Synthesis of (Purin-8-yl)- and (Purin-6-yl)phenylalanines. *Org. Biomol. Chem.* **2006**, *4*, 2278−2284.

(22) (a) Fleckenstein, C. A.; Plenio, H. Efficient Suzuki−Miyaura Coupling of (Hetero)aryl Chlorides with Thiophene- and Furanboronic Acids in Aqueous *n*-Butanol. *J. Org. Chem.* **2008**, *73*, 3236−3244. (b) Molander, G. A.; Canturk, B.; Kennedy, L. E. Scope of the Suzuki−Miyaura Cross-Coupling Reactions of Potassium Heteroaryltrifluoroborates. *J. Org. Chem.* **2009**, *74*, 973−980.

(23) Florentin, D.; Fournie-Zaluski, M. C.; Callanquin, M.; Roques, B. P. Pka and Protodeboronation of Furanboronic Acids. *J. Heterocycl. Chem.* **1976**, *13*, 1265−1272.

(24) Brown, R. D.; Buchanan, A. S.; Humffray, A. A. Protodeboronation of Thiophenboronic acids. *Aust. J. Chem.* **1965**, *18*, 1521−1525.

(25) Olah, G. A.; Narang, S. C.; Gupta, B. G. B.; Malhotra, R. Synthetic Methods and Reactions. 62. Transformations with Chlorotrimethylsilane Sodium Iodide, a Convenient in Situ Iodotrimethylsilane Reagent. *J. Org. Chem.* **1979**, *44*, 1247−1251.

(26) West, R. A.; Beauchamp, L. 2-Alkyl(aryl)- and 2,7-Dimethyl-4-substituted Aminopyrrolo [2,3-*d*]pyrimidines. *J. Org. Chem.* **1961**, *26*, 3809−3812.
(27) Robins, M. J.; Uznanski, B. Nucleic-Acid Related-Compounds. 33. Conversions of Adenosine and Guanosine to 2,6-Dichloro, 2-Amino-6-Chloro, and Derived Purine Nucleosides. *Can. J. Chem.* **1981**, *59*, 2601−2607.
(28) Gangjee, A.; Zhao, Y.; Lin, L.; Raghavan, S.; Roberts, E. G.; Risinger, A. L.; Hamel, E.; Mooberry, S. L. Synthesis and Discovery of Water-Soluble Microtubule Targeting Agents That Bind to the Colchicine Site on Tubulin and Circumvent Pgp-Mediated Resistance. *J. Med. Chem.* **2010**, *53*, 8116−8128.
(29) Seela, F.; Peng, X. 7-Functionalized 7-Deazapurine Ribonucleosides Related to 2-Aminoadenosine, Guanosine, and Xanthosine: Glycosylation of Pyrrolo[2,3-*d*]pyrimidines with 1-*O*-Acetyl-2,3,5-tri-*O*-benzoyl-D-ribofuranose. *J. Org. Chem.* **2006**, *71*, 81−90.
(30) Serafinowski, P.; Dorland, E.; Balzarini, J.; De Clercq, E. The Synthesis and Antiviral Activity of Some New S-Adenosyl-L-homocysteine Derivatives and Their Nucleoside Precursors. *Nucleosides Nucleotides* **1995**, *14*, 545−547.
(31) Denizot, F.; Lang, R. Rapid colorimetric assay for cell growth and survival: Modifications to the tetrazolium dye procedure giving improved sensitivity and reliability. *J. Immunol. Methods* **1986**, *89*, 271−277.
(32) Scudiero, D. A.; Shoemaker, R. H.; Paull, K. D.; Monks, A.; Tierney, S.; Nofziger, T. H.; Currens, M. J.; Seniff, D.; Boyd, M. R. Evaluation of a Soluble Tetrazolium/Formazan Assay for Cell Growth and Drug Sensitivity in Culture Using Human and Other Tumor Cell Lines. *Cancer Res.* **1988**, *48*, 4827−4833.
(33) Gottesman, M. M.; Fojo, T.; Bates, S. E. Multidrug resistance in cancer: Role of ATP-dependent transporters. *Nat. Rev. Cancer.* **2002**, *2*, 48−58.
(34) Noskova, V.; Dzubak, P.; Kuzmina, G.; Ludkova, A.; Stehlik, D.; Trojanec, R.; Janostakova, A.; Korinkova, G.; Mihal, V.; Hajduch, M. In vitro chemoresistance profile and expression/function of MDR associated proteins in resistant cell lines derived from CCRF-CEM, K562, A549 and MDA MB 231 parental cells. *Neoplasma* **2002**, *49*, 418−425.
(35) Muller, P. A.; Vousden, K. H. p53 mutations in cancer. *Nat. Cell Biol.* **2013**, *15*, 2−8.

2.3.1.4 Inhibition of human and mycobacterial ADK by compounds with different structural basis

SNÁŠEL J[1], NAUŠ P, DOSTÁL J, HNÍZDA A, FANFRLÍK J, BRYNDA J, BOURDERIOUX A, DUŠEK M, DVOŘÁKOVÁ H, STOLAŘÍKOVÁ J, ZÁBRANSKÁ H, POHL R, KONEČNÝ P, DŽUBÁK P, VOTRUBA I, HAJDÚCH M, REZÁČOVÁ P, VEVERKA V, HOCEK M, PICHOVÁ I. (2014). Structural basis for inhibition of mycobacterial and human adenosine kinase by 7-substituted 7-(Het)aryl-7-deazaadenine ribonucleosides., *J Med Chem*. Oct 23;57(20):8268-79.

Journal of Medicinal Chemistry

Article

pubs.acs.org/jmc

Structural Basis for Inhibition of Mycobacterial and Human Adenosine Kinase by 7-Substituted 7-(Het)aryl-7-deazaadenine Ribonucleosides

Jan Snášel,[†,#] Petr Nauš,[†,#] Jiří Dostál,[†] Aleš Hnízda,[†] Jindřich Fanfrlík,[†] Jiří Brynda,[†] Aurelie Bourderioux,[†] Michal Dušek,[‡] Hana Dvořáková,[§] Jiřina Stolaříková,[∥] Helena Zábranská,[†] Radek Pohl,[†] Petr Konečný,[⊥] Petr Džubák,[⊥] Ivan Votruba,[†,∞] Marián Hajdúch,[⊥] Pavlína Řezáčová,[†] Václav Veverka,[†] Michal Hocek,[*,†] and Iva Pichová[*,†]

[†]Institute of Organic Chemistry and Biochemistry, Academy of Sciences of the Czech Republic, Flemingovo nam. 2, 16610 Prague 6, Czech Republic

[‡]Institute of Physics ASCR, v.v.i., Na Slovance 2, 182 21 Praha 8, Czech Republic

[§]Laboratory of NMR Spectroscopy, Institute of Chemical Technology, Technicka 5, 16628 Prague 6, Czech Republic

[∥]Laboratory for Mycobacterial Diagnostics and Tuberculosis, Regional Institute of Public Health in Ostrava, Partyzánské nám. 7, 70200 Ostrava, Czech Republic

[⊥]Institute of Molecular and Translational Medicine, Faculty of Medicine and Dentistry, Palacky University and University Hospital in Olomouc, Hněvotínská 5, 77515 Olomouc, Czech Republic

Supporting Information

ABSTRACT: Adenosine kinase (ADK) from *Mycobacterium tuberculosis* (Mtb) was selected as a target for design of antimycobacterial nucleosides. Screening of 7-(het)aryl-7-deazaadenine ribonucleosides with Mtb and human (*h*) ADKs and testing with wild-type and drug-resistant Mtb strains identified specific inhibitors of Mtb ADK with micromolar antimycobacterial activity and low cytotoxicity. X-ray structures of complexes of Mtb and *h*ADKs with 7-ethynyl-7-deazaadenosine showed differences in inhibitor interactions in the adenosine binding sites. 1D ^{1}H STD NMR experiments revealed that these inhibitors are readily accommodated into the ATP and adenosine binding sites of Mtb ADK, whereas they bind preferentially into the adenosine site of *h*ADK. Occupation of the Mtb ADK ATP site with inhibitors and formation of catalytically less competent semiopen conformation of MtbADK after inhibitor binding in the adenosine site explain the lack of phosphorylation of 7-substituted-7-deazaadenosines. Semiempirical quantum mechanical analysis confirmed different affinity of nucleosides for the Mtb ADK adenosine and ATP sites.

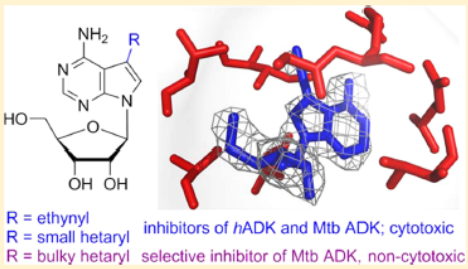

INTRODUCTION

Tuberculosis (TB) remains one of the leading public health problems worldwide and is more prevalent in the world today than at any other time in human history. In 2012, an estimated 8.6 million people developed TB, and 1.3 million died from the disease (WHO tuberculosis report 2013). In recent decades, multidrug-resistant (MDR) and even more ominous extensively drug-resistant (XDR) *Mycobacterium tuberculosis* (Mtb) strains have emerged.[1] At the same time, a high rate of HIV co-infection, especially in developing countries, has increased the susceptibility of the population to Mtb infection. Successful treatment of TB requires long courses of several antibiotics. In HIV-positive patients, TB treatment is further complicated by undesirable drug−drug interactions that decrease the therapeutic concentration of antiretrovirals by induction of the hepatic cytochrome P450 oxidase system.[2] Similar restrictions apply to coadministration of diabetes and TB drugs. Mtb can persist permanently in host lesions, evading immune surveillance. An estimated one-third of the world's population asymptomatically harbors a latent form of Mtb, with a life-long risk of disease activation and transmission. However, existing drugs do not target the latent form of Mtb. Therefore, the discovery of new molecules with new mechanisms of action is needed to address latent Mtb. New treatments may become critical as MDR and XDR Mtb incidence increases.

Enzymes involved in the biosynthesis of purine nucleotides are potential targets for development of new types of

Received: March 28, 2014
Published: September 26, 2014

compounds active against Mtb. In most organisms, purine nucleotides are formed from purine bases and phosphoribosyl 1-pyrophosphate or by phosphorylation of nucleosides in the purine salvage pathway, or they are synthesized de novo in a multistep sequence. Mtb expresses enzymes from both pathways; however, the interdependence and regulation of these processes remain unclear. Of the variety of possible target enzymes from the Mtb purine salvage pathway,[3,4] adenosine kinase (ADK, EC 2.7.1.20, Rv2202c)[5] is considered a promising target for drug development. ADK catalyzes phosphorylation of adenosine to adenosine monophosphate (AMP) in the phosphoryl transfer reaction using adenosine 5′-triphosphate (ATP) as a substrate and releasing adenosine 5′-diphosphate (ADP). ADK is present in most eukaryotes, fungi, plants, and parasites but is not commonly found in bacteria. The activity of ADK has been confirmed in Mtb,[6] and biochemical characterization indicates that this enzyme shares low structural similarity with and behaves very differently from human and other well-characterized ADKs.[3,7]

Nucleoside analogs are an important group of drugs used to treat viral infections and cancer. Certain nucleoside inhibitors are active against *Toxoplasma gondii*[8] and other parasites.[9] Several adenosine analogs with various modifications have already been tested for inhibition of Mtb ADK.[3,6,10] These studies established the promise of these compounds for drug development. In addition, diverse modified 7-deazapurine nucleosides have been reported as ADK inhibitors.[11−15] Recently, we discovered 6-hetaryl-7-deazapurine ribonucleosides with nanomolar cytostatic activities toward leukemia and cancer cell lines,[16] and we later found that these nucleosides are excellent inhibitors of Mtb ADK but only weak antimycobacterial agents.[17] Related 7-deazaadenosines bearing small five-membered heterocycles at position 7 (**1**) were also found to be nanomolar cytostatics,[18] whereas compounds bearing bulky aromatic substituents were neither cytostatic nor cytotoxic. Here, we report on the structure−activity relationship of 7-substituted 7-(het)aryl-7-deazaadenine ribonucleosides with Mtb ADK and human ADK (*h*ADK). We also describe screening of these compounds for in vitro inhibition of Mtb ADK and *h*ADK and for inhibition of two Mtb strains.

RESULTS AND DISCUSSION

Chemistry of 7-Substituted 7-Deazaadenosines. Synthesis of **1a−s** (Chart 1) was reported previously.[18] Our previous study showed that 7-deazaadenosine derivatives bearing small five-membered rings or acetylene exerted significant cytostatic/cytotoxic effects. To identify nontoxic derivatives with potential activity against Mtb ADK, we designed a series of nucleosides bearing bulky hydrophobic aromatic substituents at position 7. These substituents included substituted benzenes (**1t−aa**), polycyclic (hetero)aromatics (**1ab−af**), styrene (**1ag**), biaryls (**1ah**,**ai**), and aryl benzyl ether (**1aj**). All compounds were prepared by a single-step procedure based on the aqueous Suzuki−Miyaura cross-coupling reactions of 7-iodo-7-deazaadenosine (**2**) with the corresponding arylboronic acids (Scheme 1). The reactions generally proceeded smoothly, providing the desired 7-aryl-7-deazaadenosines **1t−aj** in good yields of 67−91% (with the exception of compound **1ai**, which was isolated in 53% yield).

Biological Activity Profiling of 7-Substituted 7-Deazapurine Derivatives. Compounds **1a−aj** were tested for inhibition of human and Mtb ADKs (for cloning, expression, and purification of these enzymes, see ref 19).

Chart 1. Numbering of Proton Positions in Modified Nucleosides and Structures of Previously Reported 7-Substituted 7-Deazaadenosines

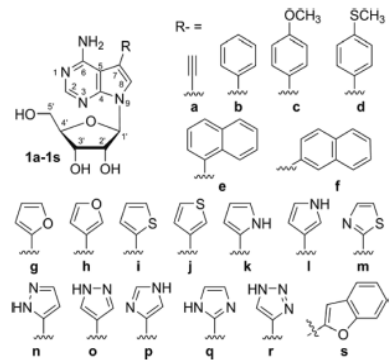

Scheme 1. Synthesis of 7-Deazaadenosines Bearing Bulky Substituents at Position 7

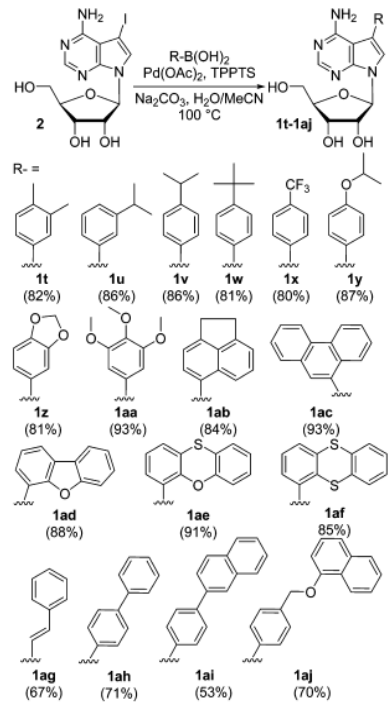

Most compounds were also tested as potential kinase substrates. The inhibition and substrate phosphorylation screening results were correlated with the compounds' in vitro cytotoxicity (MTT) against nonmalignant BJ and MRC-5 human fibroblast cell lines (Table 1). As expected, the

Table 1. Cytotoxicity, Human and Mtb ADK Inhibition, and Antimycobacterial Activity

				ADK inhibition IC_{50} (μM)			*M. tuberculosis*[d] MIC (μM)	
compd	BJ[a] CC_{50} (μM)	MRC-5 CC_{50} (μM)	ADK Phs[b] (%), human	human	Mtb	*M. bovis*[c] IC_{50} (μM)	My 331/88	Praha 131
1a	43.1 ± 3.6	13.4 ± 3.6	62	0.20 ± 0.02	0.33 ± 0.02	0.13	8	8
1b	50.9 ± 6.4	21.0 ± 3.2		>5	>10	1.34	8	8
1c	21.9 ± 1.4	61.4 ± 6.1		>5	>10	2.08	16	16
1d	18.0 ± 3.2	45.6 ± 3.5		>10	>10	0.36	4	8
1e	90.6 ± 5.8	94.4 ± 8.7		>10	>10	1.87	32	32
1f	13.9 ± 1.9	13.6 ± 1.5		>5	5.33 ± 0.65	0.39	2	4
1g	18.3 ± 2.1	9.49 ± 1.49	8	>5	2.10 ± 0.15	17.4	62.5	62.5
1h	91.5 ± 13.3	67.9 ± 14.9	9	>5	>10	8.31	16	16
1i	65.4 ± 2.6	39.4 ± 4.5	2	>5	>10	4.73	8	8
1j	12.9 ± 0.9	42.5 ± 5.3	2	>5	6.60 ± 0.51	3.93	8	8
1k	>100	99.6 ± 1.0	6	>20	4.4 ± 0.30	7.27	62.5	62.5
1l	10.1 ± 1.5	5.05 ± 0.88	20	4.5 ± 0.31	>10	1.12	62.5	62.5
1m	>100	25.1 ± 5.1	3	2.3 ± 0.17	4.5 ± 0.20	2.51	125	125
1n	9.51 ± 2.03	0.18 ± 0.13	7	>10	>10	48.0	>250	>250
1o	48.9 ± 5.3	71.2 ± 8.9	9	>10	>5	3.08	125	125
1p	0.12 ± 0.03	0.33 ± 0.04	47	13	>10	>100	>250	>250
1q	1.48 ± 0.28	0.15 ± 0.06	19	>20	>3	>100	>250	>250
1r	0.08 ± 0.02	0.10 ± 0.0	37	>20	>10	69.0	>250	>250
1s	21.2 ± 2.1	35.1 ± 3.8		>10	1.80 ± 0.20	2.27	16	16
1t	57.3 ± 1.4	37.9 ± 2.8		>20	4.9 ± 0.40	1.13	8	8
1u	>100	>100		3.3 ± 0.4	2.33 ± 0.25	6.75	32	32
1v	63.9 ± 4.4	52.9 ± 8.7		>20	>10	5.29	16	16
1w	>100	96.3 ± 5.9		>20	>10	4.54	62.5	62.5
1x	62.0 ± 9.1	78.8 ± 12.0		>10	>10	1.16	4	4
1y	59.9 ± 2.7	50.2 ± 8.8		>10	13.1 ± 1.5	3.07	32	32
1z	15.5 ± 0.7	46.0 ± 8.1		>10	>10	1.38	8	8
1aa	>100	>100		>10	>10	7.05	8	8
1ab	23.1 ± 2.5	>100		>10	>10	1.74	16	16
1ac	>100	66.0 ± 9.2		>10	>10	1.90	32	32
1ad	>100	100 ± 0.08		>10	0.6 ± 0.05	0.19	4	4
1ae	>100	95.1 ± 7.7		>20	0.3 ± 0.02	4.53	16	16
1af	>100	68.5 ± 6.3		>10	2.06 ± 0.14	44.32	62.5	125
1ag	19.6 ± 1.7	48.2 ± 9.6		>10	0.9 ± 0.12	1.30	8	8
1ah	40.6 ± 7.9	93.7 ± 6.5		>20	7.67 ± 0.81	1.68	4	4
1ai	0.12 ± 0.03	64.2 ± 12.1		>20	>10	74.42	62.5	62.5
1aj	>100	92.1 ± 12.5		>20	>10	6.39	16	32

[a]Cytotoxicity (MTT test) in BJ and MRC-5 fibroblasts. [b]Phs, ADK substrate activity (phosphorylation), conversion to 5′-phosphate (%). [c]50% growth inhibitory concentration of *Mycobacterium bovis BCG* cultivated in vitro. [d]Incubation time = 14 days. MIC of isoniazid as reference compound was 0.5 μM for the My 331/88 strain.

cytotoxicity strongly depended on the bulkiness of the substituent at position 7, with all compounds bearing bulky groups showing little to no cytotoxicity (with the exception of **1ai**, which was toxic to BJ cells). Most compounds did not significantly inhibit *h*ADK and were poor-to-moderate substrates for this enzyme. Only the 7-ethynyl derivative (**1a**) was a potent (submicromolar) *h*ADK inhibitor, while a few additional derivatives (**1l,m,u**) were inhibitory at micromolar concentrations. In contrast, most derivatives (e.g., **1f,g,j,k,m,s,t,u,y,af,ah**) showed significant inhibition of Mtb ADK with IC_{50} values in the micromolar range. Three bulky derivatives (**1ad,ae,ag**) inhibited the Mtb enzyme at submicromolar concentrations but showed no inhibitory activity toward *h*ADK. All compounds were also tested for activity against *Mycobacterium bovis* and Mtb (strain My 331/88 and drug-resistant strain Praha 131). Most compounds, except **1n–r**, were active against Mtb with in vitro minimum inhibitory concentration (MIC) ranging between 2 and 60 μM (see Table 1). The antimycobacterial activities of 14 compounds from our series of 39 nucleoside analogs correlated well with Mtb ADK inhibition. We found that **1d,i,x,aa,ab,ac,aj** were fairly active against Mtb and *M. bovis* but did not inhibit Mtb and *h*ADKs, perhaps suggesting that they can target other enzymes from the purine salvage pathway. The Mtb-ADK-specific derivative **1f** (7-(2-naphthyl)) displayed the highest antimycobacterial activity with MIC of 2 and 4 μM for the wild-type and drug-resistant Mtb strains, respectively. The nontoxic, Mtb-ADK-specific dibenzofuran derivative (**1ad**) showed the best therapeutic index. This compound displayed antimycobacterial activity with MIC of 4 μM for both Mtb strains. Compounds **1f** and **1ad** are promising lead structures for further development of antimycobacterial drugs. The lower activities of 7-deazapurine derivatives against Mtb compared to *M. bovis* could be the result of slightly different conditions used for cultivation and testing and/or the extent of compound uptake through the cell

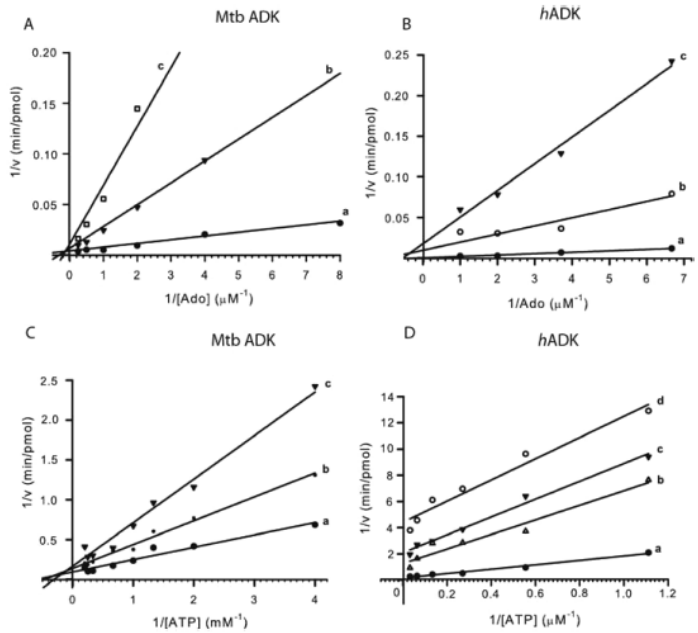

Figure 1. Kinetics of competition of **1a** with adenosine and ATP in Mtb ADK and *h*ADK binding sites. The panels show the Lineweaver−Burk plots: (A) inhibition of Mtb ADK in the presence of increasing concentrations of adenosine (Ado) (a, 0 μM; b, 0.5 μM; c, 1 μM) and 5 mM ATP; (B) inhibition of *h*ADK in the presence of increasing concentrations of Ado (a, 0 nM; b, 20 nM; c, 30 nM) and 120 μM ATP; (C) inhibition of Mtb ADK in the presence of increasing concentrations of ATP (a, 0 mM; b, 0 0.25 mM; c, 0.5 mM) and 5 μM Ado; (D) inhibition of *h*ADK in the presence of increasing concentrations of ATP (a, 0 nM; b, 15 nM; c, 30 nM; d, 60 nM) and 5 μM Ado.

wall. Therefore, our future focus will be on design of suitable prodrugs and delivery of nucleosides.

We observed differences in phosphorylation of 7-substituted 7-deazapurine nucleosides by human and Mtb ADK. While no synthesized analog was phosphorylated by Mtb ADK, several compounds served as substrates for *h*ADK (see Table 1). This may indicate differences in the structures of these enzymes and/or different binding modes of nucleoside analogs into the adenosine and ATP binding sites.

To gain insight into the mechanism of action of 7-substituted 7-deazapurine nucleosides on *h*ADK and Mtb ADK, the kinetics of compound **1a**, which inhibits both ADKs but is phosphorylated only by *h*ADK, were examined. For both enzymes, the Lineweaver−Burk double reciprocal plots of initial velocities against increasing concentrations of adenosine indicated mixed competitive inhibition (Figure 1A,B) with **1a**, suggesting inhibitor binding into either the adenosine or ATP binding sites (or simultaneously to both sites) with almost comparable affinities. The plots from competition of **1a** with ATP in Mtb ADK also showed mixed competitive inhibition (Figure 1C), but for *h*ADK nearly parallel lines for increasing concentration of ATP were detected (Figure 1D). This type of inhibition can be interpreted as a mixed uncompetitive inhibition, which suggests preferential binding of inhibitor into the already formed complex between the enzyme and ATP; however, it does not exclude binding of **1a** into the ATP site.

Crystal Structures of *h*ADK-1a and Mtb ADK-1a Complexes. To explore the binding of 7-substituted 7-deazapurine nucleosides to human and mycobacterial ADKs on a structural level, we determined crystal structures of *h*ADK and Mtb ADK in complex with **1a**, a compound that efficiently inhibits both enzymes and is specifically phosphorylated by *h*ADK.

The *h*ADK-**1a** complex crystallized in the $P2_12_12$ space group with two protein molecules in the asymmetric unit. The crystallographic model was refined to 2.5 Å resolution. Three molecules of **1a** were modeled into a well-defined electron density map (Figure S1 in Supporting Information). In both *h*ADK molecules in the asymmetric unit, **1a** binds into the substrate binding site located at the interface between a large core domain and a small lid domain. The position of **1a** mimics that of adenosine found in the crystal structure of the *h*ADK−adenosine complex (PDB code 1BX4).[20] The overall structure of the *h*ADK-**1a** complex is very similar to that of the adenosine bound enzyme. The protein adopts a closed conformation in which the small lid domain closes over the active site. Compound **1a** is completely buried in a hydrophobic pocket formed by amino acid residues Leu16, Leu40, Leu134, Ala 136, Leu138, and Phe170 (Figure 2A). The position of the base ring moiety is stabilized by a stacking interaction with the Phe170 side chain. The ethynyl moiety of **1a** is buried deep in the hydrophobic pocket and takes the place of a water molecule observed in the structure of *h*ADK with bound adenosine.

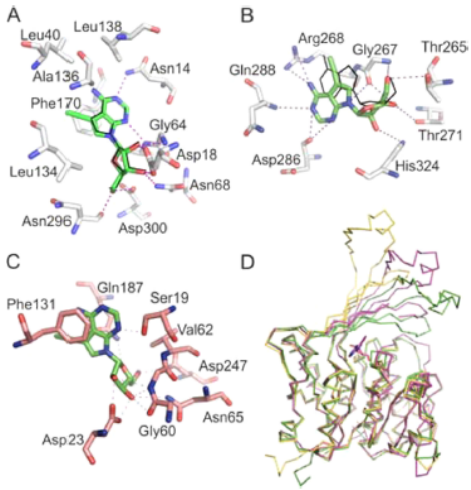

Figure 2. Binding of **1a** to the adenosine binding site (A) and ATP binding site (B) of *h*ADK and to Mtb ADK (C). Residues interacting with **1a** are shown as sticks. Polar interactions are shown by magenta dashed lines. Adenosine positions superposed from crystal structures of *h*ADK−adenosine (PDB code 1BX4)[20] or Mtb ADK−adenosine (PDB code 2PKM)[21] complexes are represented as black lines. Panel D shows superposition of the semiopen conformation of the Mtb ADK-**1a** complex (magenta) with the open conformation of Mtb ADK apo form (yellow, PDB code 2PKF) and the closed conformation of the Mtb ADK-adenosine complex (green, PDB code 2PKM).

Similar replacement of a water molecule by an iodine atom was also observed for 5-iodo-5′-deoxytubericidin (PDB code 2I6A).[7] The ribose ring of **1a** forms numerous direct hydrogen bonds with residues Asn14, Asp18, Gly64, Asn68, Asn296, and Asp300 (Figure 2A).

In one of the *h*ADK molecules in the asymmetric unit (protein chain A), an additional molecule of **1a** is bound in the ATP binding site located in the core domain about 15 Å from the adenosine binding site. Partial occupancy within the asymmetric unit points to a lower affinity of this site for **1a**. The following amino acid residues form polar contacts with **1a**: Thr265, Gly267, Arg268, Thr271, Asp286, Gln288, and His324 (Figure 1B). The pose of **1a** closely resembles the binding of adenosine molecule into ATP binding site as found in the structure of the hADK−adenosine complex (PDB code 1BX4).[20] The positions of the sugar moieties of **1a** and adenosine are very similar, but the positions of the bases are different. Interestingly, a loop surrounding the ATP binding site (and connecting β14 to α11) is partially disordered in the *h*ADK-**1a** structure, and amino acid residues 286−292 could not be modeled into a continuous electron density map.

The Mtb ADK-**1a** complex crystallized in the $P3_1$ space group with two protein molecules per asymmetric unit representing the biologically relevant Mtb ADK dimer. The final crystallographic model was refined to 2.5 Å resolution with two molecules per asymmetric unit. The quality of electron density map for residues 9−48 and 99−120 is limited suggesting that the lid domain region is partially disordered. One molecule of **1a** bound to the enzyme active site was modeled into a well-defined electron density map in both molecules in the asymmetric unit (Figure S1). A molecule of **1a** binds into the adenosine binding pocket located at the interface of the core and lid domains; the ATP binding site remains unoccupied. Compound **1a** is deeply buried in the enzyme's active site, and its position is similar to that of adenosine (Figure 2C). The base ring moiety forms a stacking interaction with Phe131, and N1 engages in a polar interaction with the side chain of Ser19. The ethynyl moiety of **1a** makes a small number of van der Waals interactions with the hydrophobic side chains of Phe115 and Phe131. The ribose ring of **1a** forms numerous direct hydrogen bonds with the side chains of Asp23, Asn65, Gln187, and Asp274 and the main chain of Gly60 (Figure 2C). The lid domain (residues 9−48 and 99−120) adopts a unique conformation in the Mtb ADK-**1a** complex. While the conformation of the lid domain is open in the free or ATP-bound enzyme, it adopts a closed conformation upon binding of adenosine in *h*ADK[20] and 2-fluoroadenosine, the only inhibitor for which the MtbADK complex structure is available (PDB code 2PKK).[21] The conformation of the lid domain in the Mtb ADK-**1a** complex structure can be described as semiopen, because its position is between the open and closed states (Figure 2D). When the closed conformation of the lid is superposed on the Mtb ADK-**1a** complex structure, steric clashes occur between the ethynyl moiety of **1a** and residues Ser130, Phe131, and Phe115. We can therefore conclude that binding of **1a** prevents formation of catalytically competent arrangement of the closed enzyme. This can serve as a structural explanation for the observation that **1a** is not phosphorylated by Mtb ADK.

Competition of 7-Substituted 7-Deazapurine Derivatives with Adenosine and ATP in Mtb and Human Adenosine Kinases. We used 1D ^{1}H STD NMR experiments

Table 2. Relative STD Enhancements of Substrate (Adenosine or ATPγS) and Inhibitor Signals in the Presence of *h*ADK or Mtb ADK[a]

	relative STD enhancement (%)													
	*h*ADK							Mtb ADK						
	Ado	ATP	**1a**	**1m**	**1u**	**1ae**	**1g**	Ado	ATP	**1a**	**1m**	**1u**	**1ae**	**1g**
H-1′	100	100	100	100	100	100	100	100	100	100	100	100	100	100
H-2	8	<1	33	57	72	33	64	44	57	63	37	42	50	43
H-8	20	<1	17	41	72	39	36	58	24	54	33	42	68	29
Ar				52	52	60	74				34	37	83	38
Ar′				78			67				45			31
Ar″							78							39

[a]Concentration of all nucleosides was kept at the 500 μM.

to establish the mode of competition of 7-hetaryl-7-deazapurine derivatives with adenosine and ATPγS for their respective binding sites and also to define the binding epitopes of the newly developed inhibitors.

First, we examined the binding behavior and mutual competition of adenosine and ATPγS to *h*ADK and Mtb ADK. For adenosine in the presence of *h*ADK, the strongest enhancement was observed for the signal from H-1′ and weaker enhancements for two aromatic proton signals H-8 and H-2 of ∼20% and ∼8% relative to H-1′ (Table 2), which suggests that protons H-1′ and H-8 are in closer contact with the protein than the rest of the substrate molecule. An analogous experiment for ATPγS yielded much weaker absolute STD enhancements, which were limited to H-1′ and NH_2. In addition, the STD enhancements induced by binding to *h*ADK of both substrates were not significantly affected in spectra obtained from their equimolar mixture, which indicates that adenosine and ATPγS do not compete and bind into their original binding sites.

The STD spectra for adenosine in the presence of Mtb ADK yielded maximum enhancement for H-1′ and moderate enhancement for H-8 and H-2 of ∼58% and ∼44% (Figure 3A, Table 2), suggesting a similar contact epitope to that observed for *h*ADK. The overall STD enhancement for ATPγS in the presence of Mtb ADK was comparable to that of adenosine, again with H-1′ being the most affected proton (Figure 3B, Table 2). However, certain differences were found for the remaining ATPγS protons in comparison with their binding to *h*ADK. There was a very weak enhancement of the NH_2 signal (<5%), and the H-2 STD signal (∼57%) was stronger than the H-8 signal (∼24%). Importantly, simultaneous addition of adenosine and ATPγS to MtbADK led to a dramatic reduction in the ATPγS enhancements, suggesting direct competition between binding of adenosine and ATPγS, as illustrated in Figure 3C. Intracellular ATP levels are generally in the low millimolar range, and adenosine is present at micromolar concentrations.[22−28] Therefore, we can speculate that ATP binds into Mtb ADK first, and conformational changes in ADK allow adenosine binding and phosphorylation in bacteria.

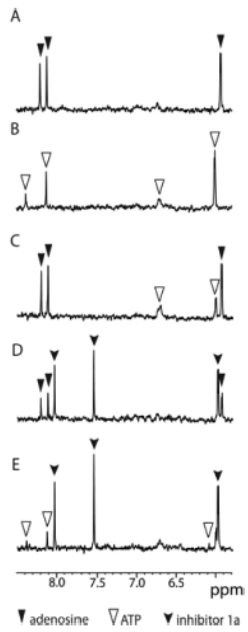

Figure 3. 1D ^{1}H STD NMR substrate/inhibitor competition experiments for Mtb ADK. (A) shows a region of the STD spectrum obtained for Mtb ADK in the presence of adenosine, while (B) shows the spectrum for the enzyme in the presence of ATPγS. (C) shows the spectrum for the mixture of substrates, with intensity of the ATPγS specific signals significantly reduced. (D) and (E) show competition of **1a** with adenosine and ATPγS illustrated by the clear drops in the STD enhancement of signals from both substrates.

We then selected compounds containing either smaller (**1a**, **1g**, **1m**) or bulkier (**1u**, **1ae**) substituents in position 7. They displayed different (**1g**, **1ae**) or comparable (**1a**, **1m**, **1u**) inhibition activities against human and mycobacterial ADK. We tested their competition with adenosine and ATPγS in the presence of either *h*ADK or Mtb ADK. All selected 7-deazaadenosines selectively competed with adenosine, as their STD enhancements were significantly reduced, but did not affect ATPγS signals in the presence of *h*ADK. This suggests significantly lower affinity of tested compounds to ATP site relative to ATPγS. The ATP site was occupied by **1a** in our crystal structure of *h*ADK, but this was due to high inhibitor excess in the crystallization experiment. However, the STD data in the presence of Mtb ADK indicated strong competition of inhibitors with both substrates (Figure 3D,E), which confirmed that these compounds can also bind into the ATP site. The STD enhancements for the substrates and inhibitors normalized to the H-1′ signal enhancement are shown in Table 2. We observed that H-1′ is subjected to the strongest STD enhancement for all inhibitors tested, independent of the protein present in sample solution. This suggests that the sugar moiety is in direct contact with the protein in all complexes. The substantial contributions from the purine protons H-2 and H-8 are found in all complexes, with approximately 50% enhancement relative to H-1′. Protein-dependent differences were found in the STD enhancements of the signals from substituents at position 7. The relative enhancements for aromatic substituent signals were higher than H-2 and H-8 enhancements in *h*ADK complexes, while they remained comparable in Mtb ADK complexes, suggesting that the substituents maintain much more extensive contacts with *h*ADK than Mtb ADK. The potential binding of 7-deazanucleosides into the ATP binding site contributes to the loss of their phosphorylation.

Binding of Selected 7-Hetaryl-7-deazapurine Derivatives to Human ADK by Protein-Detected NMR. We used two-dimensional NMR spectroscopy to study the detailed mechanism of inhibitor binding to *h*ADK. The low stability of Mtb ADK at the high concentration (100 μM) required for relatively long NMR experiments did not allow us to prepare a sample of sufficient quality for binding experiments. Initially, we analyzed 2D ^{15}N/^{1}H HSQC spectra of reference samples of ^{15}N-labeled *h*ADK in the absence and presence of adenosine or ATPγS. The 2D ^{15}N/^{1}H HSQC spectrum of free *h*ADK consisted of 270 unique signals from backbone and side chain amide groups, some subjected to extensive spectral overlaps, which corresponds to the size of the analyzed protein. Both

ligands induced a number of specific changes in the positions of signals in 2D $^{15}N/^{1}H$ HSQC spectra, indicating that this approach is suitable for studying binding modes of *h*ADK inhibitors.

Preliminary NMR experiments using ^{15}N labeled material revealed a relatively poor long-term stability of *h*ADK at temperatures above 25 °C. The 3D experiments required for backbone resonance assignment were acquired at 25 °C to minimize protein precipitation and overall material consumption. The exchange of nonlabile protons for deuterons enabled sequence-specific backbone resonance assignments; however, a certain proportion of amide groups unexpectedly did not back-exchange during protein purification in an H_2O environment and remained deuterated, as suggested by comparison of the 2D $^{15}N/^{1}H$ HSQC spectra obtained from ^{15}N and $^{2}H/^{13}C/^{15}N$-labeled *h*ADK. The high quality of NMR spectra allowed us to assign essentially all 175 detectable signals in perdeuterated *h*ADK using a previously described approach.[29,30] Detailed analysis revealed that the amide groups buried in the protein core and contributing as hydrogen bond donors were often not successfully protonated during purification in an H_2O environment. The distribution of successfully assigned backbone amide groups is illustrated in Figure S2.

As a next step, we acquired and analyzed 2D $^{15}N/^{1}H$ HSQC spectra of *h*ADK bound to the set of compounds (**1a**,**g**,**m**,**u**,**ae**) investigated by NMR 1D ^{1}H STD experiments. These data were compared with the reference spectra; we selected 17 well-resolved representative backbone amide signals in the spectrum of free *h*ADK (Table 3 and Figure 4). All compounds studied,

Table 3. Analysis of *h*ADK 2D $^{15}N/^{1}H$ HSQC Spectra in the Presence of Inhibitors[a]

	number of signals corresponding to the reference of			
inhibitor	free *h*ADK	*h*ADK + adenosine	*h*ADK + ATPγS	specific signal
1a	5	13	1	0
1g	3	14	1	0
1m	3	13	5	1
1u	5	11	3	2
1ae	6	6	8	2

[a]We selected a set of well-resolved backbone amide signals and followed their changes upon addition of selected inhibitors. Free *h*ADK and the *h*ADK in the presence of adenosine or ATPγS were used as reference samples. The signals were sorted into four distinct categories according to their behavior in the presence of an inhibitor.

with the exception of **1ae**, which contains a large 4-phenoxathiinyl group, induced changes in 2D $^{15}N/^{1}H$ HSQC spectra that closely correspond to those observed for adenosine binding, suggesting direct competition of inhibitors for the adenosine binding pocket. The spectrum of *h*ADK in the presence of **1ae** exhibited signal changes that did not unambiguously correspond to any reference spectrum, indicating that the binding mode of this inhibitor might be atypical or mixed. Additional analysis using backbone resonance assignments revealed that this compound induced specific differences compared to the reference spectrum acquired for *h*ADK in the presence of adenosine. Similar data were obtained for the isopropylphenyl derivative (**1u**) with a relatively large substituent in position 7.

Quantum Mechanical Analysis of Binding of Selected 7-Hetaryl-7-deazapurine Derivatives to Human and Mtb ADK. Complexes of *h*ADK and Mtb ADK with the compounds used for NMR competition experiments (**1a**,**g**,**m**,**u**,**ae**) were further analyzed using semiempirical quantum mechanical (SQM) based scoring function.[31,32] To build in silico models of *h*ADK complexes, we used the X-ray structure of *h*ADK in complex with two adenosine molecules (PDB code 1BX4).[20] In this structure, one adenosine molecule is located in the adenosine binding site and the second in the ATP binding site. The inhibitors were built and scored in both binding sites. The complex of *h*ADK with **1ae** could not be built because of numerous steric clashes between the inhibitor and protein. The calculated scores for the remaining inhibitors are summarized in Table 4. The inhibitors have higher affinity to the adenosine binding site (scores from −30 to −65 kcal/mol) than to the ATP binding site (scores from −12 to −23 kcal/mol). This is due to the more favorable interactions in the adenosine binding site (ΔE_{int} more negative by about 60%). These results are in good agreement with our experimental NMR finding that the inhibitors compete with higher affinity with adenosine than with ATP in the presence of *h*ADK. Compounds **1a**, **1g**, and **1m** fit well into the adenosine binding site. The 7-deaza derivative **1u** is too big to fit into the conformation of *h*ADK that was used for modeling, and its binding requires changes in the protein conformation (see Figure S3). The conformational changes significantly increased the penalty for the change of the conformational "free" energies ($\Delta G'^{w}_{int}$) of both the protein and ligand (by about 100% and 40%, respectively). This supports the NMR results showing that compounds with large substituents (**1u** and **1ae**) induce different structural changes in *h*ADK than adenosine or compounds with small substituents in position 7.

Mtb Adk complexes with the selected inhibitors were also studied using the SQM scoring function. Previous structural analyses of Mtb ADK show that binding of ATP or its analog does not change the conformation of this enzyme. However, the X-ray structure of Mtb ADK crystallized with **1a** (PDB code 4PVV) shows that the binding of adenosine analog results in movement of lid domain and formation of a semiclosed conformation. This suggests that inhibitors compete with adenosine in an open conformation. Subsequently, the binding affinity of the adenosine analogs to the adenosine site might increase when the conformation of Mtb ADK is changed from open to semiopen. To support this hypothesis, we used both the X-ray structure of Mtb ADK dimer in open conformation in complex with an ATP analog (PDB code 2PKN)[21] and the X-ray structure of semiopen conformation of Mtb ADK crystallized with **1a** to build our in silico models of Mtb ADK complexes. The closed conformation of Mtb ADK (Mtb ADK dimer crystallized with adenosine, PDB code 2PKM) did not allow us to build models. The calculated scores are summarized in Table 5, and the SQM optimized complexes of **1a** and **1ae** are shown in Figure 5. Interestingly, the inhibitors have comparable affinity to both the adenosine and ATP binding sites in the open conformation of Mtb ADK (scores ranged from −20 to −25 and from −11 to −17 kcal/mol to the ATP and adenosine binding sites, respectively). However, the affinity of 7-substituted 7-deazapurine nucleosides to the adenosine binding site increases significantly in the semiopen conformation of Mtb ADK with bound nucleosides (score from −50 to −59 kcal/mol) and is comparable to those calculated for these inhibitors bound in *h*ADK adenosine site.

dx.doi.org/10.1021/jm500497v | J. Med. Chem. 2014, 57, 8268−8279

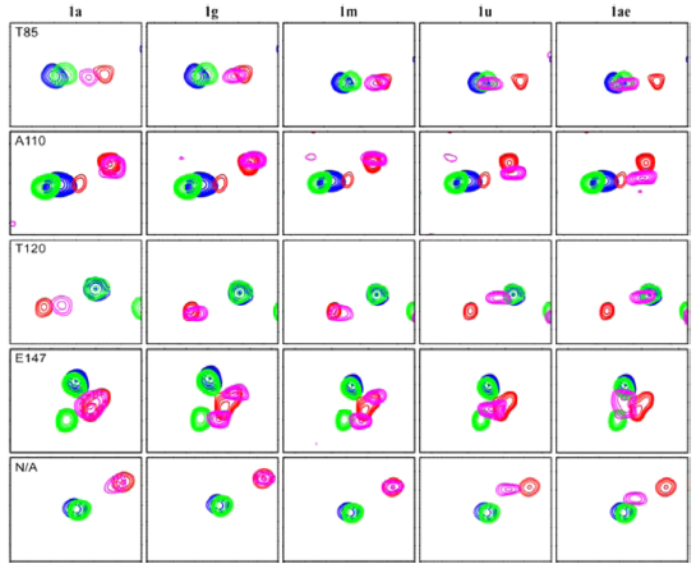

Figure 4. Binding of inhibitors to *h*ADK analyzed using 2D $^{15}N/^{1}H$ HSQC. Each row represents a different backbone amide group cross-peak (the residue number is given in the first column). Columns illustrate changes in the spectra obtained for a selected inhibitor. Contours are colored as follows: blue, free *h*ADK; green, *h*ADK in the presence of ATPγS; red, *h*ADK in the presence of adenosine; magenta, hADK in the presence of inhibitor. Concentration of all nucleosides was kept at 500 μM.

Table 4. Inhibition Constant (IC_{50}) and Score of the Studied Inhibitors to *h*ADK Calculated As a Sum of the Gas-Phase Interaction Energy (ΔE_{int}), the Interaction Solvation/Desolvation Free Energy ($\Delta\Delta G_{solv}$), the Change of the Conformational "Free" Energies of the Protein and Ligand ($\Delta G'^{w}_{conf}$(P,L)), and the Entropy Change upon Binding ($-T\Delta S_{int}$)

				Human ADK			
inhibitor	IC_{50} (μM)	score (kcal/mol)	ΔE_{int} (kcal/mol)	$\Delta\Delta G_{solv}$ (kcal/mol)	$\Delta G'^{w}_{conf}$(L) (kcal/mol)	$\Delta G'^{w}_{conf}$(P) (kcal/mol)	$-T\Delta S_{int}$ (kcal/mol)
				Adenosine Binding Site			
1a	0.2 ± 0.015	−59.7	−149.6	59.3	7.6	23	0
1g	>5	−65.0	−158.4	61.3	8.6	23.5	0
1m	2.3 ± 0.17	−56.6	−157.2	61.3	9.1	30.1	0
1u	3.3 ± 0.4	−30.6	−163.9	68.1	11.5	49.7	4
				ATP Binding Site			
1a	0.2 ± 0.015	−22.6	−93.5	43.8	2.4	24.7	0
1g	>5	−22.4	−97.1	47.3	2.5	24.8	0
1m	2.3 ± 0.17	−22.9	−95.8	49.4	2.2	21.3	0
1u	3.3 ± 0.4	−11.7	−101.5	52.7	4.6	28.5	4

■ CONCLUSIONS

A new series of 7-(het)aryl-7-deazaadenine ribonucleosides bearing small and bulky substituents in position 7 was synthesized and evaluated as potential new antimycobacterial agents. Several compounds bearing smaller substituents (e.g., **1a**) were found to inhibit both human and Mtb ADK and were cytotoxic, whereas several bulky derivatives (e.g., **1ad**, **1ae**, **1ag**) were specific inhibitors of the Mtb enzyme and were not cytotoxic. 7-(2-Naphthyl)-7-deazaadenine (**1f**) was the most active compound against Mtb strain My331/88 and drug-resistant strain Praha 131 in vitro (MIC = 2 or 4 μM, respectively), but its cytotoxicity disfavors its further development. The dibenzofuran derivative (**1ad**) had the best therapeutic index. This compound was a submicromolar Mtb-ADK-specific inhibitor and was active against Mtb strains with a MIC of 4 μmol/L. This compound is a promising lead structure for further drug development. Following binding of the 7-(het)aryl-7-deazaadenine ribonucleosides into the adenosine site, Mtb ADK adopts a unique semiopen conformation of the lid domain, and *h*ADK adopts the closed conformation. Enzyme kinetics and 1D ^{1}H STD NMR analysis of the inhibitors' competition with adenosine and ATPγS showed that 7-(het)aryl-7-deazaadenine ribonucleosides bind preferentially into the adenosine site in *h*ADK and are readily accommodated in both, to the adenosine and ATP sites in Mtb ADK. Quantum mechanical analysis indicated that these compounds have higher affinity for the ATP site of Mtb ADK in the open conformation, but movement of the lid domain increases

Table 5. Inhibition Constant (IC_{50}) and Score of Inhibitors of Mtb ADK Calculated as a Sum of Gas-Phase Interaction Energy (ΔE_{int}), the Interaction Solvation/Desolvation Free Energy ($\Delta\Delta G_{solv}$), the Change in Conformational "Free" Energies of the Protein and Ligand ($\Delta G'^{w}_{conf}$(P,L)), and the Entropy Change upon Binding ($-T\Delta S_{int}$)

	Mtb AdK						
inhibitor	IC_{50} (μM)	score (kcal/mol)	ΔE_{int} (kcal/mol)	$\Delta\Delta G_{solv}$ (kcal/mol)	$\Delta G'^{w}_{conf}$(L) (kcal/mol)	$\Delta G'^{w}_{conf}$(P) (kcal/mol)	$-T\Delta S_{int}$ (kcal/mol)
			Adenosine Binding Site in Semiopen Conformation				
1a	0.33 ± 0.02	−57.0	−131.3	63.3	2.9	8.1	0
1g	2.1 ± 0.15	−59.2	−140.7	66.9	3.4	11.3	0
1m	4.5 ± 0.2	−57.2	−141.5	68.0	4.9	11.4	0
1u	2.33 ± 0.25	−51.4	−140.8	69.5	3.8	12.1	4
1ae	0.3 ± 0.02	−49.8	−142.9	72.0	5.2	15.9	0
			Adenosine Binding Site in Open Conformation				
1a	0.33 ± 0.02	−17.4	−72.5	44.4	4.4	6.3	0
1g	2.1 ± 0.15	−16.4	−77.8	47.3	5.3	8.9	0
1m	4.5 ± 0.2	−12.9	−72.3	48.8	2	8.6	0
1u	2.33 ± 0.25	−13.3	−77.5	44.7	5.4	10.1	4
1ae	0.3 ± 0.02	−11.4	−75.1	47.2	5.3	11.2	0
			ATP Binding Site in Open Conformation				
1a	0.33 ± 0.02	−23.8	−76.2	43.6	0.9	8	0
1g	2.1 ± 0.15	−24.8	−78.8	45.5	1.1	7.4	0
1m	4.5 ± 0.2	−20.1	−75.4	44.6	1.3	9.4	0
1u	2.33 ± 0.25	−20.3	−84	46.1	2.9	10.7	4
1ae	0.3 ± 0.02	−24.3	−83.8	47.2	2.1	10.3	0

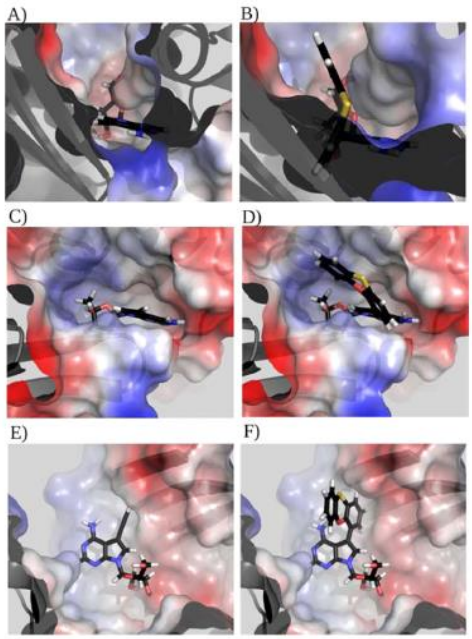

Figure 5. Model of **1a** bound to adenosine binding site in semiopen conformation (A), ATP binding site in open conformation (C) and adenosine binding site in open conformation (E) of Mtb ADK and **1ae** bound to adenosine binding site in semiopen conformation (B), ATP binding site in open conformation (D) and adenosine binding site in open conformation (F) of Mtb ADK.

binding affinity of these inhibitors in the adenosine site. Both the preferential binding of 7-(het)aryl-7-deazaadenine ribonucleosides in the Mtb ADK ATP binding site and the unique semiopen conformation of Mtb ADK during inhibitor binding in the adenosine site explain the observation that 7-(het)aryl-7-deazaadenine ribonucleosides are not phosphorylated by ADK. Similar mechanisms may also occur for deazaadenine ribonucleoside derivatives modified at other positions.

EXPERIMENTAL SECTION

Chemical Synthesis. 4-Amino-5-(3,4-dimethylphenyl)-7-(β-D-ribofuranosyl)-7*H*-pyrrolo[2,3-*d*]pyrimidine (1t). An argon-purged mixture of 4-amino-5-iodo-7-(β-D-ribofuranosyl)-7*H*-pyrrolo-[2,3-*d*]pyrimidine (**2**, 392 mg, 1 mmol), 3,4-dimethylphenylboronic acid (225 mg, 1.5 mmol), Na_2CO_3 (318 mg, 3 mmol), TPPTS (71 mg, 0.125 mmol), $Pd(OAc)_2$ (11 mg, 0.05 mmol) in water/MeCN (2:1, 5 mL) was stirred at 100 °C for 3 h. After cooling, the mixture was neutralized using aqueous HCl (1 M) and concentrated to dryness in vacuo. The residue was loaded onto silica by coevaporation from a chloroform/MeOH solution, and column chromatography (SiO_2, 0 → 2.5% MeOH in $CHCl_3$) afforded **1t** (305 mg, 82%) as a yellowish foam. Mp 120−124 °C. $[\alpha]_D$ −56.3 (*c* 0.270, DMSO). ^{1}H NMR (600.1 MHz, DMSO-d_6): 2.26 (s, 3H, CH_3-4); 2.28 (s, 3H, CH_3-3); 3.54 (bdt, 1H, J_{gem}= 11.8, $J_{5'b,4'}$ = $J_{5'b,OH}$ = 3.5, H-5′b); 3.63 (bdd, 1H, J_{gem}= 11.8, $J_{5'a,4'}$ = 3.5, H-5′a); 3.91 (td, 1H, $J_{4',5'}$ = 3.5, $J_{4',3'}$ = 3.2, H-4′); 4.10 (ddd, 1H, $J_{3',2'}$ = 5.1, $J_{3',OH}$ = 4.8, $J_{3',4'}$ = 3.2, H-3′); 4.45 (ddd, 1H, $J_{2',OH}$ = 6.5, $J_{2',1'}$ = 6.3, $J_{2',3'}$ = 5.1, H-2′); 5.14 (d, 1H, $J_{OH,3'}$ = 4.8, OH-3′); 5.22 (bm, 1H, OH-5′); 5.34 (d, 1H, $J_{OH,2'}$ = 6.6, OH-2′); 6.11 (d, 1H, $J_{1',2'}$ = 6.3, H-1′); 6.13 (bs, 2H, NH_2); 7.18 (dd, 1H, $J_{6,5}$ = 7.7, $J_{6,2}$ = 2.0, H-6-$C_6H_3Me_2$); 7.25 (d, 1H, $J_{5,6}$ = 7.7, H-5-$C_6H_3Me_2$); 7.26 (d, 1H, $J_{2,6}$ = 2.0, H-2-$C_6H_3Me_2$); 7.48 (s, 1H, H-6); 8.14 (s, 1H, H-2). ^{13}C NMR (150.9 MHz, DMSO-d_6): 19.33 (CH_3-4); 19.76 (CH_3-3); 61.92 (CH_2-5′); 70.88 (CH-3′); 74.01 (CH-2′); 85.32 (CH-4′); 87.21 (CH-1′); 100.82 (C-4a); 116.58 (C-5); 120.93 (CH-6); 126.06 (CH-6-$C_6H_3Me_2$); 129.88 (CH-2-$C_6H_3Me_2$); 130.27 (CH-5-$C_6H_3Me_2$); 132.11 (C-1-$C_6H_3Me_2$); 135.22 (C-4-$C_6H_3Me_2$); 137.10 (C-3-$C_6H_3Me_2$); 150.91 (C-7a); 151.81 (CH-2); 157.50 (C-4). IR (ATR): ν 1625, 1589, 1542, 1469, 1303, 1236, 1217, 1185, 1122, 1082, 1041, 896, 869, 828, 798, 707, 646 cm^{-1}. MS (ESI) *m*/*z* 371 (M + H), 393 (M + Na). HRMS (ESI) for $C_{19}H_{23}N_4O_4$ [M + H] calcd, 371.1714; found, 371.1713. Anal. ($C_{19}H_{22}N_4O_4$·0.8H_2O) C, H, N.

Other compounds (**1u–aj**) were prepared analogously. For characterization data, see Supporting Information.

Enzyme Preparation and Inhibitor Testing. Expression and purification of human and Mtb ADK were performed as previously described.[19] Compounds were tested for inhibition of human and Mtb ADK using previously established methods.[19]

Enzyme Kinetics. The individual assays were performed at 37 °C in 96-well microtiter plates. The reactions with both enzymes were performed in 250 mM Tris, pH 8.0, 50 mM KCl, 5 mM $MgCl_2$. When inhibitor **1a** was tested for a possible competition with adenosine, the concentration of ATP in the reaction mixtures was fixed at 5 mM for Mtb ADK or 120 μM for *h*ADK. The concentration of radiolabeled [^{3}H]adenosine varied from 0 to 1 μM. During testing of inhibitor **1a** with ATP the concentration of radiolabeled adenosine was kept at 5 μM and concentration of ATP increased from 0 to 60 nM (*h*ADK) or 0 to 0.5 mM (Mtb ADK). The individual reactions were started by the addition of enzyme, and the reaction proceeded for 4 min. Then 80 μL of samples was withdrawn and directly added to 1 mL of ice cold 0.1 M $LaCl_3$ to precipitate formed radiolabeled AMP. After keeping on ice for at least 3 h, the precipitate was collected by filtration on a glass-microfiber filter (1.2 μm pores, Sigma-Aldrich). The filters were washed with 100 mL of ice cold water, dried, and the radioactivity was measured in a liquid scintillation counter (Tri-Carb 2900 TR) after adding of 4 mL of scintillation cocktail. Two or three separate measurements were performed for best fitting the experimental data. The obtained results were analyzed using SigmaPlot (version 11) and Microsoft Excel software.

Antimycobacterial Susceptibility Testing. Compounds were tested for antimycobacterial activity against Mtb 331/88 (H37Rv) and patient-derived MDR Mtb strain Praha 131 as previously described.[33] Micromethod was used to determine the minimum inhibitory concentration (MIC). MIC values were determined after incubation at 37 °C for 14 and 21 days. The first-line anti-TB drug isoniazid (INH) was used as a reference compound.

NMR Spectroscopy. All NMR data were collected on a 600 MHz Bruker Avance spectrometer equipped with a triple-resonance (^{15}N/^{13}C/^{1}H) cryoprobe. NMR samples were prepared in a 25 mM sodium (*h*ADK) or potassium (Mtb ADK) phosphate, 15 mM $MgCl_2$, 100 mM sodium chloride buffer at pH 7.0, containing 5% D_2O/95% H_2O. NMR spectra for resonance assignment of *h*ADK were acquired from 0.35 mL samples of 0.25 mM ^{2}H/^{13}C/^{15}N protein at 25 °C. A series of triple-resonance spectra were recorded to determine sequence-specific resonance assignments for *h*ADK. In particular, we used TROSY versions of HNCACB, HN(CO)CACB, HNCA, HNCO, and HN(CA)CO experiments[34,35] with typical acquisition times of 7 ms for $^{13}C^{\alpha/\beta}$, 30 ms for $^{13}C'$, 16 ms for ^{15}N, and 70 ms for ^{1}H. The total experimental times for 3D experiments were 48–96 h.

Uniformly ^{15}N and ^{2}H/^{13}C/^{15}N labeled *h*Adk was produced from cells grown in minimal medium containing ^{15}N-ammonium sulfate and ^{13}C-D-glucose if required, as the sole nitrogen and carbon sources, and 100% D_2O when appropriate as described previously.[36] The specific binding of small molecule substrates or inhibitors to *h*ADK was monitored by changes induced in the positions of signals of 75 μM ^{15}N-labeled *h*ADK in 2D ^{15}N/^{1}H HSQC spectra acquired at 35 °C. In addition, the binding of small molecules to either *h*ADK or Mtb ADK was followed by ligand-detected saturation transfer difference (STD) experiments.[37,38] STD spectra were acquired at 20 °C using 0.55 mL samples of 5 μM unlabeled *h*ADK or Mtb ADK in the presence of a 100-fold excess (500 μM) of small molecule substrates or inhibitors with 2.5 s irradiation alternating between 0.5 ppm (on-resonance) and 20 ppm (off-resonance) using a train of 50 ms Gaussian pulses. The typical experimental time was 14 min.

Quantum Mechanical Analysis. To build in silico models, we used the X-ray structure of *h*ADK in complex with two adenosine molecules (PDB code 1BX4),[20] Mtb ADK crystallized with **1a** (PDB code 4PVV), and the X-ray structure of Mtb ADK dimer in open conformation in complex with an ATP analog (PDB code 2PKN).[21] The complexes were systematically optimized using the PM6-D3H4 method[39] combined with the COSMO solvent model[40] and fire algorithm. We only optimized amino acids within 8 Å of the inhibitors. The rest of the protein was frozen. The binding affinity was approximated by the total score expressed by eq 1.[31,32]

$$\text{score} = \Delta E_{\text{int}} + \Delta\Delta G_{\text{solv}} + \Delta G'^{\text{w}}{}_{\text{conf}}(\text{L}) + \Delta G'^{\text{w}}{}_{\text{conf}}(\text{P}) - T\Delta S_{\text{int}} \quad (1)$$

$$\Delta\Delta G_{\text{solv}} = \Delta\Delta G_{\text{int,solv}} + (\Delta G^{\text{low}}{}_{\text{solv}}(\text{L}) - \Delta G^{\text{high}}{}_{\text{solv}}(\text{L})) \quad (2)$$

Particular terms in the equation describe the gas-phase interaction energy (ΔE_{int}), the interaction solvation/desolvation free energy ($\Delta\Delta G_{\text{solv}}$), the change of the conformational "free" energy of ligand and protein ($\Delta G'^{\text{w}}{}_{\text{conf}}$(L,P)), and the entropy change upon binding ($T\Delta S_{\text{int}}$). The ΔE_{int} was calculated using the PM6-D3H4 method. The solvation free-energy change $\Delta\Delta G_{\text{int,solv}}$ was determined by the COSMO solvent model. The more accurate SMD/HF/6-31G* method was also used.[41,42] However, the SMD method is too demanding to be used for a protein, giving rise to the correction of ligand solvation/desolvation ($\Delta G^{\text{low}}{}_{\text{solv}}(\text{L}) - \Delta G^{\text{high}}{}_{\text{solv}}(\text{L})$), which is the difference between the solvation free energy calculated at high (SMD/HF/6-31G*) and low (COSMO/PM6) levels of theory.

The $\Delta G'^{\text{w}}{}_{\text{conf}}$(L,P) term is the "free" energy change between the ligand and protein in their optimal solution structure and the conformation they adopt in the complex. To evaluate $\Delta G'^{\text{w}}{}_{\text{conf}}$(L), we combined the gas phase PM6-D3H4 energy with the SMD solvation free energy. The $G'^{\text{w}}{}_{\text{conf}}$(P) term was evaluated using an annealing approach at the molecular mechanics level. The parameters for the protein were obtained from the FF03 force field; parameters for the inhibitors were obtained from the GAFF force field. The charges for the ligands were calculated using the RESP procedure at the HF/6-31G* level as recommended.[43] The isolated protein and the complex were optimized by annealing prior to standard optimization using fire algorithm. The annealing was started at 300 K, then cooled to 0 K in 1000 steps (length of each step, 1 fs) using Berendsen thermostat. For each system, eight independent runs with different starting velocities were performed, and the obtained energies were averaged. Only residues within 8 Å of the inhibitors were optimized. The rest of the protein was frozen. Finally, the $T\Delta S_{\text{int}}$ term of score was estimated using the rotatable bonds approach (i.e., 1 kcal/mol penalty for each rotatable bond in the ligand).

Protein Crystallization. For crystallization experiments at 19 °C, *h*ADK at a concentration of 10 mg/mL and Mtb ADK at a concentration of 20 mg/mL in buffer containing 20 mM Tris-Cl, pH 7.4, and 5 mM 2-mercaptoethanol were used. Prior to setting up crystallization experiments, proteins were preincubated with 5 mM **1a** for 1 h at room temperature. Initial crystallization trials were performed with the help of a Gryphon crystallization workstation (ArtRobbins) by the sitting drop vapor diffusion method in 96-well plates; 0.2 μL of protein solution was mixed with 0.2 μL of reservoir solution, and the drop was equilibrated against 200 μL of reservoir solution. The PEGs Suite and JSCG Core I Suite (QIAGEN) were used for the initial crystallization condition screen. Initial microcrystals appeared in several days. Further optimization involved changing to the hanging drop mode in 24-well crystallization plates (EasyXtal DG-Tool, QIAGEN). Optimal crystals of the hADK-**1a** complex were obtained by mixing 2 μL of protein solution with 2 μL of reservoir solution composed of 0.2 M $MgCl_2$ and 20% (w/v) PEG 3350. Crystals of the Mtb ADK-**1a** complex were obtained by mixing 3 μL of protein solution with 1 μL of reservoir solution composed of 0.1 M sodium acetate, pH 4.6, and 15% (w/v) PEG 20 000.

Data Collection and Structure Determination. For data collection, the crystals were soaked in reservoir solution supplemented with 20% (v/v) glycerol and transferred into liquid nitrogen. Diffraction data were collected at 100 K at BESSY beamline 14.2[44] in Berlin, Germany, using an MAR Mosaic 225 CCD detector. The crystals of *h*ADK and Mtb ADK in complex with **1a** diffracted up to 2.5 Å resolution. Diffraction data for *h*ADK in complex with **1a** were integrated and reduced using MOSFLM[45] and scaled using SCALA.[46] The MtbADK-**1a** crystals were of problematic character whose quality could not be optimized despite a great effort, and diffraction pattern contained extra reflections. The scaling of experimental frames and

empirical absorption correction was done with CrysAlisPro (Agilent Technologies, version 1.171.37.34) using the symmetry *P*3. Finally, the symmetry equivalent reflections were merged by JANA2006[47] and resulting reflection file was converted to the mtz format using CCP4 program suite.[48] Details of the data processing procedure are given in the Supporting Information. Crystal parameters and data collection statistics are summarized in Table S1.

The structure of the *h*ADK-**1a** complex was solved by molecular replacement using the coordinates from PDB entry 1BX4[20] as the initial model. The structure of the Mtb ADK-**1a** complex was solved by molecular replacement using coordinates from PDB entry 2PKM[5] as the initial model. Automated rebuilding was performed with the program Buccaneer.[49] Restrained refinement to 2.5 Å resolution was performed using the program REFMAC.[50] The merohedric twinning was taken into the account during rebuilding and refinement. Coot program was used for inhibitor fitting, manual rebuilding of protein chain, and addition of water molecules. Atomic coordinates and a geometry library for the inhibitor were generated using the PRODRG server.[51]

■ ASSOCIATED CONTENT

Supporting Information

Synthetic procedures and characterization data for all new compounds, additional figures, and crystallographic data. This material is available free of charge via the Internet at http://pubs.acs.org.

Accession Codes

Atomic coordinates and structure factors for the crystal structures of hADK-**1a** and Mtb ADK-**1a** have been deposited in the PDB with accession codes 4O1L and 4PVV, respectively.

■ AUTHOR INFORMATION

Corresponding Authors

*M.H.: e-mail, hocek@uochb.cas.cz; phone, +420 220183324.
*I.P.: e-mail, pichova@uochb.cas.cz; phone, +420 220183251.

Author Contributions

#J.S. and P.N. contributed equally.

Notes

The authors declare no competing financial interest.
∞I.V.: Deceased on May 25, 2014.

■ ACKNOWLEDGMENTS

This work was supported by EU-PF7 SysteMtb Collaborative Project 241587, Grant P207/11/0344 from the Czech Science Foundation, RVO 61388963 Project, Project InterBioMed LO1302, Programme "NAVRAT" LK11205 and CEITEC—open access project, No. LM2011020 from the Ministry of Education of the Czech Republic, and IOCB-Gilead Research Centre. We thank Dagmar Grundová for excellent technical assistance and H. Hoffman for editing of the manuscript.

■ ABBREVIATIONS USED

ADK, adenosine kinase; ATPγS, adenosine 5′-[γ-thio]-triphosphate; MDR, multidrug-resistant; XDR, extensively drug-resistant; CC_{50}, 50% cytotoxic concentration; IC_{50}, 50% inhibitory concentration; STD, saturation transfer difference; HSQC, heteronuclear single quantum coherence

■ REFERENCES

(1) Gandhi, N. R.; Nunn, P.; Dheda, K.; Schaaf, H. S.; Zignol, M.; van Soolingen, D.; Jensen, P.; Bayona, J. Multidrug-resistant and extensively drug-resistant tuberculosis: a threat to global control of tuberculosis. *Lancet* **2010**, *375*, 1830−1843.

(2) Niemi, M.; Backman, J. T.; Fromm, M. F.; Neuvonen, P. J.; Kivisto, K. T. Pharmacokinetic interactions with rifampicin: clinical relevance. *Clin. Pharmacokinet.* **2003**, *42* (9), 819−850.

(3) Parker, W. B.; Long, M. C. Purine metabolism in *Mycobacterium tuberculosis* as a target for drug development. *Curr. Pharm. Des.* **2007**, *13*, 599−608.

(4) Ducati, R. G.; Breda, A.; Basso, A.; Basso, L. A.; Santos, D. S. Purine salvage pathway in *Mycobacterium tuberculosis*. *Curr. Med. Chem.* **2011**, *18*, 1258−1275.

(5) Reddy, M. C. M.; Palaninathan, S. K.; Shetty, N. D.; Owen, J. L.; Watson, M. D.; Sacchettini, J. C. High resolution crystal structures of *Mycobacterium tuberculosis* adenosine kinase: insights into the mechanism and specificity of this novel prokaryotic enzyme. *J. Biol. Chem.* **2007**, *282*, 27334−27342.

(6) Long, M. C.; Escuyer, V.; Parker, W. B. Identification and characterization of a unique adenosine kinase from *Mycobacterium tuberculosis*. *J. Bacteriol.* **2003**, *185* (22), 6548−6555.

(7) Muchmore, S. W.; Smith, R. A.; Stewart, A. O.; Cowart, M. D.; Gomtsyan, A.; Mamulenko, M. A.; Yu, H.; Severin, J. M.; Bhagwat, S. S.; Lee, C. H.; Kowaluk, E. A.; Narcis, M. F.; Jakob, C. L. Crystal structures of human adenosine kinase inhibitor complexes reveal two distinct binding modes. *J. Med. Chem.* **2006**, *49* (23), 6726−6731.

(8) Al Safarjalani, O. N.; Rais, R. H.; Kim, Y. A.; Chu, C. K.; Naguib, F. N.; El Kouni, M. H. Carbocyclic 6-benzylthioinosine analogues as subversive substrates of *Toxoplasma gondii* adenosine kinase: biological activities and selective toxicities. *Biochem. Pharmacol.* **2010**, *80*, 955−963.

(9) Boison, D. Adenosine kinase: exploitation for therapeutic gain. *Pharmacol. Rev.* **2013**, *65*, 1−39.

(10) Barrow, E. W.; Westbrook, L.; Bansal, N.; Suling, W. J.; Maddry, J. A.; Parker, W. B.; Barrow, W. W. Antimycobacterial activity of 2-methyl-adenosine. *J. Antimicrob. Chemother.* **2003**, *52* (5), 801−808.

(11) Ugarkar, B. G.; DaRe, J. M.; Kopcho, J. J.; Browne, C. E., III; Schanzer, J. M.; Wiesner, J. B.; Erion, M. D. Adenosine kinase inhibitors. 1. Synthesis, enzyme inhibition and antiseizure activity of 5-iodotubercidin analogues. *J. Med. Chem.* **2000**, *43*, 2883−2893.

(12) Ugarkar, B. G.; Castellino, A. J.; DaRe, J. S.; Ramirez-Weinhouse, M.; Kopcho, J. J.; Rosengren, S.; Erion, M. D. Adenosine kinase inhibitors. 3. Synthesis, SAR and antiinflammatory activity of a series of L-lyxofuranosyl nucleosides. *J. Med. Chem.* **2003**, *46*, 4750−4760.

(13) Kim, Y. A.; Sharon, A.; Chu, C. K.; Rais, R. H.; Al Safarjalani, O. N.; Naguib, F. N. M.; el Kouni, M. H. Structure−activity relationships of 7-deaza-6-benzylthioinosine analogues as ligands of *Toxoplasma gondii* adenosine kinase. *J. Med. Chem.* **2008**, *51*, 3934−3945.

(14) Ugarkar, B. G.; Castellino, A. J.; DaRe, J. M.; Kopcho, J. J.; Wiesner, J. B.; Schanzer, J. M.; Erion, M. D. Adenosine kinase inhibitors. 2. Synthesis, enzyme inhibition and antiseizure activity of diaryltubercidin analogues. *J. Med. Chem.* **2000**, *43*, 2894−2905.

(15) Boyer, S. H.; Ugarkar, B. G.; Solbach, J.; Kopcho, J.; Matelich, M. C.; Ollis, K.; Gomez-Galeno, J. E.; Mendonca, R.; Tsuchiya, M.; Nagahisa, A.; Nakane, M.; Wiesner, J. B.; Erion, M. D. Adenosine kinase inhibitors. 5. Synthesis, enzyme inhibition and analgesic activity of erythrodiarylturbercidin analogs. *J. Med. Chem.* **2005**, *48*, 6430−6441.

(16) Nauš, P.; Pohl, R.; Votruba, I.; Džubák, P.; Hajdúch, M.; Ameral, R.; Birkus, G.; Wang, T.; Ray, A. S.; Mackman, R.; Cihlar, T.; Hocek, M. 6-(Het)aryl-7-deazapurine ribonucleosides as novel potent cytostatic agents. *J. Med. Chem.* **2010**, *53*, 460−470.

(17) Perlíková, P.; Konečný, P.; Nauš, P.; Snášel, J.; Votruba, I.; Džubák, P.; Pichová, I.; Hajduch, M.; Hocek, M. 6-Alkyl-, 6-aryl- or 6-hetaryl-7-deazapurine ribonucleosides as inhibitors of human or MTB adenosine kinase and potential antimycobacterial agents. *Med. Chem. Commun.* **2013**, *4*, 1497−1500.

(18) Bourderioux, A.; Nauš, P.; Perlíková, P.; Pohl, R.; Pichová, I.; Votruba, I.; Džubák, P.; Konečný, P.; Hajdúch, M.; Stray, K. M.; Wang, T.; Ray, A. S.; Feng, J. Y.; Birkus, G.; Cihlar, T.; Hocek, M. Synthesis and significant cytostatic activity of 7-hetaryl-7-deazaadenosines. *J. Med. Chem.* **2011**, *54*, 5498−5507.

(19) Spáčilová, P.; Nauš, P.; Pohl, R.; Votruba, I.; Snášel, J.; Zábranská, H.; Pichová, I.; Ameral, R.; Birkuš, G.; Cihlář, T.; Hocek, M. CycloSal-phosphate pronucleotides of cytostatic 6-(het)aryl-7-deazapurine ribonucleosides: synthesis, cytostatic activity, and inhibition of adenosine kinases. *ChemMedChem* **2010**, *5*, 1386−1396.
(20) Mathews, I. I.; Erion, M. D.; Ealick, S. E. Structure of human adenosine kinase at 1.5 Å resolution. *Biochemistry* **1998**, *37*, 15607−20.
(21) Reddy, M. C. M; Palaninathan, S. K.; Shetty, N. D.; Owen, J. L.; Watson, M. D.; Sacchettini, J. C. High resolution crystal structures of *Mycobacterium tuberculosis* adenosine kinase. *J. Biol. Chem.* **2007**, *282*, 27334−27342.
(22) Gribble, F. M.; Loussouarn, G.; Tucker, S. J.; Zhao, C.; Nichols, C. G.; Ashcroft, F. M. A novel method for measurement of submembrane ATP concentration. *J. Biol. Chem.* **2000**, *275*, 30046−30049.
(23) Larcombe-McDouall, J.; Buttell, N.; Harrison, N.; Wray, S. In vivo pH and metabolite changes during a single contraction in rat uterine smooth muscle. *J. Physiol.* **1999**, *518*, 783−790.
(24) Dragon, S.; Hille, R.; Gotz, R.; Baumann, R. Adenosine 3′:5′-cyclic monophosphate (cAMP) inducible pyrimidine 5′-nucleotidase and pyrimidine nucleotide metabolism of chicken embryonic erythrocytes. *Blood* **1998**, *91*, 3052−3058.
(25) Kawashima, S. Inhibition of rat liver transglutaminase by nucleotides. *Experientia* **1991**, *47*, 709−712.
(26) Koul, A.; Vranckx, L.; Dendouga, N.; Balemans, W.; van den Wyngaert, I.; Vergauwen, K.; Göhlmann, H. W.; Willebrords, R.; Poncelet, A.; Guillemont, J.; Bald, D.; Andries, K. Diarylquinolines are bactericidal for dormant mycobacteria as a result of disturbed ATP homeostasis. *J. Biol. Chem.* **2008**, *283* (37), 25273−25280.
(27) Park, J.; Gupta, R. S. Adenosine kinase and ribokinase—the RK family of proteins. *Cell. Mol. Life Sci.* **2008**, *65* (18), 2875−2896.
(28) Rao, S. P. S.; Alonso, S.; Rand, L.; Pethe, K. The protonmotive force is required for maintaining ATP homeostasis and viability of hypoxic, nonreplicating *Mycobacterium tuberculosis*. *Proc. Natl. Acad. Sci. U.S.A.* **2008**, *105*, 11945−11950.
(29) Renshaw, P. S.; Veverka, V.; Kelly, G.; Frenkiel, T. A.; Williamson, R. A.; Gordon, S. V.; Hewinson, R. G.; Carr, M. D. Sequence-specific assignment and secondary structure determination of the 195-residue complex formed by the *Mycobacterium tuberculosis* proteins CFP-10 and ESAT-6. *J. Biomol. NMR* **2004**, *30*, 225−226.
(30) Veverka, V.; Lennie, G.; Crabbe, T.; Bird, I.; Taylor, R. J.; Carr, M. D. NMR assignment of the mTOR domain responsible for rapamycin binding. *J. Biomol. NMR* **2006**, *36*, 3−3.
(31) Fanfrlik, J.; Bronowska, A. K.; Řezač, J.; Přenosil, O.; Konvalinka, J.; Hobza, P. A reliable docking/scoring scheme based on the semiempirical quantum mechanical PM6-DH2 method accurately covering dispersion and H-bonding: HIV-1 protease with 22 ligands. *J. Phys. Chem. B* **2010**, *114*, 12666−12678.
(32) Lepšík, M.; Řezač, J.; Kolař, M.; Pecina, A.; Hobza, P.; Fanfrlik, J. The semiempirical quantum mechanical scoring function for in-silico drug design. *ChemPlusChem* **2013**, *78*, 921−931.
(33) Krátký, M.; Vinšová, J.; Novotná, E.; Mandíková, J.; Wsól, V.; Trejtnar, F.; Ulmann, V.; Stolaříková, J.; Fernandes, S.; Bhat, S.; Liu, J. O. Salicylanilide derivatives block *Mycobacterium tuberculosis* through inhibition of isocitrate lyase and methionine aminopeptidase. *Tuberculosis* **2012**, *92* (5), 434−439.
(34) Salzmann, M.; Wider, G.; Pervushin, K.; Senn, H.; Wuthrich, K. TROSY-type triple-resonance experiments for sequential NMR assignments of large proteins. *J. Am. Chem. Soc.* **1999**, *121*, 844−848.
(35) Eletsky, A.; Kienhofer, A.; Pervushin, K. TROSY NMR with partially deuterated proteins. *J. Biomol. NMR* **2001**, *20*, 177−180.
(36) Wilkinson, I. C.; Hall, C. J.; Veverka, V.; Shi, J. Y.; Muskett, F. W.; Stephens, P. E.; Taylor, R. J.; Henry, A. J.; Carr, M. D. High resolution NMR-based model for the structure of a scFv-IL-1 beta complex potential for NMR as a key tool in therapeutic antibody design and development. *J. Biol. Chem.* **2009**, *284*, 31928−31935.
(37) Salzmann, M.; Pervushin, K.; Wider, G.; Senn, H.; Wuthrich, K. TROSY in triple-resonance experiments: new perspectives for sequential NMR assignment of large proteins. *Proc. Natl. Acad. Sci. U.S.A.* **1998**, *95*, 13585−13590.
(38) Mayer, M.; Meyer, B. Group epitope mapping by saturation transfer difference NMR to identify segments of a ligand in direct contact with a protein receptor. *J. Am. Chem. Soc.* **2001**, *123*, 6108−6117.
(39) Řezáč, J.; Hobza, P. Advanced corrections of hydrogen bonding and dispersion for semiempirical quantum mechanical methods. *J. Chem. Theory Comput.* **2012**, *8*, 141−151.
(40) Klamt, A.; Schuurmann, G. COSMO: a new approach to dielectric screening in solvents with explicit expressions for the screening energy and its gradient. *J. Chem. Soc., Perkin Trans. 2* **1993**, *5*, 799−805.
(41) Marenich, A. V.; Cramer, C. J.; Truhlar, D. G. Universal solvation model based on solute elektron density and on a continuum model of the solvent defined by the bulk dielectric constant and atomic surface tensions. *J. Phys. Chem. B* **2009**, *113*, 6378−6396.
(42) Frisch, M. J.; Trucks, G. W.; Schlegel, H. B.; Scuseria, G. E.; Robb, M. A.; Cheeseman, J. R.; Scalmani, G.; Barone, V.; Mennucci, B.; Petersson, G. A.; Nakatsuji, H.; Caricato, M.; Li, X.; Hratchian, H. P.; Izmaylov, A. F.; Bloino, J.; Zheng, G.; Sonnenberg, J. L.; Hada, M.; Ehara, M.; Toyota, K.; Fukuda, R.; Hasegawa, J.; Ishida, M.; Nakajima, T.; Honda, Y.; Kitao, O.; Nakai, H.; Vreven, T.; Montgomery, J. A., Jr.; Peralta, J. E.; Ogliaro, F.; Bearpark, M.; Heyd, J. J.; Brothers, E.; Kudin, K. N.; Staroverov, V. N.; Kobayashi, R.; Normand, J.; Raghavachari, K.; Rendell, A.; Burant, J. C.; Iyengar, S. S.; Tomasi, J.; Cossi, M.; Rega, N.; Millam, N. J.; Klene, M.; Knox, J. E.; Cross, J. B.; Bakken, V.; Adamo, C.; Jaramillo, J.; Gomperts, R.; Stratmann, R. E.; Yazyev, O.; Austin, A. J.; Cammi, R.; Pomelli, C.; Ochterski, J. W.; Martin, R. L.; Morokuma, K.; Zakrzewski, V. G.; Voth, G. A.; Salvador, P.; Dannenberg, J. J.; Dapprich, S.; Daniels, A. D.; Farkas, Ö.; Foresman, J. B.; Ortiz, J. V.; Cioslowski, J.; Fox, D. J. *Gaussian 09*; Gaussian, Inc.: Wallingford CT, 2009.
(43) Case, D. A.; Darden, T. A.; Cheatham, T. E., III; Simmerling, C. L.; Wang, J.; Duke, R. E.; Luo, R.; Crowley, M.; Walker, R. C.; Zhang, W.; Merz, K. M.; Wang, B.; Hayik, S.; Roitberg, A.; Seabra, G.; Kolossvary, I.; Wong, K. F.; Paesani, F.; Vanicek, J.; Wu, X., Brozell; S. R.; Steinbrecher, T.; Gohlke, H.; Yang, L.; Tan, C.; Mongan, J.; Hornak, V.; Cui, G.; Mathews, D. H.; Seetin, M. G.; Sagui, C.; Babin, V.; and Kollman, P. A. *AMBER 10*; University of California: San Francisco, CA, 2008.
(44) Mueller, U.; Darowski, N.; Fuchs, M. R.; Foerster, R.; Hellmig, M.; Paithankar, S.; Puehringer, S.; Steffien, M.; Zocher, G.; Weiss, M. S. Facilities for macromolecular crystallography at the Helmholtz−Zentrum Berlin. *J. Synchrotron Radiat.* **2012**, *19*, 442−449.
(45) Leslie, A. G. W. The integration of macromolecular diffraction data. *Acta Crystallogr.* **2006**, *D62*, 48−57.
(46) Evans, P. Scaling and assessment of data quality. *Acta Crystallogr.* **2006**, *D62*, 72−82.
(47) Petricek, V.; Dusek, M.; Palatinus, L. Crystallographic computing system JANA2006: general features. *Z. Kristallogr.* **2006**, *229*, 345−352.
(48) Winn, M. D.; Ballard, C. C.; Cowtan, K. D.; Dodson, E. J.; Emsley, P.; Evans, P. R.; Keegan, R. M.; Krissinel, E. B.; Leslie, A. G. W.; McCoy, A.; McNicholas, S. J.; Murshudov, G. N.; Pannu, N. S.; Potterton, E. A.; Powell, H. R.; Read, R. J.; Vagin, A.; Wilson, K. S. Overview of the CCP4 suite and current developments. *Acta Crystallogr.* **2011**, *D67*, 235−242.
(49) Cowtan, K. The Buccaneer software for automated model building. 1. Tracing protein chains. *Acta Crystallogr., Sect. D: Biol. Crystallogr.* **2006**, *62*, 1002−1011.
(50) Emsley, P.; Cowtan, K. Coot: model building tools for molecular graphics. *Acta Crystallogr., Sect. D: Biol. Crystallogr.* **2004**, *60*, 2126−2132.
(51) Schuettelkopf, A. W.; van Aalten, D. M. F. PRODRG—a tool for high-throughput crystallography of protein−ligand complexes. *Acta Crystallogr.* **2006**, *D60*, 1355−1363.

2.3.2 Cytosine derivatives

Cytosine derivatives are nucleoside derivatives (pyrimidine analogues), as well, and have been used in clinical practice for almost 50 years as a treatment for acute myeloid and lymphocytic leukaemia and lymphomas mostly (Klener 2010). They interfere with the synthesis of nucleosides/nucleotides (Matsuda & Sasaki 2004). Other mechanisms of action are known such as intercalation into DNA and inhibition of DNA replication by inhibition of RNA and DNA polymerases. Moreover, cytosines in the DNA sequence are very frequently methylated by DNA methyltransferase 1, as a form of epigenetic modifications of DNA. DNA methylation is very important for gene expression regulation and is very often altered in cancer cell silencing anti-onco genes and lead to hyperproliferation. Application of some cytosine derivatives can inhibit DNA methyltransferase and normalize the methylation processes in the cell (Plitta et al. 2012). Cytosine derivatives have also been successfully combined with gene therapy. By gene modification for induction of expression, prodrug activating enzymes, herpes simplex virus Type 1 thymidine kinase and cytosine deaminase from *Escherichia coli* are able to transform the nucleosidic prodrug into its active and effective state. Therefore combination of these two approaches can improve treatment and patient prognosis (Aghi et al. 1998). Thanks to its analogous structure, cytosine derivatives are able to mimic their physiological representatives and lead to DNA synthesis inhibition, even though much higher therapeutic effect is achieved by inhibition of RNA synthesis as well. This knowledge led to the development of more potent compounds which can bypass the imperfection of old structures, such as cytosine arabinosid which inhibits DNA synthesis only (Takatori et al. 1999). Many derivatives have been prepared with broader therapeutic activity, for example 1-(2-deoxy-2-methylene-b-D-erythro-pentofura-nosyl) cytosine (Takatori et al. 1999), 1-(2-deoxy-2-methylene-b-D-erythro-pentofura-nosyl) cytosine (Barkin et al. 2003), 3- aminopyridazine, 1-aminophthalazine cytosine analogues (Tomori et al. 2015) and imidazol derivatives discussed in the following article (Jansa et al. 2014). The pharmacological properties of imidazo-pyridine and imidazo-pyrimidines are very well documented and include antiviral, anticancer, antiparasitic, antibacterial, antifungal,

anti-inflammatory activity and many others. They also work as inhibitors of Syk family kinases and dopamine D4 receptor ligands. Analogues are used as a treatment for neurological and psychiatric disease, as mGluR5 receptors modulators and as potent anti-HIV and anti-HBV agents (Jansa et al. 2014).

2.3.2.1 Cytotoxic activity and cell cycle modification after treatment with cytosine derivatives

JANSA J, LYČKA A, PADĚLKOVÁ Z,GREPL M, KONEČNÝ P, HAJDÚCH M, DŽUBÁK P. (2014). New imidazo [1,2-c]pyrimidin-5(6H)-ones Derived from cytosine: Synthesis, Structure and Cytotoxic Activity. *J. Heterocyclic Chem*., DOI: 10.1002/jhet.2243

New Imidazo[1,2-*c*]pyrimidin-5(6*H*)-Ones Derived from Cytosine: Synthesis, Structure, and Cytotoxic Activity

Josef Jansa,[a,b]* Antonín Lyčka,[a] Zdeňka Padělková,[c] Martin Grepl,[d] Petr Konečný,[e,f] Marián Hajdúch,[e,f] and Petr Džubák[e,f]*

[a]Research Institute for Organic Syntheses (VUOS), Rybitví 296, CZ-533 54 Pardubice-Rybitví, Czech Republic
[b]Department of Organic Chemistry, Faculty of Science, Palacký University, 17. listopadu 1192/12 CZ-771 46 Olomouc, Czech Republic
[c]Department of General and Inorganic Chemistry, Faculty of Chemical Technology, University of Pardubice, Studentská 573, CZ-532 10 Pardubice, Czech Republic
[d]Farmak, a.s., Na Vlčinci 16/3, CZ-771 17 Olomouc, Czech Republic
[e]Institute of Molecular and Translational Medicine, Faculty of Medicine and Dentistry, Palacký University, Olomouc, Puškinova 6, CZ-775 20 Olomouc, Czech Republic
[f]University Hospital Olomouc, Ivana Petroviče Pavlova 6, CZ-77520 Olomouc, Czech Republic
*E-mail:josef.jansa@vuos.com; dzubakp@gmail.com

Received January 30, 2014
DOI 10.1002/jhet.2243
Published online 00 Month 2014 in Wiley Online Library (wileyonlinelibrary.com).

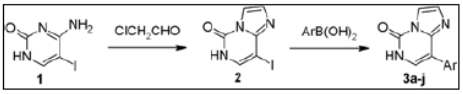

This work describes the synthesis of 8-iodoimidazo[1,2-*c*]pyrimidin-5(6*H*)-one **2** from 5-iodocytosine **1**. This compound was subjected to Suzuki cross-coupling reaction with aryl and heteroarylboronic acids. After optimization, 10 products **3a–j** were obtained in good yields 61-90%. Cytotoxic activity of all new products was evaluated on seven tumor cell lines including resistant variants and on normal human fibroblasts. Two derivatives showed promising biological activity and good therapeutic index in the case of **3h**.

J. Heterocyclic Chem., **00,** 00 (2014).

INTRODUCTION

The reaction of 2-aminopyridine, 2-aminopyrimidine, and 4-aminopyrimidine derivatives with α-halogenocarbonyl compounds is well known to produce corresponding imidazo-fused derivatives [1–3]. Imidazo[1,2-*a*]pyridine and imidazo[1,2-*a*]pyrimidine scaffolds were studied for their extensive pharmacological properties, for example, antiviral [4,5], antitubercular [6,7], anticancer [8], cytotoxic [9], antiparasitic [10], antibacterial [2], antifungal [11], cardiotonic [12], and antiinflammatory [13]. Some derivatives act as commercial drugs, from which zolpidem is widely known nonbenzodiazepine hypnotic [14].

Imidazo[1,2-*c*]pyrimidines were studied for similarly large spectrum of biological activities, such as antimicrobial [15], antimycobacterial [16], antitubercular [7], inotropic [17], antiinflammatory, analgesic, antipyretic, and ulcerogenic [18]. These compounds also act as Syk family kinases inhibitors [19,20] and dopamine D4 receptor ligands [21].

Imidazo[1,2-*c*]pyrimidine scaffolds are also formed by reaction of adenine and cytosine bases with α-halogenocarbonyl compounds. Kochetkov and coworkers first reported reaction of 9-methyladenine and 1-methylcytosine with chloroacetaldehyde, which produced corresponding ethenoderivatives [22]. Because this type of reaction became an interesting pathway for synthesis of modified nucleic acid bases with useful biological, fluorescence, and base-pairing properties [23–26].

Biological activity of some imidazo[1,2-*c*]pyrimidin-5(6*H*)-ones has been reported. Compounds with this scaffold are selective $GABA_A$ receptor ligands [27]. Recently, the large family was patented as allosteric modulators of mGluR5 receptors for treatment of neurologic and psychiatric disorders [28]. Nucleosides with this scaffold were tested as antiviral agents [29] and showed activity against hepatitis B virus [30,31] and HIV [32].

In this article, we present the access for functionalization of imidazo[1,2-*c*]pyrimidin-5(6*H*)-one scaffold by an aryl or heteroaryl ring. 8-Aryl derivatives **3a–j** were obtained from iododerivative **2** by Suzuki–Miyaura cross-coupling reaction (Scheme 1). Cytotoxic activity of all products was evaluated on tumor cell lines and normal human fibroblasts (Table 1).

RESULTS AND DISCUSSION

Chemistry. The starting 8-iodoimidazo[1,2-*c*]pyrimidin-5(6*H*)-one **2** was prepared in 86% yield by cyclization of 5-iodocytosine **1** with chloroacetaldehyde in the presence of sodium acetate. Iodine atom of **2** was substituted by an aryl or heteroaryl ring via Suzuki–Miyaura cross-coupling [33] without any need of protection of parent heterocycle **2** (Scheme 1).

Inspired by coupling of cytosine nucleosides with boronic acids [34], we first selected acetonitrile–water 2 : 1 solvent system with tetrakis(triphenylphosphine)palladium as catalyst. However, these conditions could only be used

Scheme 1. Synthesis of target imidazo[1,2-*c*]pyrimidin-5(6*H*)-ones, yields in parentheses. Reagents and conditions: (a) $ClCH_2CHO$, NaOAc, H_2O, 80°C, 4 h; (b) $ArB(OH)_2$, $Pd(dppf)Cl_2$, EtOH/H_2O, Na_2CO_3, reflux, 24 h.

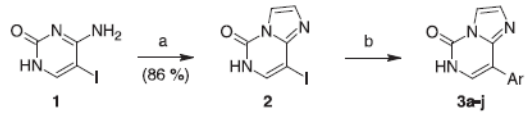

3a) Ar = phenyl (88 %)
3b) Ar = biphenyl-4-yl (81 %)
3c) Ar = 4-methoxyphenyl (90 %)
3d) Ar = 4-chlorophenyl (75 %)
3e) Ar = 4-(trifluoromethyl)phenyl (71 %)
3f) Ar = 4-formylphenyl (83 %)
3g) Ar = 4-carboxyphenyl (74 %)
3h) Ar = 4-cyanophenyl (84 %)
3i) Ar = thiophen-2-yl (61 %)
3j) Ar = pyridin-4-yl (62 %)

Table 1
Summary of cytotoxic activities (IC_{50}, μ*M*).[a]

Compound	CCRF-CEM	CEM-DNR bulk	K562	K562-Tax	A549	HCT116	HCT116p53-/-	MRC-5	BJ
2	46.15	48.99	47.37	44.63	50.00	50.00	18.61	48.33	50.00
3a	50.00	45.69	49.72	45.51	50.00	46.14	35.58	50.00	50.00
3b	8.59	2.84	15.20	8.85	10.13	20.20	15.12	7.00	0.66
3c	45.74	41.56	47.75	39.79	47.31	49.35	35.52	50.00	50.00
3d	36.87	34.84	35.81	37.70	44.69	37.53	35.89	44.45	43.71
3e	28.20	32.89	10.74	34.20	40.42	34.83	25.57	50.00	50.00
3f	32.63	20.28	34.21	23.48	9.04	50.00	18.47	50.00	48.69
3g	50.00	49.72	48.12	48.38	50.00	50.00	18.75	50.00	50.00
3h	1.45	18.84	17.71	28.72	5.07	42.49	8.83	35.27	7.29
3i	44.65	42.78	50.00	43.35	50.00	50.00	18.75	50.00	50.00
3j	50.00	46.94	50.00	46.07	50.00	50.00	18.75	50.00	50.00

[a]Cytotoxic activity was determined by MTT assay following a 3-day incubation. Values represents means of IC_{50} from three independent experiments with standard deviation ranging from 10 to 25% of the average values.

Scheme 2. Numbering of atoms in compounds **2** and **3a–j** for NMR purposes.

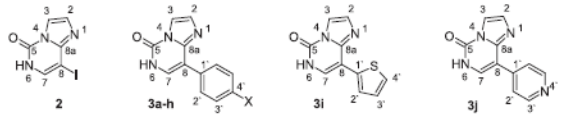

for coupling with phenylboronic and biphenyl-4-boronic acid but not for 4-methoxyphenylboronic acid (~30% conversion). When ethanol–water 2 : 1 was used as a solvent, complete conversion was observed in the coupling with 4-methoxyphenylboronic acid but lower (~80%) for coupling with 4-cyanophenylboronic acid. Then, the $Pd(dppf)Cl_2$ was used as catalyst with the aim to obtain complete conversion in case of all used boronic acids. With 3 mol% of this catalyst in ethanol–water 2 : 1, products **3a–i** were coupled in nearly quantitative conversions, detected by thin-layer chromatography. Only in the coupling of **2** with strongly deactivated 4-pyridylboronic acid, 5 mol% of $Pd(dppf)Cl_2$ in ethanol–water 4 : 1 must be used to obtain complete conversion to **3j**. Coupled products **3a–j** were obtained in 61–90% isolated yields.

Products were identified and characterized by IR, MS, and NMR spectroscopy (for atom numbering see Scheme 2). 5-Iodocytosine **1** showed three broad NH protons that mean that it exist as imino tautomer in hexadeuterated dimethyl sulfoxide (DMSO-d_6) (Scheme 3). The same tautomerism was observed in 5-bromo and 5-iodo-*N*-1-sulfonylated cytosine derivatives [35]. Complete assignment of ^1H and ^{13}C chemical shifts in compounds **2** and **3a–j** was carried out on the basis of 1D and 2D (correlation spectroscopy, heteronuclear multiple

Scheme 3. Preferred imino tautomerism of 5-iodocytosine **1**.

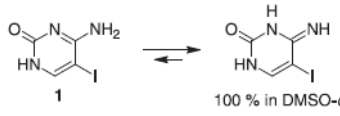

quantum coherence, and heteronuclear multiple bond correlation) NMR experiments (Table 2). ^{15}N-NMR spectra of selected derivatives were also measured.

Structure of product **3a** was confirmed by X-ray crystallography. Compound **3a** (Fig. 1) crystallizes in the orthorhombic space group *Pbca*, with eight molecules within the unit cell. To the best of our knowledge, only one analogous structure of imidazo(1,2-*c*)pyrimidin-5(6*H*)-one derivate in position 8 by a carbon atom the 3,4-etheno-5-methoxymethyl-2′-deoxycytidine [36] has been reported so far. Other two partially saturated compounds as for example *N*-methyl-6-(2-chloroethyl)-5,7-dioxo-1,2,3,5,6,7-hexahydroimidazo[1,2-*c*] pyrimidine-8-carboxamide [37] or methyl2-(1-benzyl-8-formyl-7-methoxy-5-oxo-1,2,3,5-tetrahydroimidazo[1,2-*c*]pyrimidin-3-yl)acetate [38] and two compounds with fused aromatic rings [39,40] that resemble the structural motif of **3a** were also found within the crystallographic database. Typical interatomic separations and angles for each functional group are present within the structure of **3a** [41]. A high degree of π-electron conjugation is interrupted between atoms C2-C3 and C6-N3 where the bond lengths are bit longer than is usually found for analogous distances in aromatic compounds. The torsion of the phenyl ring from the plane defined by the heterocyclic part of the molecule is 45.68(3)°.

Because of the presence of interatomic N2-H2···N3 interactions in the crystal packing of **3a** (Fig. 2), the chains of zig-zag oriented molecules (interplanar angle between two neighboring imidazopyrimidine rings is 41.0 (2)° N2-H2···N3 (Fig. 3) are observed within the crystal lattice.

Biological activity. The cytotoxic activity was analyzed on human cancer cell lines, resistant variants (CCRF-CEM, CEM-DNR, K562, K562-Tax, A549, HCT116, HCT116p53−/−, and A549) and on normal human cells (BJ and MRC-5 – normal cycling fibroblasts) to analyze the therapeutic index that is based on the ratio between the IC_{50} for normal human cells and cancer cell lines. The SAR ought to be evaluated for individual cell lines independently, because it may vary because of different tissue origin and potential molecular targets in particular cell lines. However, in our case, the trend of activity was very similar for all tested cell lines indicating similar or identical target(s), and thus, we will discuss SAR generally (Table 1).

Generally, the cytotoxic activity of the compounds is rather low; only two derivatives **3b** and **3h** are showing promising cytotoxic activity (the lowest IC_{50} = 1.45/2.84 μM). Interestingly, **3b** is showing preferential activity to CEM-DNR bulk, daunorubicin-resistant cancer cell line expressing P-glycoprotein (adenosine triphosphate-dependent transporter) and proteins from MRP family and K562-Tax, paclitaxel-resistant cancer cell line, expressing P-glycoprotein only [42]. Similarly, **3h** is showing preferential activity to CCRF-CEM, A549, and HCT116p53−/− cell line with deleted p53 protein and favorable therapeutic index to nontumor cell lines 24.32. Because P-glycoprotein positive cells are highly adenosine triphosphate dependent and the functional p53 protein is contributing to the cells survival in glucose and aminoacid deprived cells as well [43,44], the observed activity is suggesting disruption of energy metabolic pathways of the sensitive tumor cells.

Cell cycle study of the most active compound **3h** has been performed on CCRF-CEM lymphoblasts at 1× and 5× IC_{50} concentration within 24 h treatment. Finally, we did not observe any effect on cell cycle proliferation, DNA and RNA synthesis even in highest concentration (Table 3).

CONCLUSION

In conclusion, 11 new imidazo[1,2-*c*]pyrimidine-5(6*H*)-ones have been synthesized. General conditions for the Suzuki–Miyaura cross-coupling reaction were found, and all compounds were properly characterized. Cytotoxic activity is dependent on the substitution of the aryl ring, introduced by Suzuki–Miyaura cross-coupling reaction. Two derivatives showed promising activity with the lowest IC_{50} = 1.45 μM for **3h** on CCRF-CEM and IC_{50} = 2.84 μM for **3b** on resistant CEM-DNR bulk cell line. Moderate activity of some other derivatives was observed. Compound **3h** showed favorable therapeutic index to nontumor cell lines 24.32.

EXPERIMENTAL

General. The NMR spectra were measured on Bruker Avance (Rheinstetten, Germany) II 400 at 400.13 MHz (^{1}H), 100.62 MHz (^{13}C), 40.54 MHz (^{15}N), and 376.50 MHz (^{19}F) or Bruker Avance 500 at 500.13 MHz (^{1}H) and 125.67 MHz (^{13}C) in DMSO-d_6 (Rheinstetten, Germany) at ambient temperature. The ^{1}H and ^{13}C chemical shifts were referenced to the residual signal of the solvent (δ = 2.50 for ^{1}H and 39.52 for ^{13}C). The ^{15}N and ^{19}F chemical shifts were referred to external nitromethane in a coaxial capillary and internal $CFCl_3$, respectively, both having δ = 0.0.

The X-ray data for colorless crystal of **3a** (Fig. 1) were obtained at 150 K using Oxford Cryostream low-temperature device on a Nonius KappaCCD diffractometer with MoK_α radiation (λ = 0.71073 Å), a graphite monochromator, and the ϕ and χ scan mode. Data reductions were performed with DENZO-SMN [45]. The absorption was corrected by integration methods [46]. Structures were solved by direct methods (Sir92) [47] and refined by full matrix least square based on F^2 (SHELXL97) [48]. Hydrogen atoms were mostly localized on a difference Fourier map; however, to ensure uniformity of treatment of crystal, all hydrogen

Table 2

^{1}H, ^{13}C, and some ^{15}N chemical shifts (ppm) of compounds **2** and **3a–j**.

Position	2		3a		3b		3c		3d	
	δ_H	δ_C	δ_H	δ_C	δ_H	δ_C	δ_H	δ_C	δ_H	δ_C
1[b]	—	−122.6	—	−129.4	—	−129.2	—	—	—	—
2	7.90	114.1	7.87	112.6	7.89	112.6	7.85	112.5	7.85	112.6
3	7.37	132.0	7.45	132.0	7.49	129.0	7.45	132.0	7.45	132.0
4[b]	—	−190.8	—	−189.4	—	−189.3	—	—	—	—
5	—	146.1	—	145.7	—	145.7	—	145.7	—	145.6
6[b,c]	11.81	−243.3	11.90	−249.1	11.94	−248.9	11.81	—	11.95	—
7	7.58	134.2	7.52	126.5	7.63	126.5	7.44	125.4	7.57	126.9
8	—	59.8	—	110.5	—	110.0	—	110.3	—	109.1
8a	—	145.2	—	144.6	—	144.5	—	144.7	—	144.2
8-1′	—	—	—	133.1	—	132.2	—	125.4		131.9
8-2′	—	—	7.97	127.7	8.11	128.1	7.92	128.8	8.02	129.2
8-3′	—	—	7.42	128.3	7.75	126.6	6.99	113.7	7.44	128.2
8-4′	—	—	7.33	127.5	—	139.1	—	158.7	—	131.9
X	—	—	—	—	[d]	139.6	3.78	54.9	—	—

(Continues)

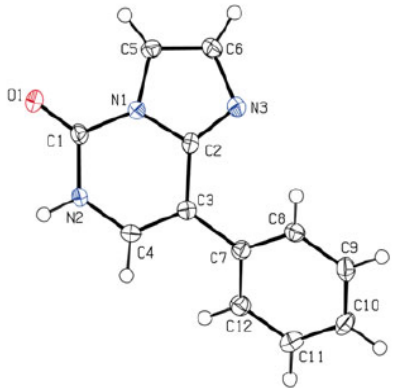

Figure 1. The molecular structure (ORTEP 50% probability level) of **3a**. Selected interatomic distances (Å), angles and interplanar angle (°): O1-C1 1.213(2), C1-N1 1.397(2), N1-C5 1.386(2), C5-C6 1.351(2), C6-N3 1.390(2), N3-C2 1.320(2), C2-C3 1.439(2), C3-C4 1.352(2), C4-N2 1.381(2), N2-C1 1.361(2), C3-C7 1.481(3); C6-N3-C2 105.29(14), N3-C2-N1 110.60(15), C2-N1-C5 107.37(14), C2-N1-C1 126.04(15), N1-C1-N2 112.78(15), C1-N2-C4 124.24(14); C2-C3-C4 versus C8-C7-C12 45.68(3). [Color figure can be viewed in the online issue, which is available at wileyonlinelibrary.com.]

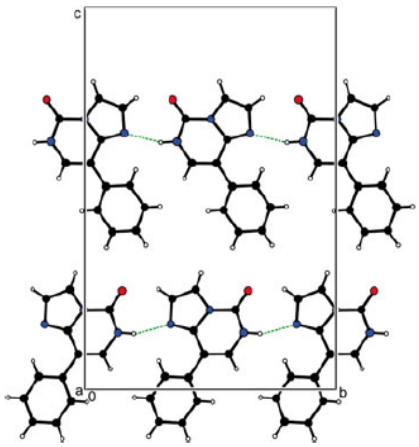

Figure 2. Interatomic N2-H2···N3 interactions of **3a**, view along axis *a*. [Color figure can be viewed in the online issue, which is available at wileyonlinelibrary.com.]

were recalculated into idealized positions (riding model) and assigned temperature factors $H_{iso}(H) = 1.2\ U_{eq}$(pivot atom) with C—H 0.93 Å for hydrogen atoms in aromatic rings and hydrogen atom for N—H bond was localized and assign from Fourier map, standard calculated distance for N—H bond is 0.86 Å.

$R_{int} = \sum |F_o^2 - F_{o,mean}^2| / \sum F_o^2$, $GOF = [\sum (w(F_o^2 - F_c^2)^2)/(N_{diffrs} N_{params})]^{1/2}$ for all data, $R(F) = \sum ||F_o| - |F_c|| / \sum |F_o|$ for observed data, $wR(F^2) = [\sum (w(F_o^2 - F_c^2)^2)/(\sum w(F_o^2)^2)]^{1/2}$ for all data.

Crystallographic data for structural analysis have been deposited with the Cambridge Crystallographic Data Centre, CCDC no. 931506 for **3a**. Copies of this information may be obtained free of charge from The Director, CCDC, 12 Union Road, Cambridge CB2 1EY, UK (fax: +44-1223-336033; E-mail: deposit@ccdc.cam.ac.uk or www: http://www.ccdc.cam.ac.uk).

Table 2
(Continued)

3e[a]		3f		3g		3h		3i		
δ_H	δ_C	δ_H	δ_C	δ_H	δ_C	δ_H	δ_C	δ_H	δ_C	^1J(C,H)
—	—	—	—	—	—	—	—	—	—	
7.85	112.7	7.89	112.7	7.88	112.7	7.88	112.7	7.87	112.8	196.8
7.45	132.0	7.49	132.0	7.48	132.0	7.46	132.0	7.49	132.0	190.5
—	—	—	—	—	—	—	—	—	—	—
—	145.6	—	145.6	—	145.6	—	145.5	—	145.4	—
11.96	—	12.09	—	12.02	—	12.10	—	11.91	—	—
7.69	128.1	7.78	128.5	7.71	127.9	7.79	128.7	7.68	125.0	182.5
—	108.9	—	109.1	—	109.4	—	109.5	—	105.7	—
—	144.1	—	144.0	—	144.2	—	143.9	—	143.4	—
	137.3	—	139.2	—	137.5	—	138.0	—	134.5	—
8.22	128.0	8.30	127.8	8.17	129.3	8.28	127.9	7.53	124.7	168.0
7.72	125.0	7.95	129.5	7.99	127.4	7.87	132.2	7.12	127.1	167.9
—	127.6	—	134.8	—	129.4	—	108.5	7.84	125.4	182.5
—	124.4	11.01	192.6	12.90	167.2	—	119.0	—	—	—

[a](δ ^{19}F) = −60.6.
[b](δ ^{15}N).
[c]J (^{15}N, ^{1}H) = 90.1 Hz.
[d]δ (^{1}H/^{13}C) = −/139.7, 7.76/126.7, 7.53/129.1, 7.42/127.6

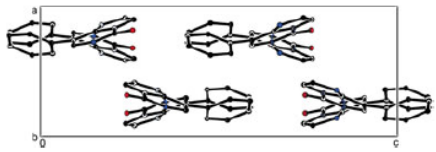

Figure 3. Crystal packing of **3a**, view along axis *b*. [Color figure can be viewed in the online issue, which is available at wileyonlinelibrary.com.]

Single crystals of **3a** (obtained by slow evaporation of acetone solution) were of sufficient quality for X-ray diffraction measurement. The crystallographic data and structure refinement parameters for compound **3a** are $C_{12}H_9N_3O$, M = 211.22, orthorhombic, *Pbca*, a = 7.2310(3), b = 13.4800(9), c = 19.9031(12) Å, $\alpha = \beta = \gamma = 90°$, Z = 8, V = 1940.03(19) Å^3, D_c = 1.446 g.cm^{-3}, μ = 0.097 mm^{-1}, T_{min}/T_{max} = 0.985/0.991; $-8 \le h \le 9$, $-17 \le k \le 14$, $-25 \le l \le 25$; 16,294 reflections measured (θ_{max} = 27.50°), 16,153 independent (R_{int} = 0.0383), 1644 with $I > 2\sigma(I)$, 146 parameters, S = 1.117, $R1$(obs. data) = 0.0484, $wR2$(all data) = 0.0940; maximum, minimum residual electron density = 0.275, −0.211 eÅ^{-3}.

High-resolution mass spectrometry (HRMS) analyses were measured with Thermo Exactive instrument (Thermo Scientific, Waltham, MA, USA). The injection was performed by autosampler of high-performance liquid chromatography apparatus Accela 1250. The chromatographic preseparation parameters: column Luna C18, 3 µm, 50×2mm i.d. (Phenomenex, Torrance, CA), mobile phase acetonitrile/water 50/50 with 0.1% of formic acid, flow rate 200 µL/min, the column temperature 30°C. Sample preparation was obtained using following procedure: The 1 mg of sample was dissolved in 10 mL of solvent acetonitrile/water 5/5 (1 min sonication), and then, 70 µL of this solution and 930 µL of the same solvent were added into vial and mixed before injection of 5 µL. High-resolution mass spectrometer Exactive based on orbitrap mass analyzer was equipped with heated electrospray ionization. The spectrometer was tuned to obtain maximum response for *m/z* 70–600. The source parameters were set to the following values: heated electrospray ionization temperature 250°C, spray voltage +3.0 kV (positive mode), transfer capillary temperature 300°C, and sheath gas/aux gas (nitrogen) flow rates 35/10. The HRMS spectra of target peaks allowed an evaluation of their elemental composition because of high intensities of their protonated molecules. The identification of the respective structures was performed with less than 0.6 ppm difference between experimental and theoretically calculated value.

IR spectra were recorded on Nicolet 6700 Fourier transform infrared spectroscopy over the range of 400–4000 cm^{-1}. Elemental analyses were performed on a Thermo Flash 2000 CHNS experimental organic analyzer. Melting points were determined on Stuart SMP3 apparatus (Barloworld Scientific, Staffordshire, UK). Reaction progress was monitored by thin-layer chromatography (dichloromethane/methanol 5:1 as mobile phase), which was performed on SiO_2 60 F_{254} plates with ultraviolet detection

Table 3
Effects of compound **3h** on cell cycle, apoptosis, and DNA/RNA synthesis in CCRF-CEM lymphoblasts (% of positive cells).

Compound	<G1	G0/G1	S	G2/M	$pH3^{Ser10}$	BrDU	BrU
Control	8.7	43.0	39.4	17.6	1.8	43.8	40.7
3h 1× IC50	7.2	41.8	41.0	17.2	2.0	44.4	41.6
3h 5× IC50	7.2	44.9	38.3	16.8	2.0	39.7	41.0

at 254 nm. Column chromatography was performed on silica gel 60. All starting materials were commercially available.

Chemistry. *5-Iodocytosine (1) [49].* Cytosine (100 g, 0.9 mol) was dissolved in the solution of 80 g of potassium hydroxide in 1500 mL of water. Then, the pulverized iodine (229 g, 0.902 mol) was added, and the mixture was stirred for 70 min at r.t. Thereafter, the reaction mixture was heated to reflux in the course of 70 min and refluxed for 2 h. After cooling to r.t., 30 mL of 20% solution of sodium thiosulfate was added, reaction mixture was stirred overnight, neutralized with 3.5 mL of acetic acid, and filtered and washed with 200 mL of water. Filter cake was suspended in 1250 mL of water and boiled for 10 min. Then cooled overnight and filtered and washed with 200 mL of water and 200 mL of methanol. Product was dried at 60°C/30 mbar. Yield 174.5 g (82%), off-white crystals, mp 238–243°C dec. (lit. 225–245°C dec.[49]), ^{1}H-NMR (400 MHz, DMSO-d_6): δ 6.54 (br s, 1H, NH), 7.80 (br s + s, 2H, NH + CH), 10.80 (br s, 1H, NH); ^{13}C-NMR (100.6 MHz, DMSO-d_6): δ 55.3, 149.5, 155.9, 164.7.

8-Iodoimidazo[1,2-c]pyrimidin-5(6H)-one (2). To the mixture of 50 g of 5-iodocytosine (0.211 mol) and 43.3 g (0.528 mol) of sodium acetate in 500 mL of water, 47.8 mL (0.422 mol) of chloroacetaldehyde (57% solution in water) was added. The mixture was stirred for 4 h at 80°C. Then, the mixture was cooled to r.t., product was filtered, washed with 400 mL of water and 100 mL of methanol. Product was dried, yield 47.4 g (86%), brown powder. Analytical sample was recrystallized from acetone and dried at 50–60°C/30 mbar to obtain off-white crystals, mp 230–235°C dec., IR (KBr): 3434, 3218, 3144, 3128, 3099, 2947, 1716, 1604, 1537, 1377, 1331, 1269, 1246, 1165, 1138, 1116, 774, 707, 642, 622, 574, and 546 cm^{-1}. HRMS *m/z* $[M+H]^+$ Calcd. for $C_6H_5IN_3O$: 261.94718, found 261.94704. *Anal.* Calcd. for $C_6H_4IN_3O$: C, 27.61; H, 1.54; N, 16.10. Found: C, 27.82; H, 1.51; N, 15.92.

General procedure for Suzuki–Miyaura cross-coupling. The mixture of 2 g (7.66 mmol) of **2**, 11.50 mmol of appropriate boronic acid, 3.25 g (30.66 mmol) of sodium carbonate, and 0.168 g (0.23 mmol) of Pd(dppf)Cl_2 (0.280 g (0.38 mmol) in case of **3j**) was placed to the flask, and argon atmosphere was introduced by three vacuum/argon cycles. First, 40 mL of ethanol and then 20 mL of water were added (48 mL of ethanol and 12 mL of water in case of **3j**), and an additional three vacuum/argon cycles were carried out. Reaction mixture was heated to reflux for 24 h, and then, the product was isolated from reaction mixture (for isolation procedure for **3b** and **3g**, refer to the succeeding texts). Thereafter, the mixture was cooled to r.t., 50 mL of water was added, and then, 6 mL of 35% hydrochloric acid was added slowly. Ethanol was evaporated at 50°C under reduced pressure. A little of active charcoal was added, and the mixture was stirred at 80°C for 10 min. The mixture was filtered over cellite and washed twice with 10 mL of 4% hydrochloric acid at 80°C. After cooling to r.t., pH of the filtrate was adjusted to 8–9 by solid sodium carbonate. Precipitated product was filtered, washed with 100 mL of water, and dried. Analytical samples of all products were recrystallized from acetone (dimethylformamide in case of **3f** and **3g**) and dried at 50–60°C/30 mbar. Pure product **3j** was obtained after column chromatography with dichloromethane/methanol 10 : 1 as a mobile phase (for NMR chemical shifts of compounds **3a-j**, refer to Table 2).

Isolation of products 3b and 3g. After refluxing reaction mixture for 24 h (refer to the previous texts) and cooling to r.t., 50 mL of water was added, and ethanol was evaporated at 50°C under reduced pressure. The resulting suspension was filtered off and washed with 50 mL of water. Crude product was dried on air overnight and recrystallized from dimethylformamide (25 mL for **3b**, 50 mL for **3g**). Product **3b** was washed with diethylether (2 × 10 mL), product **3g** with acetone (3 × 10 mL).

8-Phenylimidazo[1,2-c]pyrimidin-5(6H)-one (3a). White crystals, yield 1.27 g (88%). mp 241–243°C, IR (KBr): 3429, 3156, 3113, 3066, 2933, 2820, 2737, 2633, 1731, 1620, 1548, 1511, 1494, 1445, 1411, 1288, 1274, 1247, 1142, 1114, 886, 771, 760, 743, 735, 704, 668, and 648, 574 cm^{-1}. HRMS *m/z* $[M+H]^+$ Calcd. for $C_{12}H_{10}N_3O$: 212.08184, found 212.08173. *Anal.* Calcd. for $C_{12}H_9N_3O$: C, 68.24; H, 4.29; N, 19.89; found: C, 68.24; H, 4.25; N, 19.79.

8-(Biphenyl-4-yl)imidazo[1,2-c]pyrimidin-5(6H)-one (3b). White crystals, yield 1.78 g (81%). mp 280–287°C, IR (KBr): 3438, 3241, 3146, 3127, 3080, 2940, 2898, 1732, 1618, 1544, 1485, 1407, 1286, 1278, 1262, 1243, 1144, 1109, 918, 836, 827, 758, 740, 719, 693, abd 649, 576 cm^{-1}. HRMS *m/z* $[M+H]^+$ Calcd. for $C_{18}H_{14}N_3O$: 288.11314, found 288.11309. *Anal.* Calcd. for $C_{18}H_{13}N_3O$: C, 75.25; H, 4.56; N, 14.63; found: C, 75.58; H, 4.61; N, 14.74.

8-(4-Methoxyphenyl)imidazo[1,2-c]pyrimidin-5(6H)-one (3c). White crystals, yield 1.61 g (90%). mp 248–250°C, IR (KBr): 3435, 3160, 3068, 2999, 2932, 2845, 1723, 1709, 1619, 1610, 1546, 1515, 1462, 1407, 1298, 1276, 1256, 1183, 1141, 1113, 1024, 882, 845, 829, 800, 742, 652, 621, 572, 563, and 519 cm^{-1}. HRMS *m/z* $[M+H]^+$ Calcd. for $C_{13}H_{12}N_3O_2$: 242.09240, found 242.09249. *Anal.* Calcd. for $C_{13}H_{11}N_3O_2$: C, 64.72; H, 4.60; N, 17.42; found: C, 64.79; H, 4.59; N, 17.32.

8-(4-Chlorophenyl)imidazo[1,2-c]pyrimidin-5(6H)-one (3d). White crystals, yield 1.41 g (75%). mp 262–264°C, IR (KBr): 3437, 3146, 3130, 3067, 2743, 1747, 1617, 1549, 1510, 1486, 1412, 1402, 1287, 1266, 1246, 1144, 1112, 1099, 922, 820, 811, 777, 747, 593, 490, and 463 cm^{-1}. HRMS *m/z* $[M+H]^+$ Calcd. for $C_{12}H_9ClN_3O$: 246.04287, found 246.04287. *Anal.* Calcd. for $C_{12}H_8ClN_3O$: C, 58.67; H, 3.28; N, 17.10; Cl, 14.43; found: C, 58.79; H, 3.23; N, 16.98; Cl, 14.55.

8-[4-(Trifluoromethyl)phenyl]imidazo[1,2-c]pyrimidin-5(6H)-one (3e). White crystals, yield 1.52 g (71%). mp 235–236°C, IR (KBr): 3443, 3074, 2935, 2845, 2745, 2638, 1739, 1724, 1619, 1550, 1517, 1414, 1329, 1278, 1246, 1161, 1141, 1132, 1122, 1115, 1070, 1018, 893, 851, 744, 684, 652, 634, 619, 603, 586, and 413 cm^{-1}. HRMS *m/z* $[M+H]^+$ Calcd. for $C_{13}H_9F_3N_3O$: 280.06922, found 280.06938. *Anal.* Calcd. for $C_{13}H_8F_3N_3O$: C, 55.92; H, 2.89; N, 15.05; found: C, 56.02; H, 2.92; N, 14.95.

4-(5-Oxo-5,6-dihydroimidazo[1,2-c]pyrimidin-8-yl)benzaldehyde (3f). Off-white solid, yield 1.52 g (83%). mp 267–270°C, IR (KBr): 3438, 3147, 3131, 3068, 2859, 1748, 1695, 1615, 1607, 1568, 1550, 1503, 1487, 1411, 1395, 1293, 1279, 1248, 1215, 1167, 1143, 1126, 1112, 922, 824, 747, 685, 650, 583, 556, 493, and 476 cm^{-1}. HRMS *m/z* $[M+H]^+$ Calcd for $C_{13}H_{10}N_3O_2$: 240.07675, found 240.07669. *Anal.* Calcd. for $C_{13}H_9N_3O_2$: C, 65.27; H, 3.79; N, 17.56; found: C, 64.98; H, 3.91; N, 17.42.

4-(5-Oxo-5,6-dihydroimidazo[1,2-c]pyrimidin-8-yl)benzoic acid (3g). Off-white solid, yield 1.45 g (74%). mp >350°C dec., IR (KBr): 3435, 3147, 3131, 3064, 2850, 1744, 1701, 1678, 1611, 1548, 1502, 1486, 1437, 1412, 1327, 1291, 1279, 1245, 1184, 1137, 1112, 922, 845, 774, 758, 746, 701, 587, 556, 483, and 442 cm^{-1}. HRMS *m/z* $[M+H]^+$ Calcd. for $C_{13}H_{10}N_3O_3$: 256.07167, found 256.07152. *Anal.* Calcd. for $C_{13}H_9N_3O_3$: C, 61.18; H, 3.55; N, 16.46; found: C, 60.82; H, 3.67; N, 16.35.

4-(5-Oxo-5,6-dihydroimidazo[1,2-c]pyrimidin-8-yl)benzonitrile (3h). White crystals, yield 1.38 g (84%). mp 310–325°C dec., IR (KBr): 3432, 3219, 3175, 3086, 2942, 2227, 1723, 1624, 1606, 1549, 1509, 1413, 1287, 1274, 1243, 1143, 844, 727, 611, 571, 544, and 500 cm^{-1}. HRMS *m/z* $[M+H]^+$ Calcd. for $C_{13}H_9N_4O$: 237.07709, found 237.07699. *Anal.* Calcd. for $C_{13}H_8N_4O$: C, 66.10; H, 3.41; N, 23.72; found: C, 66.42; H, 3.48; N, 23.35.

8-(Thiophen-2-yl)imidazo[1,2-c]pyrimidin-5(6H)-one (3i). White crystals, yield 1.01 g (61%). mp 249–255°C, IR (KBr): 3420, 3157, 3069, 2922, 2847, 2743, 1726, 1709, 1611, 1553, 1519, 1499, 1405, 1287, 1250, 1241, 1141, 1114, 878, 847, 830, 731, 718, 658, 638, 591, and 571 cm^{-1}. HRMS *m/z* $[M+H]^+$ Calcd. for $C_{10}H_8N_3OS$: 218.03826, found 218.03820. *Anal.* Calcd. for $C_{10}H_7N_3OS$: C, 55.29; H, 3.25; N, 19.34; S, 14.76; found: C, 55.09; H, 3.10; N, 19.09; S, 14.56.

8-(Pyridin-4-yl)imidazo[1,2-c]pyrimidin-5(6H)-one (3j). White crystals, yield 1.01 g (62%). mp 260–263°C dec., IR (KBr): 3436, 3137, 3082, 2936, 2736, 1732, 1723, 1620, 1604, 1556, 1501, 1418, 1326, 1284, 1258, 1135, 1117, 1072, 1008, 890, 828, 758, 679, 666, 649, 618, 579, 568, 549, and 497 cm^{-1}. HRMS *m/z* $[M+H]^+$ Calcd. for $C_{11}H_9N_4O$: 213.07709, found 213.07698. *Anal.* Calcd. for $C_{11}H_8N_4O$: C, 62.26; H, 3.80; N, 26.40; found: C, 61.98; H, 3.92; N, 26.56.

Biological activity. ***MTT assay.*** As for the cytotoxic MTT assay [50], all cells were purchased from the American Tissue Culture Collection, unless otherwise indicated: The CCRF-CEM line are highly chemosensitive T-lymphoblastic leukemia cells, K562 cells were derived from patient with acute myeloid leukemia with bcr-abl translocation, A549 line is lung adenocarcinoma, HCT116 is colorectal tumor cell line, and its p53 gene knockdown counterpart (HCT116p53-/-, Horizon Discovery, Cambridge, UK) is a model of human cancers with p53 mutation frequently associated with poor prognosis. The daunorubicin-resistant subline of CCRF-CEM cells (CEM-DNR bulk) and paclitaxel-resistant subline K562-Tax were selected in our laboratory by the cultivation of maternal cell lines in increasing concentrations of daunorubicin or paclitaxel, respectively, and were characterized well in the article by Nosková *et al.* [42]. The CEM-DNR bulk cells overexpress P-glycoprotein, MRP, and LRP protein, while K562-Tax cells overexpress only P-glycoprotein, both proteins belong to family of ABC transporters and are involved in primary and/or acquired multidrug resistance phenomenon. MRC-5 and BJ are nontumor human fibroblasts. The cells were maintained in Nunc/Corning 80 cm^2 plastic tissue culture flasks and cultured in cell culture medium (DMEM/RPMI 1640 with 5 g/L glucose, 2 m*M* glutamine, 100 U/mL penicillin, 100 µg/mL streptomycin, 10% fetal calf serum, and $NaHCO_3$). Cell suspensions were prepared and diluted according to the particular cell type and the expected target cell density (25,000–30,000 cells/well based on cell growth characteristics). Cells were added by pipette (80 µL) into 96-well microtiter plates. Inoculates were allowed a preincubation period of 24 h at 37°C and 5% CO_2 for stabilization. Fourfold dilutions, in 20 µL aliquots, of the intended test concentration were added to the microtiter plate wells at time zero. All test compound concentrations were examined in duplicate. Incubation of the cells with the test compounds lasted for 72 h at 37°C, in a 5% CO_2 atmosphere at 100% humidity. At the end of the incubation period, the cells were assayed using MTT. Aliquots (10 µL) of the MTT stock solution were pipetted into each well and incubated for further 1–4 h. After this incubation period, the formazan produced was dissolved by the addition of 100 µL/well of 10% aq SDS (pH 5.5), followed by a further incubation at 37°C overnight. The optical density (OD) was measured at 540 nm with a Labsystem iEMS Reader MF (Labsystem, Helsinki, Finland). Tumor cell survival (IC_{50}) was calculated using the following equation: IC = (ODdrug-exposed well/mean ODcontrol wells) × 100%. The IC_{50} value, the drug concentration lethal to 50% of the tumor cells, was calculated from appropriate dose–response curves.

Cell cycle and apoptosis analysis. Subconfluent CCRF-CEM cells (American Tissue Culture Collection), seeded at the density of 5.10^5 cells/mL in 6-well panels, were cultivated with the 1× or 5× IC_{50} of tested compound in a humidified CO_2 incubator at 37°C in RPMI 1640 cell culture medium containing 10% fetal calf serum, 10 m*M* glutamine, 100 U/mL penicillin, and 100 µg/mL streptomycin. Control containing vehicle was harvested at the same time point (24 h). Cells were washed with cold phosphate buffered saline (PBS) and fixed in 70% ethanol overnight at 20°C. The next day, the cells were washed in hypotonic citrate buffer, treated with RNase (50 µg/mL), stained with propidium iodide, and analyzed by flow cytometry using a 488 nm single beam laser (Becton Dickinson, San Jose, CA). Cell cycle was analyzed in the program ModFitLT (Verity), and apoptosis was measured in logarithmic model as a percentage of the particles with propidium content lower than cells in G0/G1 phase (<G1) of the cell cycle. Half of the sample was used for $pH3^{Ser10}$ antibody (Sigma) labeling and subsequent flow cytometry analysis of mitotic cells.

BrDU incorporation analysis. Cells were cultured and treated as for cell cycle analysis. Before harvesting, they were pulse labeled with 10 µ*M* 5-bromo-2-deoxyuridine (BrDU) for 30 min. The cells were trypsinized, fixed with ice-cold 70% ethanol, incubated on ice for 30 min, washed with PBS, and resuspended in 2*M* HCl for 30 min at room temperature to denature their DNA. Following neutralization with 0.1*M* $Na_2B_4O_7$, the cells were washed with PBS containing 0.5% Tween-20 and 1% bovine serum albumin. They were then stained with primary anti-BrdU antibody (Exbio) for 30 min at room temperature in the dark. Cells were than washed with PBS and stained with secondary antimouse-FITC antibody (Sigma). The cells were then washed with PBS and incubated with propidium iodide (0.1 mg/mL) and RNase A (0.5 mg/mL) for 1 h at room temperature in the dark and finally analyzed by flow cytometry using a 488 nm single beam laser (FACSCalibur, Becton Dickinson).

BrU incorporation analysis. Cells were cultured and treated as for cell cycle analysis. Before harvesting, they were pulse labeled with 1 m*M* 5-bromouridine (BrU) for 30 min. The cells were fixed in 1% buffered paraformaldehyde with 0.05% of NP-40 in room temperature for 15 min and then in the refrigerator overnight. They were then washed in 1% glycin in PBS, washed in PBS, and stained with primary anti-BrDU antibody cross-reacting to BrU (Exbio) for 30 min at room temperature in the dark. Cells were than washed with PBS and stained with secondary antimouse-FITC antibody (Sigma). Following the staining, the cells were washed with PBS and fixed with 1% PBS buffered paraformaldehyde with 0.05% of NP-40. The cells were then washed with PBS, incubated with propidium iodide (0.1 mg/mL) and RNase A (0.5 mg/mL) for 1 h at room temperature in the dark, and finally analyzed by flow cytometry using a 488 nm single beam laser (FACSCalibur, Becton Dickinson).

Acknowledgments. This work was supported by Ministry of Industry and Trade of the Czech Republic (project FR-TI1/202) and by grants IGA UP LF_2014_010, CZ.1.05/2.1.00/01.0030 and study stay by CZ.1.07/2.4.00/17.0015. We thank Jan Vaněček for recording of infrared spectra and Dagmar Zvolánková for technical help.

REFERENCES AND NOTES

[1] Chunavala, K. C.; Joshi, G.; Suresh, E.; Adimurthy, S. Synthesis 2011, 4, 635.
[2] Rival, Y.; Grassy, G.; Michel, G. Chem Pharm Bull 1992, 40, 1170.
[3] Vasudevan, A.; Mavandadi, F.; Chen, L.; Gangjee, A. J Org Chem 1999, 64, 634.
[4] Gueiffier, A.; Lhassani, M.; Elhakmaoui, A.; Snoeck, R.; Andrei, G.; Chavignon, O.; Teulade, J. C.; Kerbal, A.; Essassi, E. M.; Debouzy, J. C.; Witvrouw, M.; Blache, Y.; Balzarini, J.; De Clercq, E.; Chapat, J. P. J Med Chem 1996, 39, 2856.
[5] Gudmundsson, K. S.; Johns, B. A. Bioorg Med Chem Lett 2007, 17, 2735.
[6] Moraski, G. C.; Markley, L. D.; Hipskind, P. A.; Boshoff, H.; Cho, S.; Franzblau, S. G.; Miller, M. J. ACS Med Chem Lett 2011, 2, 466.
[7] Moraski, G. C.; Markley, L. D.; Chang, M.; Cho, S.; Franzblau, S. G.; Hwang, C. H.; Boshoff, H.; Miller, M. J. Bioorg Med Chem 2012, 20, 2214.
[8] Lin, H.; Erhard, K.; Hardwicke, M. A.; Luengo, J. I.; Mack, J. F.; McSurdy-Freed, J.; Plant, R.; Raha, K.; Rominger, C. M.; Sanchez, R. M.; Schaber, M. D.; Schulz, M. J.; Spengler, M. D.; Tedesco, R.; Xie, R.; Zeng, J. J.; Rivero, R. A. Bioorg Med Chem Lett 2012, 22, 2230.
[9] Vilchis-Reyes, M. A.; Zentella, A.; Martínez-Urbina, M. A.; Guzmán, Á.; Vargas, O.; Apan, M. T. R.; Gallegos, J. L. V.; Díaz, E. Eur J Med Chem 2010, 45, 379.
[10] López-Martínez, M.; Salgado-Zamora, H.; Campos-Aldrete, M. E.; Trujillo-Ferrara, J. G.; Correa-Basurto, J.; Mexica-Ochoa, C. Med Chem Res 2012, 21, 415.
[11] Rival, Y.; Grassy, G.; Taudou, A.; Ecalle, R. Eur J Med Chem 1991, 26, 13.
[12] Andreani, A.; Rambaldi, M.; Locatelli, A.; Bossa, R.; Salvatore, G.; Galatulas, I. Eur J Med Chem 1994, 29, 339.
[13] Abignente, E.; Sacchi, A.; Laneri, S.; Rossi, F.; Amico, M. D.; Berrino, L.; Calderaro, V.; Parrillo, C. Eur J Med Chem 1994, 29, 279.
[14] Harrison, T. S.; Keating, G. M. CNS Drugs 2005, 19, 65.
[15] Bhuiyan, M. M. H.; Rahman, K. M. M.; Hossain, M. K.; Rahim, M. A.; Hossain, M. I. Croat Chem Acta 2005, 78, 633.
[16] Chhabria, M. T.; Jani, M. H. Eur J Med Chem 2009, 44, 3837.
[17] Spitzer, W. A.; Victor, F.; Don Pollock, G.; Hayes, J. S. J Med Chem 1998, 31, 1590.
[18] Abignente, E.; Arena, F.; De Caprariis, P.; Luraschi, E.; Sacchi, A.; Lampa, E.; Berrino, L.; Donnoli, D. Farmaco 1991, 46, 1099.
[19] Hirabayashi, A.; Mukaiyama, H.; Kobayashi, H.; Shiohara, H.; Nakayama, S.; Ozawa, M.; Tsuji, E.; Miyazawa, K.; Misawa, K.; Ohnota, H.; Isaji, M. Bioorg Med Chem 2008, 16, 9247.
[20] Hirabayashi, A.; Mukaiyama, H.; Kobayashi, H.; Shiohara, H.; Nakayama, S.; Ozawa, M.; Miyazawa, K.; Misawa, K.; Ohnota, H.; Isaji, M. Bioorg Med Chem 2009, 17, 284.
[21] Linz, S.; Müller, J.; Hübner, H.; Gmeiner, P.; Troschütz, R. Bioorg Med Chem 2009, 17, 4448.
[22] Kochetkov, N. K.; Shibaev, V. N.; Kost, A. A. TetrahedronLett 1971, 12, 1993.
[23] Karskela, T.; Klika, K. D.; Lönnberg, H. Collect Czech Chem Commun 2011, 76, 1043.
[24] Seela, F.; Schweinberger, E.; Xu, K.; Sirivolu, V. R.; Rosemeyer, H.; Becker, E. M. Tetrahedron 2007, 63, 3471.
[25] Kayasuga-Mikado, K.; Hashimoto, T.; Negishi, T.; Negishi, K.; Hayatsu, H. Chem Pharm Bull 1980, 28, 932.
[26] Guchhait, S. K.; Madaan, C. TetrahedronLett 2011, 52, 56.
[27] Albaugh, P. A.; Marshall, L.; Gregory, J.; White, G.; Hutchison, A.; Ross, P. C.; Gallagher, D. W.; Tallman, J. F.; Crago, M.; Cassela, J. V. J Med Chem 2002, 45, 5043.
[28] Conn, P. J.; Linsley, C. W.; Stauffer, S. R.; Bartolome-Nebreda, J. M.; Macdonald, G. J.; Conde-Ceide, S.; Jones, C. K.; Martin-Martin, M. L.; Tong H. M. PCT Int Appl Patent WO 2012125732 A1, 2012.
[29] Kifli, N.; De Clerq, E.; Balzarini, J.; Simons, C. Bioorg Med Chem 2004, 12, 4245.
[30] Mansour, T. S.; Evans, C. A.; Charron, M.; Korba, B. E. Bioorg Med Chem Lett 1997, 7, 303.
[31] Mansour, T. S.; Evans, C. A.; Siddiqui, M. A.; Zacharie, B.; Nguyen-Ba, N.; Lee, N.; Korba, B. Nucleos Nucleot 1997, 16, 993.
[32] Siddiqui, A.; Cimpoia, A.; Preville, P. PCT Int Appl Patent WO 0149700 A1, 2001.
[33] Miyaura, N.; Suzuki, A. Chem Rev 1995, 95, 2457.
[34] Raindlová, V.; Pohl, R.; Šanda, M.; Hocek, M. Angew Chem Int Ed 2010, 49, 1064.
[35] Žinić, B.; Krizmanić, I.; Vikić-Topić, D.; Žinić, M. Croat Chem Acta 1999, 72, 957.
[36] Audette, G. F.; Zoghaib, W. M.; Tourigny, G.; Gupta, S. V.; Delbaere, L. T. J. Acta Crystallogr Sect C Cryst Struct Commun 1997, 53, 1099.
[37] Basheer, A.; Rappoport, Z. J Org Chem 2006, 71, 9743.
[38] Heaney, F.; Bourke, S.; Burke, C.; Cunningham, D.; McArdle, P. J Chem Soc Perkin Trans 1 1998, 2255.
[39] Bhat, B.; Leonard, N. J. J Am Chem Soc 1992, 114, 7407.
[40] Bhat, B.; Wilson, S. R.; Leonard, N. J. Acta Crystallogr Sect C Cryst Struct Commun 1993, 49, 921.
[41] Allen, F. H.; Kennard, O.; Watson, D. G.; Brammer, L.; Orpen, A. G.; Taylor, R. J Chem Soc Perkin Trans 2 1987, S1.
[42] Nosková, V.; Džubák, P.; Kuzmina, G.; Ludková, A.; Stehlík, D.; Trojanec, R.; Janošťáková, A.; Kořínková, G.; Mihál, V.; Hajdúch, M. Neoplazma 2002, 49, 418.
[43] Maddocks, O. D. K.; Berkers, C. R.; Mason, S. M.; Zheng, L.; Blyth, K.; Gottlieb, E.; Vousden, K. H. Nature 2013, 493, 542.
[44] Maddocks, O. D. K.; Vousden, K. H. J Mol Med 2011, 89, 237.
[45] Otwinowski, Z.; Minor, W. Methods Enzymol 1997, 276, 307.
[46] Coppens, P. In Crystallographic Computing, Ahmed, F. R., Hall, S. R., Huber, C. P., Eds.; Munksgaard: Copenhagen, 1970; pp 255–270.
[47] Altomare, A.; Cascarano, G.; Giacovazzo, C.; Guagliardi, A. J Appl Crystallogr 1994, 27, 1045.
[48] Sheldrick, G. M. SHELXL-97, University of Göttingen: Göttingen, 2008.
[49] Johnson, T. B.; Johns, C. O. J Biol Chem 1906, 1, 305.
[50] Borderioux, A.; Nauš, P.; Perlíková, P.; Pohl, R.; Pichová, I.; Votruba, I.; Džubák, P.; Konečný, P.; Hajdúch, M.; Stray, K. M.; Wang, T.; Ray, A. S.; Feng, J. Y.; Birkus, G.; Cihlar, T.; Hocek, M. J Med Chem 2011, 54, 5498.

2.3.3 Hydrazone derivatives based on a Tröger´s base skeleton

Hydrazones have interesting biological properties, including antibacterial, anticancer, antiviral antimycobacterial and antifungal activity. They belong to a group of carbonyl compounds counted as aldehydes and ketones, possessing the azomethine group. Although the precise mechanism of action is not yet very well known, it is probably based on metal ion chelation or inhibition of some metabolic proteins involved in epigenetic modification, DNA and RNA synthesis and induction of oxidative stress. Hall et al. (1999) discovered that these compounds interfere with nucleic acid syntheses through amidophosphoribosidtransferase, Inosine-5-monophosphate dehydrogenase, dihydrofolate reductase, thymidylate synthase and thimidin kinase inhibition. Due to their interesting chelating properties, hydrazones have been extensively tested for their potential benefit, for example as antitumor (Lindgren et al. 2014, Kaplánek et al. 2015), antifungal (Casanova et al. 2015) antituberculotic (Mathew et al. 2015), anti-inflammatory, antiepileptic (Kumar et al. 2014) and antidiabetic (Mayer et al. 2015) agents. Moreover, these structures are known for other therapeutical properties – antimalarial, antioxidant, antiplatelet, antiparasitic, antihypertensive and cardioprotective (Singh & Raghav 2011; Ali et al. 2012; Padmini et al. 2013). Tsafack et al. (1996) tested hydrazones against *Plasmodium falciparum* and identified several molecules significantly active towards all the plasmodial stages, in micromolar and also submicromolar concentrations. A similar study with different forms of hydrazones was carried out by Walcourt at al. (2004) as well. Hydrazones in our study (2.3.3.1) were prepared to achieve DNA intercalating properties. For this purpose, Tröger´s base was used as a skeleton for the synthesis.

2.3.3.1 Cytotoxic and antibacterial activity of hydrazone derivatives

KAPLÁNEK R, HAVLÍK M, DOLENSKÝ B, RAK J, DŽUBÁK P, **KONEČNÝ P**, HAJDÚCH M, KRÁLOVÁ J, KRÁL V. (2015). Synthesis and biological activity evaluation of hydrazone derivatives based on a Tröger's base skeleton. *Bioorg Med Chem*. Apr 1; 23(7):1651-9.

Bioorganic & Medicinal Chemistry 23 (2015) 1651–1659

Contents lists available at ScienceDirect

Bioorganic & Medicinal Chemistry

journal homepage: www.elsevier.com/locate/bmc

Synthesis and biological activity evaluation of hydrazone derivatives based on a Tröger's base skeleton

Robert Kaplánek [a], Martin Havlík [a], Bohumil Dolenský [a], Jakub Rak [a], Petr Džubák [b], Petr Konečný [b], Marián Hajdúch [b], Jarmila Králová [c], Vladimír Král [a,*]

[a] Department of Analytical Chemistry, Faculty of Chemical Engineering, University of Chemical Technology, Technická 5, 166 28 Prague 6, Czech Republic
[b] Institute of Molecular and Translational Medicine, Palacky University and University Hospital in Olomouc, Faculty of Medicine and Dentistry, Hněvotínská 5, 775 15 Olomouc, Czech Republic
[c] Institute of Molecular Genetics, Academy of Sciences of the Czech Republic, Vídeňská 1083, 142 20 Prague 4, Czech Republic

ARTICLE INFO

Article history:
Received 25 November 2014
Revised 14 January 2015
Accepted 16 January 2015
Available online 23 January 2015

Keywords:
Anticancer agents
Cancer treatment
Complexation studies
Hydrazone
Tröger's base

ABSTRACT

We report the design and synthesis of novel anticancer agents based on bis-hydrazones separated by a rigid Tröger's base skeleton. This novel approach combines a biologically active moiety (hydrazone) with this scaffold (Tröger's base) to construct DNA intercalators. Evaluation of the anticancer activity of these agents using seven cancer cell lines and two healthy cell lines found that several derivatives had potent anticancer activity and excellent selectivity indexes toward cancer cells. The antimicrobial activities were tested on a set of thirteen bacterial stains, but the prepared compounds were not active. Complexation studies using biologically important metal ions demonstrated that these compounds are able to bind Cu^{2+}, Fe^{3+}, Co^{2+}, Ni^{2+} and Zn^{2+}. DNA intercalation studies showed that the compounds themselves do not interact with DNA, but their metallocomplexes do interact, most likely via intercalation into DNA.

1. Introduction

Cancer is a disease characterised by out-of-control cell growth. There are over 100 different types of cancer. Although numerous compounds show anticancer activity, many of them exhibit either unpleasant side effects or substantial toxicity. The increasingly common resistance of cancer towards currently used drugs is also problematic. A promising family of cytostatics is based on aroyl hydrazones.

(Hetero)aroyl hydrazones demonstrate a wide range of biological activities, including anti-microbial, anti-bacterial, anti-mycobacterial, anti-viral and anti-malarial activities.[1–6] In addition, they demonstrate metal ion-chelating activity and can thus be used as therapeutics for the treatment of both chronic and transfusional iron overload.[1,2,7–9] Some aroyl hydrazones have exhibited significant anticancer activity.[1,2,6,10–14]

The mechanism of the anticancer action of aroyl hydrazones is assumed to involve the chelation of metal ions, especially iron, which is crucial for the function, growth and division of cancer cells. Other possible mechanisms of action include intercalation into DNA, inhibition of the enzymes responsible for the biosynthesis of both RNA and DNA and other biological processes (such as ribonucleotide reductase, histone deacetylases and acyl transferases), the disruption of cellular metabolic processes and generation of redox systems that produce reactive oxygen species and toxicity to metabolites.[1,2,11,13–15] While not yet completely determined, the mechanism of the anticancer action of aroyl hydrazones is expected to be a combination of the above mechanisms.

The anticancer activities of (hetero)aroyl hydrazones were first described in 1959.[16] Many additional compounds have been prepared and tested over the last two decades. These hydrazones are commonly derived from pyridoxal isonicotinoyl hydrazone (PIH), which was first described in 1954 as an anti-tubercular agent[17,18] and was developed in 1979 for iron overload treatment.[19] The anticancer activities of PIH and its derivatives were discovered in 1962.[20] This class of compounds are still the subject of intense research, and many structurally diverse analogues of PIH have been recently described.[6,10,13] These aroyl hydrazones and their metallocomplexes are usually small, relatively planar molecules. These properties are favorable for intercalation into the DNA helix.

A promising strategy for the design of novel anticancer agents involves the use of multiple hydrazone-binding units that can potentially intercalate into DNA. For bis-hydrazones, the binding units are commonly connected with flexible spacer to allow the binding of one metal ion by both binding units.[21–23] Our strategy was to use a rigid spacer between the hydrazone units to facilitate

* Corresponding author. Tel.: +420 220445027.
E-mail address: Vladimir.Kral@vscht.cz (V. Král).

http://dx.doi.org/10.1016/j.bmc.2015.01.029
0968-0896/

intercalation of those units into DNA. The most promising structural motif for a spacer is based on Tröger's bases. Tröger's bases are compounds containing two arenes connected to the *b*- and *f*-sides of 1,5-methano-1,5-diazocine.[24–26] The unique structural features of Tröger's base (C_2 symmetry, rigid Δ-shape geometry, inherent chirality) result in a helical shape that can be similar or opposite to the helicity of DNA. Recently published studies have shown that Tröger's base derivatives based on acridine,[27] proflavine,[28,29] naphthalimide,[30] distamycin[31,32] or metal complexes[33] are interesting intercalators. Some Tröger's base derivatives have also been studied for their anticancer activity.[34–36]

From biological perspective, effect of the Tröger's base skeleton is unexplored area. It seems that the Tröger's base skeleton can be interesting pharmacophore useful in the design and construction of biological active compounds. Therefore explored the design and synthesis of hydrazones possessing Tröger's base skeleton and evaluated their cytostatic and antimicrobial activity, metal-binding properties and interactions with DNA.

2. Results and discussion

2.1. Synthesis of target compounds 4–14

Target hydrazones **4–14** were prepared in three synthetic steps (Scheme 1). The first step was preparation of the Tröger's base scaffold with suitable functional groups. Thus, we prepared diester **2** through the reaction of methyl 6-amino-2-naphthoate (**1**) with hexamethylenetetramine in trifluoroacetic acid (TFA) in 55% yield using procedures reported in the literature.[37,38] The diester **2** was subsequently converted into dihydrazide **3** by reaction with a large excess of hydrazine hydrate in dioxane at high temperature in 98% yield. In the last step, dihydrazide **3** was reacted with an excess of a 5-substituted 2-hydroxybenzaldehyde or a 2-*N*-heterocyclic aldehyde or ketone (molar ratio 1:2.4) in anhydrous dimethyl sulphoxide at room temperature to afford hydrazones **4–14** in high yield, 86–98%.

2.2. Biological studies

2.2.1. Cytostatic activity

The in vitro cytotoxic activities of hydrazones **4–14** were tested on the following seven cancer cell lines: CCRF-CEM (T-lymphoblastic leukaemia), CEM-DNR (T-lymphoblastic leukaemia, daunorubicin resistant), K562 (acute myeloid leukaemia) and K562-TAX (acute myeloid leukaemia, paclitaxel resistant), A549 (human lung adenocarcinoma), HCT116 (human colorectal cancer), HCT116p53−/− (human colorectal cancer, p53-deficient) and on the following two healthy cell lines: BJ (human fibroblast) and MRC-5 (human lung fibroblasts). Cytotoxic activities are presented as the IC_{50} values (Table 1). Data are expressed as the mean ± SD (μM) of the IC_{50} values for eight independent experiments. The tested compounds (**4–14**) showed cytotoxic activity at concentrations of 0.05 to >100 μM. The majority of the compounds were more active against the T-lymphoblastic leukaemia cell line CCRF-CEM than on the corresponding daunorubicin-resistant line CEM-DNR. With respect to the myeloid leukaemia K562 line and its paclitaxel-resistant form (K562-TAX), the cytotoxic activities were similar against both cell lines (except for hydrazones **12** and **13**). The IC_{50} values for the human lung adenocarcinoma cell line A549 were from 0.17 to >100 μM. The inhibitory activities for the human colorectal cancer cell line HTC116 and its p53-deficient form (HTC116p53−/−) were similar.

Comparison of the activities of our derivatives with those of other hydrazone-based compounds against the same cell lines described in the literature is difficult due to various descriptors of activity (IC_{50}, EC_{50}, GI_{50}, etc.) and experimental conditions. For example, (2-hydroxyaryl)ydene hydrazones derived from isonicotinoyl hydrazide showed IC_{50} values in the range from 0.3 to 28.4 μM

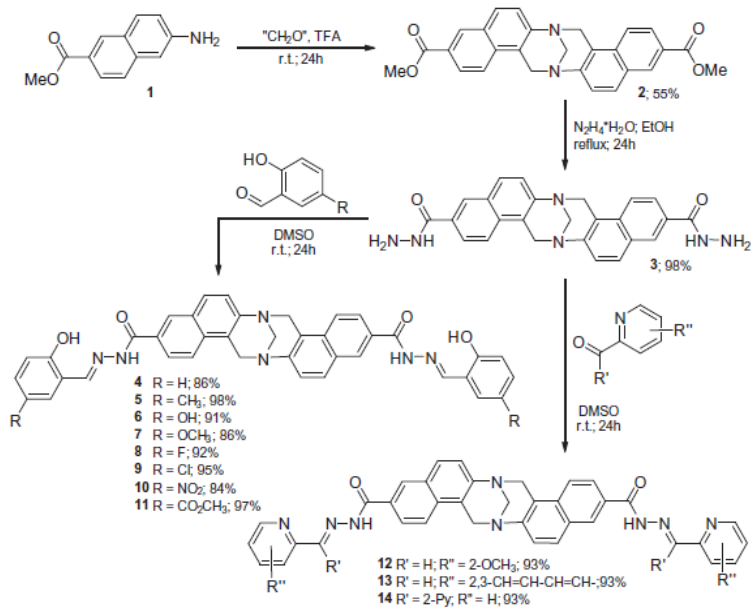

Scheme 1. Preparation of hydrazones **4–14**.

Table 1
IC_{50} values ± SD (μM) for hydrazones **4–14**

Compound	Cell line								
	CCRF-CEM	CEM-DNR	K562	K562-TAX	A549	HCT116	HCT116 p53−/−	BJ	MRC-5
4	0.36 ± 0.33	4.25 ± 1.29	0.58 ± 0.38	0.83 ± 0.09	0.98 ± 0.61	0.39 ± 0.17	0.19 ± 0.08	0.27 ± 0.19	0.39 ± 0.26
5	0.58 ± 0.43	5.36 ± 4.11	0.90 ± 1.08	1.14 ± 0.31	0.54 ± 0.25	0.62 ± 0.16	0.45 ± 0.16	0.69 ± 0.67	0.27 ± 0.30
6	0.06 ± 0.03	2.59 ± 2.27	0.44 ± 0.49	0.26 ± 0.01	0.17 ± 0.13	0.39 ± 0.23	0.12 ± 0.11	6.55 ± 4.61	0.55 ± 0.73
7	0.18 ± 0.15	2.14 ± 1.30	0.08 ± 0.05	0.21 ± 0.09	0.23 ± 0.11	0.05 ± 0.04	0.06 ± 0.03	57.15 ± 20.82	0.11 ± 0.07
8	1.58 ± 1.17	4.25 ± 1.15	2.30 ± 1.09	2.36 ± 0.84	1.24 ± 0.58	0.64 ± 0.35	0.81 ± 0.41	54.14 ± 28.47	29.03 ± 15.12
9	42.14 ± 13.06	>100	>100	>100	>100	>100	>100	>100	>100
10	>100	>100	>100	>100	>100	>100	>100	>100	88.77 ± 17.53
11	5.62 ± 1.24	28.17 ± 7.50	9.76 ± 4.34	21.23 ± 1.59	11.93 ± 5.00	10.30 ± 4.56	9.47 ± 3.42	87.42 ± 10.59	95.37 ± 7.17
12	36.56 ± 3.67	6.71 ± 2.75	55.59 ± 13.20	2.93 ± 0.84	>100	85.73 ± 17.40	>100	>100	>100
13	0.58 ± 0.53	6.29 ± 2.70	0.82 ± 1.01	10.14 ± 6.05	18.58 ± 3.10	17.66 ± 6.86	25.30 ± 38.05	>100	>100
14	0.91 ± 0.52	2.08 ± 1.03	0.64 ± 0.39	0.56 ± 0.05	2.03 ± 1.17	0.46 ± 0.09	0.78 ± 0.45	2.09 ± 1.90	1.03 ± 1.02

Legend: CCRF-CEM (T-lymphoblastic leukaemia), CEM-DNR (T-lymphoblastic leukaemia, daunorubicin resistant), K562 (acute myeloid leukaemia), K562-TAX (acute myeloid leukaemia, paclitaxel resistant), A549 (human lung adenocarcinoma), HCT116 (human colorectal cancer), HCT116p53−/− (human colorectal cancer, p53-deficient), BJ (human fibroblast) and MRC-5 (human lung fibroblasts).

(HCT116),[39] from quinoxalin-2-hydrazine in the range from 1.8 to 14.2 μM (HCT116),[40] from benzoisoindoline-based hydrazide in the range from 5.8 to more than 50 μM (HCT116) and more than 50 μM (A549),[41] from 1-arylmethyl-3-aryl-1*H*-pyrazole-5-carbohydrazide in the range 3.7–10.8 (A549)[42] or from benzoisothiazol-based hydrazides in the range of 0.5 to more than 100 μM (CCRF-CEM) and (2-*N*-heteroaryl)ydene hydrazones derived from benzoxazole-2-hydrazine showed IC_{50} values in the range from 0.004 to more than 50 μM (CCRF-CEM).[43,44] These examples indicate that anticancer effect is strongly dependent on the structure of both aldehyde/ketone and hydrazine/hydrazide part of hydrazone molecule.

From a structural perspective, the most active compounds possessed the 2-hydroxy-5-methoxybenzylidene (hydrazone **7**), 2-hydroxy-5-fluorobenzylidene (hydrazone **8**), quinolin-2-ylmethylidene (hydrazone **13**) and di(2-pyridyl)methylidene moieties (hydrazone **14**). No correlation was observed between electronic effect of substituents and anticancer activity. The lipophilicity of the compounds is well known to play an important role in their penetration through cell membrane. The lipophilicities of the all synthesized compounds were expressed as partition coefficient log *P* values (determined using ChemBioDraw Ultra v13; data are not shown). Unfortunately, log *P* values have not shown any correlation with the anticancer activity. This result indicated that lipophilicity of the tested hydrazones do not affect their anticancer activity.

The selectivity indexes toward cancer cells (Table 2) were calculated as a ratio of the average IC_{50} values for BJ and MRC-5 cells and the IC_{50} values for the corresponding cancer cell line (or the average IC_{50} value for all cancer cell lines for the overall selectivity index). Thus, the selectivity index represents the selectivity for a specific cancer cell line. In Table 2, the highest selectivity index values are highlighted in blue (SI >100) and green (100 > SI > 10). Compound **7** ($SI_{overall}$ = 68.0), compound **8** ($SI_{overall}$ = 22.1) and compound **13** ($SI_{overall}$ = 8.8) showed the best selectivity toward all cancer cells.

To better understand molecular mechanism of the cytostatic effect of the prepared hydrazones the most active compounds were tested for their effect on cell cycle alterations, apoptosis, and DNA and RNA synthesis using CCRF-CEM T-lymphoblastic leukaemia cells (Table 3). The analyses were performed at equiactive concentrations corresponding to 1 × IC_{50} and 5 × IC_{50} for a 24 h treatment interval. All tested compounds (**4–8**, **11**, **13** and **14**) induced apoptosis at the 5 × IC_{50} concentration; at the 1 × IC_{50} concentration, only compound **8** displayed significant apoptosis. Compounds **4**, **5** and **8** resulted in pronounced induction of apoptosis at the 5 × IC_{50} concentration, which was accompanied by significant inhibition of DNA synthesis and a decrease in the percentage of mitotic $pH3^{ser10}$ + cells. Compounds **8** and **13** exhibited dose-dependent inhibition of RNA synthesis.

Above mentioned results indicated, that structure–activity relationships of hydrazone derivatives based on a Tröger's base skeleton are more complex.

2.2.2. Antimicrobial activity

The prepared compounds were also tested for their antimicrobial activity against the following standard reference gram-positive and gram-negative bacterial strains: *Enterococcus faecalis*

Table 2
Selectivity indexes (SI) toward cancer cells for hydrazones **4–14**

Compound	Selectivity indexes (SI)							
	CCRF-CEM	CEM-DNR	K562	K562-TAX	A549	HCT116	HCT116 p53−/−	Overall
4	0.9	0.1	0.6	0.4	0.3	0.8	1.7	0.3
5	0.8	0.1	0.5	0.4	0.9	0.8	1.1	0.4
6	63.2	1.4	8.0	13.8	20.9	9.1	29.0	6.2
7	162.3	13.3	357.2	137.7	123.2	622.3	495.0	68.0
8	26.3	9.8	18.1	17.6	33.6	64.9	51.0	22.1
9	2.4	1.0	1.0	1.0	1.0	1.0	1.0	1.1
10	0.9	0.9	0.9	0.9	0.9	0.9	0.9	0.9
11	16.3	3.2	9.4	4.3	7.7	8.9	9.7	6.6
12	2.7	14.9	1.8	34.1	1.0	1.2	1.0	1.8
13	172.0	15.9	121.9	9.9	5.4	5.7	4.0	8.8
14	1.7	0.7	2.4	2.8	0.8	3.4	2.0	1.5

SI = [average IC_{50} values for BJ and MRC-5 cells]/[IC_{50} values for corresponding cancer cell line]. The highest SI values are highlighted in blue (SI >100) and green (100 > SI > 10).

Table 3
Summary of cell cycle, apoptosis (sub G1), mitosis (pH3), and DNA (BrdU+) and RNA (BrU+) synthesis analyses (only compounds with IC_{50}/CCRF-CEM cell line <10 μM)

Compound	% of total cell populations						
	Apoptosis	G0/G1	S	G2/M	$pH3^{Ser10}$+	DNA synthesis (BrdU+)	RNA synthesis (BrU+)
Control	4.81	40.93	43.23	15.82	1.98	47.7	46.25
4 1 × IC_{50}	18.07	30.60	50.31	19.09	0.62	50.71	59.79
4 5 × IC_{50}	50.23	43.33	37.75	18.92	0.01	5.94	83.92
5 1 × IC_{50}	14.09	40.52	44.83	14.65	1.04	38.67	33.57
5 5 × IC_{50}	54.07	38.43	46.78	14.79	0.22	5.17	26.44
6 1 × IC_{50}	3.99	37.38	44.72	17.9	2.34	50.15	48.47
6 5 × IC_{50}	9.74	21.32	58.22	20.46	2.39	55.96	43.16
7 1 × IC_{50}	12.97	30.00	54.03	15.97	0.99	50.98	63.95
7 5 × IC_{50}	21.74	39.05	48.55	12.40	0.67	31.78	56.37
8 1 × IC_{50}	40.42	31.50	55.45	13.05	0.30	13.69	63.13
8 5 × IC_{50}	58.01	41.10	42.41	16.49	0.15	1.54	4.37
11 1 × IC_{50}	12.85	48.63	38.54	12.83	1.19	46.43	28.66
11 5 × IC_{50}	14.56	31.26	55.48	13.26	0.86	54.61	21.03
13 1 × IC_{50}	8.40	46.09	38.56	15.35	1.65	52.93	44.00
13 5 × IC_{50}	10.73	46.56	39.87	13.57	1.52	43.36	16.94
14 1 × IC_{50}	12.04	28.27	61.24	10.49	0.53	57.31	60.37
14 5 × IC_{50}	24.51	3.63	68.14	28.23	1.72	55.69	55.90

Data are expressed as a percentage of the total cellular population.

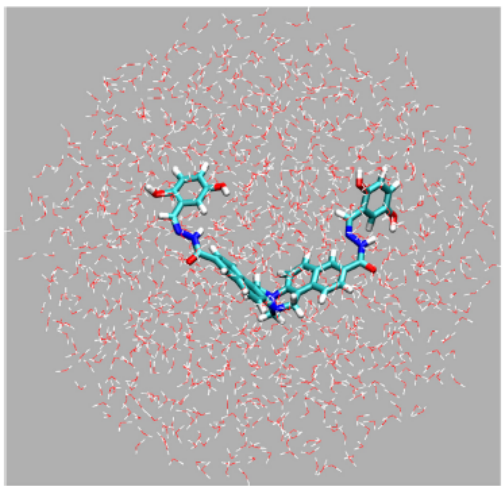

Figure 1. QD/MD simulated structure of hydrazone **6**.

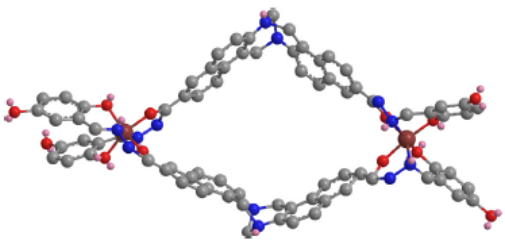

Figure 2. QD/MD simulated structure of metallocomplex of 2 Fe(III) ions with two molecules of hydrazone **6** (legend: grey—carbon, blue—nitrogen, red—oxygen, pink—electron pair, dark-red—iron, hydrogen not shown for clarity).

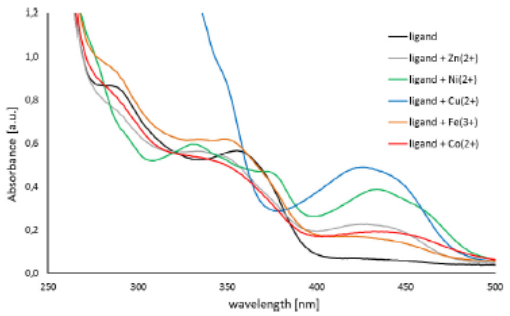

Figure 3. UV/vis spectra of hydrazone **5** and their metallocomplexes with Co^{2+}, Cu^{2+}, Fe^{3+}, Ni^{2+} and Zn^{2+} ions.

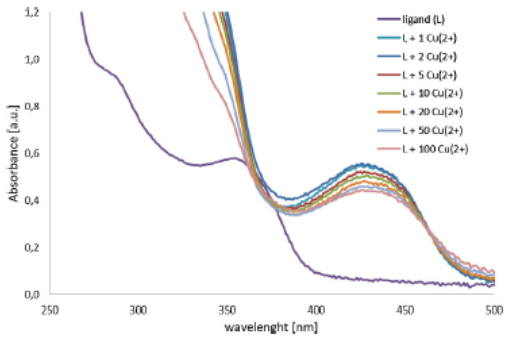

Figure 4. UV/vis titration of hydrazone **5** using Cu^{2+} ions (0–100 concentration equivalent).

CCM 4224, *Staphylococcus aureus CCM 3953*, *Escherichia coli CCM 3954*, *Pseudomonas aeruginosa CCM 395*, methicillin-resistant staphylococci (*Staphylococcus aureus MRSA 4591* and *Staphylococcus haemolyticus A/16568*) and multidrug-resistant strains (*Escherichia coli C/16702* and *Pseudomonas* aeruginosa A/16575, *Candida albicans*, *Candida crusei*, *Candida tropicalis*, *Candida parapsilosis* and *Mycobacterium bovis BCG*). Hydrazones **4–14** did not show

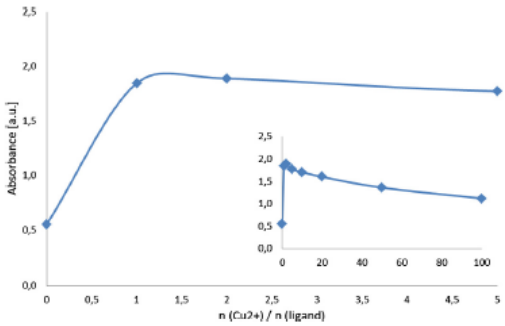

Figure 5. UV/vis titration of hydrazone **5** using Cu^{2+} ions (figure: 0–5 concentration equivalents, inset: 0–100 equiv) at 330 nm.

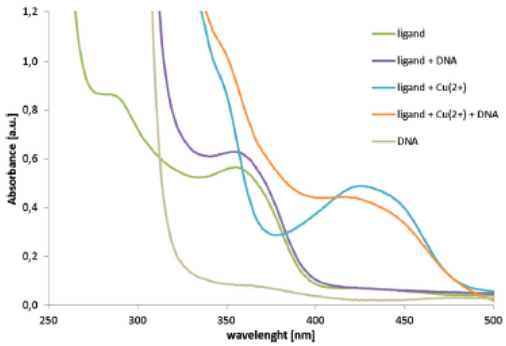

Figure 6. UV/vis spectra of hydrazone **5**, hydrazone **5** with DNA, hydrazone **5** metallocomplex with Cu^{2+}, hydrazone **5** metallocomplex with Cu^{2+} with DNA and DNA.

any antimicrobial activity in the concentration ranges tested (up to 200 μM or up to 100 μM for *Mycobacterium bovis*).

2.3. Quantum dynamic/molecular dynamic simulations

Native conformations of prepared compounds were investigated using quantum dynamic/molecular dynamic (QD/MD) calculations. As shown on Figure 1. the Tröger's base skeletons of the prepared hydrazones have rigid V-shaped geometry. Distance between both metal-binding units does not enable the formation of a 1:1 intramolecular complex with the metal ions but formation of 2:2 is possible (shown on Fig. 2).

2.4. Analytical studies

The chelation of iron and other biologically important metal ions that are necessary to ensure the growth and division of tumour cells may be the primary mechanism of action of aroyl hydrazone-based anticancer agents. The abilities of hydrazones **4–14** to bind the Fe^{2+}, Fe^{3+}, Co^{2+}, Cu^{2+}, Ni^{2+}, Zn^{2+}, Mn^{2+} and Cr^{3+} ions were investigated. Chelation of ions such as Ca^{2+} or Mg^{2+} could lead to serious trouble; thus, interactions with these cations were also investigated. The V-shaped geometry of the Tröger's base skeletons of the prepared hydrazones did not enable the formation of a 1:1 intramolecular complex with the metal ions. Titration demonstrated that the hydrazones chelated the metal ions with stability constants in the order Co^{2+}, $Cu^{2+} > Fe^{3+} > Ni^{2+} \approx Zn^{2+}$ (an overview shown on Figure 3., an example of titration shown on Figs. 4 and 5). Interactions with other metal ions (Ca^{2+}, Mg^{2+}, Fe^{2+}, Mn^{2+} and Cr^{3+}) were not observed.

The DNA intercalation studies showed that hydrazones **4–14** do not interact with DNA alone, but their metallocomplexes with Co^{2+}, Cu^{2+}, Fe^{3+}, Ni^{2+} and Zn^{2+} exhibit spectral changes after the addition of DNA (see Fig. 6). These data indicate that metallocomplexes interact with DNA. The complexation of metal ion by hydrazone moiety stabilized geometry of binding unit. Binding moiety became rigid with geometry closed to planar. This geometry of binding moiety allows intercalation into DNA. Thus, we expected that observed interaction of metallocomplexes with DNA is based on intercalation mechanism.

Spectral changes as a function of pH indicate pKa values of prepared compound as shown on Figure 7. Dashed lines correspond to pH values when protonation of compound is changed. The compound exists in the same protonation form both in the physiological pH (pH = 7.4) and in the pH values inside cancer cells (pH = 5–7).

3. Conclusion

In conclusion, we prepared a series of hydrazone derivatives based on a Tröger's base skeleton (**4–14**) in three synthetic steps with high overall yields. The anticancer activity of the prepared hydrazones was tested on nine cell lines. Eight compounds (**4–8**, **11**, **13** and **14**) showed high cytotoxic activity on all tested leukemic and cancer cell lines. The best results were obtained for compounds **6–8**, **11** and **13**, which show excellent selectivity against

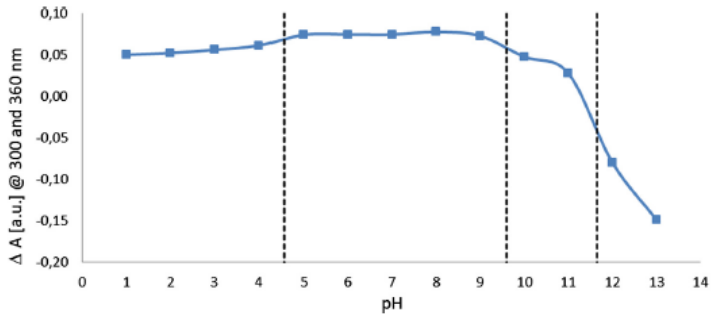

Figure 7. Spectral changes of hydrazone **5** as a function of pH. Dashed lines correspond to pK_a values.

leukaemic cells. Compounds **7**, **8** and **13** showed superior selectivity for all leukaemic and cancer cell lines compared to healthy cell lines. The prepared compounds did not show any antimicrobial activity.

Complexation studies with biologically important metal ions demonstrated that these compounds could bind to the Co^{2+}, Cu^{2+}, Fe^{3+}, Ni^{2+} and Zn^{2+} ions. DNA interaction studies showed that the compounds do not interact with DNA alone, but their metallocomplexes with Co^{2+}, Cu^{2+}, Fe^{3+}, Ni^{2+} and Zn^{2+} interact, probably through intercalation into DNA.

Our results demonstrate that hydrazones with Tröger's base skeletons are a promising class of potent cytostatic agents with high selectivity toward leukaemia and cancer cells. Tröger's base-hydrazone conjugates are good candidates for further synthetic modification and subsequent testing of anticancer activity on wider panel of cancer cell lines, in vivo testing and pharmacokinetics.

4. Experimental

4.1. Chemistry

4.1.1. Measurements and materials

All chemicals were purchased from commercial suppliers and used without further purification. NMR spectra were recorded on Varian Gemini 300 HC (300.077 MHz) at room temperature (~25 °C) in DMSO-d_6. The chemical shifts (δ) are presented in ppm, and coupling constants (J) are presented in Hz. In some cases, ^{13}C NMR spectra were not recorded due to insufficient solubility. The program MestReNova v. 8.01 was used for processing the NMR spectra. Mass spectra were obtained using electrospray ionisation (ESI) with a LTQ Orbitrap spectrometer. Elemental analysis was carried out using Elementar Vario El III analyser.

4.1.2. Preparation of dihydrazide

Diester **2**[37,38] (439 mg; 1 mmol) was dissolved in dioxane (20 mL) at 100 °C. Hydrazine hydrate (4 mL, 80 mmol) was added, and the reaction mixture was stirred at 100 °C for 24 h. The reaction mixture was evaporated to dryness in vacuo. An aliquot of isopropanol (20 mL) was added to the dried mixture. The solid was filtered off, washed with isopropanol (10 mL) followed by diethyl ether (20 mL) and then dried in vacuo to obtain 430 mg (98%) of dihydrazide **3**.

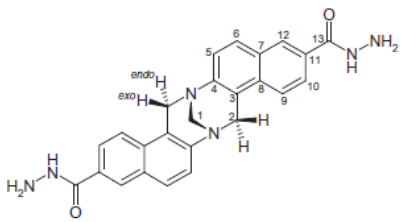

^{1}H NMR (DMSO-d_6): δ 9.93 (br s, 2H), 8.30 (d, 2H, J = 1.2 Hz), 7.91 (dd, 2H, J_1 = 8.9 Hz, J_2 = 1.2 Hz), 7.78 (d, 2H, J = 8.9 Hz), 7.78 (d, 2H, J = 8.9 Hz), 7.43 (d, 2H, J = 8.9 Hz), 4.97 (d, 2H, J = 17.0 Hz), 4.76 (d, 2H, J = 17.0 Hz), 4.45 (s, 2H). ^{1}H NMR (300 MHz, pyridine-d_5): δ 11.04 (vbr s, 2H, NH), 8.68 (d, 2H, J = 1.5 Hz, H12), 8.40 (dd, 2H, J_1 = 8.8 Hz, J_2 = 1.5 Hz, H10), 7.84 (d, 2H, J = 8.8 Hz, H9), 7.76 (d, 2H, J = 8.8 Hz, H6), 7.53 (d, 2H, J = 8.8 Hz, H5), 5.19 (signal merged with water signal, NH_2), 5.02 (d, 2H, J = 17.0 Hz, H2^{exo}), 4.88 (d, 2H, J = 17.0 Hz, H2^{endo}), 4.50 (s, 2H, H1). ^{13}C APT NMR (75 MHz, pyridine-d_5): δ 168.49 (C13), 148.20 (C4), 133.75 (C8), 131.17 (C11), 131.04 (C7), 129.35 (C6), 129.04 (C12), 126.58 (C5), 125.85 (C10), 122.65 (C9), 122.45 (C3), 67.22 (C1), 56.40 (C2). Full assignment based on correlation gHSQC and gHMBC spectra. Anal. Calcd for $C_{25}H_{22}N_6O_2$: C, 68.48; H, 5.06; N, 19.17. Found: C, 68.46; H, 5.09; N, 19.17. HRMS (ESI$^+$) calcd for $C_{25}H_{22}N_6O_2Na$ [M+Na]$^+$: 461.16965, found: 461.16956.

4.1.3. Preparation of hydrazones

General procedure: Dihydrazide **3** (120 mg; 275 µmol) was treated with carbonyl compound (660 µmol; 1.2 equiv) in anhydrous DMSO (4 mL) at rt for 24 h. Diethyl ether (30 mL) was then added, and the precipitated solid was filtered off, washed with a diethyl ether-acetonitrile mixture (4:1 v/v; 3 × 20 mL) and dried in vacuo to obtain the hydrazone.

4.1.3.1. Hydrazone 4. 153 mg (86%). ^{1}H NMR (DMSO-d_6): 12.23 (s, 2H), 11.30 (s, 2H), 8.67 (s, 2H), 8.45 (d, 2H, J = 0.6 Hz), 8.01 (dd, 2H, J_1 = 8.8 Hz, J_2 = 0.6 Hz), 7.89 (m, 4H), 7.53 (m, 4H), 7.30 (m, 2H), 6.94 (m, 4H), 5.05 (d, 2H, J = 17.0 Hz), 4.84 (d, 2H, J = 17.0 Hz), 4.50 (s, 2H). ^{1}H NMR (300 MHz, pyridine-d_5): δ 13.12 (br s, 2H), 12.51 (vbr s, 2H), 8.84 (s, 2H), 8.65 (d, 2H, J = 1.5 Hz), 8.38 (dd, 2H, J_1 = 8.7 Hz, J_2 = 1.5 Hz), 7.80 (d, 2H, J = 8.7 Hz), 7.67 (d, 2H, J = 8.9 Hz), 7.51 (d, 2H, J = 8.9 Hz), 7.42 (br d, 2H, J = 7.6 Hz), 7.32 (br t, 2H, J = 7.7 Hz), 7.22 (covered by solvent signal), 6.91 (td, 2H, J_1 = 7.4 Hz, J_2 = 1.2 Hz), 4.99 (d, 2H, J = 17.0 Hz), 4.84 (d, 2H, J = 17.0 Hz), 4.48 (s, 2H). ^{13}C APT NMR (75 MHz, pyridine-d_5): δ 164.78, 159.64, 150.0 (covered by solvent signal), 148.59, 134.04, 132.25 CH, 131.17 CH, 130.76, 130.36, 129.75 CH, 129.34 CH, 126.70 CH, 126.12 CH, 122.82 CH, 122.48, 120.12 CH, 119.81, 117.84 CH, 67.12 CH_2, 56.33 CH_2. Anal. Calcd for $C_{39}H_{30}N_6O_4$: C, 72.43; H, 4.68; N, 13.00. Found: C, 72.41; H, 4.70; N, 12.99. HRMS (ESI$^+$) calcd for $C_{39}H_{30}N_6O_4Na$ [M+Na]$^+$: 669.22207, found: 669.22186.

4.1.3.2. Hydrazone 5. 182 mg (98%). ^{1}H NMR (DMSO-d_6): δ 12.21 (s, 2H), 11.05 (s, 2H), 8.62 (s, 2H), 8.44 (d, 2H, J = 0.6 Hz), 8.00 (dd, 2H, J_1 = 8.8 Hz, J_2 = 0.6 Hz), 7.90 (d, 2H, J = 8.8 Hz), 7.88 (d, 2H, 8.8 Hz), 7.51 (d, 2H, J = 8.8 Hz), 7.35 (d, 2H, J = 1.2 Hz), 7.10 (dd, 2H, J_1 = 8.4 Hz, J_2 = 1.2 Hz), 6.83 (d, 2H, J = 8.4 Hz), 5.04 (d, 2H, J = 17.3 Hz), 4.83 (d, 2H, J = 17.3 Hz), 4.49 (s, 2H), 2.25 (s, 6H). ^{1}H NMR (300 MHz, pyridine-d_5): δ 13.14 (br s, 2H, NH), 12.33 (vbr s, 2H, OH), 8.87 (s, 2H, H14), 8.65 (d, 2H, J = 1.8 Hz, H12), 8.38 (dd, 2H, J_1 = 8.7 Hz, J_2 = 1.8 Hz, H10), 7.79 (d, 2H, J = 8.7 Hz, H9), 7.67 (br d, 2H, J = 8.8 Hz, H6), 7.50 (d, 2H, J = 8.8 Hz, H5), 7.21 (H20, covered by solvent signal), 7.14 (d, 2H, J = 8.3 Hz), 7.10 (dd, 2H, J_1 = 8.3 Hz, J_2 = 1.7 Hz), 4.98 (d, 2H, J = 16.9 Hz), 4.83 (d, 2H, J = 16.9 Hz), 4.47 (s, 2H), 2.13 (s, 6H, H21). ^{13}C APT NMR (75 MHz, pyridine-d_5): δ 164.82 (C13), 157.51 (C16), 150.0 (C14, covered by solvent signal), 148.58 (C4), 134.02 (C8), 133.06 (C18), 131.22 (C20), 130.76 (C7), 130.40 (C11), 129.76 (C12), 129.34 (C6), 128.95 (C19), 126.69 (C5), 126.14 (C10), 122.81 (C9), 122.47 (C3), 119.48 (C15), 117.66 (C17), 67.11 (C1), 56.32 (C2), 20.65 (C21). Full assignment based on correlation gCOSY, NOESY1D, gHSQC and gHMBC spectra. Anal. Calcd for $C_{41}H_{34}N_6O_4$: C, 72.98; H, 5.08; N, 12.46. Found: C, 72.97; H, 5.10; N, 12.47. HRMS (ESI$^+$) calcd for $C_{41}H_{34}N_6O_4Na$ [M+Na]$^+$: 697.25337, found: 697.25305.

4.1.3.3. Hydrazone 6. 170 mg (91%). ^{1}H NMR (DMSO-d_6): δ 12.11 (s, 2H), 10.40 (s, 2H), 9.00 (s, 2H), 8.61 (s, 2H), 8.44 (s, 2H), 8.00 (d, 2H, J = 8.8 Hz), 7.89 (d, 2H, J = 8.8 Hz), 7.87 (d, 2H, 8.8 Hz), 7.51 (d, 2H, J = 8.8 Hz), 6.99 (s, 2H), 6.75 (s, 4H), 5.04 (d, 2H, J = 16.8 Hz), 4.82 (d, 2H, J = 16.8 Hz), 4.49 (s, 2H). ^{1}H NMR (300 MHz, pyridine-d_5): δ 13.02 (br s, 2H), 11.93 (br s, 2H), 11.13 (vbr s, 2H), 8.90 (br s, 2H, H14), 8.66 (s, 2H, H12), 8.38 (br d, 2H, J = 8.1, H10), 7.79 (d, 2H, J = 8.1, H9), 7.68 (d, 2H, J = 8.6, H6), 7.50 (d, J = 8.6, H5), 7.37 (br s, 2H; covered by signal solvent at

7.22 ppm at 75 °C, H20), 7.22 (4H, covered by solvent signal; two doublets J = 8.8 at 7.19 and 7.16 ppm at 75 °C, H17 and H18), 4.99 (d, J = 16.8, $H2^{exo}$), 4.83 (d, 2H, J = 16.8, $H2^{endo}$), 4.48 (s, 2H, H1). ^{13}C APT NMR (75 MHz, pyridine-d_5): δ 164.75, 152.70, 152.01, 150.0 (C14, covered by solvent signal), 148.57, 134.02, 130.78, 130.48, 129.73 (C12), 129.37 (C6), 126.69 (C5), 126.13 (C10), 122.81 (C9), 122.48, 120.56 (C17 or C18), 120.21, 118.60 (C17 or C18), 116.98 (C20), 67.13 (C1), 56.33 (C2). Partial assignment based on correlation gCOSY and gHSQC spectra. Anal. Calcd for $C_{39}H_{30}N_6O_6$: C, 69.02; H, 4.46; N, 12.38. Found: C, 69.00; H, 4.48; N, 12.35. HRMS (ESI$^+$) calcd for $C_{39}H_{30}N_6O_6Na$ [M+Na]$^+$: 701.21190, found: 701.21198.

4.1.3.4. Hydrazone 7. 167 mg (86%). ^{1}H NMR (DMSO-d_6): δ 12.21 (s, 2H), 10.70 (s, 2H), 8.65 (s, 2H), 8.44 (d, 2H, J = 1.0), 8.00 (dd, 2H, J_1 = 8.8 Hz, J_2 = 1.0 Hz), 7.90 (d, 2H, J = 8.8 Hz), 7.87 (d, 2H, 8.8 Hz), 7.51 (d, 2H, J = 8.8 Hz), 7.13 (d, 2H, J = 2.6 Hz), 6.92 (dd, 2H, J_1 = 8.8 Hz, J_2 = 2.6 Hz), 6.86 (d, 2H, J = 8.8 Hz), 5.04 (d, 2H, J = 16.9 Hz), 4.83 (d, 2H, J = 16.9 Hz), 4.49 (s, 2H), 3.73 (s, 6H). Anal. Calcd for $C_{41}H_{34}N_6O_6$: C, 69.68; H, 4.85; N, 11.89; O, 13.58. Found: C, 68.67; H, 4.87; N, 11.90. HRMS (ESI$^+$) calcd for $C_{41}H_{34}N_6O_6Na$ [M+Na]$^+$: 729.24320, found: 729.24329.

4.1.3.5. Hydrazone 8. 173 mg (92%). ^{1}H NMR (DMSO-d_6): δ 12.27 (s, 2H), 11.03 (s, 2H), 8.66 (s, 2H), 8.45 (s, 2H), 8.00 (d, 2H, J = 8.8 Hz), 7.90 (d, 2H, J = 8.8 Hz), 7.87 (d, 2H, J = 8.8 Hz), 7.51 (d, 2H, J = 8.8 Hz), 7.44 (dd, 2H, J_1 = 8.9 Hz, J_2 = 2.6 Hz), 7.15 (m, 2H), 6.93 (m, 2H), 5.05 (d, 2H, J = 16.9 Hz), 4.83 (d, 2H, J = 16.9 Hz), 4.49 (s, 2H). ^{1}H NMR (300 MHz, pyridine-d_5): δ 13.20 (br s, 2H, NH), 12.36 (vbr s, 2H, OH), 8.90 (s, 2H, H14), 8.66 (d, 2H, J = 1.7 Hz, H12), 8.38 (dd, 2H, J_1 = 8.8 Hz, J_2 = 1.7 Hz, H10), 7.81 (d, 2H, J = 8.8 Hz, H9), 7.68 (br d, 2H, J = 8.8 Hz, H6), 7.51 (d, 2H, J = 8.8 Hz, H5), 7.44 (br d, 2H, 8.8 Hz, H20), 7.11 (m, 4H, H17 and H18), 4.99 (d, 2H, J = 17.0 Hz, $H2^{exo}$), 4.84 (d, 2H, J = 17.0 Hz, $H2^{endo}$), 4.48 (s, 2H, H1). ^{13}C APT NMR (75 MHz, pyridine-d_5): δ 164.92 (C13), 157.21 (d, J = 235.6 Hz, C19), 155.64 (C16), 148.63 (C4), 147.94 (C14), 134.06 (C8), 130.75 (C7), 130.30 (C11), 129.83 (C12), 129.36 (C6), 126.72 (C5), 126.15 (C10), 122.84 (C9), 122.49 (C3), 120.69 (d, J = 7.5 Hz, C15), 118.78 (d, J = 22.7 Hz, C18), 118.78 (d, J = 7.8 Hz, C17), 115.87 (d, J = 24.1 Hz, C20), 67.11 (C1), 56.32 (C2). ^{19}F NMR (282 MHz, pyridine-d_5): δ −131.6 (dt, J_1 = 8.8 Hz, J_2 = 6.6 Hz). Partial assignment based on correlation gCOSY, and gHMBC spectra. Anal. Calcd for $C_{39}H_{28}F_2N_6O_4$: C, 68.62; H, 4.13; N, 12.31. Found: C, 68.61; H, 4.16; N, 12.31. HRMS (ESI$^+$) calcd for $C_{39}H_{28}F_2N_6O_4Na$ [M+Na]$^+$: 705.20323, found: 705.20313.

4.1.3.6. Hydrazone 9. 187 mg (95%). ^{1}H NMR (DMSO-d_6): δ 12.30 (s, 2H), 11.30 (s, 2H), 8.65 (s, 2H), 8.45 (s, 2H), 8.00 (d, 2H, J = 8.8 Hz), 7.90 (d, 2H, J = 8.8 Hz), 7.88 (d, 2H, J = 8.8 Hz), 7.68 (d, 2H, J = 1.2 Hz), 7.51 (d, 2H, J = 8.8 Hz), 7.32 (dd, 2H, J_1 = 8.8 Hz, J_2 = 1.2 Hz), 6.95 (d, 2H, J = 8.8 Hz), 5.05 (d, 2H, J = 16.9 Hz), 4.83 (d, 2H, J = 16.9 Hz), 4.49 (s, 2H). ^{1}H NMR (300 MHz, pyridine-d_5): δ 13.24 (br s, 2H), 12.61 (vbr s, 2H), 8.87 (s, 2H, H14), 8.65 (d, 2H, J = 1.6 Hz, H12), 8.38 (dd, 2H, J_1 = 8.7 Hz, J_2 = 1.6 Hz, H10), 7.80 (d, 2H, J = 8.7 Hz, H9), 7.66 (br d, 2H, J = 8.8 Hz, H6), 7.65 (d, J = 2.6 Hz, H20), 7.51 (d, 2H, J = 8.8 Hz, H5), 7.29 (dd, 2H, J_1 = 8.7 Hz, J_2 = 2.6 Hz, H18), 7.10 (d, 2H, J = 8.7 Hz, H17), 4.99 (d, 2H, J = 16.9 Hz, $H2^{exo}$), 4.84 (d, 2H, J = 16.9 Hz, $H2^{endo}$), 4.48 (s, 2H, H1). ^{13}C APT NMR (75 MHz, pyridine-d_5): δ 164.94 (C13), 158.06 (C16), 148.63 (C4), 147.70 (C14), 134.06 (C8), 131.68 (C18), 130.73 (C7), 130.23, 129.85 (CH), 129.80 (CH), 129.35 (CH), 126.71 (CH), 126.14 (CH), 124.46 (C19), 122.83 (CH), 122.49 (C3), 121.50 (C15), 119.30 (CH), 67.10 (C1), 56.31 (C2). Partial assignment based on correlation gCOSY and gHMBC spectra. Anal. Calcd for $C_{39}H_{28}Cl_2N_6O_4$: C, 65.46; H, 3.94; N, 11.74. Found: C, 65.47; H, 3,98; N, 11.72. HRMS (ESI$^+$) calcd for $C_{39}H_{28}Cl_2N_6O_4Na$ [M+Na]$^+$: 737.14413, found: 737.14414.

4.1.3.7. Hydrazone 10. 170 mg (84%). ^{1}H NMR (DMSO-d_6): δ 12.38 (s, 2H), 12.35 (s, 2H), 8.77 (s, 2H), 8.60 (s, 2H), 8.46 (s, 2H), 8.17 (d, 2H, J = 8.0 Hz), 8.08–7.80 (m, 6H), 7.51 (d, 2H, J = 8.9 Hz), 7.11 (d, 2H, J = 8.9 Hz), 5.05 (d, 2H, J = 16.8 Hz), 4.84 (d, 2H, J = 16.8 Hz), 4.50 (s, 2H). Anal. Calcd for $C_{39}H_{28}N_8O_8$: C, 63.58; H, 3.83; N, 15.21. Found: C, 63.54; H, 3.85; N, 15.19. HRMS (ESI$^+$) calcd for for $C_{39}H_{28}N_8O_8Na$ [M+Na]$^+$: 759.19223, found: 759.19183.

4.1.3.8. Hydrazone 11. 203 mg (97%). ^{1}H NMR (DMSO-d_6): δ 12.29 (s, 2H), 11.84 (s, 2H), 8.74 (s, 2H), 8.45 (s, 2H), 8.29 (s, 2H), 8.01 (d, 2H, J = 8.9 Hz), 7.94–7.82 (m, 6H), 7.51 (d, 2H, J = 8.5 Hz), 7.03 (d, 2H, J = 8.5 Hz), 5.05 (d, 2H, J = 17.0 Hz), 4.83 (d, 2H, J = 17.0 Hz), 4.50 (s, 2H), 3.84 (s, 6H). Anal. Calcd for $C_{43}H_{34}N_6O_8$: C, 67.71; H, 4.49; N, 11.02. Found: C, 67.69; H, 4.52; N, 10.99. HRMS (ESI$^+$) calcd for $C_{43}H_{34}N_6O_8Na$ [M+Na]$^+$: 785.23303, found: 785.23279.

4.1.3.9. Hydrazone 12. 173 mg (93%). ^{1}H NMR (DMSO-d_6): δ 12.11 (s, 2H), 8.44 (s, 4H), 8.10 - 7.73 (m, 8H), 7.58 (d, 2H, J = 8.0 Hz), 7.51 (d, 2H, J = 8.8 Hz), 6.86 (d, 2H, J = 8.0 Hz), 5.04 (d, 2H, J = 17.1 Hz), 4.83 (d, 2H, J = 17.1 Hz), 4.49 (s, 2H), 3.89 (s, 6H). Anal. Calcd for $C_{39}H_{32}N_8O_4$: C, 69.22; H, 4.77; N, 16.56. Found: C, 69.22; H, 4.79; N, 16.58. HRMS (ESI$^+$) calcd for $C_{39}H_{32}N_8O_4Na$ [M+Na]$^+$: 699.24387, found: 699.24420.

4.1.3.10. Hydrazone 13. 183 mg (93%). ^{1}H NMR (DMSO-d_6): δ 12.36 (s, 2H), 8.65 (s, 2H), 8.47 (s, 2H), 8.43 (d, 2H, J = 8.8 Hz), 8.43 (d, 2H, J = 8.8 Hz), 8.10 - 7.87 (m, 10H), 7.79 (m, 2H), 7.64 (m, 2H), 7.53 (d, 2H, J = 8.9 Hz), 5.06 (d, 2H, J = 17.0 Hz), 4.85 (d, 2H, J = 17.0 Hz), 4.51 (s, 2H). Anal. Calcd for $C_{45}H_{32}N_8O_2$: C, 75.40; H, 4.50; N, 15.63. Found: C, 75.38; H, 4.53; N, 15.60. HRMS (ESI$^+$) calcd for $C_{45}H_{32}N_8O_2Na$ [M+Na]$^+$: 739.25404, found: 739.25391.

4.1.3.11. Hydrazone 14. 197 mg (93%). ^{1}H NMR (DMSO-d_6): δ 8.97 (d, 2H, J = 8.8 Hz), 8.62 (d, 2H, J = 8.8 Hz), 8.39 (s, 2H), 8.10 - 7.85 (m, 14H), 7.69 - 7.42 (m, 8H), 5.06 (d, 2H, J = 16.8 Hz), 4.85 (d, 2H, J = 16.8 Hz), 4.51 (s, 2H). Anal. Calcd for $C_{47}H_{34}N_{10}O_2$: C, 73.23; H, 4.45; N, 18.17. Found: C, 73.21; H, 4.47; N, 18.18. HRMS (ESI$^+$) calcd for $C_{47}H_{34}N_{10}O_2Na$ [M+Na]$^+$: 793.27584, found: 793.27594.

4.2. Biological tests

4.2.1. Cytotoxic MTT assay

All cells were purchased from the American Tissue Culture Collection (ATCC). The CCRF-CEM line is derived from T lymphoblastic leukaemia and has high chemosensitivity. K562 cells are from an acute myeloid leukaemia patient sample with bcr-abl translocation. HCT116 is a colorectal tumour cell line, and its p53 gene knock-down counterpart (HCT116p53−/−, Horizon Discovery, UK) is a model of human cancers with p53 mutation, which is frequently associated with poor prognosis. The A549 line is a lung adenocarcinoma. The daunorubicin-resistant subline of CCRF-CEM cells (CEM-DNR bulk) and paclitaxel-resistant subline K562-TAX were selected in our laboratory by the cultivation of maternal cell lines in increasing concentrations of daunorubicin or paclitaxel, respectively. The CEM-DNR bulk cells overexpress MRP-1 protein, while K562-TAX cells overexpress P-glycoprotein; both proteins belong to the family of ABC transporters and are involved in the primary and/or acquired multidrug resistance phenomenon. MRC-5 and BJ were used as non-tumour controls and represent human fibroblasts. The cells were maintained in Nunc/Corning 80

cm^2 plastic tissue culture flasks and cultured in cell culture medium (DMEM/RPMI 1640 with 5 g/L glucose, 2 mM glutamine, 100 U/mL penicillin, 100 μg/mL streptomycin, 10% foetal calf serum and $NaHCO_3$). Cell suspensions were prepared and diluted according to the particular cell type and the expected target cell density (25,000–30,000 cells/well based on cell growth characteristics). Cells were added by pipette (80 μL) to 96-well microtiter plates. Inoculates were pre-incubated for 24 h at 37 °C and 5% CO_2 for stabilisation. Four-fold dilutions, in 20-μL aliquots, of the intended test concentration were added to the microtiter plate walls at time zero. All test compound concentrations were examined in duplicate. Incubation of the cells with the test compounds was performed for 72 h at 37 °C in a 5% CO_2 atmosphere at 100% humidity. At the end of the incubation period, the cells were assayed using MTT. Aliquots (10 μL) of the MTT stock solution were pipetted into each well and incubated for a further 1–4 h. After this incubation period, the formazan produced was dissolved by the addition of 100 μL/well 10% aq SDS (pH 5.5), followed by further incubation at 37 °C overnight. The optical density (OD) was measured at 540 nm with a Labsystem iEMS Reader MF. Tumour cell survival (IC_{50}) was calculated using the following equation: $IC = (OD_{drug\text{-}exposed\ well}/\text{mean}\ OD_{control\ wells}) \times 100\%$. The IC_{50} value, the drug concentration lethal to 50% of the tumour cells, was calculated from the appropriate dose-response curves.

4.3. Flow cytometric analysis

4.3.1. Cell cycle and apoptosis analysis

A suspension of CCRF-CEM cells (ATCC), seeded at a density of 1.10^6 cells/ mL in 6-well panels, was cultivated with the 1 × IC_{50} or 5 × IC_{50} of the tested compound in a humidified CO_2 incubator at 37 °C in RPMI 1640 cell culture medium containing 10% foetal calf serum, 10 mM glutamine, 100 U/mL penicillin, and 100 μg/mL streptomycin. The treated cells and control sample containing vehicle were harvested at the same time point (24 h). After a further 24 h, cells were washed with cold 1× PBS and fixed in 70% ethanol added dropwise and then stored overnight at −20 °C. Cells were then washed in hypotonic citrate buffer, treated with RNase (50 μg/mL) and stained with propidium iodide. Flow cytometry using a 488 nm single beam laser (Becton Dickinson) was used for measurement. The cell cycle was analysed with the program ModFitLT (Verity), and apoptosis was measured using a logarithmic model expressed as the percentage of the particles with propidium content lower than cells in the G0/G1 phase (<G1) of the cell cycle. Half of the sample was used for $pH3^{Ser10}$ antibody (Sigma) labelling and subsequent flow cytometry analysis of mitotic cells.

4.3.2. BrdU incorporation analysis

The same cultivation procedure used in the previous method was used for BrdU analysis. Before harvesting, 10 μM 5-bromo-2-deoxyuridine (BrdU) was added to the cells for pulse labelling for 30 min. The cells were fixed with ice-cold 70% ethanol and stored overnight. Before analysis, they were incubated on ice for 30 min, washed with 1× PBS, and resuspended in 2 M HCl for 30 min at room temperature to denature their DNA. Following neutralisation with 0.1 M $Na_2B_4O_7$ (Borax), the cells were washed with 1× PBS containing 0.5% Tween-20 and 1% BSA. The cells were then stained with primary anti-BrdU antibody (Exbio) for 30 min at room temperature in the dark. Cells were washed with 1× PBS and stained with secondary anti-mouse-FITC antibody (Sigma). The cells were then washed with 1× PBS again and incubated with propidium iodide (0.1 mg/mL) and RNase A (0.5 mg/mL) for 1 h at room temperature in the dark and afterwards analysed by flow cytometry using a 488 nm single beam laser (FACSCalibur, Becton Dickinson).

4.3.3. BrU incorporation analysis

Cells were cultured and treated as above. Before harvesting, cells were pulse labelled with 1 mM 5-bromouridine (BrU) for 30 min. The cells were then fixed in 1% buffered paraformaldehyde with 0.05% NP-40 at room temperature for 15 min and then stored at 4 °C overnight. Before measurement, they were then washed in 1% glycine in 1× PBS, washed in PBS again, and stained with a primary anti-BrDU antibody that crossreacts with BrU (Exbio) for 30 min at room temperature in the dark. After another washing step in 1× PBS, cells were stained with secondary anti-mouse-FITC antibody (Sigma). Following the staining, cells were washed with 1× PBS and fixed with 1% PBS-buffered paraformaldehyde with 0.05% NP-40 for 1 h. The cells were then washed with 1× PBS, incubated with propidium iodide (0.1 mg/mL) and RNase A (0.5 mg/mL) for 1 h at room temperature in the dark and finally analysed by flow cytometry using a 488 nm single beam laser (FACSCalibur, Becton).

4.3.4. Antimicrobial activity assay

Mycobacterium bovis BCG (strain isolated from the commercially available live vaccine SSI obtained from Statens Serum Institute) was used as a prototype mycobacterium to assess the activity of the compounds on living and proliferating cells. Briefly, the mycobacterial cell suspensions were prepared and diluted in culture medium (Difco Middlebrook 7H9 Broth supplemented with Middlebrook ADC Growth Supplement FD019 and 0.04% of Tween 80) to the approximate target cell density (100 000 microbes/well). Cells were added by pipette (80 μL) to 96-well microtiter plates. Four-fold dilutions, in 20 μL aliquots, of the intended test concentration were added to the microtiter plate wells at time zero. All tested compound concentrations were examined in duplicate. Incubation of the cells with the test compounds lasted for 120 h at 37 °C, 5% CO_2 and 100% humidity. At the end of the incubation period, the living cells were assayed using MTT. Aliquots (10 μL) of the MTT stock solution were pipetted into each well and incubated for a further 1–4 h. After this incubation period, the formazan produced was dissolved by the addition of 100 μL/well 10% aq SDS (pH = 5.5) followed by a further incubation at 37 °C overnight. The optical density was measured at 540 nm on a microarray reader. The 50% growth inhibitory concentration (IC_{50}) was calculated from the appropriate dose–response curves. The tested bacterial strains were selected to include both Gram-positive and Gram-negative standard reference bacteria with good susceptibility to antimicrobial agents. However, multidrug-resistant bacteria were tested simultaneously because their frequency in both the human population and the environment continues to increase and must be considered. The following reference strains (labelling according to the Czech Collection of Microorganisms, Czech Republic) were used: *Enterococcus faecalis CCM 4224*, *Staphylococcus aureus CCM 3953*, *Escherichia coli CCM 3954*, *Pseudomonas aeruginosa CCM 3955*. We also used strains isolated from the clinical specimens of patients hospitalised at the University Hospital Olomouc (Czech Republic): methicillin-resistant staphylococci (*Staphylococcus aureus MRSA 4591* and *Staphylococcus haemolyticus A/16568*), multidrug-resistant strains of *Escherichia coli C/16702* and *Pseudomonas* aeruginosa A/16575. Similarly, the effectiveness against *Candida albicans*, *Candida crusei*, *Candida tropicalis* and *Candida parapsilosis* was also determined.

Bacterial and yeast suspensions were prepared as follows. The tested strains were inoculated on blood agar and Sabouraud dextrose agar and incubated for 24 h/37 °C. Four to five isolated colonies were dissolved in 2 mL of Mueller Hinton broth (Himedia) and incubated for 1 h/37 °C., The broth was then diluted in a Petri dish in 10 mL of distilled water and inoculated in microtiter plates.

MIC assessment. Antimicrobial efficacy was tested by the standard dilution micromethod, and the minimal inhibition

concentrations (MIC) required for inhibition of bacterial growth were determined. Samples were diluted exponentially and tested in microtiter plates in Brain Heart Infusion broth (Himedia). Plates were inoculated into a standard quantity of microbes ($10^{5,6}$ CFU/mL). The MIC was read after 24 and 48 h of incubation at 37 °C for bacteria and yeast, respectively, as the minimum inhibitory concentration of the tested substance that inhibited the growth of the bacterial or *Candida* strain.

MBC/MBS assessment (minimal bactericidal/bacteriostatic concentration). To assess bactericidal (ability of the compound to kill bacteria) or bacteriostatic (ability of the compound to inhibit bacterial growth) properties of the compound, 5 μL of the bacterial suspension from microtiter plates with the determined MIC was inoculated on blood agar (bacteria) or on Sabouraud dextrose agar (yeasts) and incubated for 24 or 48 h at 37 °C for bacteria and yeast, respectively. The bactericidal/bacteriostatic properties of the compounds were determined by the negative or positive growth of bacterial colonies.

4.4. Metal-binding studies

Binding studies of hydrazones **4**–**14** with the chlorides of metal ions (Fe^{2+}, Fe^{3+}, Co^{2+}, Cu^{2+}, Cr^{3+}, Ni^{2+}, Zn^{2+}, Mn^{2+}, Ca^{2+} and Mg^{2+}) were performed using UV/vis spectroscopy in DMSO. The corresponding hydrazone (0.03 mM) solution in DMSO (100 mL) was titrated using a semi-automatic titration system (peristaltic pump, flow-cuvette, syringe pump) with the continuous addition of a stock solution of metal ions (6 mM, 10 mL/h). The spectra were collected every 30 sec. DNA binding studies were performed similar way: hydrazone (0.03 mM) solution or solution of hydrazone (0.03 mM) with metal ion (0.3 mM) in DMSO (100 mL) was titrated using a semi-automatic titration system with the continuous addition of a stock solution of low molecular weight DNA (6 mM of a DNA basepairs, 10 mL/h).

4.5. Theoretical studies

Native conformations of prepared compounds were investigated using quantum dynamic/molecular dynamic (QD/MD) calculations performed by the TeraChem 1.45 software (PetaChem, LLC.).[45–47] Each compound (calculated using quantum dynamics) was placed into a drop of water (calculated by molecular dynamics). The QD calculations were performed using the 6-31G basis set and the BLYP method with DFT corrections, as implemented in the software.[46,47] The MD calculations were performed using the TIP3P force field; the water sphere radius was 20 Å (typically containing approximately 1040 water molecules), and the density was 1 g/mL with spherical boundary conditions. The simulation ran for 20 ps with a time step of 1 fs.

Acknowledgements

The authors are grateful to the Ministry of Education, Youth and Sport of the Czech Republic, for the project CZ.1.07/2.3.00/30.0060 supported by the European Social Fund and program NPU I LO1304. This work was supported by the Grant Agency of the Czech Republic, project GAP303/11/1291; by the Technology Agency of the Czech Republic, project TE01020028.

Supplementary data

Supplementary data associated with this article can be found, in the online version, at http://dx.doi.org/10.1016/j.bmc.2015.01.029. These data include MOL files and InChiKeys of the most important compounds described in this article.

References and notes

1. Liu, Z. D.; Hider, R. C. *Coord. Chem. Rev.* **2002**, *232*, 151.
2. Tam, T. F.; Leung-Toung, R.; Li, W. R.; Wang, Y. S.; Karimian, K.; Spino, M. *Curr. Med. Chem.* **2003**, *10*, 983.
3. Meyer, D. *Curr. Pharm. Des.* **2006**, *12*, 1943.
4. Melnyk, P.; Leroux, V.; Sergheraert, C.; Grellier, P. *Bioorg. Med. Chem. Lett.* **2006**, *16*, 31.
5. Rollas, S.; Kucukguzel, S. G. *Molecules* **2007**, *12*, 1910.
6. Narang, R.; Narasimhan, B.; Sharma, S. *Curr. Med. Chem.* **2012**, *19*, 569.
7. Kalinowski, D. S.; Richardson, D. R. *Chem. Res. Toxicol.* **2007**, *20*, 715.
8. Crisponi, G.; Remelli, M. *Coord. Chem. Rev.* **2008**, *252*, 1225.
9. Sharpe, P. C.; Richardson, D. R.; Kalinowski, D. S.; Bernhardt, P. V. *Curr. Top. Med. Chem.* **2011**, *11*, 591.
10. Buss, J. L.; Greene, B. T.; Turner, J.; Torti, F. M.; Torti, S. V. *Curr. Top. Med. Chem.* **2004**, *4*, 1623.
11. Richardson, D. R.; Kalinowski, D. S.; Lau, S.; Jansson, P. J.; Lovejoy, D. B. *Biochim. Biophys. Acta* **2009**, *1790*, 702.
12. Dandawate, P.; Khan, E.; Padhye, S.; Gaba, H.; Sinha, S.; Deshpande, J.; Swamy, K. V.; Khetmalas, M.; Ahmad, A.; Sarkar, F. H. *Bioorg. Med. Chem. Lett.* **2012**, *22*, 3104.
13. Mackova, E.; Hruskova, K.; Bendova, P.; Vavrova, A.; Jansova, H.; Haskova, P.; Kovarikova, P.; Vavrova, K.; Simunek, T. *Chem. Biol. Interact.* **2012**, *197*, 69.
14. Saletta, F.; Rahmanto, Y. S.; Siafakas, A. R.; Richardson, D. R. *J. Biol. Chem.* **2011**, *286*, 35396.
15. Buss, J. L.; Torti, F. M.; Torti, S. V. *Curr. Med. Chem.* **2003**, *10*, 1021.
16. Wiley, R. H.; White, H. K.; Irick, G. *J. Org. Chem.* **1959**, *24*, 1784.
17. Sah, P. P. T. *J. Am. Chem. Soc.* **1954**, *76*, 300.
18. Libermann, D.; Rist, N.; Grumbach, F.; Moyeux, M.; Gauthier, B.; Rouaix, A.; Maillard, J.; Himbert, J.; Cals, S. *Bull. Soc. Chim. Fr.* **1954**, *21*, 1430.
19. Hoy, T.; Humphrys, J.; Williams, A.; Ponka, P.; Jacobs, A. *Br. J. Haematol.* **1979**, *43*, 443.
20. Wiley, R. H.; Clevenger, R. L. *J. Med. Pharm. Chem.* **1962**, *5*, 1367.
21. Umarov, B. B.; Khusenov, K. S.; Ishankhodzhaeva, M. M.; Parpiev, N. A.; Gaibullaev, K. S. *Zh. Org. Khim.* **1996**, *32*, 93.
22. Lal, R. A.; Basumatary, D.; Chanu, O. B.; Lemtur, A.; Asthana, M.; Kumar, A.; De, A. K. *J. Coord. Chem.* **2011**, *64*, 300.
23. Zhao, L.; Qu, S. Y.; He, C.; Zhang, R.; Duan, C. Y. *Chem. Commun.* **2011**, *47*, 9387.
24. Dolensky, B.; Elguero, J.; Kral, V.; Pardo, C.; Valik, M. *Adv. Heterocycl. Chem.* **2007**, *93*, 1.
25. Sergeyev, S. *Helv. Chim. Acta* **2009**, *92*, 415.
26. Runarsson, O. V.; Artacho, J.; Warnmark, K. *Eur. J. Org. Chem.* **2012**, 7015.
27. Tatibouet, A.; Demeunynck, M.; Andraud, C.; Collet, A.; Lhomme, J. *Chem. Commun.* **1999**, 161.
28. Baldeyrou, B.; Tardy, C.; Bailly, C.; Colson, P.; Houssier, C.; Charmantray, F.; Demeunynck, M. *Eur. J. Med. Chem.* **2002**, *37*, 315.
29. Ricci, C. G.; Netz, P. A. *J. Braz. Chem. Soc.* **2012**, *23*, 1334.
30. Veale, E. B.; Gunnlaugsson, T. *J. Org. Chem.* **2010**, *75*, 5513.
31. Valik, M.; Malina, J.; Palivec, L.; Foltynova, J.; Tkadlecova, M.; Urbanova, M.; Brabec, V.; Kral, V. *Tetrahedron* **2006**, *62*, 8591.
32. Valik, M.; Dolensky, B.; Petrickova, H.; Vasek, P.; Kral, V. *Tetrahedron Lett.* **2003**, *44*, 2083.
33. Claessens, N.; Pierard, F.; Bresson, C.; Moucheron, C.; Kirsch-De, A. *J. Inorg. Biochem.* **2007**, *101*, 987.
34. Johnson, R. A.; Gorman, R. R.; Wnuk, R. J.; Crittenden, N. J.; Aiken, J. W. *J. Med. Chem.* **1993**, *36*, 3202.
35. Gaslonde, T.; Leonce, S.; Pierre, A.; Pfeiffer, B.; Michel, S.; Tillequin, F. *Tetrahedron Lett.* **2011**, *52*, 4426.
36. Paul, A.; Maji, B.; Misra, S. K.; Jain, A. K.; Muniyappa, K.; Bhattacharya, S. *J. Med. Chem.* **2012**, *55*, 7460.
37. Havlik, M.; Kral, V.; Kaplanek, R.; Dolensky, B. *Org. Lett.* **2008**, *10*, 4767.
38. Tatar, A.; Cejka, J.; Kral, V.; Dolensky, B. *Org. Lett.* **2010**, *12*, 1872.
39. Kumar, H. S. N.; Parumasivam, T.; Jumaat, F.; Ibrahim, P.; Asmawi, M. Z.; Sadikun, A. *Med. Chem. Res.* **2014**, *23*, 269.
40. Rodrigues, F. A. R.; Bomfim, I. D.; Cavalcanti, B. C.; Pessoa, C. D.; Wardell, J. L.; Wardell, S. M. S. V.; Pinheiro, A. C.; Kaiser, C. R.; Nogueira, T. C. M.; Low, J. N.; Gomes, L. R.; de Souza, M. V. N. *Bioorg. Med. Chem. Lett.* **2014**, *24*, 934.
41. Zhao, Y.; Hui, J.; Wang, D.; Zhu, L.; Fang, J. H.; Zhao, X. D. *Chem. Pharm. Bull.* **2010**, *58*, 1324.
42. Xia, Y.; Fan, C. D.; Zhao, B. X.; Zhao, J.; Shin, D. S.; Miao, J. Y. *Eur. J. Med. Chem.* **2008**, *43*, 2347.
43. Easmon, J.; Purstinger, G.; Thies, K. S.; Heinisch, G.; Hofmann, J. *J. Med. Chem.* **2006**, *49*, 6343.
44. Moorthy, N. S. H. N.; Cerqueira, N. S.; Ramos, M. J.; Fernandes, P. A. *Med. Chem. Res.* **2012**, *21*, 133.
45. Ufimtsev, I. S.; Martinez, T. J. *J. Chem. Theory Comput.* **2009**, *5*, 2619.
46. Grimme, S.; Antony, J.; Ehrlich, S.; Krieg, H. *J. Chem. Phys.* **2010**, *132*.
47. Grimme, S.; Ehrlich, S.; Goerigk, L. *J. Comput. Chem.* **2011**, *32*, 1456.

2.3.4 Benzothiazole Hydrazones analysed for their intracellular activity (Unpublished data)

3 Results and summary

The causes and development of cancer, bacterial, inflammatory and other diseases are discovered and better understood every year. However, together with the emerging multi-drug resistance issue, existing treatments are very often inadequate and need to be adjusted or substituted by novel drugs with different molecular targets and mechanisms of action. Many different groups of potentially active compounds are designed and tested all over the world. The main issues are the high financial costs combined with advanced instruments requirements. Many interesting compounds, effective *in vitro*, fail clinical trials. This is frequently caused by inappropriate and inadequate settings in the early phases of research. Mainly, cell culture conditions rarely represent the real environment in the human body during the disease progression. Standardly used 2D cultures lack the heterogeneity and complexity of spatially diversified cells, caused by 3 dimensional structures, subsequent oxygen depletion and chaotic blood distribution created under natural conditions. Therefore it is necessary for *in vitro* experiments to approximate conditions as *in vivo*. 3D models and matrices, together with co-cultivation with SDF (stroma derived fibroblasts) partially enable mimicking of natural development, hypoxic conditions and co-option of surrounding cells. This guarantees more efficient selection of compounds with better outcome in clinical trials (Das, Konečný 2015; Appendix I). Many groups of compounds have been tested for their anticancer or antibacterial activities proving either rather general cytotoxic effects, or desirably targeting specific molecules necessary for development, reproduction and growth of cancer cells and bacteria.

We have screened several related groups of compounds for their anticancer and antibacterial activities based on their structure – activity relationship. Several potentially active compounds have been selected after flow cytometric and cytotoxicity screening and were used as model compounds for further synthesis. Derivatives of ribonucleosides, apart from the fact that by their actions affect the cell cycle of cancer cells and inhibit their RNA synthesis and induced apoptosis, display significant antibacterial, specifically antimycobacterial activities.

Regarding cytotoxicity, **7-Hetaryl-7-deazaadenine ribonucleosides** have proven to have cytostatic activity at low nanomolar concentration which is in contrast to agents from the group of 7-aryl-7-deazaadenines, which display significantly worse activity. In general, nucleosides with 5-membered heterocycles at position 7 evince *in vitro* antiproliferative impact on both, haematological and solid tumors. Although, as mentioned above, these compounds were able to inhibit RNA synthesis in treated cells, direct inhibition of human RNA polymerase II was very weak with a rapid onset of apoptosis (Bourderioux et al. 2011).

Representatives of the **6-alkyl, 6-aryl or 6-hetaryl-7-deazapurines** proved to have many interesting properties. In the range of micromolar and submicromolar concentrations, they were able to significantly inhibit growth and reproduction of *Mycobacterium bovis* and *smegmatis.* Some results point to similar cytotoxicity to Rifampicin. They were specifically designed to inhibit mycobacterial ADK by binding to its ATP and adenosine binding sites. Synthesis was adjusted accordingly. The cytotoxicity of these structures was strongly dependent on the substituent at position six and its bulkiness. Among the most active compounds, were those with five-membered heterocycles. In contrast, the general toxicity of bulky aryl group bearing derivatives was very low. It has been confirmed that the measured compounds were not a substrate for MTB ADK and most of them successfully inhibited it. Individual groups alkyl-substituents were poor inhibitors of MTB ADK. On the other hand, aryl- and hetaryl-substituted 7-deazapurines (7-fluoro, 7-chloro-derivatives included) strongly inhibited adenosine kinase in submicromolar and low nanomolar concentrations. For the group of phenyl bearing five-membered hetaryl groups at position 6, inhibition of ADK was significantly selective for the mycobacterial form, while human ADK was unaffected and with serious general toxicity, which makes these structures the most promising. 6-furyl substituted compounds inhibited both hADK and MTB ADK with poor selectivity. Derivatives with a bulky aryl group were active in low nanomolar concentrations for MTB ADK, micromolar concentration for hADK, respectively with very low cytotoxicity. Interestingly, the *in vitro* antimycobacterial activity of these compounds was very low, with only one exception, compound 1a, which displayed submicromolar IC50.

Nevertheless, this compound was generally highly toxic with a low TI (Perlíková et al. 2013; Snášel et al. 2014). Targeting directly the MTB and human ADK, using wild and drug-resistant bacterial strains, structures with micromolar activity were identified from the group of 7-(Het)aryl-7-deazaadenine ribonucleosides. These compounds selectively inhibited this enzyme at micromolar concentration and low cytotoxicity. Preferential active binding site for tested compounds proved to be different for each form of ADK. For the human form of ADK, the adenosine site is the place of binding, whereas for MTB ADK, both ATP and adenosine binding sites are occupied by these inibitors. The molecule with the best therapeutic index was the dibenzofuran derivative and this displayed significant specific submicromolar MTB ADK inhibition with MIC 4 μM for mycobacterial strains. Binding of these molecules to their preferential sites, change the conformation of ADK. MTB ADK after binding of tested compounds acquires a semi-open conformation of the lid domain. Human ADK, on the other hand, has a closed conformation (Snášel et al. 2014).

Different modifications, such as **7-hetaryl-deazaadenosines, 6-substituted 7-(Het) aryl-7-deazapurines** and their relatives **6-alkyl substituents** were prepared and analysed for their biological activities. Except for mycobacterial ADK, some successfully inhibited the human form in micromolar concentration, as well. Rather than the binding sites of MTB ADK, ATP and adenosine, adenosine binding site is preferential in hADK. In relation to anticancer activity, distinct inhibition of RNA synthesis and induction of apoptosis was observed. Nevertheless, RNA polymerase itself was inhibited very weakly. Hence other mechanisms must be involved. Among others, antiparasitic and antiviral activities are connected to this group of compounds. Compared to the previous group, **6-methoxy-, 6-methylsulfanyl-, 6-methyloamino- and 6methyl-7-(2-furyl)-deazapurines** were prepared and tested. They showed toxicity in the range of low nanomolar concentrations but most of the compounds were less active then the ones mentioned above (Nauš 2014).

Cytosine derivative compounds have proven to have activity towards the CEM cell line in micromolar concentrations and served as structures for further modification to obtain better therapeutic properties. These structures are known as $GABA_A$ receptor

ligands and their nucleoside modifications prove to have some antiviral activity, as well. Some of them display selective activity towards drug-resistant cell lines (CEM-DNR, K562-TAX), though the cell cycle was not affected even in high concentrations. As most promising compounds, molecules with the label 3b and 3h were selected. 3b compound has a micromolar activity toward the CEM cell line and 3h is selectively active towards daunorubicine resistant CEM cells. This molecule also has a favourable therapea utic index (Jansa et al. 2014).

Another group of compounds analysed for their anticancer/antibacterial effects are the **Hydrazone derivatives**. These structures are constructed on Tröger´s base skeleton and allow them to work as DNA intercalating agents. They also have chelating properties (binding Cu^{2+}, Fe^{3+}, Co^{2+}, Ni^{2+}, Zn^{2+}) and their complexes interact with DNA. The IC50 values for some of these drugs are in micromoles and in some cases; we were able to see quite a high therapeutic index and therefore selectivity towards cancer cells. In correlation with the previously mentioned tested groups, these structures do not have significant antimicrobial activity and considering the cell cycle, inhibition of DNA and RNA synthesis was observed in some cases but all in concentrations 5x IC50. Otherwise the effect on the cell cycle was indistinct. The therapeutic activity of these compounds is probably connected to some other mechanisms of action. The tested compounds were poor antimicrobial agents. Anticancer activity with high selectivity against leukemic cells was observed for 10 different compounds (6, 7, 8, 11 and 13). The best therapeutic index was found for 3 structures (7, 8 and 13).

4 References

Aghi, M., Kramm, C. M., Chou, T. C., Breakefield, X. O., & Chiocca, E. a. (1998). Synergistic anticancer effects of ganciclovir/thymidine kinase and 5-fluorocytosine/cytosine deaminase gene therapies. *Journal of the National Cancer Institute*, *90*(5), 370–380.

Akins, R. E., Rockwood, D., Robinson, K. G., Sandusky, D., Rabolt, J., & Pizarro, C. (2010). Three-dimensional culture alters primary cardiac cell phenotype. *Tissue Engineering. Part A*, *16*(2), 629–641. doi:10.1089/ten.tea.2009.0458

Ali, R., Marella, A., Alam, T., & Naz, R. (2012). Review Of Biological Activities Of Hydrazones. *Indonesian Journal of Pharmacy*, *23*(4), 193–202.

Arora, A., & Scholar, E. (2005). Role of tyrosine kinase inhibitors in cancer therapy. *Journal of Pharmacology and Experimental Therapeutics*, *315*(3), 971–979. http://doi.org/10.1124/jpet.105.084145

Asthana, A., & Kisaalita, W. S. (2012). Microtissue size and hypoxia in HTS with 3D cultures. *Drug Discovery Today*, *17*(15-16), 810–817. doi:10.1016/j.drudis.2012.03.004

Asthana, A., & Kisaalita, W. S. (2013). Biophysical microenvironment and 3D culture physiological relevance. *Drug Discovery Today*, *18*(11-12), 533–540. doi:10.1016/j.drudis.2012.12.005

Ayabe, T., Shimizu, T., Tomita, M., Yano, M., Nakamura, K., Onitsuka, T. (2011). Emergent completion pneumonectomy for postoperative hemorrhage from rupture of the infected pulmonary artery in lung cancer surgery. Case Reports in Surgery Volume 2011 (2011), Article ID 902062, 4 pages

Bakuła, Z., Napiórkowska, A., Kamiński, M., Augustynowicz-Kopeć, E., Zwolska, Z., Bielecki, J., & Jagielski, T. (2015). Second-line anti-tuberculosis drug resistance and its

genetic determinants in multidrug-resistant *Mycobacterium* tuberculosis clinical isolates. *Journal of Microbiology, Immunology and Infection*. doi:10.1016/j.jmii.2015.04.003

Barkin, J. L., Faust, M. D., & Trenkle, W. C. (2003). Cytosine analogues from substituted acetonitriles via Thorpe condensation. *Organic Letters*, *5*(18), 3333–3335. http://doi.org/10.1021/ol035223j

Barretina J, Caponigro G, Stransky N, et al. (2012). The Cancer Cell Line Encyclopedia enables predictive modelling of anticancer drug sensitivity. *Nature*. 2012; 483(7391):603–607.

Barrios-Payán, J., Saqui-Salces, M., Jeyanathan, M., Alcántara-Vazquez, A., Castañon-Arreola, M., Rook, G., & Hernandez-Pando, R. (2012). Extrapulmonary locations of *mycobacterium tuberculosis* DNA during latent infection. *Journal of Infectious Diseases*, *206*(8), 1194–1205. doi:10.1093/infdis/jis381

Beck, J. N., Singh, A., Rothenberg, A. R., Elisseeff, J. H., & Ewald, A. J. (2013). The independent roles of mechanical, structural and adhesion characteristics of 3D hydrogels on the regulation of cancer invasion and dissemination. *Biomaterials*, *34*(37), 9486–9495. doi:10.1016/j.biomaterials.08.077

Berridge M., Tan A., McCoy K., Wang R. (1996). The Biochemical and Cellular Basis of Cell Proliferation Assays that Use Tetrazolium Salts. *Biochemica*.;4:14–19.

Berridge M., Herst P., Tan A. (2005). Tetrazolium dyes as tools in cell biology: New insights into their cellular reduction. *Biotechnology Annual Review*; 11:127–152

Berning, S. E. (2001). The role of fluoroquinolones in tuberculosis today. *Drugs*, *61*(1), 9–18. http://doi.org/10.2165/00003495-200161010-00002

Betts, J. C., Lukey, P. T., Robb, L. C., McAdam, R. a., & Duncan, K. (2002). Evaluation of a nutrient starvation model of *Mycobacterium tuberculosis* persistence by gene and

protein expression profiling. *Molecular Microbiology*, *43*(3), 717–731. doi:10.1046/j.1365-2958.2002.02779.x

Billis, A., Meirelles L., Freitas, L., Magna, L., Reis, L., Ferreira U. (2012). Influence of focal and diffuse extraprostatic extension and positive surgical margins on biochemical progression following radical prostatectomy. *Int. Braz. J. Urol.* 38, 175–184.

Birgersdotter, A., Sandberg, R., & Ernberg, I. (2005). Gene expression perturbation *in vitro* - A growing case for three-dimensional (3D) culture systems. *Seminars in Cancer Biology*, *15*(5 SPEC. ISS.), 405–412. doi:10.1016/j.semcancer.2005.06.009

Bobeck, D. R., Schinazi, R. F., & Coats, S. J. (2010). Advances in nucleoside monophosphate prodrugs as anti-HCV agents. *Antiviral Therapy*, *15*(7), 935–950. http://doi.org/10.3851/IMP1667

Bourderioux, A., Nauš, P., Perlíková, P., Pohl, R., Pichová, I., Votruba, I., … Hocek, M. (2011). Synthesis and significant cytostatic activity of 7-hetaryl-7- deazaadenosines. *Journal of Medicinal Chemistry*, *54*(15), 5498–5507. http://doi.org/10.1021/jm2005173

Brennan, P. J. (2003). Structure, function, and biogenesis of the cell wall of *Mycobacterium tuberculosis*. *Tuberculosis*, *83*(1-3), 91–97. doi:10.1016/S1472-9792(02)00089-6

Breslin, S., & O'Driscoll, L. (2013). Three-dimensional cell culture: The missing link in drug discovery. *Drug Discovery Today*, *18*(5-6), 240–249. doi:10.1016/j.drudis.2012.10.003

Bugrim, A., Nikolskaya, T., & Nikolsky, Y. (2004). Early prediction of drug metabolism and toxicity : systems biology approach and modeling and suggest directions for their integration .,*Drug Discovery Today*, *9*(3), 127–135.

Butina, D., Segall, M. D., & Frankcombe, K. (2002). Predicting ADME properties *in silico*: Methods and models. *Drug Discovery Today*, *7*(11), 83–88. http://doi.org/10.1016/S1359-6446(02)02288-2

Casanova, B., Muniz, M., de Oliveira, T., de Oliveira, L., Machado, M., Fuentefria, A., Gosmann G. And Gnoatto S. (2015). Synthesis and Biological Evaluation of Hydrazone Derivatives asAntifungal Agents. *Molecules (Basel, Switzerland)* vol. 20 (5) p. 9229-41

Castel, D., Pitaval, A., Debily, M. A., & Gidrol, X. (2006). Cell microarrays in drug discovery. *Drug Discovery Today*, *11*(13-14), 616–622. doi:10.1016/j.drudis.2006.05.015

Choy, Y. Bin, & Prausnitz, M. R. (2011). The rule of five for non-oral routes of drug delivery: Ophthalmic, inhalation and transdermal. *Pharmaceutical Research*, *28*(5), 943–948. http://doi.org/10.1007/s11095-010-0292-6

Das, V., Bruzzese, F., Konečný, P., Iannnell, F., Budillon, A., & Hajdúch, M. (2015). Pathophysiologically relevant *in vitro* tumor models for drug screening. *Drug Discovery Today*. http://doi.org/10.1016/j.drudis.2015.04.004

Dixon, J. E., Shah, D. a, Rogers, C., Hall, S., Weston, N., Parmenter, C. D. J., … Shakesheff, K. M. (2014). Combined hydrogels that switch human pluripotent stem cells from self-renewal to differentiation. *Proceedings of the National Academy of Sciences of the United States of America*, *111*(15), 5580–5. doi:10.1073/pnas.1319685111

Du, Q., Dai, G., Long, Q., Yu, X., Dong, L., Huang, H., & Xie, J. (2013). *Mycobacterium tuberculosis* rrs A1401G mutation correlates with high-level resistance to kanamycin, amikacin, and capreomycin in clinical isolates from mainland China. *Diagnostic Microbiology and Infectious Disease*, *77*(2), 138–142. doi:10.1016/j.diagmicrobio.2013.06.031

Eglen, R. M., Gilchrist, A., & Reisine, T. (2008). The use of immortalized cell lines in GPCR screening: the good, bad and ugly. *Combinatorial Chemistry & High Throughput Screening*, *11*(7), 560–565.

Erlanson, D. a. (2006). Fragment-based lead discovery: a chemical update. *Current Opinion in Biotechnology*, *17*(6), 643–652.

Fennema, E., Rivron, N., Rouwkema, J., van Blitterswijk, C., & De Boer, J. (2013). Spheroid culture as a tool for creating 3D complex tissues. *Trends in Biotechnology*, *31*(2), 108–115. doi:10.1016/j.tibtech.2012.12.003

Fernandes, T. G., Diogo, M. M., Clark, D. S., Dordick, J. S., & Cabral, J. M. S. (2009). High-throughput cellular microarray platforms: applications in drug discovery, toxicology and stem cell research. *Trends in Biotechnology*, *27*(6), 342–349. doi:10.1016/j.tibtech.2009.02.009

Fischbach, C., Chen, R., Matsumoto, T., Schmelzle, T., Brugge, J. S., Polverini, P. J., & Mooney, D. J. (2007). Engineering tumors with 3D scaffolds. *Nature Methods*, *4*(10), 855–860. doi:10.1038/nmeth1085

Florczyk, S. J., Wang, K., Jana, S., Wood, D. L., Sytsma, S. K., Sham, J. G., … Zhang, M. (2013). Porous chitosan-hyaluronic acid scaffolds as a mimic of glioblastoma microenvironment ECM. *Biomaterials*, *34*(38), 10143–10150. doi:10.1016/j.biomaterials.2013.09.034

Friedrich, J., Seidel, C., Ebner, R., & Kunz-Schughart, L. A. (2009). Spheroid-based drug screen: considerations and practical approach. *Nat. Protocols*, *4*(3), 309–324. Retrieved from http://dx.doi.org/10.1038/nprot.2008.226

Fukuoka, M. et al. Multi-institutional randomized phase II trial of gefitinib for previously treated patients with advanced non-small-cell lung cancer (The IDEAL 1 Trial) [corrected]. J. Clin. Oncol. 21, 2237–2246 (2003);

Gagneux, S., DeRiemer, K., Van, T., Kato-Maeda, M., de Jong, B. C., Narayanan, S., … Small, P. M. (2006). Variable host-pathogen compatibility in *Mycobacterium tuberculosis*. *Proceedings of the National Academy of Sciences of the United States of America*, *103*(8), 2869–2873. doi:10.1073/pnas.0511240103

Gagneux, S., & Small, P. M. (2007). Global phylogeography of *Mycobacterium tuberculosis* and implications for tuberculosis product development. *Lancet Infectious Diseases*, *7*(5), 328–337. doi:10.1016/S1473-3099(07)70108-1

Gao, S., Calcagni, M., Welti, M., Hemmi, S., Hild, N., Stark, W. J., … Buschmann, J. (2014). Proliferation of ASC-derived endothelial cells in a 3D electrospun mesh: Impact of bone-biomimetic nanocomposite and co-culture with ASC-derived osteoblasts. *Injury*, *45*(6), 974–980. doi:10.1016/j.injury.2014.02.035

Geetharamani, G., Padma, M., & Pandian, J. A. (2015). A New Therapeutic Applications for Drug Repositioning on the Cloud Computing, 119–129.

Gidrol, X., Fouqué, B., Ghenim, L., Haguet, V., Picollet-D'hahan, N., & Schaack, B. (2009). 2D and 3D cell microarrays in pharmacology. *Current Opinion in Pharmacology*, *9*(5), 664–668. doi:10.1016/j.coph.2009.05.002

Gillet, J., Calcagno, A., Varma, S., Marino, M., Green, L., Vora, M., Patel, C., Orina, J., Eliseeva, T., Singal, V., Padmanabhan, R., Davidson, B., Ganapathi, R., Sood, A., Rueda, B., Ambudkar, S., Gottesman, M. (2011). Redefining the relevance of established cancer cell lines to the study of mechanisms of clinical anti-cancer drug resistance. *Proc Natl Acad Sci* U S A. Nov 15;108(46):18708-13. doi: 10.1073/pnas.1111840108.

Glickman, M. S., Jacobs, W. R., York, N., & Ave, M. P. (2001). Microbial pathogenesis of *Mycobacterium tuberculosis* : Dawn of a Discipline, *Cell*. *104*, 477–485.

Gutierrez, M., Master, S., & Singh, S. (2004). Autophagy Is a Defense Mechanism Inhibiting BCG and *Mycobacterium tuberculosis* Survival in Infected Macrophages. *Cell*, *119*, 753–766. doi:10.1016/j.cell.2004.11.038

Hall, I. H., Peaty, N. J., Henry, J. R., Easmon, J., Heinisch, G., & Pürstinger, G. (1999). Investigations on the mechanism of action of the novel antitumor agents 2-benzothiazolyl, 2-benzoxazolyl, and 2-benzimidazolyl hydrazones derived from 2-acetylpyridine. *Archiv Der Pharmazie*, *332*(4), 115–123.

Hann, M. M. (2011). Molecular obesity, potency and other addictions in drug discovery. *MedChemComm*, *2*(5), 349. http://doi.org/10.1039/c1md00017a

Harris, J., De Haro, S. a., Master, S. S., Keane, J., Roberts, E. a., Delgado, M., & Deretic, V. (2007). T Helper 2 Cytokines Inhibit Autophagic Control of Intracellular *Mycobacterium tuberculosis*. *Immunity*, *27*(3), 505–517. doi:10.1016/j.immuni.2007.07.022

Harris, J., Master, S. S., De Haro, S. a., Delgado, M., Roberts, E. a., Hope, J. C., … Deretic, V. (2009). Th1-Th2 polarisation and autophagy in the control of intracellular mycobacteria by macrophages. *Veterinary Immunology and Immunopathology*, *128*(1-3), 37–43. doi:10.1016/j.vetimm.2008.10.293

Horman, S. R., To, J., & Orth, A. P. (2013). An HTS-compatible 3D colony formation assay to identify tumor-specific chemotherapeutics. *Journal of Biomolecular Screening*, *18*(10), 1298–308. doi:10.1177/1087057113499405

Houben, E. N. G., Nguyen, L., & Pieters, J. (2006). Interaction of pathogenic mycobacteria with the host immune system. *Current Opinion in Microbiology*, *9*(1), 76–85. doi:10.1016/j.mib.2005.12.014

Howell, P. M., Liu, Z., & Khong, H. T. (2010). Demethylating agents in the treatment of cancer. *Pharmaceuticals*, *3*(7), 2022–2044. http://doi.org/10.3390/ph3072022

Jahnz-Wechmann, Z., Framski, G., Januszczyk, P., & Boryski, J. (2015). Bioactive fused heterocycles: Nucleoside analogs with an additional ring. *European Journal of Medicinal Chemistry*, *97*, 388–396. http://doi.org/10.1016/j.ejmech.2014.12.026

Janin, Y. L. (2007). Antituberculosis drugs: ten years of research. *Bioorganic & Medicinal Chemistry*, *15*(7), 2479–2513. http://doi.org/10.1016/j.bmc.2007.01.030

Jansa, J., Lyčka, A., Padělková, Z.,Grepl, M., Konečný, P., Hajdúch, M., Džubák, P. New imidazo [1,2-c]pyrimidin-5(6H)-ones Derived from cytosine: Synthesis, Structure and Cytotoxic Activity. J. Heterocyclic Chem., DOI: 10.1002/jhet.2243

Jiguet-Jiglaire C, Cayol M, Mathieu S, Jeanneau C, Bouvier-Labit C, Ouafik L, El-Battari (2014). A. Noninvasive near-infrared fluorescent protein-based imaging of tumor progression and metastases in deep organs and intraosseous tissues. J Biomed Opt. 2014 Jan;19(1):16019. doi: 10.1117/1.JBO.19.1.016019

Jiguet Jiglaire, C., Baeza-Kallee, N., Denicolaï, E., Barets, D., Metellus, P., Padovani, L., … Fernandez, C. (2014). Ex vivo cultures of glioblastoma in three-dimensional hydrogel maintain the original tumor growth behavior and are suitable for preclinical drug and radiation sensitivity screening. *Experimental Cell Research*, *321*(2), 99–108. doi:10.1016/j.yexcr.2013.12.010

Jordheim, L. P., Durantel, D., Zoulim, F., & Dumontet, C. (2013). Advances in the development of nucleoside and nucleotide analogues for cancer and viral diseases. *Nature Reviews. Drug Discovery*, *12*(6), 447–64. http://doi.org/10.1038/nrd4010

Kachel, V., Fellner-Feldegg, H., and Menke, E. (1990). Hydrodynamic properties of flow cytometry instruments. In Flow Cytometry and Sorting (M. R. Melamed, T. Lindmo, and M.L. Mendelsohn, eds.) pp. 27-44 .Wiley-Liss, New York.

Kaplánek, R., Havlík, M., Dolenský, B., Rak, J., Džubák, P., Konečný, P., … Král, V. (2015). Synthesis and biological activity evaluation of hydrazone derivatives based on a Tröger's base skeleton. *Bioorganic & Medicinal Chemistry*, *23*(7), 1651–1659. http://doi.org/10.1016/j.bmc.2015.01.029

Kaplánek, R., Jakubek, M., Rak, J., Kejík, Z., Havlík, M., Dolenský, B., … Král, V. (2015). Caffeine-hydrazones as anticancer agents with pronounced selectivity toward T-lymphoblastic leukaemia cells. *Bioorganic Chemistry*, *60*, 19–29. http://doi.org/10.1016/j.bioorg.2015.03.003

Kato, S., Moulder, S. L., Ueno, N. T., Wheler, J. J., Meric-, F., Kurzrock, R., & Janku, F. (2015). Challenges and perspective of drug repurposing strategies in early phase clinical trials, *2*(6).

Keane, J., Balcewicz-Sablinska, M. K., Remold, H. G., Chupp, G. L., Meek, B. B., Fenton, M. J., & Kornfeld, H. (1997). Infection by Mycobacterium tuberculosis promotes human alveolar macrophage apoptosis. *Infection and Immunity*, *65*(1), 298–304.

Keserü, G. M., & Makara, G. M. (2009). The influence of lead discovery strategies on the properties of drug candidates. *Nature Reviews. Drug Discovery*, *8*(3), 203–212. http://doi.org/10.1038/nrd2796

Kim, J. Bin. (2005). Three-dimensional tissue culture models in cancer biology. *Seminars in Cancer Biology*, *15*(5), 365–377. doi:10.1016/j.semcancer.2005.05.002

Kimlin, L. C., Casagrande, G., & Virador, V. M. (2013). *In vitro* three-dimensional (3D) models in cancer research: An update. *Molecular Carcinogenesis*, *52*(3), 167–182. doi:10.1002/mc.21844

Klener P., Klener P. Jr. (2010). Nová protinádorová léčiva a léčebné strategie v onkologii, Grada Publishing, 1. vydání, 232 stran, ISBN 978-80-247-2808-7

Kris, M., Natale, R., Herbst R., Lynch, T., Prager, D., Belani, C., Shiller, J., Kelly, K., Spiridonidis, H., Sandler, A., Albain, K., Cella, D., Wolf, M., Averbuch, S., Ochs, J. (2003) Efficacy of gefitinib, an inhibitor of the epidermal growth factor receptor tyrosine kinase, in symptomatic patients with non–small cell lung cancer: A randomized trial. *JAMA*, *290*(16), 2149–2158. Retrieved from http://dx.doi.org/10.1001/jama.290.16.2149

Kumar, N., Chauhan, L. S., Dashora, N., & Sharma, C. S. (2014). Review Article Anticonvulant potential of Hydrazone derivatives, *Sch. Acad. J.Pharm.*, *3*(5), 366–373.

Kumar, S. (2015). Drug Targets for Cancer Treatment: An Overview. *Medicinal Chemistry*, *5*(3), 115–123. http://doi.org/10.4172/2161-0444.1000252

Lau, C. L., Kovacevic, M., Tingleff, T. S., Forsythe, J. S., Cate, H. S., Merlo, D., … Beart, P. M. (2014). 3D Electrospun scaffolds promote a cytotrophic phenotype of cultured primary astrocytes. *Journal of Neurochemistry*, *130*(2), 215–226. doi:10.1111/jnc.12702

Leiba, J., Carrère-Kremer, S., Blondiaux, N., Dimala, M. M., Wohlkönig, A., Baulard, A., … Molle, V. (2014). The *Mycobacterium tuberculosis* transcriptional repressor EthR is negatively regulated by Serine/Threonine phosphorylation. *Biochemical and Biophysical Research Communications*, *446*(4), 1132–1138. doi:10.1016/j.bbrc.2014.03.074

Li, A. P. (2001). Screening for human ADME/Tox drug properties in drug discovery. *Drug Discovery Today*, *6*(7), 357–366. http://doi.org/10.1016/S1359-6446(01)01712-3

Li, C. Y., Wood, D. K., Huang, J. H., & Bhatia, S. N. (2013). Flow-based pipeline for systematic modulation and analysis of 3D tumor microenvironments. *Lab on a Chip*, *13*(10), 1969–78. doi:10.1039/c3lc41300d

Lindgren, E. B., de Brito, M. a., Vasconcelos, T. R. a., de Moraes, M. O., Montenegro, R. C., Yoneda, J. D., & Leal, K. Z. (2014). Synthesis and anticancer activity of (E)-2-benzothiazole hydrazones. *European Journal of Medicinal Chemistry*, *86*, 12–16. http://doi.org/10.1016/j.ejmech.2014.08.039

Lipinski, C. a, Lombardo, F., Dominy, B. W., & Feeney, P. J. (2001). Experimental and computational approaches to estimate solubility and permeability in drug discovery and development settings1PII of original article: S0169-409X(96)00423-1. The article was originally published in Advanced Drug Delivery Reviews 23 (1997) 3–25.1. *Advanced Drug Delivery Reviews*, *46*(1-3), 3–26. http://doi.org/10.1016/S0169-409X(00)00129-0

Lipinski, C. a. (2000). Drug-like properties and the causes of poor solubility and poor permeability. *Journal of Pharmacological and Toxicological Methods*, *44*(1), 235–249. http://doi.org/10.1016/S1056-8719(00)00107-6

Lipinski, C. a. (2004). Lead- and drug-like compounds: The rule-of-five revolution. *Drug Discovery Today: Technologies*, *1*(4), 337–341. http://doi.org/10.1016/j.ddtec.2004.11.007

Liu, P. T., & Modlin, R. L. (2008). Human macrophage host defense against *Mycobacterium tuberculosis. Current Opinion in Immunology*, *20*(4), 371–376. doi:10.1016/j.coi.2008.05.014

Long, M. C., & Parker, W. B. (2006). Structure-activity relationship for nucleoside analogs as inhibitors or substrates of adenosine kinase from Mycobacterium tuberculosis. I. Modifications to the adenine moiety. *Biochemical Pharmacology*, *71*(12), 1671–1682. http://doi.org/10.1016/j.bcp.2006.03.006

Lorenzi, P., Reinhold, W., Varma, S., Hutchinson, A., Pommier, Y., Chanock, S., Weinstein, J. (2009). DNA fingerprinting of the NCI-60 cell line panel. *Mol Cancer Ther.* Apr;8(4):713-24.

Malikova, N. P., Burakova, L. P., Markova, S. V., & Vysotski, E. S. (2014). Characterization of hydromedusan Ca2+-regulated photoproteins as a tool for measurement of Ca2+concentration. *Analytical and Bioanalytical Chemistry*, *406*(23), 5715–5726. http://doi.org/10.1007/s00216-014-7986-2

Marshall, N., Goodwin, C., Holt, S. (1995). A critical assessment of the use of microculture tetrazolium assays to measure cell growth and function. *Growth Regul.*;5(2):69–84.

Marzo, I., & Naval, J. (2013). Antimitotic drugs in cancer chemotherapy: Promises and pitfalls. *Biochemical Pharmacology*, *86*(6), 703–710. http://doi.org/10.1016/j.bcp.2013.07.010

Massarelli, E., Varella-Garcia, M., Tang, X., Xavier, A. C., Ozburn, N. C., Liu, D. D., … Wistuba, I. I. (2007). KRAS mutation is an important predictor of resistance to therapy with epidermal growth factor receptor tyrosine kinase inhibitors in non-small-cell lung cancer. *Clinical Cancer Research : An Official Journal of the American Association for Cancer Research*, *13*(10), 2890–2896. http://doi.org/10.1158/1078-0432.CCR-06-3043

Mathew, B., Suresh, J., Ahsan, M. J., & Mathew, G. E. (2015). Hydrazones as a Privileged Structural Linker in Antitubercular Agents : A Review Hydrazones as a Privileged Structural Linker in Antitubercular Agents : A Review, (August).

Matsuda, A., Sasaki, T. (2004). Antitumor activity of sugar-modified cytosine nucleosides. *Cancer Science*, *95*(2), 105–111. http://doi.org/10.1111/j.1349-7006.2004.tb03189.x

Mayer, J., Starý, J. (2002). Leukemie. Grada Publishing, 266-268.

Mayer, N., Schweiger, M., Melcher, M.-C., Fledelius, C., Zechner, R., Zimmermann, R., & Breinbauer, R. (2015). Structure-activity studies in the development of a hydrazone based inhibitor of adipose-triglyceride lipase (ATGL). *Bioorganic & Medicinal Chemistry*, *23*(12), 2904–2916. http://doi.org/10.1016/j.bmc.2015.02.051

McDermott U, Sharma SV, Settleman J. (2008). High-throughput lung cancer cell line screening for genotype-correlated sensitivity to an EGFR kinase inhibitor. *Methods Enzymol*. 2008;438:331–341;

Mdluli, K., & Spigelman, M. (2006). Novel targets for tuberculosis drug discovery. *Current Opinion in Pharmacology*, *6*(5), 459–467. http://doi.org/10.1016/j.coph.2006.06.004

Mehta, G., Hsiao, A. Y., Ingram, M., Luker, G. D., & Takayama, S. (2012). Opportunities and challenges for use of tumor spheroids as models to test drug delivery and efficacy. *Journal of Controlled Release*, *164*(2), 192–204. doi:10.1016/j.jconrel.2012.04.045

Menéndez-Arias, L., Alvarez, M., & Pacheco, B. (2014). Nucleoside/nucleotide analog inhibitors of hepatitis B virus polymerase: mechanism of action and resistance. *Current Opinion in Virology*, *8C*, 1–9. http://doi.org/10.1016/j.coviro.2014.04.005

Moore, M. J., Goldstein, D., Hamm, J., Figer, A., Hecht, J.,…...Parulekar, W. (2007). Erlotinib plus gemcitabine compared with gemcitabine alone in patients with advanced pancreatic cancer: a phase III trial of the National Cancer Institute of Canada Clinical Trials Group. J. Clin. Oncol. 25, 1960–1966;

Mosmann T. (1983). Rapid colorimetric assay for cellular growth and survival: Application to proliferation and cytotoxicity assays. J. Immunol. Meth.;65:55–63.

Mueller, P., & Pieters, J. (2006). Modulation of macrophage antimicrobial mechanisms by pathogenic mycobacteria. *Immunobiology*, *211*(6-8), 549–556. doi:10.1016/j.imbio.2006.06.004

Mulhall, H. J., Hughes, M. P., Kazmi, B., Lewis, M. P., & Labeed, F. H. (2013). Epithelial cancer cells exhibit different electrical properties when cultured in 2D and 3D environments. *Biochimica et Biophysica Acta*, *1830*(11), 5136–41. doi:10.1016/j.bbagen.2013.07.008

Muthyala, R. (2012). Orphan/rare drug discovery through drug repositioning. *Drug Discovery Today: Therapeutic Strategies*, *8*(3-4), 71–76. http://doi.org/10.1016/j.ddstr.2011.10.003

Nauš, P., Caletková, O., Konečný, P., Džubák, P., Bogdanová, K., Kolář, M., … Hocek, M. (2014). Synthesis, cytostatic, antimicrobial, and anti-HCV activity of 6-substituted 7-(het)aryl-7-deazapurine ribonucleosides. *Journal of Medicinal Chemistry*, *57*(3), 1097–1110. http://doi.org/10.1021/jm4018948

Neve, R., Chin, K., Fridlyand J., Yeh, J., Baehner, F., ……Gray, J. (2006). A collection of breast cancer cell lines for the study of functionally distinct cancer subtypes. Cancer Cell 10, 515–527;

Nivens, D. E., McKnight, T. E., Moser, S. a., Osbourn, S. J., Simpson, M. L., & Sayler, G. S. (2004). Bioluminescent bioreporter integrated circuits: Potentially small, rugged and inexpensive whole-cell biosensors for remote environmental monitoring. *Journal of Applied Microbiology*, *96*(1), 33–46. http://doi.org/10.1046/j.1365-2672.2003.02114.x

Noskova, V., Dzubak, P., Kuzmina, G., Ludkova, a., Stehlik, D., Trojanec, R., Hajduch, M. (2002). *In vitro* chemoresistance profile and expression/function of MDR associated proteins in resistant cell lines derived from CCRF-CEM, K562, A549 and MDA MB 231 parental cells. *Neoplasma*, *49*(6), 418–425.

Olakanmi, O., Britigan, B. E., & Schlesinger, L. S. (2000). Gallium disrupts iron metabolism of mycobacteria residing within human macrophages. *Infect. Immun.*, *68*, 5619–5627. Retrieved from http://dx.doi.org/10.1128/IAI.68.10.5619-5627.2000

Paez, J. G., Jänne, P. A., Lee, J. C., Tracy, S., Greulich, H., Gabriel, S., … Meyerson, M. (2004). EGFR Mutations in Lung Cancer: Correlation with Clinical Response to Gefitinib Therapy. *Science* , *304* (5676), 1497–1500. http://doi.org/10.1126/science.1099314

Padhy, B., & Gupta, Y. (2011). Drug repositioning: Re-investigating existing drugs for new therapeutic indications. *Journal of Postgraduate Medicine*, *57*(2), 153–160. http://doi.org/10.4103/0022-3859.81870

Padmini, K., Preethi, P. J., Divya, M., Rohini, P., Lohita, M., Swetha, K., & Kaladar, P. (2013). A Review on Biological Importance of Hydrazones, *International Journal of Pharma Research & Review*, August 2013; 2(8):43-58

Pałasz, A., & Cież, D. (2015). In search of uracil derivatives as bioactive agents. Uracils and fused uracils: Synthesis, biological activity and applications. *European Journal of Medicinal Chemistry*, *97*, 582–611. http://doi.org/10.1016/j.ejmech.2014.10.008

Pampaloni, F., Reynaud, E. G., & Stelzer, E. H. K. (2007). The third dimension bridges the gap between cell culture and live tissue, *8*(october), *Nature reviews, Molecular Cell Biology*, Volume 8, 839–845.

Pastor-Anglada, M., Felipe, A., & Javier Casado, F. (1998). Transport and mode of action of nucleoside derivatives used in chemical and antiviral therapies. *Trends in Pharmacological Sciences*, *19*(10), 424–430. http://doi.org/10.1016/S0165-6147(98)01253-X

Perlíková, P., Konečný, P., Nauš, P., Snášel, J., Votruba, I., Džubák, P., … Hocek, M. (2013). 6-Alkyl-, 6-aryl- or 6-hetaryl-7-deazapurine ribonucleosides as inhibitors of human or MTB adenosine kinase and potential antimycobacterial agents. *MedChemComm*, *4*(11), 1497. http://doi.org/10.1039/c3md00232b

Perola, E. (2010). An analysis of the binding efficiencies of drugs and their leads in successful drug discovery programs. *Journal of Medicinal Chemistry*, *53*(7), 2986–2997. http://doi.org/10.1021/jm100118x

Pickl, M., & Ries, C. H. (2009). Comparison of 3D and 2D tumor models reveals enhanced HER2 activation in 3D associated with an increased response to trastuzumab. *Oncogene*, *28*(3), 461–468. doi:10.1038/onc.2008.394

Pieters, J. (2008). *Mycobacterium tuberculosis* and the Macrophage: Maintaining a Balance. *Cell Host and Microbe*, *3*(6), 399–407. doi:10.1016/j.chom.2008.05.006

Plitta, B., Adamska, E., Giel-Pietraszuk, M., Fedoruk-Wyszomirska, A., Naskręt-Barciszewska, M., Markiewicz, W. T., & Barciszewski, J. (2012). New cytosine derivatives as inhibitors of DNA methylation. *European Journal of Medicinal Chemistry*, *55*, 243–254. http://doi.org/10.1016/j.ejmech.2012.07.024

Radzioch, D., Hudson, T., Boulé, M., Barrera, L., Urbance, J. W., Varesio, L., & kamene, E. (1991). Genetic resistance/susceptibility to mycobacteria: phenotypic expression in bone marrow derived macrophage lines. *Journal of Leukocyte Biology*, *50*(3), 263–272.

Reid, B. G., Jerjian, T., Patel, P., Zhou, Q., Yoo, B. H., Kabos, P., … Labarbera, D. V. (2014). Live multicellular tumor spheroid models for high-content imaging and screening in cancer drug discovery. *Current Chemical Genomics and Translational Medicine*, *8*(Suppl 1), 27–35. doi:10.2174/2213988501408010027

Reddy, M. C. M., Palaninathan, S. K., Shetty, N. D., Owen, J. L., Watson, M. D., & Sacchettini, J. C. (2007). High resolution crystal structures of *Mycobacterium tuberculosis* adenosine kinase: Insights into the mechanism and specificity of this novel prokaryotic enzyme. *Journal of Biological Chemistry*, *282*(37), 27334–27342. http://doi.org/10.1074/jbc.M703290200

Reynolds, C. H., Bembenek, S. D., & Tounge, B. a. (2007). The role of molecular size in ligand efficiency. *Bioorganic and Medicinal Chemistry Letters*, *17*(15), 4258–4261. http://doi.org/10.1016/j.bmcl.2007.05.038

Rimann, M., & Graf-Hausner, U. (2012). Synthetic 3D multicellular systems for drug development. *Current Opinion in Biotechnology*, *23*(5), 803–809. doi:10.1016/j.copbio.2012.01.011

Riss, T., Moravec, R., Niles, A., et al. (2013). Cell Viability Assay. Eli Lilly & Company and the National Center for Advancing Translational Sciences; Assay Guidance Manual [Internet]. Bethesda (MD)

Saltz, L. B., Meropol N., Loehrer, P., Needle, M., Kopit, J., Mayer, R. (2004). Phase II trial of cetuximab in patients with refractory colorectal cancer that expresses the epidermal growth factor receptor. J. Clin. Oncol. 22, 1201–1208;

Shapiro, H.M. (2003). Practical Flow Cytometry, chapter 7.5 Fluorescent Labels and Protein Dyes, Covalent labels for antibodies and other molecules, 328-332, 4th ed., pp. 681, Wiley Liss, New York

Shepherd, F. A., Pereira, J., Ciuleanu, T., Hirsch, V., ….Seymour, L. (2005). Erlotinib in previously treated non-small-cell lung cancer. N. Engl. J. Med. 353, 123–132 ;

Schaible, U. E., & Kaufmann, S. H. E. (2004). Iron and microbial infection. *Nat Rev Micro*, *2*(12), 946–953. Retrieved from http://dx.doi.org/10.1038/nrmicro1046

Sikic, B. I. (1999). New approaches in cancer treatment. *Ann Oncol*, *10 Suppl 6*, 149–153.

Singh, M., & Raghav, N. (2011). Biological activities of hydrazones: A review. *International Journal of Pharmacy and Pharmaceutical Sciences*, *3*(4), 26–32. http://doi.org/10.1186/1752-153X-5-2; Rollas, S., Kiiciikguzel, S.G., Biological Activities of Hydrazone Derivatives (2007) Molecules, 12, pp. 1910-1939; Yadav, J., Pandeya, S.N., Nath, G., Singh, S.P., Synthesis and antibacterial evaluation of some hydrazones of flavanoid derivatives (2010) J Chem Pharm Res, 2 (4), pp. 558-563;

Snášel, J., Nauš, P., Dostál, J., Hnízda, A., Fanfrlík, J., Brynda, J., … Pichová, I. (2014). Structural Basis for Inhibition of Mycobacterial and Human Adenosine Kinase by 7-Substituted 7-(Het)aryl-7-deazaadenine Ribonucleosides. *Journal of Medicinal Chemistry*, *57*(20), 8268–8279. http://doi.org/10.1021/jm500497v

Sos, M. L., Michel, K., Zander, T., Weiss, J., Frommolt, P., Peifer, M.,…..Thomas, R. (2009). Predicting drug susceptibility of non small cell lung cancers based on genetic lesions. *J. Clin. Invest*. 119, 1727–1740.

Stinson, S. F., Alley, M., Kopp, W., Fiebig, H., Mullendore, L., Pittman, A., Kenney, S., Keller, J., Boyd, M. (1992). Morphological and immunocytochemical characteristics of human tumor cell lines for use in a disease-oriented anticancer drug screen. *Anticancer Res*. 12, 1035–1053 (1992

Sudo, R., Chung, S., Zervantonakis, I. K., Vickerman, V., Toshimitsu, Y., Griffith, L. G., & Kamm, R. D. (2009). Transport-mediated angiogenesis in 3D epithelial coculture. *The*

FASEB Journal : Official Publication of the Federation of American Societies for Experimental Biology, *23*(7), 2155–2164. doi:10.1096/fj.08-122820

Sun, T., Jackson, S., Haycock, J. W., & MacNeil, S. (2006). Culture of skin cells in 3D rather than 2D improves their ability to survive exposure to cytotoxic agents. *Journal of Biotechnology*, *122*(3), 372–381. doi:10.1016/j.jbiotec.2005.12.021

Sundaramurthy, V., & Pieters, J. (2007). Interactions of pathogenic mycobacteria with host macrophages. *Microbes and Infection*, *9*(14-15), 1671–1679. doi:10.1016/j.micinf.2007.09.007

Takatori, S., Kanda, H., Takenaka, K., Wataya, Y., Matsuda, A., Fukushima, M., Shiammoto, Y., Tanaka, M., Sasaki, T. (1999). Antitumor mechanisms and metabolism of the novel antitumor nucleoside analogues , 1- (3-C-ethynyl- b - D -ribo-pentofuranosyl) cytosine and 1- (3-C-ethynyl- b - D - ribo-pentofuranosyl) uracil, 97–104.

Takiff, H., & Guerrero, E. (2011). Current prospects for the fluoroquinolones as first-line tuberculosis therapy. *Antimicrobial Agents and Chemotherapy*, *55*(12), 5421–5429. http://doi.org/10.1128/AAC.00695-11

Tarcsay, Á., Nyíri, K., & Keserú, G. M. (2012). Impact of lipophilic efficiency on compound quality. *Journal of Medicinal Chemistry*, *55*(3), 1252–1260. http://doi.org/10.1021/jm201388p

Thatcher, N., Chang, A., Parikh, P., Rodriquez Pereira, J. et al. (2005). Gefitinib plus best supportive care in previously treated patients with refractory advanced non-small-cell lung cancer: results from a randomised, placebo-controlled, multicentre study (Iressa Survival Evaluation in Lung Cancer). Lancet 366, 1527–1537.

Theodosopoulos, T., Yiallourou, A., Dafnios, N., Polymeneas, G. et al. (2012) Right Kocher's incision: a feasible and effective incision for right hemicolectomy: a retrospective study. *World J. Surg. Oncol*. 10, 101

Tomori, T., Miyatake, Y., Sato, Y., Kanamori, T., Masaki, Y., Ohkubo, A., … Seio, K. (2015). Synthesis of Peptide Nucleic Acids Containing Pyridazine Derivatives As Cytosine and Thymine Analogs, and Their Duplexes with Complementary Oligodeoxynucleotides. *Organic Letters*, *17*(6), 1609–1612. http://doi.org/10.1021/acs.orglett.5b00522

Torzilli, G., Procopio F., Palmisano, A., Donadon, M. et al. (2011) Total or partial anatomical resection of segment 8 using the ultrasound-guided finger compression technique. *HPB (Oxford)* 13, 586–591

Tsafack, A., Loyevsky, M., Ponka, P., & Cabantchik, Z. I. (1996). Mode of action of iron (III) chelators as antimalarials. IV. Potentiation of desferal action by benzoyl and isonicotinoyl hydrazone derivatives. *Journal of Laboratory and Clinical Medicine*, *127*(6), 574–582. http://doi.org/10.1016/S0022-2143(96)90148-1

Vermorken, J. B. et al. (2007). Open-label, uncontrolled, multicenter phase II study to evaluate the efficacy and toxicity of cetuximab as a single agent in patients with recurrent and/or metastatic squamous cell carcinoma of the head and neck who failed to respond to platinum-based therapy. *J. Clin. Oncol*. 25, 2171–2177

Verveer, P. J., Swoger, J., Pampaloni, F., Greger, K., Marcello, M., & Stelzer, E. H. K. (2007). High-resolution three-dimensional imaging of large specimens with light sheet-based microscopy. *Nature Methods*, *4*(4), 311–313. doi:10.1038/nmeth1017

Walcourt, A., Loyevsky, M., Lovejoy, D. B., Gordeuk, V. R., & Richardson, D. R. (2004). Novel aroylhydrazone and thiosemicarbazone iron chelators with anti-malarial activity against chloroquine-resistant and -sensitive parasites. *International Journal of Biochemistry and Cell Biology*, *36*(3), 401–407. http://doi.org/10.1016/S1357-2725(03)00248-6

Worthington Biochemical Online Tissue Dissociation Guide. Santangelo, C. 2011. Worthington Biochemical Corporation. date of access (http://www.worthington-biochem.com/tissuedissociation/basic.html).

World Health Organization. (2014). Global tuberculosis report 2014 (WHO/HTM/TB/2014.08). doi:WHO/HTM/TB/2014.08

Xu, W. S., Parmigiani, R. B., & Marks, P. a. (2007). Histone deacetylase inhibitors: molecular mechanisms of action. *Oncogene*, *26*(37), 5541–5552. http://doi.org/10.1038/sj.onc.1210620

Xu, Z., Ba, M., Zhou, H., Cao, Y., Tang, C., Yang, Y., … Guo, C. (2014). 2,4,5-Trisubstituted thiazole derivatives: a novel and potent class of non-nucleoside inhibitors of wild type and mutant HIV-1 reverse transcriptase. *European Journal of Medicinal Chemistry*, *85*, 27–42. http://doi.org/10.1016/j.ejmech.2014.07.072

Yadav, R. R., Khan, S. I., Singh, S., Khan, I. a., Vishwakarma, R. a., & Bharate, S. B. (2015). Synthesis, antimalarial and antitubercular activities of meridianin derivatives. *European Journal of Medicinal Chemistry*, *98*, 160–169. http://doi.org/10.1016/j.ejmech.2015.05.020

Yamamoto, M. et al. (2012) Clinical outcomes of laparoscopic surgery for advanced transverse and descending colon cancer: a single-center experience. *Surg. Endosc*. 26, 1566–1572

Yliperttula, M., Chung, B. G., Navaladi, A., Manbachi, A., & Urtti, A. (2008). High-throughput screening of cell responses to biomaterials. *European Journal of Pharmaceutical Sciences*, *35*(3), 151–160. doi:10.1016/j.ejps.2008.04.012

Younger, H. M., Bathgate, a. J., & Hayes, P. C. (2004). Review article: Nucleoside analogues for the treatment of chronic hepatitis B. *Alimentary Pharmacology and Therapeutics*, *20*(11-12), 1211–1230. http://doi.org/10.1111/j.1365-2036.2004.02211.

Zhang, Y., Post-Martens, K., & Denkin, S. (2006). New drug candidates and therapeutic targets for tuberculosis therapy. *Drug Discovery Today*, *11*(1-2), 21–27. http://doi.org/10.1016/S1359-6446(05)03626-3

Zhang, X., Betzi, S., Morelli, X., & Roche, P. (2014). Focused chemical libraries - design and enrichment: an example of protein-protein interaction chemical space. *Future Medicinal Chemistry*, (August 2015). http://doi.org/10.4155/fmc.14.57

Zumla, A., Nahid, P., & Cole, S. T. (2013). Advances in the development of new tuberculosis drugs and treatment regimens. *Nature Reviews. Drug Discovery*, *12*(5), 388–404. http://doi.org/10.1038/nrd4001

5 Bibliography

5.1 Original articles and reviews

BOURDERIOUX, A., NAUŠ, P., PERLÍKOVÁ, P., POHL, R., PICHOVÁ, I., VOTRUBA, I., DŽUBÁK, P., KONEČNÝ, P., HAJDÚCH, M., STRAY, K.M., WANG, T., RAY, A. S., FENG, J.Y., BIRKUS, G., CIHLÁŘ, T., HOCEK, M. Synthesis and Significant Cytostatic Activity of 7-Hetaryl-7-deazaadenosines. Journal of Medicinal Chemistry, 2011, vol. 2011, no. 54, s. 5498-2623. ISSN: 0022-2623. IF (2010): 5.207.

SPENEROVA, M., P. DZUBAK, J. SROVNAL, L. RADOVA, R. BURIANOVA, **P. KONECNY**, S. SALKOVA, Z. NOVY, D. POSPISILOVA, J. STARY, B. BLAZEK, J. HAK, T. VOTAVA, P. TIMR, E. KAISEROVA, E. BUBANSKA, V. MIHAL a M. HAJDUCH. Combination of prednisolone and low dosed dexamethasone exhibits greater *in vitro* antileukemic activity than equiactive dose of prednisolone and overcomes prednisolone drug resistence in acute childhood lymphoblastic leukemia. *Biomedical Papers of the Medical Faculty of the University Palacký, Olomouc, Czech Republic*. 2012, **156**, (DOI: 10.5507/bp.2012.059). ISSN 1213-8118. IF (2011): 0.702.

PERLÍKOVÁ, P., **KONEČNÝ, P**. NAUŠ, J. SNÁŠEL, I. VOTRUBA, P. DŽUBÁK, I. PICHOVÁ, M. HAJDÚCH a M. HOCEK. 6-Alkyl-, 6-aryl- or 6-hetaryl-7-deazapurine ribonucleosides as inhibitors of human or MTB adenosine kinase and potential antimycobacterial agents. *MedChemComm.* 2013, 4(11), 1497-1500. ISSN 2040-2503. IF (2012): 2.722.

NAUŠ, P., O. CALETKOVÁ, **P**. **KONEČNÝ,** P. DŽUBÁK, K. BOGDANOVÁ, M. KOLÁŘ, J. VRBKOVÁ, L. SLAVĚTÍNSKÁ, E. TLOUŠŤOVÁ, P. PERLÍKOVÁ, M. HAJDÚCH a M. HOCEK. Synthesis, cytostatic, antimicrobial, and anti-HCV activity of 6-substituted 7-(het)aryl-7-deazapurine ribonucleosides. *Journal of Medicinal Chemistry*. 2014, **57**(3), 1097-1110. ISSN 0022-2623. IF (2012): 5.614.

TOMÁNKOVÁ K, KOLÁŘOVÁ H, PIŽOVA K, BINDER S, **KONEČNY P**, KRIEGOVA E, MALINA L, HORAKOVA J, MALOHLAVA J, KEJLOVA K, JIROVA D. Cytotoxicity and Antioxidative Effects of Herbal and Fruit Extracts *In Vitro, Food Biophysics* 2014, 9:267–276, DOI 10.1007/s11483-014-9349-0 IF (2013): 1.551

JANSA J, LYČKA A, PADĚLKOVÁ Z,GREPL M, KONEČNÝ P, HAJDÚCH M, DŽUBÁK P. New imidazo [1,2-c]pyrimidin-5(6H)-ones Derived from cytosine: Synthesis, Structure and Cytotoxic Activity. *J. Heterocyclic Chem*. 2014, DOI: 10.1002/jhet.2243 IF (2014): 0.873

SNÁŠEL J[1], NAUŠ P, DOSTÁL J, HNÍZDA A, FANFRLÍK J, BRYNDA J, BOURDERIOUX A, DUŠEK M, DVOŘÁKOVÁ H, STOLAŘÍKOVÁ J, ZÁBRANSKÁ H, POHL R, **KONEČNÝ P**, DŽUBÁK P, VOTRUBA I, HAJDÚCH M, REZÁČOVÁ P, VEVERKA V, HOCEK M, PICHOVÁ I. Structural basis for inhibition of mycobacterial and human adenosine kinase by 7-substituted 7-(Het)aryl-7-deazaadenine ribonucleosides., J Med Chem. 2014 Oct 23;57(20):8268-79. doi: 10.1021/jm500497v. Epub 2014 Oct 8. IF (2014): 5.447

KAPLÁNEK R[1], HAVLÍK M[1], DOLENSKÝ B[1], RAK J[1], DŽUBÁK P[2], **KONEČNÝ P**[2], HAJDÚCH M[2], KRÁLOVÁ J[3], KRÁL V[4]. Synthesis and biological activity evaluation of hydrazone derivatives based on a Tröger's base skeleton. Bioorg Med Chem. 2015 Apr 1; 23(7):1651-9. doi: 10.1016/j.bmc.2015.01.029. Epub 2015 Jan 23. IF (2015): 2.793

DAS V[1], BRUZZESE F[2], **KONEČNÝ P**[1], IANNELLI F[2], BUDILLON A[2], HAJDÚCH M[3]. Pathophysiologically relevant *in vitro* tumor models for drug screening. Drug Discov Today. 2015 Apr 20. pii: S1359-6446(15)00148-8. doi: 10.1016/j.drudis.2015.04.004. [Epub ahead of print], IF (2015): 6.691

PIZOVA K[1], BAJGAR R[2], FILLEROVA R[3], KRIEGOVA E[3], CENKLOVA V[2], LANGOVA K[4], **KONEČNÝ, P** KOLAROVA H[2]. C-MYC and C-FOS expression changes and cellular aspects of the photodynamic reaction with photosensitizers

TMPyP and ClAlPcS2. J Photochem Photobiol B. 2015 Jan;142: 186-96. doi: 10.1016/j.jphotobiol.2014.12.003. Epub 2014 Dec 9. IF (2015): 2.960

KONEČNÝ P, GURSKÁ S, ZNOJEK P, SCHADICH E, HAJDUCH M, DZUBAK P. Reprofilování jako úspěšná strategie hledání nových léčiv. Acta Medicinae (Farmakologická léčba). Submitted 10/2015.

5.2 Abstracts in periodics

KONEČNÝ, P. – DŽUBÁK, P. – SOURAL, M. – HLAVÁČ, J. – FRYDRYCH, I. – RYLOVÁ, G. – HAJDÚCH, M. Flow cytometric profiling of 2-Phenylsubstituted-3-Hydroxyquinolin-4(1H)-one-Carboxamides and their anticancer activities. In Towards toxicity assessment without animals. The 28th Workshop of SSCT and FINSCOPA Seminar, 21.-23.9.2011, Tampere, Finland, 2011, s. 47. (vol.-, no.-, ISBN: 978-951-44-8558-9).

KONEČNÝ, P. – DŽUBÁK, P. – FRYDRYCH, I. – ŠPENEROVÁ, M. – JANOŠŤÁKOVÁ, A. – SROVNAL, J. – MIHÁL, V. – HAJDÚCH, M. Prediction of Therapeutic Response to Corticoids for Children Patients with ALL. Sborník abstrakt konference: Nová léčiva závažných lidských onemocnění, 2011, s. 11-12. (vol.-, no.-,ISSN/ISBN:-)

DŽUBÁK, P. – VÁGNEROVÁ, H. – FRYDRYCH, I. – **KONEČNÝ, P**. – ŘEHULKA, J. – JANOŠŤÁKOVÁ, A. – GANDALÁKOVÁ, A. – HAJDÚCH, M. Prodrug formy triterpenů s protinádorovou aktivitou. In VII. DNY DIAGNOSTICKÉ, PREDIKTIVNÍ A EXPERIMENTÁLNÍ ONKOLOGIE. Onkologie, 2011, s. B16-B17. (vol. 5, Suppl.B, ISSN: 1802-4475). BEZ IF.

RYLOVÁ, G. – DŽUBÁK, P. – ŠPENEROVÁ, M. – JANOŠŤÁKOVÁ, A. – FRYDRYCH, I. – **KONEČNÝ, P**. – HOLUB, D. – OŽDIAN, T – DOLEŽAL, D. – SOURAL, M. – HLAVÁČ, J. – HAJDÚCH, M. Molecular targets and biological aktivity of quinolinone derivatives with anticancer effect. In VII. DNY DIAGNOSTICKÉ, PREDIKTIVNÍ A EXPERIMENTÁLNÍ ONKOLOGIE. Onkologie, 2011, s. B16. (vol. 5, Suppl.B, ISSN: 1802-4475). BEZ IF.

FRYDRYCH, I. – **KONEČNÝ, P**. – DŽUBÁK, P. – RADOVÁ, L. – HAJDÚCH, M. Comparative study of distinct effects of chemotherapeutic drugs on cell cycle. In Towards toxicity assessment without animals. The 28th Workshop of SSCT and FINSCOPA Seminar, 21.-23.9.2011, Tampere, Finland, 2011, s. 47-48. (vol.-, no.-, ISBN: 978-951-44-8558-9). BEZ IF

RYLOVÁ, G. – DŽUBÁK, P. – ŠPENEROVÁ, M. – JANOŠŤÁKOVÁ, A. – FRYDRYCH, I. – **KONEČNÝ**, **P**. – HOLUB, D. – OŽDIAN, T. – DOLEŽAL, D. – SOURAL, M. – HLAVÁČ, M. – HAJDÚCH, M. Biological activity and protein targets of quinoline derivatives with anticancer effect. In Book of Abstracts, 5th Central and Eastern European Proteomic Conference, 2011, s. 61. (vol. -, no.-, ISSN/ISBN: -).

RYLOVÁ, G. – DŽUBÁK, P. – ŠPENEROVÁ, M. – JANOŠŤÁKOVÁ, A. – FRYDRYCH, I. – **KONEČNÝ, P**. – HOLUB, D. – OŽDIAN, T. – DOLEŽAL, D. – SOURAL, M. – HLAVÁČ, J. – HAJDÚCH, M. Biological Activity and Molecular Targets of Quinoline Derivatives with Anticancer Effect. In Sborník abstrakt konference: Nová léčiva závažných lidských onemocnění, 2011, s. 19. (vol.-, no.-, ISSN/ISBN: -). BEZ IF.

ŠPENEROVÁ, M. – SROVNAL, J. – DŽUBÁK, P. – FRYDRYCH, I. – **KONEČNÝ, P**. – JANOŠŤÁKOVÁ, A. – ŠÁLKOVÁ, S. – KYLAROVÁ, K. – RŮŽKOVÁ, V. – RADOVÁ, L. – HAJDÚCH, M. – STARÝ, J. – TIMR, P. – HAK, J. – BLAŽEK, B. – ČERNÁ, Z. – KAISEROVÁ, E. – BUBANSKÁ, E. – MIHÁL, V. STUDY OF CORTICOID RESISTANCE IN CHILDHOOD ACUTE LYMPHOBLASTIC LEUKEMIA. In Biomed. Pap. Med. Fac. Univ. Palacky Olomouc, 2010, s. S3. (vol. 154, no. 4, ISSN: 1213-8118). BEZ IF.

ŘEHULKA, J. – DŽUBÁK, P. – HOLUB, D. – OŽDIAN, T. – KAMENÍČKOVÁ, A. – **KONEČNÝ, P**. – FRYDRYCH, I. – ŠÁLKOVÁ, S. – ŠAREK, J. – KVASNICA, M. – VLK, M. – HAJDÚCH, M. Diverse Gross of triterpenoid compounds derived from betulinic acid rapidly inducing apoptosis and G2/M block.

In VI. DNY DIAGNOSTICKÉ, PREDIKTIVNÍ A EXPERIMENTÁLNÍ ONKOLOGIE. Onkologie, 2010, s. 24. (vol. 4, Suppl.A., ISSN: 1803-5922).

FRYDRYCH, I. – DŽUBÁK, P. – SOURAL, M. – HLAVÁČ, J. – FUNK, P. – **KONEČNÝ, P**. – HAJDÚCH, M. 2-Substituted-3-Hydroxyquinoline-4(1H)-one-Carboxamides as potential anticancer drugs. In VI. DNY DIAGNOSTICKÉ, PREDIKTIVNÍ A EXPERIMENTÁLNÍ ONKOLOGIE. Onkologie, 2010, s. 24. (vol. 4, Suppl.A., ISSN: 1803-5922).

RYLOVÁ, G. – DŽUBÁK, P. – ŠPENEROVÁ, M. – JANOŠŤÁKOVÁ, A. – FRYDRYCH, I. – **KONEČNÝ,** P. – HOLUB, D. – OŽDIAN, T. – DOLEŽAL, D. – SOURAL, M. – HLAVÁČ, J. – HAJDÚCH, M. Affinity purification coupled to mass spektrometry-approach to drug target identification. In VI. DNY DIAGNOSTICKÉ, PREDIKTIVNÍ A EXPERIMENTÁLNÍ ONKOLOGIE. Onkologie, 2010, s. 14. (vol. 4, Suppl.A., ISSN: 1803-5922).

ŠPENEROVÁ, M. – SROVNAL, J. – DŽUBÁK, P. – FRYDRYCH, I. – **KONEČNÝ, P**. – JANOŠŤÁKOVÁ, A. – ŠÁLKOVÁ, S. – KYLAROVÁ, K. – RŮŽKOVÁ, V. – RADOVÁ, L. – HAJDÚCH, M. – STARÝ, J. – TIMR, P. – HAL, J. – BLAŽEK, B. – ČERNÁ, Z. – KAISEROVÁ, E. – BUBANSKÁ, E. – MIHÁL, V. Studium rezistence na kortikoidy u dětské akutní lymfoblastické leukemie. In VI. DNY DIAGNOSTICKÉ, PREDIKTIVNÍ A EXPERIMENTÁLNÍ ONKOLOGIE. Onkologie, 2010, s. 12-13. (vol. 4, Suppl.A., ISSN: 1803-5922).

DŽUBÁK, P. – KOPŘIVA, F. – POTĚŠIL, J. – JANOŠŤÁKOVÁ, A. – FRYDRYCH, I. – **KONEČNÝ, P**. – BURIÁNOVÁ, R. – HAJDÚCH, M. Lymphocyte mdr1 expression and clinical relevance of mdr1 polymorphism in asthmatic children treated by inhaled corticosteroids. In VI. DNY DIAGNOSTICKÉ, PREDIKTIVNÍ A EXPERIMENTÁLNÍ ONKOLOGIE. Onkologie, 2010, s. 12. (vol. 4, Suppl.A., ISSN: 1803-5922).

RYLOVÁ G. – DŽUBÁK P. – JANOŠŤÁKOVÁ A. – FRYDRYCH I. – **KONEČNÝ P**. – HOLUB D. - OŽDIAN T. – DOLEŽAL D. – SOURAL M. – HLAVÁČ J. – HAJDÚCH M. Biological activity and molecular target of quinolinone

derivatives with anticancer effect. In IX. DNY DIAGNOSTICKÉ, PREDIKTIVNÍ A EXPERIMENTÁLNÍ ONKOLOGIE. 2013. Abstract book, s. A23. BEZ IF.

ŠTĚPÁNkOVÁ J. – DŽUBÁK P. – PETŘÍK M. – NOVÝ Z. – **KONEČNÝ P**. – GRUNER B. – ŠÍCHA V. – BRYNDA J. – DOLEŽAL D. – HAJDÚCH M. Intratumoral pH alteration following carborans treatment. In IX. DNY DIAGNOSTICKÉ, PREDIKTIVNÍ A EXPERIMENTÁLNÍ ONKOLOGIE. 2013. Abstract book, s. A23. BEZ IF.

5.3 Conference lectures

KONEČNÝ, P. – DŽUBÁK, P. – FRYDRYCH, I. – ŠPENEROVÁ, M. – JANOŠŤÁKOVÁ, A. – SROVNAL, J. – MIHÁL, V. – HAJDÚCH, M. Prediction of Therapeutic Response to Corticoids for Children Patients with ALL. Sborník abstrakt konference: Nová léčiva závažných lidských onemocnění, 2011, s. 11-12. (vol.-, no.-,ISSN/ISBN:-)BEZ IF

KONEČNÝ, P. – DŽUBÁK, P. – SOURAL, M. – HLAVÁČ, J. – FRYDRYCH, I. – RYLOVÁ, G. – KOCIS, P. – HAJDÚCH, M. Flow cytometric profiling of 2-Phenylsubstituted-3-Hydroxyquinolin-4(1H)-one-Carboxamides and their anticancer activities. In VII. DNY DIAGNOSTICKÉ, PREDIKTIVNÍ A EXPERIMENTÁLNÍ ONKOLOGIE. Onkologie, 2011, s. B17. (vol. 5, Suppl.B, ISSN: 1802-4475). BEZ IF.

KONEČNÝ P. – DŽUBÁK P. – SOURAL M. – HLAVÁČ J. – FRYDRYCH I. – RYLOVÁ G. – KOCIS P. – HAJDÚCH M. SAR analýza 2-fenylsubstituovaných-3-hydroxychinolin-4(1H)-one-karboxamidů na základě jejich vlivu na regulaci buněčného cyklu a toxicity vůči vybraným nádorovým buněčným liniíM. In VIII. DNY DIAGNOSTICKÉ, PREDIKTIVNÍ A EXPERIMENTÁLNÍ ONKOLOGIE. Onkologie, 2012, s. B25 (vol. 6, Suppl. B. ISSN: 1803 – 5922). Bez IF. (MSM 6198959216, LC07017);

KONEČNÝ P. – DŽUBÁK P. – HOCEK M. – HAJDÚCH M. Nucleosides – compounds with combined therapeutical activities. In IX. DNY DIAGNOSTICKÉ, PREDIKTIVNÍ A

KONEČNÝ P.- ONDRYÁŠOVÁ H.- TROJANEC R. – Chromosome sorting using BD FACS Aria II.Flow cytometry seminar, I.T.A Intertact, BD Bioscience

6 Appendix

DAS V[1], BRUZZESE F[2], **KONEČNÝ P**[1], IANNELLI F[2], BUDILLON A[2], HAJDÚCH M[3]. Pathophysiologically relevant *in vitro* tumor models for drug screening. Drug Discov Today. 2015 Apr 20. pii: S1359-6446(15)00148-8. doi: 10.1016/j.drudis.2015.04.004. [Epub ahead of print]

ELSEVIER

Pathophysiologically relevant *in vitro* tumor models for drug screening

Viswanath Das[1,3,4], Francesca Bruzzese[2,3,4], Petr Konečný[1,3,4], Federica Iannelli[2,3,4], Alfredo Budillon[2,3,4] and Marián Hajdúch[1,3,4]

[1] Institute of Molecular and Translational Medicine, Faculty of Medicine and Dentistry, Palacky University Olomouc, Hněvotínská 5, 779 00 Olomouc, Czech Republic
[2] Experimental Pharmacology Unit, Istituto Nazionale per lo Studio e la Cura dei Tumori Fondazioni Giovanni Pascale – IRCCS, 80131 Naples, Italy
[3] EATRIS Headquarters, Giovanni Migliaccio, De Boelelaan 1118, 1081 HZ Amsterdam, The Netherlands

The alarming rate of failure of clinical trials is a major hurdle in cancer therapy that partly results from the inadequate use of *in vitro* tumor models for the screening of promising hits and leads in preclinical studies. 2D cultures of cancer cell lines that are primarily used for drug screening do not adequately recapitulate tumor microenvironment (TME) complexities compared with 3D cancer cell cultures and tumor-derived primary cell cultures. In this review, we focus on the potential use of *in vitro* tumor models that reproduce *in vivo* tumor complexities for effective drug selection in the preclinical stages of drug development.

Introduction

The identification of new drugs and predicting drug responses in patients with cancer are major challenges facing researchers in the translation of laboratory discoveries to the bedside. Interestingly, anticancer drugs have the lowest 'likelihood of approval' and highest nonlead indication in clinical trials, and only one in 15 drugs entering clinical development is approved by the US Food and Drug Administration [1]. This high attrition rate is attributed to several factors, including inadequate use of *in vitro* tumor models for drug selection during the preclinical stages of drug development [2].

2D cultures of immortalized cancer cells have been used for the past few decades as primary *in vitro* tumor models in the high-throughput screening (HTS) of anticancer drugs. However, the limitation imposed by the use of 2D cultures of cancer cells has become increasingly apparent only recently. The immortalization and prolonged culture of cancer cells on 2D surfaces can alter their response to anticancer drugs. Drugs that show significant toxicity in 2D cultures, such as cisplatin and fluorouracil, display reduced toxicity in 3D cultures of cancer cells (Fig. 1). By contrast, trastuzumab, which has enhanced activity in 3D cultures, shows reduced cytotoxic effects in 2D cultures [3]. In addition to differences in drug effects, the transcriptomic analysis of cancer cell lines of different tumor types also reveals no correlation with their clinical counterparts [4]. This lack of correlation results from the fact that 2D cultures of cancer cells do not adequately recapitulate the *in vivo* conditions of tumors that critically alter drug penetration and/or response. Therefore, studies now emphasize the use of cell models that closely reproduce the *in vivo* features of tumors, and circumvent radical genotypic and phenotypic alterations resulting from prolonged culture in 2D surfaces. In this review, we discuss the use of pathophysiologically relevant *in vitro* tumor models in preclinical studies, and highlight advances in high throughput (HT)-compatible 3D culture platforms for the screening of potential anticancer drugs under a more biologically relevant microenvironment.

Pathophysiologically relevant *in vitro* tumor models

Culture of patient-derived primary tumor cells

The introduction of the National Cancer Institute 60 (NCI60) cell line panel comprising 60 human tumor cell lines was a major scientific endeavor in anticancer drug research. However, in the clinic, targeted anticancer drugs are often limited to small subset of

Corresponding author: Hajdúch, M. (marian.hajduch@upol.cz)
[4] All authors contributed equally to this article.

http://dx.doi.org/10.1016/j.drudis.2015.04.004

Please cite this article in press as: Das, V. et al. Pathophysiologically relevant *in vitro* tumor models for drug screening, Drug Discov Today (2015), http://dx.doi.org/10.1016/j.drudis.2015.04.004

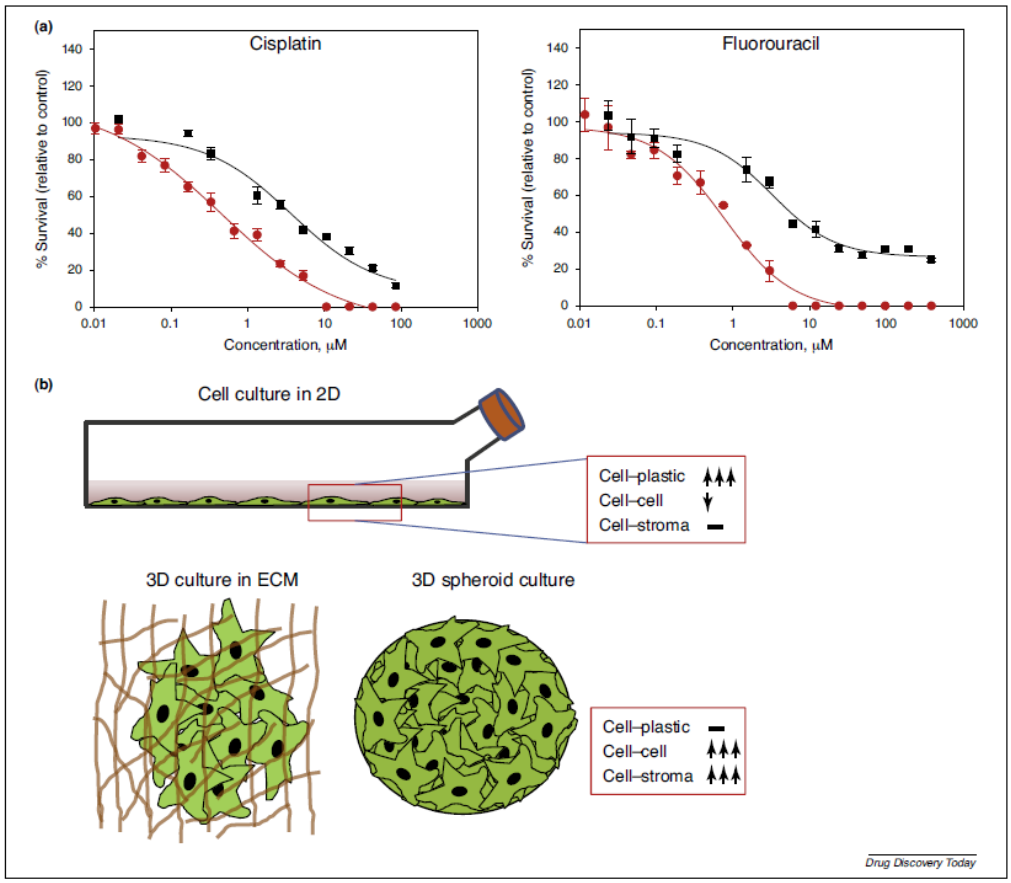

FIGURE 1

Characteristics differences in 2D and 3D cultures of cells. **(a)** Colorectal carcinoma HT29 cells cultured in 2D (red lines) and 3D (black lines) show a significant difference in survival response to the anticancer drugs cisplatin and fluorouracil, which are used clinically for the treatment of colorectal cancer. **(b)** Cells cultured as a monolayer on plastic surfaces are exposed to significant artificial conditions that alter their morphological and cellular behavior. By contrast, 3D cultures of cells in extracellular matrix (ECM) or as multicellular spheroids reproduce the microenvironment experienced by cells under physiological conditions.

patients, rendering the composition of the NCI60 panel inadequate for capturing low-frequency responses. Cultures of patient-derived tumor cells are now being recognized as important *in vitro* models for drug discovery studies because of their close resemblance to primary tumors (Table 1). Primary cells express endogenous targets at levels that closely resemble the disease, enabling the robust quantification of clinically relevant endpoints, such as drug efficacy, resistance to therapy, and biomarker discovery. Novel drugs characterized using primary cells act in a more predictable manner compared with those characterized using cancer cells [5].

Ex vivo cultures of cancer-associated fibroblasts (CAFs) recapitulate tumor-associated stroma that alters cancer cell response to drugs. CAFs are one of the major constituents of the stroma implicated in tumorigenesis and resistance, and differ from normal fibroblasts in the expression of several genes and proteins [6,7]. Signaling factors secreted by CAFs significantly affect the TME, and serve as biomarkers for cancer diagnosis. CAFs from patients with prostate cancer express high levels of the cytokine, chemokine ligand 14 (CXCL14), and CAF-produced CXCL14, but not recombinant CXCL14, stimulates cancer cell proliferation and migration [8]. Compared with normal stroma, reactive stroma from patients with prostate cancer has significantly altered gene expression [9]. Additional upregulated factors in CAFs but not normal fibroblasts from patients with prostate cancer have

Please cite this article in press as: Das, V. et al. Pathophysiologically relevant *in vitro* tumor models for drug screening, Drug Discov Today (2015), http://dx.doi.org/10.1016/j.drudis.2015.04.004

TABLE 1

Advantages and limitations of 2D and 3D cell cultures, and the culture of patient-derived primary tumor cells for the screening of anticancer compounds

Method	Advantages	Limitations
Cell line culture in 2D	Easy to culture Good viability Easy to image and suitable for endpoint assays Highly compatible with HTS Economical compared with other systems Significant 2D data available	Few cell–cell and cell–stroma interactions No histological morphology of tumor of origin Do not replicate heterogeneity seen in tumor regions Different genetic makeup compared with original tissue
3D culture	Oxygen and nutrient gradient of tumors Many cell–cell and cell–stroma interactions Distinct histological morphology of tumor of origin Hypoxia-induced cell cycle alterations reflecting microregions of tumors HT-compatible 3D culture plates available	Assays are laborious Requires higher drug concentrations compared with 2D cultures Requires advanced imaging systems Current high content imaging not suitable for 3D imaging Lacks tumor vasculature Relatively expensive compared with 2D cultures HTS compatibility still developing
Primary tumor cell culture	Recapitulates tumor heterogeneity Recapitulates tumor microenvironment Few mutations	Difficult to isolate Contamination with nontumor cells Limited life span Long-term culture not possible No standardized methods available Reduced reproducibility Low HTS applicability

recently been identified [10]. Of particular interest was growth differentiation factor 15 (GDF15), a potential regulator of prostate cancer progression in the stromal cells from prostate tissue. GDF15-expressing fibroblasts were found to stimulate the growth, migration, and invasion of prostate cancer cells [10]. In addition to local tumor-promoting activity, GDF15-expressing fibroblasts also stimulated the outgrowth of distant, otherwise indolent cancer cells. This study demonstrated for the first time the tumor-initiating potency of stroma from malignant tumors.

Finally, another important issue that has led investigators to shift their focus from cell lines to primary tumors is the role of cancer stem cells (CSCs) in cancer development. A subset of CSCs that are quiescent and resistant to chemotherapeutic agents are thought to be responsible for disease relapse and development of acquired resistance to therapies [11]. Malignant pleural effusions (MPEs) obtained from patients with lung cancer are a source of cancer-initiating cells and constitute an excellent model to study inter- and intratumoral heterogeneity. 3D cultures of MPE-derived cells induced the upregulation of markers of stemness and, when implanted in mice, reproduced the histopathological features of the tumor of origin [12]. However, the use of different CSC markers and isolation methodologies has resulted in conflicting data, highlighting the lack of sensitive methods to isolate CSCs. Recently, a group of autofluorescent cells in tumors of different types were identified that show typical features of CSCs [13]. This subset of cells with CSC-like features could serve as an attractive tool for screening anticancer compounds that specifically target CSCs.

Although there is emerging interest in the use of primary cancer cells for HTS, not all research facilities have access to patients from whom they can obtain viable tumor tissues for isolation of cells. Additionally, challenges associated with the isolation of cancerous cells from solid tumors and their long-term culture in an *in vitro* environment limit the use of primary cells in drug screening. Methodologies to isolate tumor specimens vary based on the tissue of origin, and are not always reproducible in establishing primary cultures. Furthermore, the cultivation of cells from dissociated tumors in 2D cultures results in the lack of architectural diversity and heterogeneity. These limitations have encouraged researchers to look for more advanced methods of establishing primary cell lines. Circulating tumor cells (CTCs) enable the real-time study of drug susceptibility changes in patients with tumors that acquire new mutations. Although the isolation of viable CTS is technically challenging, a recent microfluidic-based technology demonstrated for the first time the feasibility of CTC cultures from patients with breast cancer for individualized therapy [14].

3D cultures of cancer cells

Cells in living organisms are affected by their surrounding microenvironment in ways that we do not yet fully understand. Cells in 2D cultures have significantly fewer cell–cell and cell–stroma interactions compared with cells in 3D cultures that affect cellular behavior and significantly alter responses to drugs (Fig. 1). Studies now implicate resistance in solid tumors via spatial dimension-mediated oncogenic signaling pathways that promote cell survival and proliferation [15]. For example, responses to trastuzumab are sensitive to dimerization of human epidermal growth factor receptor (HER2), and patients with high levels of HER2 homodimers responded positively to trastuzumab and other anti-HER therapies [16]. In 2D cultures of SK-BR-3 cells, HER2 formed heterodimers and activated signaling pathways that facilitated cell survival and induce resistance to trastuzumab [3]. However, a change to 3D culture resulted in the homodimerization of HER2 and enhanced trastuzumab-induced inhibition of SK-BR-3 cells, mimicking clinical responses to trastuzumab therapy.

Tumors have a heterogeneous microenvironment and crosstalk between cancer and stromal cells affects cell behavior and response to drugs in 3D cultures (Fig. 2). Human mesenchymal stem cells

Please cite this article in press as: Das, V. et al. Pathophysiologically relevant *in vitro* tumor models for drug screening, Drug Discov Today (2015), http://dx.doi.org/10.1016/j.drudis.2015.04.004

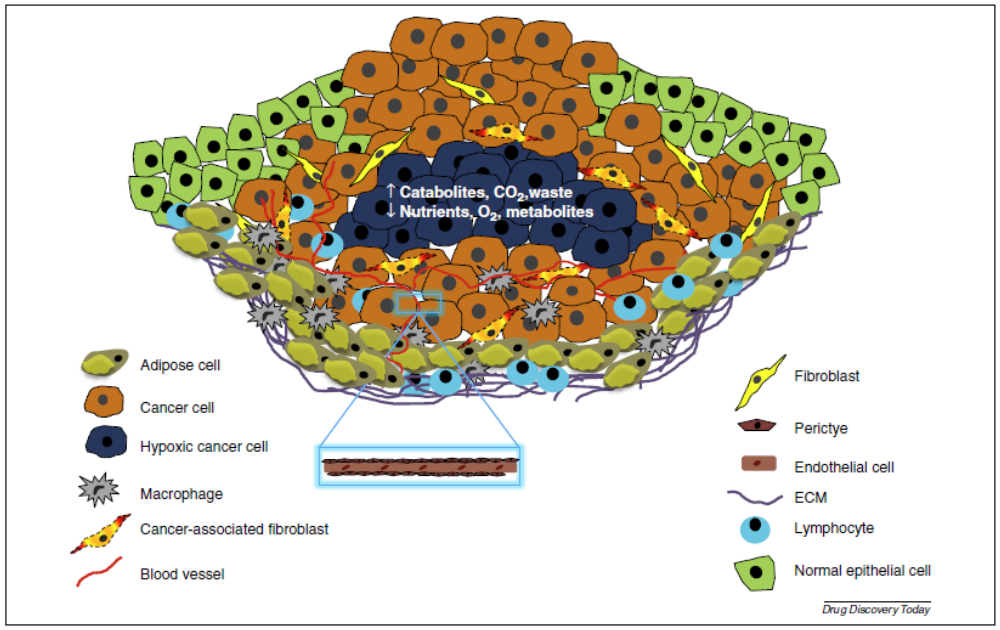

FIGURE 2

Heterogeneous tumor microenvironment. Solid tumors have a heterogeneous microenvironment comprising cancer cells and a reactive stroma containing pericytes, endothelial cells, normal epithelial cells and fibroblasts, cancer-associated fibroblasts, immune cells (such as lymphocytes and macrophages), and a dense mesh of extracellular matrix (ECM). The lining of capillaries with endothelial cells and pericytes that wrap around them are presented in the magnified window. Poor vascularization within tumors results in high levels of catabolites, CO_2, and waste, and low levels of metabolites, O_2, and nutrients in the tumor core. This results in the development of a necrotic core surrounded by hypoxic cells that show increased resistance to anticancer agents.

from bone marrow increased the metastatic potency of otherwise weakly metastatic breast cancer cells in a 3D microenvironment but not in 2D cultures [17]. 3D cell–extracellular matrix (ECM) interactions regulate the expression of proangiogenic molecules, such as vascular endothelial growth factor, interleukin 8 (IL-8), and basic fibroblast growth factor [18,19]. Similarly, IL-8 expression was upregulated only when breast cancer and glioblastoma U87 cells were co-cultured in 3D, which increased the number of cell–ECM interactions [19].

One of the most evident effects of 3D growth is seen in individual cell morphology. Breast and ovarian epithelial cancer cell 3D cultures show distinct histological morphology of tumor of the origin compared with cultures of the same cells in 2D [20]. Forced apical–basal cell polarity experienced by cells of mesenchymal origin in 2D cultures greatly altered their function and response to drug-induced apoptosis [21]. Cell morphology alterations also affected cell secretory pathways, and stimulated secretion of IL-8 in OSCC-3 cells in 3D cultures [19]. The 3D microenvironment induces epithelial–mesenchymal transition in human epithelial ovarian cancer cells [22]. Primary hepatocytes undergo rapid dedifferentiation, and lose hepatocyte-specific characters and metabolic competence in 2D compared with 3D cultures [23]. Not surprisingly, hepatocellular carcinoma cells show significant differences in gene expression and response to drugs in 2D versus 3D conditions [23].

Transition from a 2D to 3D environment in many cells also induces the altered expression of genes and proteins linked to tumorigenesis that serve as biomarkers and drug targets [24,25]. Ovarian epithelial cells express endometriosis-associated genes and show histological features of endometriosis lesions only when cultured in 3D [26]. Unlike 2D cultures, expression of P-glycoprotein (P-gp) in 3D multicellular spheroids (MCS) is cell cycle dependent and G_0/G_1 block upregulates P-gp expression [27]. Most cells in 2D cultures proliferate exponentially compared with 3D cultures, which display a gradient of cells in different phases of the cell cycle, mirroring conditions of tumor microregions [28]. Immunohistochemical analyses show the presence of an outer layer of proliferating cells in MCS of human pancreatic cancer cells [29]. Not surprisingly, paclitaxel-induced expression of apoptosis-related caspase 8 was limited mainly to the outer region of proliferating cells rather than to the inner layers of quiescent cells in MCS [28]. Likewise, osteosarcoma cells cultured in 3D showed G_1 cell cycle arrest, altered expression of cyclin B1 and p21, and resistance to doxorubicin and cisplatin [15].

Another important characteristic of solid tumors recapitulated in 3D but not 2D cultures of cancer cells is the development of

Please cite this article in press as: Das, V. et al. Pathophysiologically relevant *in vitro* tumor models for drug screening, Drug Discov Today (2015), http://dx.doi.org/10.1016/j.drudis.2015.04.004

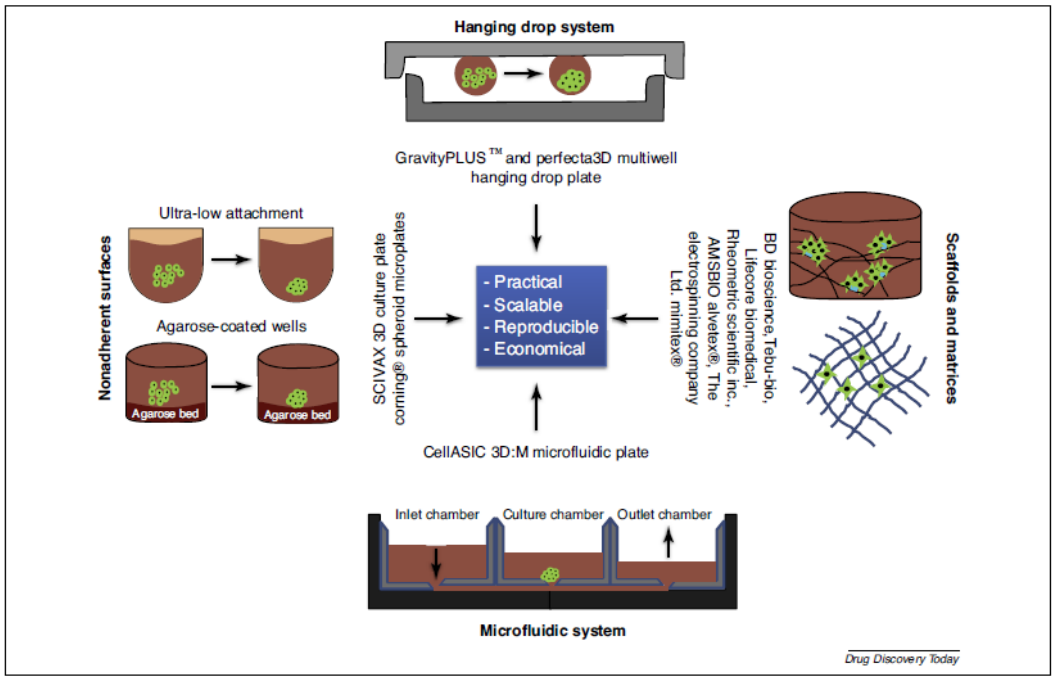

FIGURE 3

High throughput-compatible 3D culture techniques for drug–target and cell–cell interaction studies. Four commonly used methods of 3D mono- and co-culture of cancer cells and nonmalignant cells are presented that have undergone significant modifications over the past few years. Currently, several commercial 3D cultures plates are available for the high throughput screening (HTS) of anticancer drugs under more physiologically relevant microenvironments.

hypoxia resulting from the limited supply of oxygen and nutrients. Hypoxia affects many cellular functions and is implicated in tumorigenesis, and chemo- and radioresistance. Reports now strongly suggest a role of hypoxia in altering individual cell heterogeneity and the distribution of drugs within tumors [30,31]. The altered response to drugs in solid tumors has also been attributed to altered metabolic pathways that result in high levels of ATP in tumor cells compared with normal tissues. Increased aerobic glycolysis in tumors results in increased glucose uptake and high levels of lactate. Compared with 2D cultures, lactate accumulation was significantly higher in 3D culture medium, suggesting a shift to glycolysis for energy production [32]. Additionally, 3D cultures also show increased expression of lactate dehydrogenase A (LDHA), which is induced in hypoxic conditions and linked to poor prognosis in solid tumors [32]. Intriguingly, high lactate levels combined with hypoxic conditions in 3D cultures resulted in the overexpression of P-gp and multidrug resistance-associated protein 1, which alter the accumulation of drugs and their efficacy [32].

HT-compatible 3D culture platforms for effective characterization of drugs

HTS is a powerful state-of-the-art research tool for the identification of novel therapeutic compounds. Currently, several standardized methods are available for the 3D culture of cancer cells (Fig. 3). Below, we briefly discuss four commonly used techniques for 3D culture that have undergone significant modifications for HT compatibility and reliable screening of drugs under more physiological conditions.

3D cultures on nonadherent surface

Liquid-overlay technique (LOT) is a routinely used simple and inexpensive method of 3D culture on a nonadherent surface for the screening of anticancer drugs [33–36]. Although a simple method, coating of microtiter plates with nonadherent substrates, cell seeding, and medium exchange are prone to human error, which has been overcome by the use of automated liquid handling systems in LOT [37]. The availability of commercial nonadherent 3D culture plates has further simplified LOT. For example, 3D cultures of cells in ultra-low attachment plates from Corning Life Sciences (Netherlands) are amenable to automated imaging and cell migration and invasion assays on a HT scale [38]. Similarly, NanoCulture® culture plates from SCIVAX USA, Inc. enable simple and rapid assays for HTS of anticancer drugs in 3D cultures [39]. Furthermore, recent studies demonstrated the feasibility of these plates for the 3D culture of several cancer cell lines, and of patient-derived tumor cells for potential application in individualized chemotherapy [39,40]. Multiple MCS formed per well in these

Please cite this article in press as: Das, V. et al. Pathophysiologically relevant *in vitro* tumor models for drug screening, Drug Discov Today (2015), http://dx.doi.org/10.1016/j.drudis.2015.04.004

plates raised the possibility of the generation of MCS of variable size. However, studies have now shown that multiple MCS per well have equal size distribution and reproducibility across different plates [39,40].

Hypoxia and mass transfer limitations are significant resistance-associated factors that differ greatly in spheroids of different sizes [41]. Altered spheroid geometry is reported to affect the pharmacokinetics of drugs [41], making the generation of uniform-sized MCS an important requirement for 3D culture techniques for drug treatment assays.

Hanging drop 3D cultures

Hanging drop cultures (HDCs) is another 3D culture method that has undergone significant improvement for HT compatibility. Efficiency, throughput, and the long-term culture of MCS were some of the major issues that restricted the use of conventional HDC methods in HTS assays. However, the availability of commercial plates that are compatible with automatic liquid handling and imaging has significantly simplified HDCs [42,43]. Using GravityPLUS™ hanging drop plates from Insphero AG (Switzerland), Amann *et al.* [44] co-cultured non-small cell lung cancer cells with lung fibroblasts to study stroma–tumor interactions in 3D. They reported the increased expression of vimentin and decreased levels of E-cadherin, indicating epithelial to mesenchymal transition in the 3D microenvironment. Efforts are underway to make HDC more practical and amenable to HTS. Tung and coworkers [42] developed improved HDC plates that prevent osmolality shifts in culture medium resulting from excessive evaporation. Additional improved technicalities enable easy medium exchange with minimal damage to MCS. The suitability of 3D cultures in these plates for HTS studies was investigated using fluorescent and calorimetric assays on epithelial carcinoma MCS treated with standard anticancer drugs. Interestingly, both assays did not require removal of treated samples to a new microplate for analysis. The authors have further amended their HDC plates for the co-culture of two or more fluorescent cell types to generate MCS with concentric layers of multicolored cells that are attractive models for studying heterotypic cellular interactions in the 3D microenvironment [43].

Matrices and scaffolds for 3D cultures

Lately, the use of matrices and scaffolds has gained significant attention for the culture of primary cells from patient-derived tumor samples in 3D. Jiguet Jiglaire *et al.* [45] described the culture of primary glioblastoma cells on hyaluronic acid (HA)-based hydrogels for preclinical drug screening in a more *in vivo* setting. Matrix stiffness significantly affects several cell functions that alter the cellular response to drugs [46]. ECM and hydrogel-based cell cultures are important tools for studying the effect of matrix stiffness on cell functions and cell response to anticancer drugs in 3D. Hydrogels with varying matrix components allow cell growth under a controlled microenvironment, enabling the expression of genes associated with matrix synthesis and remodeling [47,48]. Altering matrix stiffness to that observed in solid tumors results in characteristic changes in cells that mirror the clinical parameters of invasive tumors [48]. Collagen–HA matrices are also in use to culture MCS of multiple cell types that enable the study of cell–cell interactions in 3D [49]. The potential use of chitosan–HA-based scaffolds for the culture of patient-derived tumor cells in 3D is currently being explored for individualized therapy [50]. Hydrogels can be used on a large scale for MCS generation and testing of potential anticancer drugs [28,51]. Currently, hydrogel scaffolds are easily adaptable to 96-well plates [45], and their potential use in 384- and 1536-well plates will have significant impact on 3D drug research and HTS.

Microfluidic 3D cell cultures

TME complexities that result in significant drug failure in clinical studies have motivated researchers to develop improved cell culture methods for the robust selection of anticancer drugs. Compared with other 3D culture systems, microfluidic systems enable drug screening under a more spatiotemporally controlled microenvironment to study the role of cell–cell and cell–matrix interactions, and cell–volume ratios on drug effects in real time [52,53]. Furthermore, control over parameters such as hydrodynamic stress, chemical gradient, and fluid flow enables cell growth under more physiological microfluidic conditions.

Microfluidics culture of rat primary hepatocytes and retinal microvascular endothelial cells (rMVECs) enables the dynamic study of angiogenesis in 3D [54]. Unlike 2D cultures, where rMVECs form sheet-like structures, rMVECs form biologically relevant 3D capillary structures in microfluidic devices. Bersini *et al.* [52] developed a 3D microfluidic model for the culture of breast cancer cells with human bone marrow-derived mesenchymal stem cells and endothelial cells. Such biomimicking microfluidic triculture systems are valuable *in vitro* tools to study the transendothelial migration of breast carcinomas surrounded by a bone-like matrix, and drug effects under co-culture conditions in 3D [52,55]. Microfluidic 3D co-culture platforms have also been extended to the personalized treatment of cancer in the clinic. 3D co-culture of patient-derived primary cancer and stromal cells on microfluidic chips was used to determine treatment regimens for patients with lung cancer [56]. Microfluidics also offer an efficient platform to monitor the inhibitory effects of drugs on epithelial–mesenchymal transition, and to determine the precise dosages required for the inhibition of tumor metastasis [57]. Microfluidic culture plates from CellASIC (USA) are available in a 96-well format for long-term 3D culture under perfused conditions and for screening of anticancer drugs using existing laboratory techniques [58].

Concluding remarks

3D cultures have tremendous potential for the effective selection of promising anticancer drugs in preclinical stages and to significantly reduce drug failure rates in clinical trials; however, several challenges currently limit 3D HT preclinical studies (Table 1). Current 3D culture methods reproduce only a subset of real-tissue conditions at a given time and, therefore, vary in their ability to replicate *in vivo* tumor conditions completely. These limitations are reflected in the discrepancies between various studies using similar controlled settings. Additionally, not all cell types are suitable for a particular 3D culture method, and there are few reports on 3D cultures from primary tumor cells.

Currently, medium exchange in most of 3D systems is possible either manually or using an automatic liquid handling system. However, the development of improved methods that enable the

Please cite this article in press as: Das, V. et al. Pathophysiologically relevant *in vitro* tumor models for drug screening, Drug Discov Today (2015), http://dx.doi.org/10.1016/j.drudis.2015.04.004

continuous flow of nutrient and waste removal will benefit the use of 3D cultures for HTS. Although 4D cultures with continuous nutrient flow and waste removal provide improved conditions for the study of tumor biology [59], their potential use in HTS remains unexplored. Additionally, 3D culture systems that allow the development of vascular networks that closely mimic TME in MCS will improve HTS with 3D cultures under more realistic physiological conditions. Interestingly, a recent study reported the development of a microfluidic system that reproduces 'leaky' tumor microvasculature in 3D cultures [60].

HTS in 3D cultures also require advanced microscopic techniques to quantify drug effects not only in outer MCS layers, but also within MCS [61–63]. Current confocal microscopy systems are not fully suitable for deep tissue imaging and the dynamic quantification of 3D cultures [38]. Light-sheet microscopy and other imaging systems that have been reported suitable for imaging of 3D structures have yet to be tested in HT platforms [61,64,65].

The recent surge in the use of 3D cell cultures for drug screening has significantly bridged the gap between 2D assays and animal studies. Furthermore, the 'Tissue Chip' initiative by the National Institutes of Health for the development of 3D human tissue chips for toxicology studies will have a significant effect on biomedical research [66]. The co-culture of cancer cells with other components of the TME in 3D enables crosstalk to determine the precise mechanism of action of drugs under more biologically relevant conditions. Additionally, the use of 3D platforms for the culture of patient-derived primary tumor cells will considerably facilitate the effective bench-to-bed translation of potential lead compounds and reinforce the concept of personalized medicine.

Acknowledgments

This work was supported by grants from the Czech Ministry of Education, Youth and Sports (CZ.1.07/2.3.00/30.0041 to V.D.; LO1304 to M.H.), the Czech Ministry of Health (NT14282 to M.H.), the Technological Agency of the Czech Republic (TE01020028 to M.H.), the Italian Ministry of Health, and Ricerca Corrente 2013 (RF-2011-02346914 to A.B.).

References

1 Hay, M. *et al.* (2014) Clinical development success rates for investigational drugs. *Nat. Biotechnol.* 32, 40–51
2 Iacombe, D. and Liu, Y. (2013) The future of clinical research in oncology: where are we heading to? *Chin. Clin. Oncol.* 2, 9
3 Pickl, M. and Ries, C.H. (2009) Comparison of 3D and 2D tumor models reveals enhanced HER2 activation in 3D associated with an increased response to trastuzumab. *Oncogene* 28, 461–468
4 Gillet, J.P. *et al.* (2011) Redefining the relevance of established cancer cell lines to the study of mechanisms of clinical anti-cancer drug resistance. *Proc. Natl. Acad. Sci. U. S. A.* 108, 18708–18713
5 Eglen, R.M. *et al.* (2008) The use of immortalized cell lines in GPCR screening: the good, bad and ugly. *Comb. Chem. High Throughput Screen.* 11, 560–565
6 Bozóky, B. *et al.* (2013) Novel signatures of cancer-associated fibroblasts. *Int. J. Cancer* 133, 286–293
7 Bremnes, R.M. *et al.* (2011) The role of tumor stroma in cancer progression and prognosis: emphasis on carcinoma-associated fibroblasts and non-small cell lung cancer. *J. Thorac. Oncol.* 6, 209–217
8 Augsten, M. *et al.* (2009) CXCL14 is an autocrine growth factor for fibroblasts and acts as a multi-modal stimulator of prostate tumor growth. *Proc. Natl. Acad. Sci. U. S. A.* 106, 3414–3419
9 Dakhova, O. *et al.* (2009) Global gene expression analysis of reactive stroma in prostate cancer. *Clin. Cancer Res.* 15, 3979–3989
10 Bruzzese, F. *et al.* (2014) Local and systemic protumorigenic effects of cancer-associated fibroblast-derived GDF15. *Cancer Res.* 74, 3408–3417
11 Subramaniam, D. *et al.* (2010) Cancer stem cells: a novel paradigm for cancer prevention and treatment. *Mini-Rev. Med. Chem.* 10, 359–371
12 Mancini, R. *et al.* (2011) Spheres derived from lung adenocarcinoma pleural effusions: molecular characterization and tumor engraftment. *PLoS ONE* 6, e21330
13 Miranda-Lorenzo, I. *et al.* (2014) Intracellular autofluorescence: a biomarker for epithelial cancer stem cells. *Nat. Methods* 11, 1161–1169
14 Yu, M. *et al.* (2014) *Ex vivo* culture of circulating breast tumor cells for individualized testing of drug susceptibility. *Science* 345, 216–220
15 Tan, P.H.S. *et al.* (2013) Three-dimensional spatial configuration of tumour cells confers resistance to chemotherapy independent of drug delivery. *J. Tissue Eng. Regen. Med.* http://dx.doi.org/10.1002/term.1800
16 Ghosh, R. *et al.* (2011) Trastuzumab has preferential activity against breast cancers driven by HER2 homodimers. *Cancer Res.* 71, 1871–1882
17 Karnoub, A.E. *et al.* (2007) Mesenchymal stem cells within tumour stroma promote breast cancer metastasis. *Nature* 449, 557–563
18 Lu, P. *et al.* (2012) The extracellular matrix: a dynamic niche in cancer progression. *J. Cell Biol.* 196, 395–406
19 Fischbach, C. *et al.* (2009) Cancer cell angiogenic capability is regulated by 3D culture and integrin engagement. *Proc. Natl. Acad. Sci. U. S. A.* 106, 399–404
20 Kenny, P.A. *et al.* (2007) The morphologies of breast cancer cell lines in three-dimensional assays correlate with their profiles of gene expression. *Mol. Oncol.* 1, 84–96
21 Baker, B.M. and Chen, C.S. (2012) Deconstructing the third dimension: how 3D culture microenvironments alter cellular cues. *J. Cell Sci.* 125, 3015–3024
22 Kuo, C.T. *et al.* (2012) Configurable 2D and 3D spheroid tissue cultures on bioengineered surfaces with acquisition of epithelial–mesenchymal transition characteristics. *NPG Asia Mater.* 4, e27
23 Chang, T.T. and Hughes-Fulford, M. (2014) Molecular mechanisms underlying the enhanced functions of three-dimensional hepatocyte aggregates. *Biomaterials* 35, 2162–2171
24 He, W. *et al.* (2014) Proteomic comparison of 3D and 2D glioma models reveals increased HLA-E expression in 3D models is associated with resistance to NK cell-mediated cytotoxicity. *J. Proteome Res.* 13, 2272–2281
25 Lee, J.M. *et al.* (2013) A three-dimensional microenvironment alters protein expression and chemosensitivity of epithelial ovarian cancer cells *in vitro*. *Lab Invest.* 93, 528–542
26 Brueggmann, D. *et al.* (2014) Novel three-dimensional *in vitro* models of ovarian endo-metriosis. *J. Ovarian Res.* 7, 17
27 Wartenberg, M. *et al.* (2002) Modulation of intrinsic P-glycoprotein expression in multi-cellular prostate tumor spheroids by cell cycle inhibitors. *Biochim. Biophys. Acta* 1589, 49–62
28 Loessner, D. *et al.* (2014) Engineered microenvironments provide new insights into ovarian and prostate cancer progression and drug responses. *Adv. Drug Deliv. Rev.* 79–80C, 193–213
29 Laurent, J. *et al.* (2013) Multicellular tumor spheroid models to explore cell cycle check-points in 3D. *BMC Cancer* 13, 73
30 Di Paolo, A. and Bocci, G. (2007) Drug distribution in tumors: mechanisms, role in drug resistance, and methods for modification. *Curr. Oncol. Rep.* 9, 109–114
31 Luoto, K. *et al.* (2013) Tumor hypoxia as a driving force in genetic instability. *Genome Integr.* 4, 5
32 Longati, P. *et al.* (2013) 3D pancreatic carcinoma spheroids induce a matrix-rich, chemo-resistant phenotype offering a better model for drug testing. *BMC Cancer* 13, 95
33 Costa, E.C. *et al.* (2014) Optimization of liquid overlay technique to formulate heterogenic 3D co-cultures models. *Biotechnol. Bioeng.* 111, 1672–1685
34 Khaitan, D. *et al.* (2006) Establishment and characterization of multicellular spheroids from a human glioma cell line: implications for tumor therapy. *J. Transl. Med.* 4, 12
35 Ma, H. *et al.* (2012) Multicellular tumor spheroids as an *in vivo*-like tumor model for three-dimensional imaging of chemotherapeutic and nano material cellular penetration. *Mol. Imaging* 11, 487–498
36 Mikhail, A.S. *et al.* (2013) Multicellular tumor spheroids for evaluation of cytotoxicity and tumor growth inhibitory effects of nanomedicines *in vitro*:

Please cite this article in press as: Das, V. et al. Pathophysiologically relevant *in vitro* tumor models for drug screening, Drug Discov Today (2015), http://dx.doi.org/10.1016/j.drudis.2015.04.004

a comparison of docetaxel-loaded block copolymer micelles and Taxotere®. *PLOS ONE* 8, e62630
37 Wenzel, C. *et al.* (2014) 3D high-content screening for the identification of compounds that target cells in dormant tumor spheroid regions. *Exp. Cell Res.* 323, 131–143
38 Vinci, M. *et al.* (2012) Advances in establishment and analysis of three-dimensional tumor spheroid-based functional assays for target validation and drug evaluation. *BMC Biol.* 10, 29
39 Yoshii, Y. *et al.* (2015) High-throughput screening with nanoimprinting 3D culture for efficient drug development by mimicking the tumor environment. *Biomaterials* 51, 278–289
40 Yoshii, Y. *et al.* (2011) The use of nanoimprinted scaffolds as 3D culture models to facilitate spontaneous tumor cell migration and well-regulated spheroid formation. *Biomaterials* 32, 6052–6058
41 Leung, B.M. *et al.* (2015) Media additives to promote spheroid circularity and compactness in hanging drop platform. *Biomater. Sci.* 3, 336–344
42 Tung, Y.C. *et al.* (2011) High-throughput 3D spheroid culture and drug testing using a 384 hanging drop array. *Analyst* 136, 473–478
43 Hsiao, A.Y. *et al.* (2012) 384 hanging drop arrays give excellent Z-factors and allow versatile formation of co-culture spheroids. *Biotechnol. Bioeng.* 109, 1293–1304
44 Amann, A. *et al.* (2014) Development of an innovative 3D cell culture system to study tumour-stroma interactions in non-small cell lung cancer cells. *PLOS ONE* 9, e92511
45 Jiguet Jiglaire, C. *et al.* (2014) *Ex vivo* cultures of glioblastoma in three-dimensional hydrogel maintain the original tumor growth behavior and are suitable for preclinical drug and radiation sensitivity screening. *Exp. Cell Res.* 321, 99–108
46 Schrader, J. *et al.* (2011) Matrix stiffness modulates proliferation, chemotherapeutic response, and dormancy in hepatocellular carcinoma cells. *Hepatology* 53, 1192–1205
47 Pedron, S. *et al.* (2013) Regulation of glioma cell phenotype in 3D matrices by hyaluronic acid. *Biomaterials* 34, 7408–7417
48 Wang, C. *et al.* (2014) Bioengineered 3D brain tumor model to elucidate the effects of matrix stiffness on glioblastoma cell behavior using PEG-based hydrogels. *Mol. Pharm.* 11, 2115–2125
49 Campbell, J.J. *et al.* (2014) A 3D *in vitro* co-culture model of mammary gland involution. *Integr. Biol.* 6, 618–626
50 Florczyk, S.J. *et al.* (2013) Porous chitosan-hyaluronic acid scaffolds as a mimic of glioblastoma microenvironment ECM. *Biomaterials* 34, 10143–10150
51 Song, H.H.G. *et al.* (2014) Hydrogels to model 3D *in vitro* microenvironment of tumor vascularization. *Adv. Drug Deliv. Rev.* 79–80, 19–29
52 Bersini, S. *et al.* (2014) A microfluidic 3D *in vitro* model for specificity of breast cancer metastasis to bone. *Biomaterials* 35, 2454–2461
53 Hagemann, T. *et al.* (2008) 'Re-educating' tumor-associated macrophages by targeting NF-κB. *J. Exp. Med.* 205, 1261–1268
54 Sudo, R. *et al.* (2009) Transport-mediated angiogenesis in 3D epithelial coculture. *FASEB J.* 23, 2155–2164
55 Niu, Y. *et al.* (2014) Validating antimetastatic effects of natural products in an engineered microfluidic platform mimicking tumor microenvironment. *Mol. Pharm.* 11, 2022–2029
56 Xu, Z. *et al.* (2013) Application of a microfluidic chip-based 3D co-culture to test drug sensitivity for individualized treatment of lung cancer. *Biomaterials* 34, 4109–4117
57 Aref, A.R. *et al.* (2013) Screening therapeutic EMT blocking agents in a three-dimensional microenvironment. *Integr. Biol.* 5, 381–389
58 Chen, S.Y. *et al.* (2011) Microfluidic array for three-dimensional perfusion culture of human mammary epithelial cells. *Biomed. Microdevices* 13, 753–758
59 Mishra, D.K. *et al.* (2014) Gene expression profile of A549 cells from tissue of 4D model predicts poor prognosis in lung cancer patients. *Int. J. Cancer* 134, 789–798
60 Prabhakarpandian, B. *et al.* (2015) Synthetic tumor networks for screening drug delivery systems. *J. Control. Release* 201, 49–55
61 Pampaloni, F. *et al.* (2013) High-resolution deep imaging of live cellular spheroids with light-sheet-based fluorescence microscopy. *Cell Tissue Res.* 352, 161–177
62 Celli, J.P. *et al.* (2014) An imaging-based platform for high-content, quantitative evaluation of therapeutic response in 3D tumour models. *Sci. Rep.* 4, 3751
63 Leong, D.T. and Ng, K.W. (2014) Probing the relevance of 3D cancer models in nanomedicine research. *Adv. Drug Deliv. Rev.* 79-80, 95–106
64 Verveer, P.J. *et al.* (2007) High-resolution three-dimensional imaging of large specimens with light sheet-based microscopy. *Nat. Methods* 4, 311–313
65 Reynaud, E. *et al.* (2008) Light sheet-based fluorescence microscopy: more dimensions, more photons, and less photodamage. *HFSP J.* 2, 266–275
66 Fabre, K.M. *et al.* (2014) Organs-on-chips (microphysiological systems): tools to expedite efficacy and toxicity testing in human tissue. *Exp. Biol. Med.* 239, 1073–1077

Please cite this article in press as: Das, V. et al. Pathophysiologically relevant *in vitro* tumor models for drug screening, Drug Discov Today (2015), http://dx.doi.org/10.1016/j.drudis.2015.04.004